Liliana Napolitano

A multidisciplinary approach for the early diagnosis of Alzheimer's disease and potential therapeutic applications

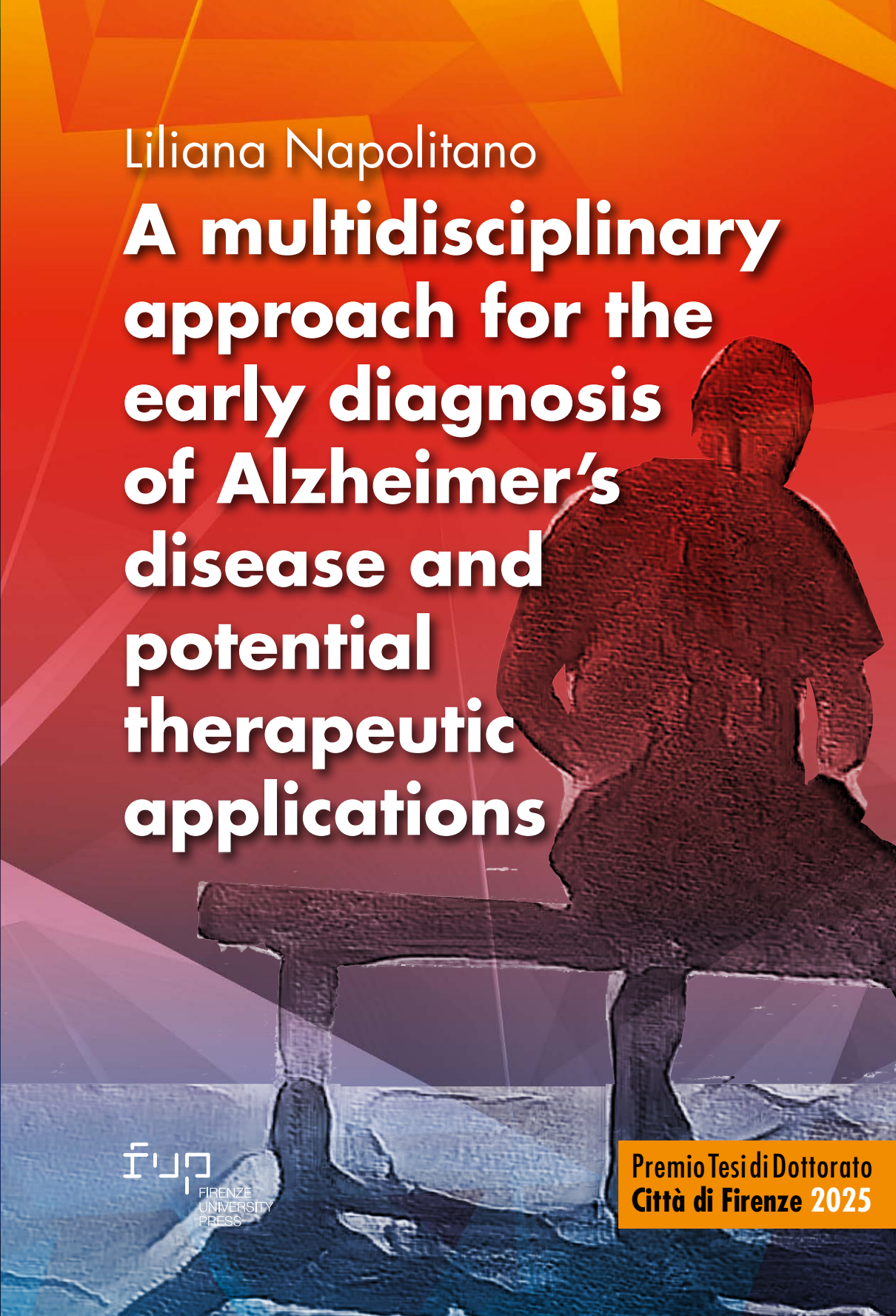

FIRENZE UNIVERSITY PRESS

Premio Tesi di Dottorato
Città di Firenze 2025

PREMIO TESI DI DOTTORATO CITTÀ DI FIRENZE
ISSN 3103-3881 (PRINT) | ISSN 3103-3989 (ONLINE)
– 12 –

PREMIO TESI DI DOTTORATO
Commissione giudicatrice, anno 2025

Anna Dolfi, Presidente della commissione

Piero Baglioni, Area Scientifica
Paola Bruni, Area Biomedica
Franco Cambi, Area Umanistica e della Formazione
Pietro Costa, Area Scienze Sociali
Fabrizio Desideri, Area Umanistica e della Formazione
Daniele Dominici, Area Scientifica
Stefano Manetti, Area Tecnologica
Massimo Morisi, Area Scienze Sociali
Raffaele Paloscia, Area Tecnologica
Alessandro Petretto, Area Scienze Sociali
Domenico Prisco, Area Biomedica
Maria Chiara Torricelli, Area Tecnologica
Luca Uzielli, Area Tecnologica
Marcello Verga, Area Umanistica e della Formazione

Liliana Napolitano

A multidisciplinary approach for the early diagnosis of Alzheimer's disease and potential therapeutic applications

FIRENZE UNIVERSITY PRESS
2026

A multidisciplinary approach for the early diagnosis of Alzheimer's disease and potential therapeutic applications / Liliana Napolitano. - Firenze : Firenze University Press, 2026.
(Premio Tesi di Dottorato Città di Firenze ; 12)

https://books.fupress.com/isbn/9791221509939

ISSN 3103-3881 (print)
ISSN 3103-3989 (online)
ISBN 979-12-215-0992-2 (Print)
ISBN 979-12-215-0993-9 (PDF)
ISBN 979-12-215-0994-6 (XML)
DOI 10.36253/979-12-215-0993-9

Graphic design: Alberto Pizarro Fernández, Lettera Meccanica SRLs

Published by Firenze University Press
Firenze University Press
Università degli Studi di Firenze
via Cittadella, 7, 50144 Firenze, Italy
www.fupress.com

This book is printed on acid-free paper
Printed in Italy

Table of contents

FUP Best Practice in Scholarly Publishing (DOI 10.36253/fup_best_practice)

Liliana Napolitano, *A multidisciplinary approach for the early diagnosis of Alzheimer's disease and potential therapeutic applications*, © 2026 Author(s), CC BY 4.0, published by Firenze University Press, ISBN 979-12-215-0993-9, DOI 10.36253/979-12-215-0993-9

Introduction

1. Alzheimer's Disease

Alzheimer's disease (AD) is a chronic and fatal neurodegenerative disease and the most common form of dementia, affecting ca. 60-70% of 55 million people worldwide (2023 Alzheimer's disease facts and figures). Furthermore, researchers from the Institute for Health Metrics and Evaluation at the University of Washington School of Medicine, as reported at AAIC 2021, anticipate arise in dementia cases, estimating that the number of affected people will nearly triple to exceed 152 million by 2050 (2021 Alzheimer's disease facts and figures; World Health Organization, 2021) becoming one of the most expensive, lethal, and burdening diseases worldwide (Alzheimer Europe, 2020).

AD is characterized by well-defined pathophysiological mechanisms (Alzheimer *et al.* 1995; Blessed, Tomlinson and Roth 1968; Glenner and Wong 1984; De Strooper and Karran 2016; Guo *et al*. 2020; Kim *et al*. 2023) leading to memory loss and difficulties with thinking, language and problem-solving skills. Neuropathologically, the AD is characterized by the presence of extracellular neurotic plaques, arising from the accumulation of the amyloid-beta (Aβ) peptide, and intracellular neurofibrillary tangles, composed of the hyperphosphorylated microtubule-associated tau protein (Glenner and Wong 1984; Kosik, Joachim and Selkoe 1986) as schematically represented in Figure 1.

These deposits are thought to play a crucial role in neurodegeneration, leading to several cytotoxic pathways such as excessive stimulation of neurotransmitter receptors, loss of calcium homeostasis, inflammation and depletion of energy and neuronal factors (Li S. *et al*. 2009; Heneka *et al*. 2015; Popugaeva, Pchitskaya and Bezprozvanny 2018; Butterfield and Halliwell 2019). However, recent studies have shown that the deposition of amyloid in the brain represents the first sign of the disease, preceding the clinical diagnosis of dementia by up to 20 years (Jack *et al*. 2013b; Jansen *et al*. 2015; Winblad *et al*. 2016; Vermunt *et al*. 2019). Indeed, AD

Liliana Napolitano, liliana98.napolitano@gmail.com, 0009-0004-3087-286X

Referee List (DOI 10.36253/fup_referee_list)
FUP Best Practice in Scholarly Publishing (DOI 10.36253/fup_best_practice)

Book References DOI 10.36253/979-12-215-0993-9.references

presents a pre-symptomatic period that may last a few years, if not over a decade, before cognitive symptoms (Sperling *et al*. 2011; Villemagne *et al*. 2013), a mild cognitive impairment (MCI), which is characterized by a detectable cognitive deficiency without impact of daily activities (Albert *et al*. 2011; Brodaty *et al*. 2013) and regarded as an intermediate, transitional period from normal cognition to AD, when the disorder is evident as a form of dementia (McKhann *et al*., 2011; Albert *et al*. 2011; Brodaty *et al*. 2013).

The aforementioned phases are characterized by several clinical symptoms. Indeed, different studies at this time showed that episodic memory loss (*i.e*., amnesia) is usually the earliest and most prominent aspect of the AD dementia (Walsh and Selkoe 2004; Bäckman *et al*. 2005; Sperling *et al*. 2011; Weintraub, Wicklund and Salmon 2012).

These findings were consistent with neuropathologic studies that showed extensive AD pathology occurring earliest in medial temporal lobe (MTL) structures (*e.g*., hippocampus, entorhinal cortex), and responsible for episodic memory loss (Hyman *et al*. 1984; Bondi, Edmonds, and Salmon 2017). Furthermore, a deficit in language skills (*i.e.*, aphasia) was observed relatively early during AD, with deficits in confrontation naming, verbal fluency (especially in semantic categories), and a reduced ability to recall learned facts (*e.g.*, the number of days in a year) (Hodges, Graham and Patterson 1995; Nebes 1989; Bondi, Edmonds, and Salmon 2017). In addition, deficits in "executive" functions responsible for the simultaneous mental manipulation of information, concept formation, problem solving, and cue-directed behavior, have been found to develop during AD (Bondi *et al.* 1994; Lafleche and Albert 1995; Perry and Hodges 1999; Bondi, Edmonds, and Salmon 2017). The gradual decline in cognitive function, therefore, contributes substantially to the loss of autonomy and reduced quality of life suffered by patients (Heyman *et al*. 1996; Whitehouse *et al*. 1997; Corey-Bloom 2002).

1.1 Etiology and genetics

AD can be classified into early-onset and late-onset AD. Early-onset AD accounts for approximately 1– 6% of all cases and manifests roughly between 30 and 60 years of age. The late-onset form, accounting for around 90% of cases, has an age of onset later than 60 years of age (Revi 2020). Besides the age of onset of symptoms, the early and late forms of AD differ in many clinical, neuropsychological, neuropathological and neuroimaging variables (Mendez 2017). Indeed, the existence of AD "variants", as posterior cortical atrophy (PCS) (Hof *et al*. 1997; Renner *et al.* 2004) and a frontal variant of AD (Johnson *et al.* 1999) has complicated the clinical and neuropsychological differentiation of AD from other neurodegenerative diseases that may have a different underlying focal pathology such as Frontotemporal Lobe Dysfunction (FTLD), Dementia with Lewy Bodies (DLB), or Primary Progressive Aphasia (PPA) (Bondi, Edmonds, and Salmon 2017). In addition, genetics play a crucial role in AD, with a heritability of 58–79% for late-onset disease and over 90%

for the early-onset one, respectively (Sims, Hill and Williams 2020). Dominantly inherited mutations in amyloid-β precursor protein (APP), presenilin 1 (PSEN1), and presenilin 2 (PSEN2) are associated with early onset AD (Karch, Cruchaga and Goate 2014).

APP is located on chromosome 21q21. Dominant mutations in this gene account for approximately 14% of early onset autosomal dominant cases of AD, with more than 30 mutations described (Guerreiro, Gustafson and Hardy 2012; TCW and Goate 2017). Two recessive APP mutations, A673V and E693Δ, were also reported to cause early onset AD (Guerreiro, Gustafson and Hardy 2012). The majority of mutations in APP cluster in the region that is adjacent to or within the Aβ domain; however, early genetic studies only sequenced the exons encoding the Aβ sequence (16 and 17), leaving the possibility that variants may exist elsewhere in APP, thus causing or increasing the risk for AD (Karch, Cruchaga and Goate 2014). PSEN1 is located on chromosome 14q24.3, while its homologue, PSEN2, is located on chromosome 1q31-q42. PSEN1 and PSEN2 are structurally similar integral membrane proteins containing nine transmembrane domains with a hydrophilic intracellular loop region (Guerreiro, Gustafson and Hardy 2012) and critical components of the γ-secretase complex, which cleaves APP into Aβ fragments (Karch, Cruchaga and Goate 2014).

In late-onset AD, the strongest genetic risk factor is the apolipoprotein E (APOE) genotype. APOE, which encodes the brain's major cholesterol transporter, has three common alleles: ε2 (8.4% estimated allele frequency in the population), ε3 (77.9%), and ε4 (13.7%) (Liu *et al.* 2013). APOE ε4 contributes to AD risk via a multitude of mechanisms, including enhanced aggregation and decreased clearance of the Aβ peptide, increased tau phosphorylation, neuronal network hyperexcitability, reduced glucose metabolism, impaired vascular and mitochondrial function (Liu *et al.* 2013).

Genome-wide association studies have identified more than 20 additional common genetic variants that modify the risk of late-onset AD (Carmona, Hardy and Guerreiro 2018). These genes converge in biological pathways involving lipid metabolism, innate immunity, and endocytosis; the effects of each one on AD risk is small (odds ratios of approximately 0.8 to 0.9 for protective alleles and 1.1 to 1.2 for risk alleles) and not clinically meaningful (Rabinovici 2019). The genetic landscape of AD is entirely reported in Figure 2.

2. Protein misfolding

Protein misfolding diseases is believed to be the primary cause of several neurodegenerative diseases, including AD. These diseases are characterized by a generic failure of the proteostasis network (PN), that is composed of the protein translation machinery (PTM), molecular chaperones (MC), the ubiquitin-proteasome system (UPS) and the autophagy-lysosome pathway (ALP), that together cooperate to maintain proteins in a soluble non-aggregated state (Brehme *et al.* 2014; McKinnon and Tabrizi 2014; Martinez-Lopez, Athonvarangkul and Singh 2015). Schematic representation of altered proteostatsis system in Figure 3.

2.1 Protein translation machinery (PTM)

As the foundation of translational control, PTM directly influences the quality and quantity of newly synthesized peptides, which in turn affects cellular adaptation (Jackson, Hellen and Pestova 2010; Yuan, Zhou and Xu 2024). Once mRNA has entered the translation pool, the remaining steps are completed by the translation machinery, which is primarily composed of ribosomes, transfer RNA (tRNA), and translation factors (TrFs), including initiation factors (eIFs), elongation factors (eEFs), and termination factors (eRFs) (Jackson, Hellen and Pestova 2010).

In MCI and AD dementia, several studies showed altered composition of ribosomes, abnormal expression levels of certain transcription factors, and impaired protein synthesis in cortical areas (Sajdel-Sulkowska and Marotta 1984; Ferrer 2002; Ding *et al.* 2005; Li *et al.* 2004; Hernández-Ortega *et al.* 2016). The main modifications implicated increased RNA oxidation as evidenced by increased 8-hydroxyguanosine immunoreactivity, reduced rRNA levels and capacity of isolated polyribosomes to incorporate S35 methionine into protein (Ginsberg *et al.* 1998; Nunomura *et al.* 2001; Ding *et al.* 2005; Hernández-Ortega *et al.* 2016). Furthermore, other studies have shown that the nuclear organizer region (NOR) surface/total nucleus surface is reduced (Nyhus *et al.* 2019; Brooks 2024), and that the rDNA promoter is hyper-methylated in AD, thus suggesting epigenetic silencing of rDNA at very specific times of AD progression (Pietrzak *et al.* 2011). Overall, these results indicate that many processes related to protein production, from the nucleus and nucleolus to the ribosome, are affected AD brain.

2.2 Molecular chaperones (MC)

Chaperones are crucial for maintaining cellular proteostasis by aiding in protein folding, preventing aggregation, and facilitating degradation of misfolded proteins (Chiti and Dobson 2017; Scalia *et al*. 2021; Kravats,Wickner and Camberg 2022). Cellular stress, arising from factors like heat shock or oxidative stress, increases the burden of misfolded proteins, leading to elevated chaperone synthesis as a protective response (Kravats,Wickner and Camberg 2022). Chaperones are categorized based on sequence homology and molecular weight into distinct families, such as Hsp40, Hsp60, Hsp70, Hsp90 and others, each contributing uniquely to the complex network of proteostasis maintenance (Kim *et al*. 2013; Camberg *et al*. 2013).

In pathological stages, chaperones and co-chaperones lose their ability to fold and degrade by the lysosome, and proteins such as tau and Aβ accumulate in the brain tissue of AD patients (Gorantla and Chinnathambi 2018; Batko *et al*. 2024). Studies have shown that Hsp90, an essential heat shock protein (Hsp) (Taipale, Jarosz and Lindquist 2010; Batko *et al*. 2024), plays a crucial role in AD. Alonso and coworkers, have proven that Hsp90 may regulate tau phosphorylation and dephosphorylation (Alonso *et al*. 2018). Moreover, certain co-chaperones like

Protein Phosphatase 5 (PP5), Cell Division Cycle 37 (Cdc37), and Calcyclin Binding Protein/Siah-1 Interacting Protein (CacyBP/SIP) contribute to tau dephosphorylation, which may help to prevent its aggregation (Jinwal *et al*. 2011; Wasik *et al*. 2013). However, the activity or proper localization of these enzymes often declines or is disrupted with age, potentially disrupting this protective mechanism. Conversely, the co-chaperone C-terminus of Hsc70-interacting protein (CHIP) facilitates tau degradation through ubiquitination, and its dysfunction results in tau accumulation (Dickey *et al*. 2008). Another important chaperone in AD context is Hsp70. Hsp70 enhances the Aβ clearance through the upregulation of Insulin Degrading Enzyme (IDE) and Transforming Growth Factor-β1 (TGF-β1) (Lu *et al*. 2014). IDE is an Aβ-degrading enzyme that increases the clearance of Aβ. TGF-β1 is a key cytokine involved in inflammatory response regulation in the brain and has been suggested to slow down AD progression. Precisely, TGF-β1 leads to Aβ clearance through activation of phagocytic microglia (Lu *et al*. 2014).

These findings suggest that age-related changes in Hsp90 co-chaperone and Hsp70 function may play a significant role in the development of neurodegenerative diseases like AD, where tau pathology is a key hallmark.

2.3 The ubiquitin-*p*roteasome system (UPS) and the autophagy-lysosome pathway (ALP)

The ubiquitin proteasome system (UPS) and autophagy-lysosome pathway (ALP) are predominant methods of proteolysis in cells. Many small proteins that have completed their cellular functional roles or are aberrantly folded are linked to a small protein, called ubiquitin, for degradation by the 26S proteasome, a multi-subunit proteolytic complex, being eliminated through the UPS pathways (Kleiger and Mayor 2014). In contrast, large protein aggregates and cellular organelles undergo degradation by the ALP (Bento *et al*. 2016). Failure of these protein degradation systems is associated with disrupted proteome homeostasis as well as development of pathogenic diseases as AD, Parkinson's Disease (PD), Huntington's Disease and other neurodegenerative disorders (Kinger *et al*. 2024). In order to recognize and degrade proteins, the UPS use a tagging system through the action of three well-known enzymes called the ubiquitin-modifying enzymes: E1, E2 and E3 (Amm, Sommer and Wolf 2014). For UPS activation, E1 ubiquitin-activating enzyme (UBA1/UBE1) firstly interacts with ubiquitin proteins. Subsequently, the second enzyme from cascade, E2 ubiquitin conjugating enzyme, binds and activates ubiquitin and aids in its translocation to the final enzyme in cascade, E3 ubiquitin-ligase (Hershko and Ciechanover 1998; Ciechanover and Brundin 2003; Stewart *et al*. 2016).

In AD, tau filaments can impair and decrease proteasome activity, leading to neurodegeneration (Keck *et al*. 2003). Moreover, Aβ was observed to increase the E1 enzyme, probably to maintain ubiquitin-dependent proteolytic pathway (Lopez Salon *et al*. 2003; Kinger *et al*. 2024). Additionally, in neuronal cells exposed to Aβ, there was an observed induction of the ubiquitin-conjugating

enzyme E2-25 kDa/Huntingtin interacting protein 2 (E2-25K/HIP2). This increase in HIP2 was potentially linked to a compromised proteasome function (Song *et al*. 2003). Furthermore, E3 is able to degrade APP through HRD1 domain (Kaneko *et al*. 2010). However, increasing levels of insoluble HRD1 due to oxidative stress, may lead to APP accumulation and following Aβ production (Saito *et al*. 2010; Kaneko *et al*. 2012; Saito *et al*. 2014; Kinger *et al*. 2024). Unfortunately, the UPS is not the only altered network. Indeed, ALP results to be impacted as well. Under physiological conditions, Aβ undergoes lysosomal degradation, but this process appears to be impaired in AD. In this context, Pickford and coworkers demonstrated that decreased levels of the autophagic component Beclin 1 were linked to neurodegeneration, especially during the early stages of the disease (Pickford *et al*. 2008). In addition, their studies have shown that transcription factor levels, as the nuclear factor of activated T-cells (NFAT), could modulate chaperone-mediated autophagy. Indeed, NFAT is a transcription factor for lysosome-associated membrane protein 2 (LAMP2) gene (Valdor *et al*. 2014). Decreased NFAT has been linked to reduced chaperone-mediated autophagy and increased regulator of calcineurin 1 (RCAN1), which is also observed in AD. Besides transcription factors, other proteins have an important impact on macro autophagy, such as PSEN1. PSEN1 is fundamental for targeting vacuolar H^+-ATPases (v-ATPase) to lysosomes, lowering lysosomal lumen pH, essential for autophagic protein breakdown. Alterations in lysosomal proteolysis, results in toxic protein build-up and neuron death in AD (Lee *et al*. 2010; Kinger *et al*. 2024).

3. The Amyloid-β peptide

3.1 Structure and function of APP

APP is a transmembrane protein expressed in various tissues, especially in the central nervous system (CNS), where the major isoform encompasses 695 amino acid residues (Jakob-Roetne and Jacobsen 2009; Nalivaeva and Turner 2013). APP can undergo two major proteolytic pathways, the non-amyloidogenic and the amyloidogenic one (Figure 4). The non-amyloidogenic pathway begins with α-secretase-mediated cleavage of APP at amino acid 687 (in the APP 770 isoform) which releases the ectodomain, soluble APP α (APPsα), into the extracellular space. As a result, a C-terminal fragment of APP (83 amino acids in length, CTF83 or αCTF) remains embedded in the plasma membrane. Cleavage of CTF83 by γ-secretase releases a small p3 fragment into the extracellular space and the APP intracellular domain (AICD) into the cytoplasm (Nalivaeva and Turner 2013).

Unlike sAPPβ and Aβ, sAPPα was shown to possess neurotrophic and neuroprotective functions. Indeed, sAPPα reduces tau hyper-phosphorylation by inhibiting β-site amyloid precursor protein cleaving enzyme 1 (BACE1) and glycogen synthase kinase (GSK)-3β activity in cultured cells and transgenic

presenilin 1 and APP (PSAPP) mouse model (De Strooper 2003; Obregon *et al*. 2012; Deng *et al*. 2015). The amyloidogenic processing begins with β-secretase-mediated APP cleavage at amino acid 671 (in the APP 770 isoform) and results in the release of a small and soluble ectodomain, APP β (sAPPβ), into the extracellular space. A larger APP C-terminal fragment composed of 99 amino acids (CTF99, or βCTF) remains embedded in the plasma membrane. Finally, the cleavage of CTF99 by γ-secretase releases Aβ peptide into the extracellular space and the AICD into the cytoplasm, respectively (Figure 4; Wilkins and Swerdlow 2017). Aβ peptide is a 38- to 43-amino acids residue peptide and is mainly produced intracellularly in vesicles like endosomes, and then released in the extracellular space of healthy brain during neuronal activity (Jarrett, Berger and Lansbury 1993; Saido and Leissring 2012; Cheignon *et al*. 2018).

Overall, the function of APP is not fully understood. It has been assumed to relate to several processes, such as cell adhesion, due to its interaction with laminin and collagen and its co-localization with integrins, specifically within neuronal axons (Yamazaki, Koo and Selkoe 1997; Young-Pearse *et al*. 2008). Furthermore, sAPPα may stimulate the differentiation of neuronal stem cells into an astrocytic phenotype (Caillé *et al*. 2004). sAPPβ has been described as a less potent protectant, or even as a harmful agent for neurons (Chasseigneaux and Allinquant 2012), as it can cause neuronal death and axonal pruning by binding to the death receptor 6 (DR6; Nikolaev *et al*. 2009).

3.2 Aβ peptide aggregation

Approximately 50 human pathologies are associated with the deposition of amyloid, primarily composed of a single misfolded peptide or protein (Chiti and Dobson 2017). These conditions, collectively termed protein misfolding diseases (or protein conformational diseases), arise from the conversion of soluble, functional peptides or proteins into highly ordered, insoluble fibrillar aggregates (Chiti and Dobson 2006). This aberrant aggregation process disrupts cellular homeostasis and contributes to the pathogenesis of various debilitating diseases. Among these pathologies, neurodegenerative disorders, including AD, represent nowadays very common and detrimental medical conditions in the industrialized countries. Aβ plays a main role in the process of fibrillogenesis in AD. Precisely, Aβ belongs to the class of "natively disordered" proteins, existing in the monomeric state in an equilibrium mixture of many conformers (Roychaudhuri *et al*. 2009). Moreover, its two isoforms, $A\beta_{40}$ and $A\beta_{42}$, are normal constituents of cerebrospinal fluid (CSF) (Frost *et al*. 2003). Both the $A\beta_{40}$ and $A\beta_{42}$ monomers are dominated by random coil segments in their typical ensembles (Vivekanandan *et al*. 2011; Somavarapu and Kepp 2015).

The process of fibrillogenesis begins with amyloid monomers that, through a slow and often rate-limiting process called primary nucleation (k_n), assemble to form a variety of oligomeric species. These oligomers can then undergo further aggregation into short, flexible, irregular protofibrils, or alternatively, they can

participate in secondary nucleation events (k_2), catalyzing the formation of new aggregates on their surfaces. These protofibrils mature and elongate (k_p) into insoluble fibrils, which in turn can also serve as templates for secondary nucleation, significantly accelerating the overall fibrillization process and leading to their rapid accumulation extracellularly. (Figure 5; Westermark 2005; Cohen *et al*. 2013; Chiti and Dobson 2017; Reiss *et al*. 2018). Precisely, $A\beta_{42}$ tends to accumulate in extracellular fibrils, whereas $A\beta_{40}$, which represents the large majority of produced Aβ (LaFerla, Green and Oddo 2007), tends to be more stable in the monomeric conformation (Hubin *et al*. 2014).

Aβ fibrils, whether obtained *in vivo* from AD patients or *in vitro*, consistently exhibit a threadlike morphology with diameters ranging from 7 to 13 nm, as visualized by electron microscopy (EM) or atomic force microscopy (AFM). These fibrils, often microns in length, typically comprise 2 to 8 protofilaments, each with a diameter of approximately 2 to 7 nm. These protofilaments intertwine, forming twisted structures or associate laterally to create flat ribbons. Notably, while less common, fibrils composed of a single protofilament have also been observed (Paravastu *et al*. 2008; Wasmer *et al*. 2008; Chiti and Dobson 2017). Fibrils possess a cross-β structure, in which β-strands are oriented perpendicularly to the fibril axis and assembled into β-sheets that run the length of the fibril, as initially detected using X-ray fiber diffraction (Sunde and Blake 1997; Chiti and Dobson 2017), with recent support from Fourier transform infrared spectroscopy (FTIR), solid-state nuclear magnetic resonance (ssNMR), and X-ray crystallography (Paravastu *et al*. 2008; Zandomeneghi *et al*. 2004; Eisenberg and Jucker 2012; Chiti and Dobson 2017) and Cryo-EM. Aβ fibril's structure representation showed in Figure 6 (Kollmer *et al*. 2019).

Although amyloid fibrils represent the main pathological hallmark of AD, increasing evidence suggests that small, soluble oligomers, are the major agents responsible for neurotoxicity in AD (Kayed *et al*. 2003; Benilova, Karran and De Strooper 2012; Chiti and Dobson 2017; Selkoe 2019). The size of Aβ oligomers is distributed over a wide molecular weight range (from < 10 kDa to > 100 kDa), with structural polymorphisms in oligomers of similar sizes (Sakono and Zako 2010). Indeed, Aβ oligomers are organized in different structures ranging from dimers (Sakono and Zako 2010), trimers (Sakono and Zako 2010), tetramers (Walsh *et al*. 2000, Chen and Glabe 2006), pentamers (Ahmed *et al*. 2010), nonamers and dodecamers (referred to as Aβ*56) (Sakono and Zako 2010), and amyloid derived-diffusible ligands (ADDLs; Lambert *et al*. 1998; Sakono and Zako 2010). Furthermore, previous studies have shown that oligomer size distribution was very different between $A\beta_{42}$ and $A\beta_{40}$, indicating that their oligomerization pathways are different (Bitan *et al*. 2003; Sakono and Zako 2010).

Despite the small structural difference between these two peptides, they display distinct clinical, biological, and biophysical behaviors (Bitan *et al*. 2003). The concentration of secreted $A\beta_{42}$ is ~ 10% that of $A\beta_{40}$, yet the longer form is the predominant component in parenchymal plaques (Bitan *et al*. 2003). Indeed, an increase in the $A\beta_{42}/A\beta_{40}$ concentration ratio is associated with familial forms of

early-onset AD (Scheuner *et al*. 1996; Golde, Eckman and Younkin 2000). In addition, $A\beta_{42}$ displays enhanced neurotoxicity with respect to $A\beta_{40}$ (Younkin 1995; Selkoe 1999; Dahlgren *et al*. 2002; Bitan *et al*. 2003), because of the additional presence of hydrophobic residues at the C-terminal, that makes $A\beta_{42}$ more aggregation-prone than the $A\beta_{40}$ form, and so more toxic to neurons (Finder *et al*. 2010). Lambert *et al*. reported the formation of small Aβ globular oligomers (5 nm in diameter) in Ham's-F12 medium from a synthetic $A\beta_{42}$ amyloid peptide, which were referred to as ADDLs (Lambert *et al*. 1998). Importantly, ADDLs strongly bound to the dendritic arbors of cultured neurons, blocked long term potentiation (LTP) and caused neuronal cell death (Lambert *et al*. 1998; Wang *et al*. 2002). The finding of ADDLs in soluble brain extracts from human AD brains using ADDL-specific antibodies supports the idea that their presence in human AD brain is strongly associated with the disease (Sakono and Zako 2010). Moreover, a study by Yamamoto and collaborators showed the formation of toxic Aβ oligomers in the presence of the GM1 ganglioside (Yamamoto *et al*. 2007). These oligomers were spherical, with a diameter of 10–20 nm and a molecular mass of 200–300 kDa, therefore much larger than ADDLs (Sakono and Zako 2010). Furthermore, Aβ monomers produced extracellularly can interact with GM1, and Aβ complexes with GM1 have been found in AD brains (Yanagisawa 2007). These observations support the idea that extracellular soluble Aβ oligomers could be formed by GM1 (Sakono and Zako 2010). Later, Ladiwala and coworkers characterized two $A\beta_{42}$ oligomers, referred to as A+ and A-, found that they were both globular in shape and had size of 6.2 ± 0.5 nm or 6.1 ± 0.6 nm, respectively, in height (Ladiwala *et al*. 2012). Such oligomers were also compared to ADDLs and fibrillar conformers formed at high concentrations of $A\beta_{42}$ monomeric protein, which appeared to possess an elongated morphology as observed by AFM (Figure 7) (Banchelli *et al*. 2020).

Despite their structural similarity, A- oligomers showed a much lower toxicity than the A+ oligomers when the metabolic activity was assessed through the (3-[4,5- dimethylthiazol-2-yl]-2,5 diphenyl tetrazolium bromide (MTT) reduction inhibition assay and membrane integrity was evaluated via lactate dehydrogenase (LDH) activity assay in differentiated PC12 cells and primary cultures of rat embryonic cortical neurons (Ladiwala *et al*. 2012). Furthermore, fibrils were reported to be mildly toxic to neuronal cells (Ladiwala *et al*. 2012), whereas A+ oligomers show a higher neurotoxicity due to the presence of an array of aminoacidic residues on their surface exposing hydrophobic groups, as well as tyrosine (Tyr) and lysine (Lys) residues, that are linked to a higher neurotoxicity with respect to that of A- oligomers and amyloid fibril. The detrimental effects appear to result from an aberrant interaction with cellular components, such as membrane, small metabolites, proteins or other macromolecules (Chiti and Dobson 2006; Banchelli *et al*. 2020). Schematic representation of A+ and A- oligomers is reported in Figure 8.

4. The amyloid hypothesis and pathogenic pathways

A dominant theory for the pathology of AD is the "amyloid hypothesis", which describes a complex sequence of pathogenic events responsible for neurodegeneration (Figure 9; Hardy and Allsop 1991; Selkoe 1991; Hardy and Selkoe 2002). According to this hypothesis, the aberrant accumulation of the Aβ peptide, following the amyloidogenic processing of the APP, results in the production of cytotoxic complexes, such as small and soluble oligomers, which accumulation triggers a cascade of pathogenic events, including the alteration of mitochondrial functions, oxidative stress and calcium dyshomeostasis (Braak and Braak 1994).

Although our primary focus will be on the amyloid cascade hypothesis and the description of related pathogenic pathways, it is important to acknowledge the existence and growing importance of alternative hypotheses and mechanisms implicated in the pathogenesis of AD. These include, but are not limited to, the vascular hypothesis, which emphasises the role of cerebrovascular dysfunction (Iadecola 2017), prion-like tau protein aggregation (Goedert, Masuda-Suzukake, Falcon 2017), neuroinflammation (Heneka *et al*. 2015) and metabolic dysfunction (De la Monte and Tong 2014).

The vascular hypothesis of AD posits that cerebrovascular dysfunction is a key contributor to its pathogenesis. Indeed, AD brains have microvascular alteration and more atherosclerosis in intracranial vessels than age matched controls (Love and Miners 2016; Iadecola 2017). Furthermore, it was observed that AD pathology and ischemic lesions frequently coexist in the same brain (Schneider *et al*. 2007; Toledo *et al*. 2013; Iadecola 2017), and that ischemic lesions lower the threshold for clinical dementia leading to neurodegeneration (Kapasi, DeCarli and Schneider 2017; Iadecola 2017). Beyond amyloid, the prion-like propagation of tau protein, independent of or synergistic with amyloid, is gaining support. This mechanism suggests that misfolded tau seeds can spread throughout the brain, templating further misfolding and driving neurofibrillary tangle formation (Goedert, Masuda-Suzukake and Falcon 2017). Moreover, neuroinflammation, once considered a secondary response to amyloid plaques, is now understood as a powerful driver of neurodegeneration. Indeed, in AD pathology, microglia's ability to phagocytose Aβ decreases (Hansen, Hanson and Sheng 2018) and actively contribute to neurodegeneration through the release of toxic substances and regulation of synaptic function (Hong *et al*. 2016; Miao *et al*. 2023). Furthermore, metabolic dysfunction, including insulin resistance and mitochondrial abnormalities, has been implicated in AD. These metabolic impairments can disrupt neuronal function, increase oxidative stress, and promote the accumulation of toxic protein aggregates (De la Monte and Tong 2014). It is likely that these diverse pathways interact and influence each other, contributing to the complex and heterogeneous nature of AD.

4.1 Plasma membrane disruption

The cell membrane consists of a semi permeable lipid bilayer. It regulates the transport of materials entering and exiting the cell. In 1972, Singer and Nicolson proposed the *fluid- mosaic model*, describing the cellular membrane as a double layer of lipids in a lamellar liquid-crystalline phase (Singer and Nicolson 1972). Nowadays, membranes are considered to be increasingly complex, characterized by lipid/proteins assemblies, with lateral and transverse asymmetries, different patchiness and variable thickness with an elevated protein presence (Engelman 2005; Nicolson 2014; Fabiani and Antollini 2019).

Several fundamental biochemical reactions crucial for cell life, such as metabolic and signaling reactions involving G-protein, histamine, Gamma-Aminobutyric acid (GABA) or glutamate receptors and other, take place in cell membranes, making them a key agent in almost all cellular physiological and pathological processes (Li G. *et al*. 2009; Fabiani and Antollini 2019). Lipids, such as fatty acids, cholesterol (chol), endocannabinoids, arachidonic acid metabolites such as prostaglandins, leukotrienes and epoxyeicosatrienoic acids, and many others, are major plasma membrane constituent with important implications (Fabiani and Antollini 2019). Chol, cardiolipin, phosphatidylinositol-4,5-biphosphate (PIP2) and glycolipids influence the action of numerous transmembrane proteins, as reported in several research papers (Lee 2003; Barenholz 2004; Barrera, Zhou and Robinson 2013; Fabiani and Antollini 2019).

In AD, Mason and coworkers in 1992 demonstrated that isolated brain membranes derived from AD patients had lower levels of cholesterol, disadvantaging the insertion of Aβ into the membrane (Mason *et al*. 1992). Thus, Aβ remains attached to the cellular membrane surface leading to plaques formation (Ji, Wu and Sui 2002). Taking advantage of confocal microscopy and fluorescence anisotropy, Cecchi and colleagues showed an inverse correlation between chol content and membrane perturbation (Cecchi *et al*. 2009). It has also been shown that increasing chol reduces amyloid-induced membrane disruption by modifying the raft domain properties (Cecchi *et al*. 2009; Fabiani and Antollini 2019).

Another important lipid in Aβ-membrane interaction is GM1, an important component of the raft domains (Lin *et al*. 2008), as previously reported. Precisely, increasing chol levels enhance gangliosides clustering, which is supposed to influence and modulate Aβ oligomerization. The interaction between clusters and Aβ peptides can induce Aβ aggregation in β-sheet rich structures in a concentration dependent way (McLaurin *et al*. 1998; Ariga *et al*. 2001; Kakio *et al*. 2001, 2002; Matsuzaki 2007; Fabiani and Antollini 2019). The binding Aβ/GM1 cluster promotes a conformational change depending on the protein density of the membrane. At low peptide/lipid ratios the transition from random coil to α-helix conformation is favored, while at high peptide/lipid ratios the fibrils formation is promoted, due to Aβ-sheet rich structure organization (Matsuzaki, Kato and Yanagisawa 2010; Fukunaga *et al*. 2012; Cascella *et al*. 2017; Fabiani

and Antollini 2019). Representative interaction Aβ/ganglioside is shown in Figure 10. Closer examination of the mechanism of Aβ interaction with GM1 suggests that Aβ oligomers, which have increased hydrophobicity compared to Aβ monomers as reported in *section 3.2*, mainly bind to GM1, activating sequential changes such as membrane biophysical and ion permeability disruption, leading to Aβ-mediated synaptotoxicity (Hong *et al*. 2014; Fabiani and Antollini 2019).

Notwithstanding, all the evidence leads us to assess a direct role of gangliosides in Aβ oligomerization, another Aβ oligomerization mechanism has also been observed, without being dependent on Aβ/ganglioside interaction, suggesting that other lipid components or raft glycans may also be involved (Kim, Yi and Ko 2006; Fabiani and Antollini 2019).

In addition to the role of lipids in Aβ-induced neurotoxicity, three main membrane damage models have been proposed (Cheng *et al*. 2013).

The first model is based on the generation of a stable transmembrane protein pores determined by the interaction between amyloidogenic protein, in its monomeric or oligomeric form, with the membrane lipid bilayer (Sciacca, La Rosa and Milardi 2021). Consistently, Pollard and colleagues reported that Aβ interacting with lipid membranes could lead to the formation of calcium (Ca^{2+})-permeable channels, inducing cell death (Pollard, Rojas and Arispe 1993; Sciacca, La Rosa and Milardi 2021). Indeed, other evidence suggested that blocking Ca^{2+} influx reduces the Aβ oligomer neurotoxicity and insoluble $Aβ_{40}$ and $Aβ_{42}$ levels in AD mice (Samad *et al*. 2017; Cascella and Cecchi 2021). Moreover, elevated intracellular Ca^{2+} activates calcineurin (CaN) and phosphatases like PP1, involved in long-term depression (Reese and Taglialatela 2011; Cascella and Cecchi 2021).

The second model is represented by the membrane destabilization via a "carpet model", determined by the interaction of prefibrillar species with the cellular membranes resulting in an asymmetric pressure between both layers (Sciacca, La Rosa and Milardi 2021). Proximal or distant pressure relief with respect to the protein determines leakage of small molecules, leading to membrane disruption (Hebda and Miranker 2009; Sciacca, La Rosa and Milardi 2021).

The third model is described as a "detergent-like mechanism". This model is determined by an asymmetric pressure caused by peptides carpeting the cellular membrane, leading to the loss of lipid from one or both leaflets of the bilayer (Bode *et al*. 2019; Sciacca, La Rosa and Milardi 2021). Precisely, this detergent-like mechanism may result in a thinner membrane or in the formation of a hole (Sciacca, La Rosa and Milardi 2021).

In conclusion, the Aβ-induced neurotoxicity described through these three mechanisms contributes to the neuronal damage observed in AD. Indeed, a deep understanding of these mechanisms is crucial for the development of therapeutic strategies counteract disease progression. A schematic representation of the aforementioned models in Figure 11.

4.2 Mitochondrial dysfunction

Mitochondrial dysfunction plays a crucial role in the pathogenesis of AD (Rai *et al*. 2020). Mitochondria are ubiquitous intracellular organelles and they represent the primary source for the generation of biological energy in the cell in the form of ATP (Cadonic, Sabbir and Albensi 2016; Bhatia *et al*. 2022). Mitochondria contain an outer membrane, which is freely permeable to small molecules and ions, and an inner one, impermeable to most molecules and ions (Cadonic, Sabbir and Albensi 2016), which contains the electron transport chain (ETC), ADP-ATP translocases, ATP synthases, and numerous other membrane transport systems. The ETC and the ATP synthases dispersed throughout this membrane are directly involved in the generation of ATP from the potential energy stored in substrates (*i.e*. glucose) (Cadonic, Sabbir and Albensi 2016). In the early 1980s, fluorodeoxyglucose positron emission tomography (FDG PET) studies showed that brains of AD patients utilized less glucose than those of control subjects, thus leading to confusion and loss of temporary memory in the early stages of disease (Swerdlow 2018). Further evidence of impaired glucose metabolism in AD patients comes from the cohort autopsy conducted within the Baltimore Longitudinal study of aging evaluating the ratios of concentrations of glycolytic amino acids, serine, glycine, and alanine to glucose and quantifying the protein levels of neuronal (GLUT3) and astrocytic (GLUT1) transporters (An *et al*. 2018). The study revealed that the severity of AD symptoms were directly linked to the decreased glycolytic flux that downregulate GLUT3 levels and increase tissue glucose concentrations, establishing that impaired glucose metabolism was connected to the progression of AD (An *et al*. 2018; Bhatia *et al*. 2022). In addition, Aβ can enter the matrix through the TOM/TIM channels, thus leading to mitochondrial dysfunction (Hashimoto *et al*. 2003). Indeed, cultured PC12 cells maintained in the presence of $A\beta_{42}$ oligomers showed reduced electron transport chain enzyme activities (Pereira, Santos and Oliveira 1998; Swerdlow 2018). Post-mortem studies on AD patients have revealed a decrease in the levels and activity of α-ketoglutarate dehydrogenase complex (a rate-limiting enzyme of the TCA cycle) in the temporal cortex, parietal cortex, and hippocampus regions (Sheu *et al*. 1994; Mastrogiacoma *et al*. 1996; Kish 1997; Bhatia *et al*. 2022). Cytochrome oxidase and pyruvate dehydrogenase enzymes were also found to be deficient in AD patients (Sorbi, Bird and Blass 1983; Sheu *et al*. 1985; Parker, Filley and Parks 1990, Bhatia *et al*. 2022). $A\beta_{42}$ oligomers were also reported to impair respiratory chain function in isolated mitochondria (Canevari, Clark and Bates 1999; Swerdlow 2018). Moreover, Aβ can affect mitochondrial function by binding heme groups, which reduces their functionality as redox centers in the ETC. This event occurs predominantly at the heme groups of complex IV of the ETC (Santos *et al*. 2010; Cadonic, Sabbir and Albensi 2016). Furthermore, Aβ may also bind to Aβ-binding alcohol dehydrogenase (ABAD), resulting in an increase in reactive oxygen species (ROS) generation through impairment in complex IV molecular O2 processing, reduced cytochrome c release, and decrease in ATP production (Santos *et al*. 2010; Cadonic, Sabbir and

Albensi 2016). In the early stages of AD, a reduced axonal transport of mitochondria has been reported, as well as fewer mitochondria within neurons, with the remaining organelles presenting significant alterations in size and shape (Esteves and Arduino 2009; Zhu *et al*. 2013). Mitochondrial dysfunctions reported above are represented in Figure 12.

4.3 Calcium dyshomeostasis

Calcium ions (Ca^{2+}) regulate the function of various enzymes and proteins and play an important role as secondary messengers in signal transduction pathways, including cell survival, proliferation, differentiation and apoptosis (Clapham 2007; Cascella and Cecchi 2021). Ca^{2+} is also involved in the regulation of multiple neuronal and astrocytic functions, such as neurotransmitter release, synaptic plasticity, membrane excitability, gene transcription, proliferation and cell death (Berridge 1998; Berridge, Lipp and Bootman 2000; Cascella and Cecchi 2021). A wide variety of Ca^{2+} channels are present in the plasma membrane with a diverse distribution. In particular, N-methyl-D-aspartate receptor (NMDAR) and α-amino-3-hydroxy-5-methyl-4-isoxazolepropionic acid receptor (AMPAR) regulate the Ca^{2+} influx from extracellular to intracellular space by performing fine-tuning (Cascella and Cecchi 2021).

The "calcium hypothesis", firstly postulated by Khachaturian in 1989 following major experimental studies by the group of Landfield and colleagues, investigated how the activation of the amyloidogenic pathway can reshape neuronal Ca^{2+} signaling pathways responsible for cognition (Khachaturian 1989). According to this hypothesis, the depolarization-repolarization cycles in which Ca^{2+} influx from the extracellular space plays a critical role, are responsible for many of the neuronal dysfunction observed in brain disorders in older people. Several studies support the notion that embrane disruption induced by Aβ aggregates allows the entry of small molecules and ions, mainly free Ca^{2+} (Peters *et al*. 2015). Moreover, it was reported that Aβ cause the formation of stable pores and ion channels, usually defined as "annular protofibrils", thereby resulting in perturbation of Ca^{2+} influx (Lin, Bhatia and Lal 2001; Kagan, Azimov and Azimova 2004; Arispe, Diaz and Simakova 2007). Based on these findings, numerous researchers have focused their attention on the effects of Aβ aggregates on Ca^{2+} channels in neuronal cells. Specifically, the blockade of Ca^{2+} influx was reported to reduce the neurotoxicity of Aβ oligomers and the levels of insoluble $A\beta_{40}$ and $A\beta_{42}$ in the hippocampus of AD transgenic mice (Samad *et al*. 2017; Cascella and Cecchi 2021). Increasing evidence suggests that one of the most important Aβ targets is NMDAR (Popugaeva, Pchitskaya and Bezprozvanny 2018). NMDARs are cationic channels gated by the neurotransmitter glutamate, having critical roles in excitatory synaptic transmission, plasticity, as well as in excitotoxicity in the CNS (Kamat *et al*. 2016); their activation leads to massive Ca^{2+} fluxes into the postsynaptic cells (Kamat *et al*. 2016). Previous studies have shown that Aβ in its oligomeric form can increase the vulnerability of neurons to excitotoxicity,

which is caused by excessive NMDARs activation with subsequent cell calcium overload (Mattson *et al*. 1992; Mattson 2004; Popugaeva, Pchitskaya and Bezprozvanny 2018). The resulting activation of downstream signal transduction pathways triggers a cascade of pathological events leading to synaptic disruption and neuronal loss. In addition, Aβ-induced synaptic degeneration also involves surface removal and endocytosis of AMPARs, thus increasing calcium dysregulation and neuronal loss (Tu *et al*. 2014). Neurotoxic mechanisms induced by Aβ oligomers are briefly reported in Figure 13.

4.4 Oxidative stress

Oxidative stress is a condition produced by the imbalance between oxidants and antioxidants in a biological system (Singh *et al*. 2019). Neuronal vulnerability to ROS is emerging as a key detrimental factor responsible for AD pathogenesis. The brain consumes a large amount of oxygen for proper functioning, and mitochondria present in neuronal cells are responsible for the production of a large amount of free radicals and ROS, due to the high accessibility of oxygen in these organelles (Angelova and Abramov 2018).

In pathogenic conditions, such AD, dysfunctional mitochondria are less efficient producers of ATP but more efficient producers of ROS (Wang *et al*. 2014). ROS significantly contribute to the deterioration of neuronal cells via modulating the function of biomolecules (DNA, RNA, lipids, and proteins), and processes (nucleic acid oxidation, lipid peroxidation) in the cell (Halliwell and Gutteridge 2015). The ROS primarily involved in neurodegeneration are hydrogen peroxide (H_2O_2), superoxide anion (O^{2-}), and the highly reactive hydroxyl radical (HO^-). In addition, reactive nitrogen species (RNS), such as nitric oxide (NO) also have a deleterious effect on neurons (Singh *et al*. 2019). Several studies have shown that Aβ-induced oxidative imbalance is responsible for the elevated levels of lipid peroxidation by products (*e.g*., 4-hydroxynones, malondialdehyde), protein oxidation (*e.g*., carbonyl), and DNA/RNA oxidation (*e.g*., 8-hydroxylguanosine, 8-hydroxydeoxyguanosine) (Praticò 2008; Zhao and Zhao 2013; Wang *et al*. 2014; Singh *et al*. 2019).

Moreover, increasing evidence has shown that various metals are involved in the pathogenesis of AD, such as iron, zinc, copper. Many enzymes require metals for their proper function, but the interaction of Aβ with redox active metals hinders their enzymatic function. Furthermore, the binding of Aβ to copper in its redox state promotes the aggregation process (Greenough, Camakaris and Bush 2013; Singh *et al*. 2019). Finally, zinc dyshomeostasis occurs in the inflammatory response to insoluble Aβ plaques, leading to abnormal zinc release and increased oxidative stress (Huang, Zhang and Chen 2016; Singh *et al*. 2019).

5. Biomarkers

The term "biomarker" or "biological marker" refers to a broad subcategory of medical signs that can be measured accurately and reproducibly (Strimbu and

Tavel 2010). In 1998, the National Institutes of Health Biomarkers Definitions Working Group defined a biomarker as an indicator of a normal, or either pathogenic, biological process, or a pharmacological response to a therapeutic intervention that can be evaluated and measured (Biomarkers Definitions Working Group 2001; Strimbu and Tavel 2010).

5.1 The A/T/N classification

The A/T/N classification system for AD biomarkers, where "A" indicates Aβ biomarker concentrations, "T" identifies the level of tau biomarkers, and "N" refers to neurodegeneration biomarkers, is used to distinguish three groups of biomarkers based on different neuropathological mechanisms (Jack *et al*. 2018).

The first category involves indicators of Aβ deposition: the CSF of AD patients is characterized by a reduced level of $A\beta_{42}$ concentration (by ~50% with respect to healthy subjects) (Olsson *et al*. 2016; Zetterberg and Bendlin 2021). $A\beta_{42}$ is normally mobilized from the interstitial fluid of the brain into the CSF and blood, probably through the lymphatic system (Rasmussen, Mestre and Nedergaard 2018). The reduction in $A\beta_{42}$ levels in AD is due to its aggregation in the brain parenchyma. Diagnostic accuracy for Aβ pathology can be increased by dividing the aggregation-prone $A\beta_{42}$ concentration by soluble $A\beta_{40}$; both are products of the same APP-processing pathway, but $A\beta_{40}$, in contrast to $A\beta_{42}$, remains soluble in AD. The CSF $A\beta_{42}/A\beta_{40}$ ratio is influenced by interindividual differences in amyloidogenic APP-processing (high vs. low Aβ producers) and is close to 100% concordant with amyloid PET (Hansson *et al*. 2019; Zetterberg and Bendlin 2021); discordant cases CSF-positive and PET-negative, often become PET-positive within a few years (Lewczuk *et al*. 2017; Hansson *et al*. 2019; Zetterberg and Bendlin 2021).

The second major AD neurodegenerative biomarkers are increased levels of CSF total (t-tau) and phosphorylated (p-tau) tau protein (Fagan *et al*. 2009; Shaw *et al*. 2009; Jack and Holtzman 2013), atrophy on structural MRI (Vemuri *et al*. 2009; Dickerson and Wolk 2012; Jack and Holtzman 2013), and hypometabolism on FDGPET (Jagust 2010). Blennow and coworkers demonstrated that tau pathology could be reflected with biomarkers through ELISA assay capturing specifically tau protein phosphorylated threonine 181 (p-tau 181) and 231 (p-tau231) (Blennow *et al*. 1995). P-tau species seem to predict progression from MCI to dementia (Mattsson *et al*. 2009) and are highly accurate in differential diagnosis of AD (Ewers *et al*. 2015). In accordance with the National Institute on Aging and the Alzheimer's Association (NIA-AA) research framework and novel International World Group (IWG) criteria, another biomarker proposed to reflect tau pathology is PET imaging, targeting AD-specific tau deposits, which do not occur in other neurodegenerative diseases with tau pathology (Ossenkoppele *et al*. 2018; Simrén *et al*. 2023).

The third major category is neurodegeneration, defined as the process of progressive neuronal loss. Importantly, CSF levels of $A\beta_{42}$ and amyloid PET are

specific for Aβ deposition, whereas these changes are not specific in AD (Jack *et al*. 2002; Simrén *et al*. 2023). In subjects with AD, both FDG PET and MRI follow a modality-specific pattern that is typical of AD (Senjem *et al*. 2005; Jack and Holtzman 2013). One of the first pathological alterations is the temporal lobes atrophy mainly in the hippocampal region. Although it is not a specific diagnostic marker, rate of change predicts disease progression accurately (Frisoni *et al*. 2010). Generally, an MRI is highly recommended for patients seeking medical advice for cognitive decline (Simrén *et al*. 2023). Complementary, FDG PET gives information on decreased neuronal glucose metabolism. This technique not only assesses functional decline but also directly measures neuronal loss, typically observed in the posterior cingulate and temporo-parietal regions. The distinct patterns associated with various neurodegenerative diseases make this a valuable tool for differentiating between them (Chételat *et al*. 2020; Simrén *et al*. 2023). Fluid biomarkers proposed to reflect neurodegeneration involve CSF neurofilament light (NfL), the main component of the neuroaxonal cytoskeleton (Friede and Samorajski 1970). Unfortunately, the CSF sampling is an invasive and expensive procedure and amyloid PET has limited availability (and not insignificant radiation exposure); consequently, a blood biomarker for brain Aβ pathology would be an important step toward precision medicine and to perform clinical follow-up of patients with cognitive disorders (Olsson *et al*. 2016; Zetterberg and Bendlin 2021; Mielke and Fowler 2024). Recently, it has been observed that $A\beta_{42}$ levels in relation to $A\beta_{40}$ (measured by immunoprecipitation mass spectrometry or ultrasensitive enzyme-linked immunosorbent assays) reflect brain Aβ pathology with relatively high accuracy as compared to both amyloid PET and CSF $A\beta_{42}/A\beta_{40}$ ratio (Janelidze *et al*. 2016; Ovod *et al*. 2017; Zetterberg and Bendlin 2021), although evaluation against neuropathology is equally necessary (Zetterberg and Bendlin 2021). The main synaptic biomarkers are neurogranin (Ng) in CSF, as well as the synaptic vesicle glucoprotein 2A (SV2A). The most established astrocytic biomarker is the chitinase-3-like protein 1 (YKL-40) in CSF, and another promising biomarker is glial fibrillary acidic protein (GFAP) in CSF and plasma that highlights astrocytic activation/degeneration (Antonell *et al*. 2014; Zetterberg and Bendlin 2021). An overview of the AD biomarkers continuum is reported in Table 1.

Recently, new criteria for AD diagnosis have been introduced, expanding the biological framework for AD diagnosis and specifying further categories within the ATN system. In this context, *α*-Synuclein (*α*Syn) was found to be involved in the pathophysiology of AD (Twohig and Nielsen 2019). In 2024, Bellomo and coworkers found a significant proportion of AD patients (30%) being positive to *α*Syn seed amplification assays (*α*S-SAAs) in all clinical stages of AD. Furthermore, the *α*S-SAAs positivity was associated with a more marked cognitive decline (Bellomo *et al.* 2024). From this evidence, the introduction of synucleinopathy as a new criterion for AD diagnosis represent a successful strategy for the selection of AD patients who may benefit from anti-*α*Syn therapies (Bellomo *et al*. 2024).

5.2 Temporal evolution of AD biomarkers in the CSF

Biomarkers could change linearly with time, exponentially or with a sigmoidal way. Initially, the temporal evolution of AD biomarkers was based on observations in elderly subjects through the cognitive continuum (Jack *et al*. 2008, 2009, 2010a; Mormino *et al*. 2009; Perrin, Fagan and Holtzman 2009; Jack and Holtzman 2013). These initial models assumed that amyloid biomarkers were the first to become abnormal, followed by biomarkers of tau-related neurodegeneration and finally by overt clinical symptoms. Notably, a further model proposed that the general or functional form for biomarker evolution was sigmoidal with time (Jack *et al*. 2010a).

Subsequently, empirical studies in elderly individuals (Buchhave *et al*. 2012; Förster *et al*. 2012; Jack *et al*. 2010b; Landau *et al*. 2012; Lo *et al*. 2011; Villemagne *et al*. 2011, 2013; Jack and Holtzman 2013) and in autosomal dominant mutation carriers (Bateman *et al*. 2012; Reiman *et al*. 2012; Jack and Holtzman 2013) showed that the order of biomarker alteration was consistent with that proposed in models. In addition, these data also showed that the class of biomarkers related to Aβ followed a sigmoidal shape over time (Caroli and Frisoni 2010; Fleisher *et al*. 2012; Jack *et al*. 2012, 2013; Villemagne *et al*. 2013; Jack and Holtzman 2013).

In 2013, Jack, Jr. and Holtzman proposed three different sets of biomarker models, each culminating in the common clinical phenotype of AD dementia (Jack and Holtzman 2013). Specifically, they proposed the "Pure AD biomarker model: Amyloid first", where the temporal ordering pattern in this model corresponds to the sequence of molecular events proposed in the amyloid cascade hypothesis (Glenner and Wong 1984; Hardy and Selkoe 2002; Jack and Holtzman 2013). Initially, this model is characterized by the overproduction and aggregation of $A\beta_{42}$ and decreased clearance, resulting in the formation of amyloid plaques. CSF $A\beta_{42}$ and amyloid PET are the first biomarkers to become abnormal. Following the deposition of $A\beta_{42}$ aggregates, tauopathy is induced in the medial temporal lobe and promotes its spread into the neocortex. Tauopathy results in detectable abnormalities in MRI and FDG PET imaging biomarkers of structural neurodegeneration. At this stage, clinical symptoms follow the MRI and FDG PET abnormalities (Reed *et al*. 2010; Vemuri *et al*. 2011). In the early and intermediate clinically symptomatic stages of the disease, amyloid biomarkers approach a plateau while MRI, FDG PET, and tau tend to increase (Jack and Holtzman 2013). In the late phase of the disease, all biomarkers approach a plateau. Unfortunately, systematic studies on the progression of biomarkers in the end stage of disease have not been done because of difficulties in performing (Jack and Holtzman 2013). An explicative model of temporal evolution of AD biomarkers is represented in Figure 14.

5.3 Putative CSF biomarkers based on the novel concept of generic protein misfolding and proteotoxicity

The current literature demonstrates a clear association between protein misfolding and the deterioration of PN, with numerous studies indicating that disrupted PN status is linked to an elevated propensity for proteins to lose solubility and form various types of self-assemblies that are often challenging to detect (Hipp, Park and Hartl 2014). As previously mentioned in *section 2*, in the AD pathological conditions, the PN status results to be highly disrupted and unregulated, leading to the formation of misfolded oligomers and highly structured fibrils. In particular, small oligomers composed of the $_{42}$-residue form of Aβ, formed in the initial stages of the aggregation process or released from mature fibrils, have emerged as a significant focus in the study of AD pathogenesis (Kayed *et al*. 2004; Benilova, Karran and De Strooper 2012; Evangelisti *et al*. 2016; Bigi *et al*. 2023b; Bigi e*t al*. 2024b). Indeed, elevated oligomer levels in the brain have been linked to the progression of pathology and have been shown to correlate more strongly with the severity of dementia than mature fibrils (Cline *et al*. 2018; Selkoe 2019; Bigi *et al*. 2024b). Therefore, the ageing-related accumulation of protein aggregates is both a result and a cause of PN decline, creating a vicious cycle that ultimately leads to its collapse (Balchin, Hayer-Hartl and Hartl 2016; Labbadia and Morimoto 2015). Thus, the presence of aggregates of a specific protein increases the propensity of numerous others to undergo aggregation into proteotoxic oligomeric species. This scenario is evidenced by the observation that in every neurodegenerative disease the primary protein deposits are often associated with deposits of other proteins that are neither the cause nor a defining feature of that disease (Ferrer *et al*. 2001; Amador-Ortiz *et al*. 2007; Nakashima-Yasuda *et al*. 2007; Schwab *et al*. 2008; Colom-Cadena *et al*. 2013; Sengupta *et al*. 2015; Hepp *et al*. 2016; Nonaka, Masuda-Suzukake and Hasegawa 2018; Twohig and Nielsen 2019).

In this context, Bigi and Fani with their colleagues, decided to compare CSF samples derived from AD patients and control subjects in a novel Italian study named PRAMA (Proteomics, Radiomics & Machine learning-integrated strategy for precision medicine for Alzheimer's). Precisely, we investigated the presence of protein instability with biophysical methods, and correlated proteotoxicity, in the form of misfolded protein oligomers able to induce cell dysfunction in cultured cells using cell viability assays (Bigi *et al*. 2024a).

This approach expands beyond the detection of misfolded $A\beta_{42}$ and tau proteins, which constitute a minor fraction of the CSF proteome. Instead, it focuses on analysing the entire CSF proteome for misfolded proteins, grounded in the experimental evidence that AD involves a broader failure of protein homeostasis and the potential presence of misfolded protein species beyond Aβ and tau (Bigi *et al*. 2024a).

Our findings indicated that AD CSF samples exhibited elevated solvent exposure of tryptophan residues within the proteome, increased concentrations of large protein species, and elevated concentrations of protein species capable of

inducing an influx of calcium ions from the extracellular space to the cytosol of cultured cells. We can assess that these observations suggest the presence of protein misfolding, protein aggregation, and proteotoxicity. This result broadens the scope of our investigation to encompass the entire proteome, rather than focusing on specific proteins such as $A\beta_{42}$, t-tau, p-tau and numerous other individual proteins that are currently being explored as potential AD biomarkers in clinical settings (Bigi *et al*. 2024a).

6. Blood-based biomarkers in AD

The invasiveness of the lumbar puncture (LP) and the high cost of clinical procedure, such as PET imaging, make these two techniques not suitable for extensive use in primary care (Löppönen *et al*. 2003; Simrén *et al*. 2023). For this reason, researchers have felt the need to switch from CSF to blood-based biomarkers, mainly due to the large availability of samples and the drastic reduction in costs. Unfortunately, early attempts to detect and measure brain proteins in blood were extensively unsuccessful (Olsson *et al*. 2016). Finally, the development of ultrasensitive assays has made it possible to translate the CSF biomarkers reflecting AT(N) pathologies into the blood (Simrén *et al*. 2023). Although blood biomarkers are promising for early diagnosis and monitoring of AD, their diagnostic accuracy is not yet comparable to that of CSF biomarkers. Therefore, CSF analysis remains the gold standard for confirmation of diagnosis (Leuzy *et al*. 2022).

6.1 The A/T/N classification in plasma

For the first plasma biomarkers category, only recent studies have reported lower plasma $A\beta_{42}/A\beta_{40}$ in AD patients, being in accordance with PET or CSF measures. The first pioneering study was conducted by Ovod and colleagues only in 2017 (Ovod *et al*. 2017). The primary challenge with plasma Aβ as a biomarker lies in its small fold-changes between amyloid-positive and -negative individuals, potentially due to matrix effects and peripheral Aβ expression (Benedet *et al*. 2022; Simrén *et al*. 2023). This contributes to its modest association with CSF $A\beta_{42}/A\beta_{40}$ and Aβ PET, necessitating highly robust assays to minimize misclassifications arising from pre-analytical and analytical variations (Benedet *et al*. 2022). The weak correlation between current candidate methods (Pannee *et al*. 2021) further underscores the need for substantial advancements before their clinical utility can be established beyond research settings.

Concerning the second biomarkers category, recent and promising studies have shown that highly specific immunoassays for p-tau181 (Karikari *et al*. 2020), p-tau217 (Palmqvist *et al*. 2020), and p-tau231 (Ashton *et al*. 2021) are able to detect AD early changes in tau release long time before the onset of symptoms (Palmqvist *et al*. 2020; O'Connor *et al*. 2021; Simrén *et al*. 2023). Accordingly, Janelidze and coworkers have shown that plasma p-tau predicts conversion from a cognitively unimpaired condition (CU) to MCI and finally to

AD dementia (Janelidze *et al*. 2020). For p-tau, the diagnostic accuracy, as determined by the area under the curve (AUC), distinguishes symptomatic AD from differential diagnoses and healthy controls consistently around 0.9 in most studies conducted in well-characterised research cohorts. (Karikari *et al*. 2020; Palmqvist *et al*. 2020; Ashton *et al*. 2021). In conclusion, plasma p-tau might represent the most promising biomarker for use in routine clinical chemistry as a complement of CSF biomarkers, as well as for use in clinical trials as a tool for prescreening and enrichment strategies (Simrén *et al*. 2023).

For the latter plasma biomarkers category, NfL in blood strongly correlates with NfL CSF (Gisslén *et al*. 2016; Hansson *et al*. 2017; Giacomucci *et al*. 2022). However, the interindividual differences observed in seemingly healthy elderly individuals are substantial due to the presence of concomitant pathologies affecting the central and peripheral axons of the older population. Therefore, the specificity is limited. Nevertheless, a very low NfL concentration (*i.e*. clearly normal) is unlikely to be compatible with neurodegenerative diseases, such as AD (Ashton *et al*. 2021; Simrén *et al*. 2023). A further potential application of NfL is to assess the efficacy as disease- modifying drugs become more widely available. Moreover, effective treatment should result in a decline in NfL levels, as observed in individuals affected by spinal muscular atrophy (SMA), a genetic neurodegenerative disease that primarily affects children. (Olsson *et al*. 2019) In conclusion, NfL is a stable biomarker, demonstrating consistency throughout the analytical, pre-analytical and biological phases, and holds promise as a diagnostic indicator, as well as a tool for monitoring treatment efficacy and disease progression in AD. An overview of plasma biomarkers in AD is reported in Table 2.

6.2 Antibodies as diagnostic and therapeutic tools for AD

One of the greatest unmet medical challenges facing our society is the development of effective methods for diagnosing and treating of AD. Notably, the identification of early diagnostic biomarkers would enable the development of new and effective treatments for this disease (Yu and Watts 2013).

Antibodies, also known as immunoglobulins, are proteins with a high binding specificity with the target. The structure of a classical immunoglobulin G (IgG) consists of four chains, as reported in Figure 15: two heavy chains and two light ones. The light chains have a variable region (V_L) and a constant one, whereas the heavy chains possess a variable region (V_H) and a constant one, divided into three homology regions (Edelman 1970). These chains are held together by weak force and by interchain sulfur-sulfur bonds between corresponding pairs of cysteines (Edelman 1970).

The target recognition of the antigen is performed by both the variable portions of the light and heavy chains (Edelman 1970), thus making antibodies highly accurate tools for the recognition of biomarkers of pathological interest, due to their high specificity and affinity for target (Perchiacca *et al*. 2012).

Antibodies can be divided into monoclonal (mAbs) (Milstein 1980), that bind a single epitope, and polyclonal antibodies, that recognize multiple epitopes on the same antigen.

7. Core immunochemistry approaches for AD research and clinical practice

7.1 ELISA assay

Nowadays, the clinical routine measurement procedures are based on enzyme-linked immuno-sorbent assays (ELISA) (classical or automated, such as the Lumipulse ® and Elecsys® technology) (Veerabhadrappa *et al*. 2020), but there have been several approaches and attempts to detect levels of CSF biomarkers.

Major efforts have been made to develop an ELISA assay specific for Aβ oligomers, the Aβ conformer considered to be the most toxic one. Unfortunately, their detection in CSF sample derived from AD patients is very challenging given their heterogenous and transient nature and their low concentration in biological fluids. Indeed, CSF $A\beta_{42}$ oligomers concentration ranged between 0.1 and 10 pg/ml (Savage *et al*. 2014).

In 2007, it was developed an assay using flow cytometry in conjunction with fluorescence resonance energy transfer, revealing that oligomeric Aβ is detectable in control patients even without dementia (Santos *et al*. 2007). Later, a sandwich ELISA assays with a single antibody (Ban50) have been used to detect high molecular weight (HMW) oligomers demonstrating that an increase in Aβ oligomers in CSF is associated with cognitive decline (Fukumoto *et al*. 2010; Herskovits *et al*. 2013). Another measurement procedure includes the Alzbio3 assay, a multiparametric test performed on the Luminex platform. This assay is able to detect Aβ and tau proteins in the same sample and has a diagnostic accuracy similar to traditional flat plate ELISAs (Le Bastard *et al*. 2013; Herskovits *et al*. 2013).

7.2 Single Molecule Array (SIMOA)

In 2010, Rissin and coworkers introduced a new technique called Single Molecule Array (SIMOA) (Rissin et al. 2010). This assay employs an antibody-coated bead to capture the target antigen, followed by a biotinylated detection antibody. The construct is then labeled with streptavidin-β-galactosidase (SBG). Upon addition of a fluorogenic substrate, β- galactosidase activity generates fluorescent product within each well. This digital readout, where each bead represents a single molecule, enables the detection of analytes at concentrations far below the limits of conventional ELISA. The fluorescence intensity within the sample well is subsequently quantified using spectrofluorimetry. This measurement is then compared against a standard curve with known concentrations, enabling the calculation of the analyte's concentration within the sample. The primary distinction lies in the use of antibody-coated microscopic

beads in Simoa, which allows for the isolation of individual antigen-bead complexes and the application of a Poisson distribution for signal analysis, enhancing sensitivity compared to standard ELISA (Rissin et al. 2010). The principle of Simoa is represented in Figure 16.

In their study, Chatziefstathiou and coworkers, tested the diagnostic performance of a panel of four biomarkers Glial fibrillary acidic protein (GFAP), NfL, tau, Ubiquitin Carboxyl-Terminal Hydrolase L1 (UCH-L1) in CSF samples derived from AD and FTD patients and control subjects using the SIMOA platform. They demonstrated that GFAP and tau were the most valuable markers to discriminate AD from FTD patients, while NfL, tau and UCH-L1 were most valuable to differentiate between FTD and control subjects (Chatziefstathiou *et al*. 2024).

In another study, Wojdała and colleagues, evaluated two different immunoassays targeting different regions of the Aβ peptide performing a method comparison in both CSF and plasma and assessing the diagnostic performance across the AD continuum (Wojdała *et al*. 2024). They observed that while both $A\beta_{42}/A\beta_{40}$ assays allowed them to effectively discriminate between control subjects and different AD stages, the assay targeting the amyloid N-terminal region provided the best diagnostic performance in plasma (Wojdała *et al*. 2024). From both these studies, the SIMOA techniques proved to be an excellent tool, able to discriminate between different AD biomarkers and neurodegenerative diseases, assessing its differential diagnostic potential.

7.3 Chemiluminescence immune-sorbent assay (CLEIA) and electrochemiluminescence immune-sorbent assay (ECLIA).

CLEIA and ECLIA are alternative methods which adopt chemiluminescence to generate signal. Basically, chemiluminescence techniques are based on the generation of luminescence, meaning that radiation is emitted, which is being generated when an electron transits from an excited state to the ground one (Simrén *et al*. 2023). The resultant energy in the atom is released in the form of light, which is then detected (Cinquanta, Fontana and Bizzaro 2017).

The classical CLEIA is based on mixing the necessary reagents in a proper and controlled manner, whereases the ECLIA reaction is activated by changing an electrode potential. This allows the control of both the time of the reaction and the position (Miao 2008; Simrén *et al*. 2023). Nowadays, fully automated platforms used for measuring different CSF biomarkers in clinical routine are provided by Elecsys on the Cobas platform (Roche), and Lumipulse (Fujirebio) utilizing ECLIA and CLEIA, respectively (Simrén *et al*. 2023).

8. Sequence-specific and conformational antibodies against Aβ

Immunotherapy using anti-Aβ antibody is one of the most promising approaches for AD treatment (Murakami 2014). Antibodies can be divided into sequence-specific and conformational antibodies. Sequence-specific antibodies

are able to recognize six to ten amino acid residues and they are used to identify the primary structure of the protein (Edelman 1970). Indeed, the monoclonal sequence-specific antibodies 6E10 was the first anti-amyloid monoclonal antibody against Aβ and one of the most widely used antibodies in AD research. In particular, the epitopes for 6E10 maps to residues 1-16 of Aβ (Baghallab *et al*. 2018). However, most clinical studies using conventional sequence- specific antibodies have encountered significant difficulties. This is presumably due to their aspecific detection of non-pathological conformers, such as monomer, fibrils of Aβ and APP, together with pathological oligomers (Murakami 2014).

Conversely, conformation dependent antibodies have been reported to specifically recognize distinct assembly states of amyloids, such as prefibrillar oligomers or fibrils (Kayed *et al*. 2007). In 2001, Lambert and colleagues demonstrated that ADDLs are effective antigens for the induction of antibodies with therapeutic potential (Lambert *et al*. 2001). Two antibodies, referred to as M93 and M94, detected assembled forms of Aβ, which were toxic both *in vitro* and *in vivo*, but weakly associated with Aβ in its physiological monomeric state. Deepening their potency and specificity, this study demonstrated that antibodies are useful for screening compounds that delay ADDL formation and enable ADDLs detection both in cultured hippocampal neurons and in the AD affected brain (Lambert *et al*. 2001).

Two years later, Kayed and colleagues developed the A11 polyclonal antibody, an anti- oligomer antibody, which is capable of recognizing *in vitro* a structural common epitope to oligomeric conformers formed by several distinct proteins (Kayed *et al*. 2004). They studied *in vivo* the ability of A11 antibodies to neutralize the toxicity of oligomeric forms of all amyloid species on cell cultures (Kayed *et al*. 2004). They even observed that the amount of oligomer specific antibody deposition was significantly lower than the total Aβ, comprehending that oligomers do not accumulate over time, but tend to aggregate into fibrillar structures that are undetected by this oligomer specific antibody (Kayed *et al*. 2004).

In a subsequent study, Kayed and colleagues developed the OC conformational polyclonal antibody, that was able to recognize a generic epitope associated with amyloid fibrils and soluble fibrillar oligomers formed by different proteins, and that is absent in prefibrillar oligomers, specifically recognized by the A11 conformational polyclonal antibody (Kayed *et al*. 2007). Starting from these observations, the researchers hypothesized that there were at least two distinct types of amyloid oligomers: prefibrillar oligomers and fibrillar ones (Figure 17). The fact that the OC antibody recognized small soluble oligomers in the 250 kDa range of dimers that are not recognized by A11 indicates that these oligomeric species are conformationally bound to fibrils and distinct from prefibrillar oligomers (Kayed *et al*. 2007).

In 2014, Savage and collaborators developed a novel conformational antibody specific for $A\beta_{42}$ ADDLs, called 19.3. Specifically, the researchers developed a robust assay to quantify oligomers from CSF, that resulted to be significantly elevated in AD CSF compared with aged controls (Savage *et al*. 2014).

9. Anti-Aβ monoclonal antibodies approved in clinical trials for AD treatment

Over the past 25 years, several mAbs have been engineered to bind and eliminate Aβ (Karran and De Strooper 2022) from the brain of AD patients and are currently under investigation in clinical trials (Bigi *et al*. 2024b). The Aβ plaque reduction catalyzed by mAbs specific for different Aβ conformers is retained to involve the activation of microglia, following the phagocytosis of fibrillar Aβ and degradation through the endosomal/lysosomal system, as reported in Figure 18 (Cummings *et al*. 2024).

Nowadays, a mAb called Lecanemab, has received the U.S. Food and Drug Administration (FDA) approval (Swanson *et al*. 2021). However, the path to approval is often challenging. Aducanumab, which initially received accelerated FDA approval (Sims *et al*. 2023; Fletcher 2023), was subsequently withdrawn by its manufacturer, Biogen, in 2024 due to limited clinical efficacy (Alzheimer's Disease and Dementia, 2024). Another mAb, such as Donanemab (Sims *et al*. 2023; Fletcher 2023), is currently under investigation, while Remternetug is in Phase III clinical trials (Alzforum 2023). Development of Gantererumab, another mAb, was terminated after it failed to meet primary endpoints in clinical trials (Boess *et al*. 2021; Ostrowitzki *et al*. 2012).

9.1 Lecanemab

Lecanemab (BAN2401; Leqembi.) is a humanized IgG1 antibody based on the mouse mAb158 (Englund *et al*. 2007) that specifically binds to Aβ protofibrils. Lecanemab was approved in January 2023 by FDA, and it is recommended to patients with MCI or mild AD dementia with positive amyloid PET or CSF biomarkers, consistent with AD. (FDA Office of the Commissioner 2023). In phase III, Lecanemab showed to slow down the cognitive decline of AD patients compared with controls treated with placebo. (van Dyck *et al*. 2023). Furthermore, amyloid PET plaque levels were reduced in patients treated with Lecanemab, and all CSF and plasma biomarkers were decreased by Lecanemab compared to the placebo except for NfL, showing no drug-placebo difference (Cummings *et al*. 2024). Unfortunately, infusion-related reactions (26.4%), intracerebral hemorrhages (17.3%), and cerebral edema (12.6%) were the most common adverse effects (van Dyck *et al*. 2023). Furthermore, non-carriers of the APOE ε4 allele in the under Lecanemab treatment had the lowest incidence of hemorragies (11.9%) and cerebral edema (5.4%); whereas ε4 heterozygotes had a higher incidence of both (van Dyck *et al*. 2023; Cummings *et al*. 2024). Lecanemab received accelerated approval from the FDA based on its Aβ lowering activity in the Phase IIb study, which showed a reasonable likelihood of predicting clinical benefit. Based on the results of the study "CLARITY AD", Lecanemab received standard FDA approval (van Dyck *et al*. 2023).

9.2 Aducanumab

Aducanumab (BIIB037; Aduhelm™) is a humanIgG1 mAb (IgG1-mAb) specific for an N-terminal epitope composed by amino acids 3–7 of the $A\beta_{42}$ peptide, with a higher affinity for fibrillar aggregates compared with monomers (Arndt *et al*. 2018). This mAb was recommended for patients with MCI or mild dementia who were positive for amyloid PET or CSF studies (Sevigny *et al*. 2016). In phase III, Aducanumab decreased, in a dose-dependent manner, the CSF p-tau levels and plasma p-tau (Budd Haeberlein *et al*. 2022). In addition, pooled results from a small sample of patients showed a dose-dependent decrease in tau PET standardized uptake value ratio (SUVR) in precise brain regions, demonstrating that Aducanumab directly affects both an upstream biomarker of AD (Aβ plaque) and downstream biomarkers of AD (CSF and plasma p-tau; tau PET). Reductions in amyloid PET SUVR correlated with reductions in plasma p-tau 181 levels. Taken together, these results support the hypothesis that Aβ accumulation triggers downstream tau pathology and subsequent clinical decline, and that removal of aggregated Aβ in the brain via Aducanumab treatment results in clinical benefit (Herring *et al*. 2021; Chen *et al*. 2024). Unfortunately, intracerebral hemorrhages and Amyloid-Related Imaging Abnormalities (ARIA) were the most common adverse effects at high-dose of mAbs (Sevigny et al. 2016; Herring *et al*. 2021; Chen *et al*. 2024). However, after 48 months of treatment with Aducanumab, the Aβ plaques were reduced in a dose- and time- dependent manner, as visible by amyloid PET (Herring *et al*. 2021; Cummings *et al*. 2024; Chen *et al*. 2024). Unfortunately, Aducanumab has been discontinued by Biogen in 2024, due to limited clinical efficacy and the discontinuation of confirmatory trials needed for full FDA approval (Alzheimer's Disease and Dementia, 2024).

9.3 Donanemab

Donanemab (LY3002813; N3pG) is a humanised IgG1 mAb developed from mouse mE8-IgG2a (Demattos *et al*. 2012). It recognises the N-terminal pyroglutamate form of Aβ, binds to deposited Aβ plaques and activates microglia-mediated clearance (Demattos *et al*. 2012; Cummings *et al*. 2024). Several phase III studies were conducted to investigate the Donanemab treatment, and one phase III trial is complete. In patients with intermediate tau levels and clinical AD symptoms, Donanemab showed to reduce the cognitive decline by 35% in Clinical Dementia Rating – Sumb of Boxes and led to 40% less decline in activities of daily living (Eli Lilly and Company 2023). Cerebral edema appeared in 24% of participants who were treated with Donanemab, with 6.1% experiencing symptomatic edema (Cummings *et al*. 2024). Cerebral hemorrhages occurred in 31% of participants treated with Donanemab and 13% receiving placebo. Based on these results, standard approval of Donanemab by the FDA is anticipated (Eli Lilly and Company 2023; Sims *et al*. 2023).

9.4 Remternetug

Remternetug (LY3372993) is an N3pG-AB mAb, specific for pyroglutamate Aβ, and able to target Aβ plaques (Alzforum 2023). In this moment, Remternetug is tested in a phase III study, which has as primary outcome to measure the percentage of participants who reach Aβ clearance on PET, and as a secondary outcome to measure changes of Aβ plaque on PET from baseline, monitor the time necessary to reach the Aβ plaque reduction, measure of the pharmacokinetics trough serum concentration, and number of participants with treatment emergent anti-drug antibodies (Cummings *et al*. 2024). Moreover, participants who have received placebo, will be treated with Remternetug for additional 52 weeks of time, while participants treated with mAb are going to be treated with placebo (Alzforum 2023; Cummings *et al*. 2024).

9.5 Gantenerumab

Gantenerumab (RO4909832; R1450) is the first fully human IgG1 monoclonal antibody against Aβ in clinical development (Ostrowitzki *et al*. 2012). It recognizes both the N- terminal and the central amino acids of the Aβ peptide. It initiates cell-mediated clearance via the recruitment of microglia (Ostrowitzki *et al*. 2012; Cummings *et al*. 2024). Two phase III clinical trials, designated GRADUATE I and GRADUATE II, were conducted to assess the efficacy of Gantenerumab in mitigating cognitive decline in patients with early-stage AD. The results demonstrated that, although Gantenerumab was effective in reducing amyloid plaques, it did not achieve the primary endpoint of slowing clinical decline as measured by the Clinical Dementia Rating-Sum of Boxes (Boess *et al*. 2021; Ostrowitzki *et al*. 2022). An overview of these mAbs is represented in Table 3.

10. Camelid antibodies

Over the past decade, several monoclonal antibodies engineered to bind and eliminate Aβ aggregates have been developed, some of which have been applied to human trials. Despite some promising clinical data, the great majority of therapeutic trials of Aβ have so far failed to improve cognition in MCI patients (Selkoe 2019), primarily because of too late treatment and massive adverse reactions. However, the experience gained from these trials has provided important clues to enable the development of improved treatments.

In the early 1990s, antibodies composed only of the heavy chains and missing the light chains were identified in the serum of the camelid family and they were called "camelid antibodies" (Hamers-Casterman *et al*. 1993). The camelid heavy-chain antibodies (HcAbs) include only two constant domains in contrast with three constant domains present in conventional antibodies (Figure 19) (Hamers-Casterman *et al*. 1993).

Due to the lack of a light chain, the antigen binding site of heavy-chain

antibodies is formed by one single domain: the VHH domain (Hamers-Casterman *et al*. 1993) also defined as nanobodies or single-domain antibodies (sdAbs). Notably, like classical monoclonal antibodies, nanobodies exhibit high target specificity and affinity but their small size (one-tenth of a full-length IgG) makes them highly stable, soluble, able to access hidden epitopes, and functionally expressed within the cell as intrabodies (Muyldermans 2013). Their low immunogenic potential due to their high sequence homology to human and mouse V_H domains and their low molecular weight significantly reduce the intrinsic toxicity characterizing conventional antibodies, making them great tools for basic research and potential candidates for diagnostic and therapeutic purposes (Muyldermans 2013; Ackaert *et al*. 2021). Nowadays, sdAbs have been shown to be useful probes for the study of amyloid aggregation and for the prevention of amyloid- induced cytotoxicity and cell death (Aprile *et al*. 2020).

10.1 DesAb-O antibody

In the recent years, Aprile and coworkers introduced a scanning method based on the use of rationally designed single-domain (VH) antibodies (DesAbs) for sequence-activity relationship studies (Sormanni, Aprile and Vendruscolo 2015; Aprile *et al*. 2017; Sormanni, Aprile and Vendruscolo 2018, Aprile *et al*. 2020). Using this strategy, they identified the DesAb-$A\beta_{29\text{-}36}$ antibody, targeting a structural epitope formed by residues 29-36 of $A\beta_{42}$, present in oligomeric aggregates and buried in the core of the cross-β structure of mature fibrils (Colvin *et al*. 2016; Aprile *et al*. 2020), resulting in low binding of DesAb-$A\beta_{29\text{-}36}$ to these conformers, as well as to the monomeric protein (Aprile *et al*. 2017; Aprile *et al*. 2020). Therefore, they applied a rational design to generate a battery of DesAbs, targeting epitopes in the region of residues 29-36 of $A\beta_{42}$, and performing experimental screening to identify one, later called DesAb-O, that exhibited the best affinity and binding selectivity for the oligomers of $A\beta_{42}$, rather than its monomeric and fibrillar forms (Aprile *et al*. 2020) as represented in Figure 20.

Given the high affinity of DesAb-O for $A\beta_{42}$ oligomers, we investigated the ability of DesAb-O to selectively detect preformed $A\beta_{42}$ oligomers both *in vitro* and in cultured neuronal cells, by using dot-blot, ELISA immunoassay and super-resolution STED microscopy, and to counteract the toxicity induced by the oligomers, monitoring their interaction with neuronal membrane and the resulting mitochondrial impairment. We then applied this approach to CSF samples (CSFs) from AD patients as compared to age- matched control subjects (Bigi *et al*. 2024b). Moreover, in another study, with the aim of improve the outstanding ability of DesAb-O, we designed a dimeric structure of this sdAbs, adding a flexible $(GGGGS)_3$ linker to the C-terminus, allowing the protein a wide range of movement and the connection of two monomeric domains (Napolitano *et al*. in preparation).

11. Aim of the thesis

Current diagnostic criteria for AD include the use of CSF biomarkers such as the decreased CSF $A\beta_{42}/A\beta_{40}$ ratio due to $A\beta_{42}$ levels reduction, and the increased levels of total and phosphorylated tau (t-tau and p-tau, respectively). Despite their widely recognized diagnostic relevance, such biomarkers often produce uncertain results, both in terms of false positives and negatives, especially in the early AD, thus rendering the research and identification of novel biomarkers of fundamental importance for supporting the existing ones to gain sensitivity and specificity. In addition, the NIA-AA recommended a biomarker-grounded biological, rather than syndromal, definition of AD, involving biomarkers able to reflect pathophysiological changes occurring already in the early stages of AD.

All the classical protein-based biomarkers reveal the levels of specific proteins, including $A\beta_{42}$ and tau; however, as a proteinopathy, AD is characterized by a generic failure of the proteostasis network, which does not maintain proteins in a native, non-aggregated functional state. Building on this idea, we have extended our attention to the status of the entire proteome, performing an array of biophysical and cellular analyses on CSF samples from AD patients and healthy subjects, with the aim to identify new and putative biomarkers comparing their ability to discriminate between AD and non-AD cases with those of classical ones.

In this context of altered proteostasis, increasing evidence also suggests that small soluble Aβ oligomers, rather than mature Aβ fibrils, are the main agents responsible for neurotoxicity in AD. Recently, sdAbs have been proposed as promising tools for the early diagnosis and therapy for AD. Thus, the second aim of the study was to investigate the ability of DesAb-O to selectively detect $A\beta_{42}$ oligomers both *in vitro* and in cultured cells and to neutralize their associated neurotoxicity. Furthermore, we have investigated its ability to discriminate the CSFs of AD patients from those derived from age-matched control subjects by using immune-enzymatic assays and STED microscopy.

Finally, with the aim of improving the already incredible binding avidity and specificity of DesAb-O and obtain a more accurate sdAb able to detect oligomers at even lower concentrations, we have engineered the structure of DesAb-O by designing a dimeric sdAb: the Dimeric-DesAb-O. We have performed biophysical experiments to characterise its ability to interfere with the $A\beta_{42}$ aggregation process and studied its specificity and selectivity for $A\beta_{42}$ oligomers. Furthermore, we have studied the ability of Dimeric-DesAb-O to counteract the toxicity induced by $A\beta_{42}$ oligomers and CSFs of AD patients on neuronal cells, demonstrating the neuroprotective ability of this dimeric sdAb at lower concentrations as compared to DesAb-O.

Overall, this thesis aims to identify novel CSF biomarkers for AD and to explore the application of sdAbs as promising tools for the early diagnosis and therapy of AD. Overall, this research seeks to contribute to the development of more effective diagnostic tools and therapeutic interventions for a future AD cure.

12. Introduction: figures and tables

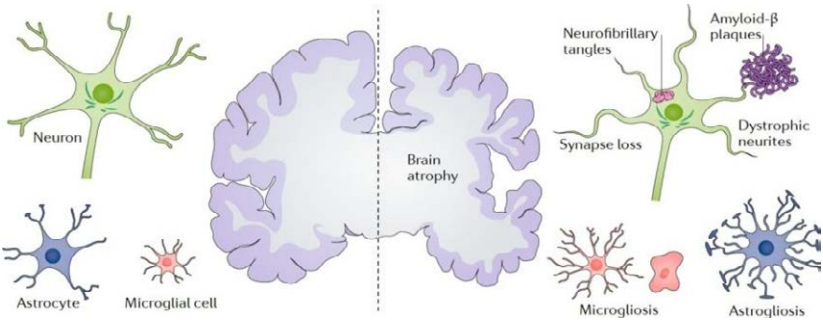

Figure 1 - Pathologic features of AD. Anatomically, AD is characterized by brain atrophy associated with loss of synapses and neurons. Microscopically, deposition of extracellular Aβ plaques and intraneuronal neurofibrillary tangles, in association with dystrophic neurites and loss of synapses, as well as microgliosis and astrogliosis (Adapted from Congdon and Sigurdsson, 2018).

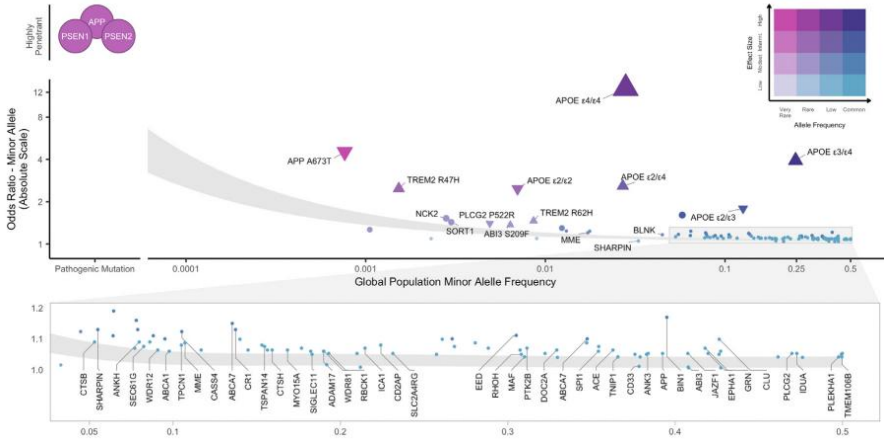

Figure 2 - Visual representation of genetic architecture of AD/dementia. This scheme illustrates the distinction between rare, high-penetrance mutations in genes such as APP, PSEN1 and PSEN2, which are strongly associated mwith early-onset familial AD, and the more prevalent variants identified by genome- wide association studies (GWAS), which confer lower risk for the more common late-onset AD. Furthermore, it shows the difficulties and possibilities inherent in elucidating the intricate genetic underpinnings of AD, as evidenced by the influence of allele frequency and effect size on the statistical capacity to identify AD-associated genetic variants (Adapted from Andrews *et al*. 2023).

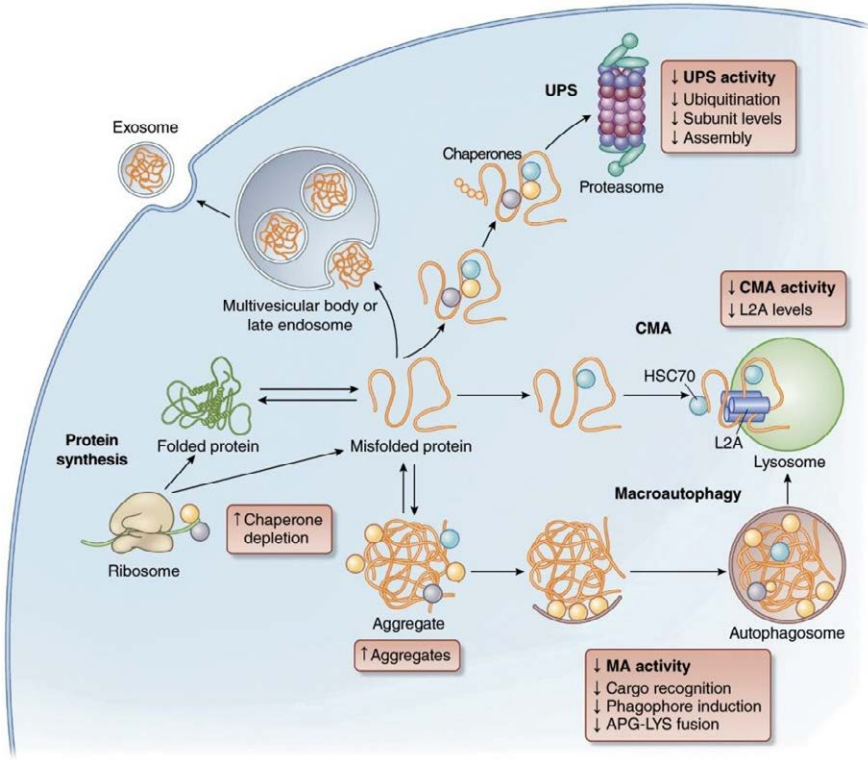

Figure 3 - Altered intracellular proteostasis systems. The intracellular proteostasis is regulated by chaperones, the ubiquitin-proteasome system (UPS) and autophagy. Chaperones, depicted as blue, yellow, and gray circles, facilitate the folding of proteins. In the event of an unsuccessful folding process, chaperones direct the unfolded protein for proteasomal (often subsequent to ubiquitination) or lysosomal degradation. In chaperone-mediated autophagy (CMA), soluble proteins may enter the lysosomal lumen via a membrane transporter. Once misfolded proteins have aggregated into oligomers or insoluble aggregates, they can only be removed from the cytosol by undergoing degradation in lysosomes via macroautophagy (MA) or via exosomes. The brown boxes indicate the alterations that occur with age in the intracellular proteostasis networks. APG-LYS: autophagosome-lysosome; HSC70: heat-shock cognate protein of 70kDa; L2A: lysosome-associated membrane protein type 2A (Adapted from Kaushik and Cuervo 2015)

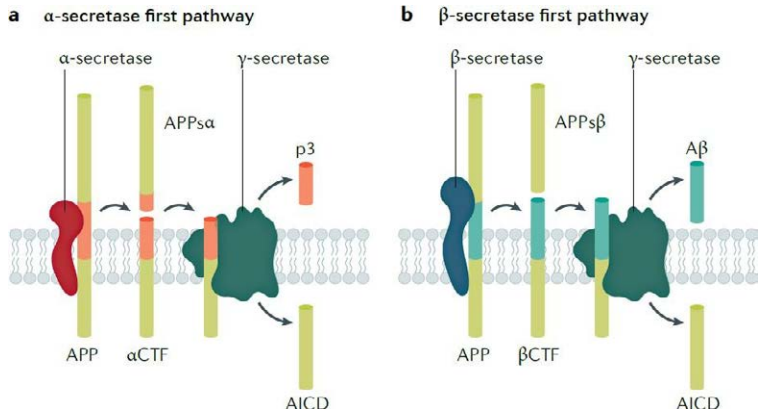

Figure 4- Proteolytic cleavage of APP. A) In the non-β-amyloidogenic pathway, APP is cleaved by α-secretase leading to the formation of sAPPα and α CTF, which in turn is cleaved by γ-secretase to produce the extracellular peptide p3 and the intracellular fragment AICD (Sewell 2007). B) Aβ is formed in the amyloidogenic pathway through cleavage of APP by β-secretase into sAPPβ and β CTF, the latter of which will be cleaved again by γ-secretase, producing Aβ and AICD (Adapted from Knopman *et al*. 2021).

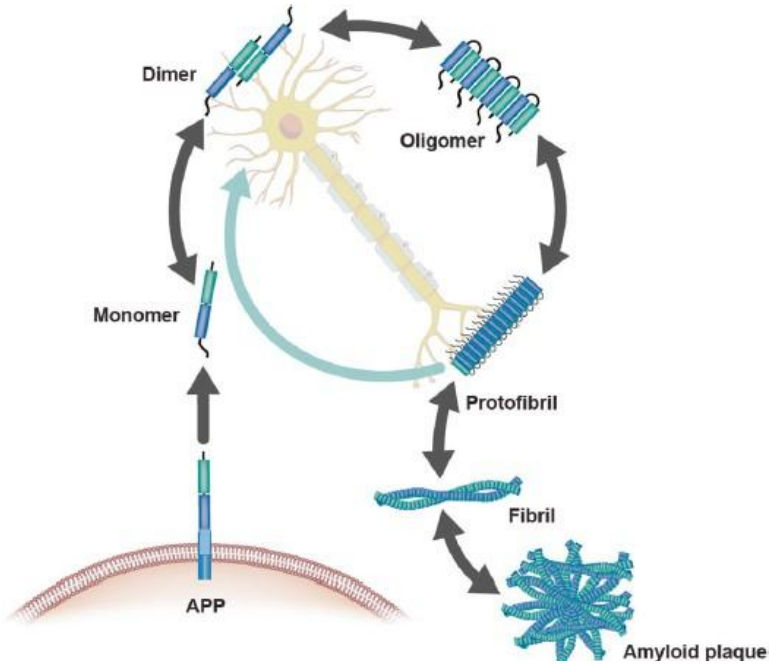

Figure 5 - Species of Aβ aggregation and evidence for reversible states: the Aβ cycle. Aβ aggregation species can exist as monomers, dimers, oligomers, protofibrils, fibrils, and amyloid plaques. These species exist in an equilibrium state in which one form can convert to another bidirectionally (Adapted from Hampel *et al*. 2021b).

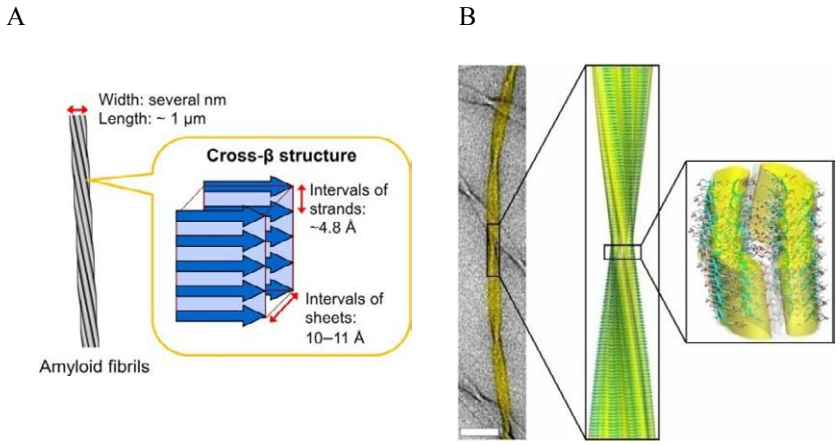

Figure 6 – Aβ fibrils structure representation. A) Schematic representation of the structure of an Aβ fibril. Aβ fibril typically have a needle-like and unbranched morphology, consisting of several protofilaments a few nanometers wide and about a micrometer long, which are bundled together laterally. Each protofilament has a cross-β structure. This means that the β strands are stacked perpendicular to the long axis of the fibril (Adapted from Chatani *et al*. 2021). B) Detailed view of the atomic resolution structure of the triplet fibril (middle). The background image of the fibril (left) was obtained by Transmission Electron Microscopy (TEM). (Scale bar, 50 nm.) The surface of the fibril (Right) is shown at 1.0 σ (white) and 2.2 σ (yellow) above the mean density, respectively, and the constituent β-sheets are shown as ribbons; oxygen, carbon and nitrogen atoms are shown in red, gray and blue, respectively (Adapted from Fitzpatrick *et al*. 2013).

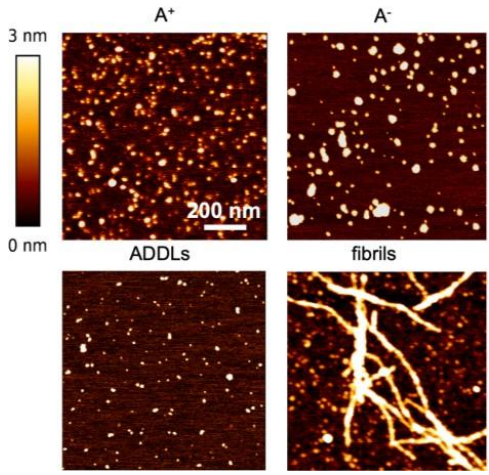

Figure 7 - AFM images of $A\beta_{42}$ oligomers (A+, A-, ADDLs) and $A\beta_{42}$ fibrils. The AFM revealing height values of 4.4 ± 2.4 nm for A+, 4.4 ± 1.5 nm for A-, 3.9 ± 1.2 nm for ADDLs (Adapted from Banchelli *et al*. 2020).

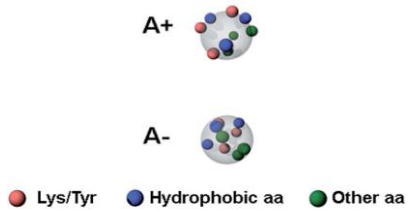

Figure 8 - Schematic picture of the A+ and A- oligomers generated from $A\beta_{42}$. Toxic A+ oligomers are characterized by exposure of hydrophobic clusters (blue), as well as of Tyr and Lys residues (red) (Adapted from Banchelli *et al*. 2020).

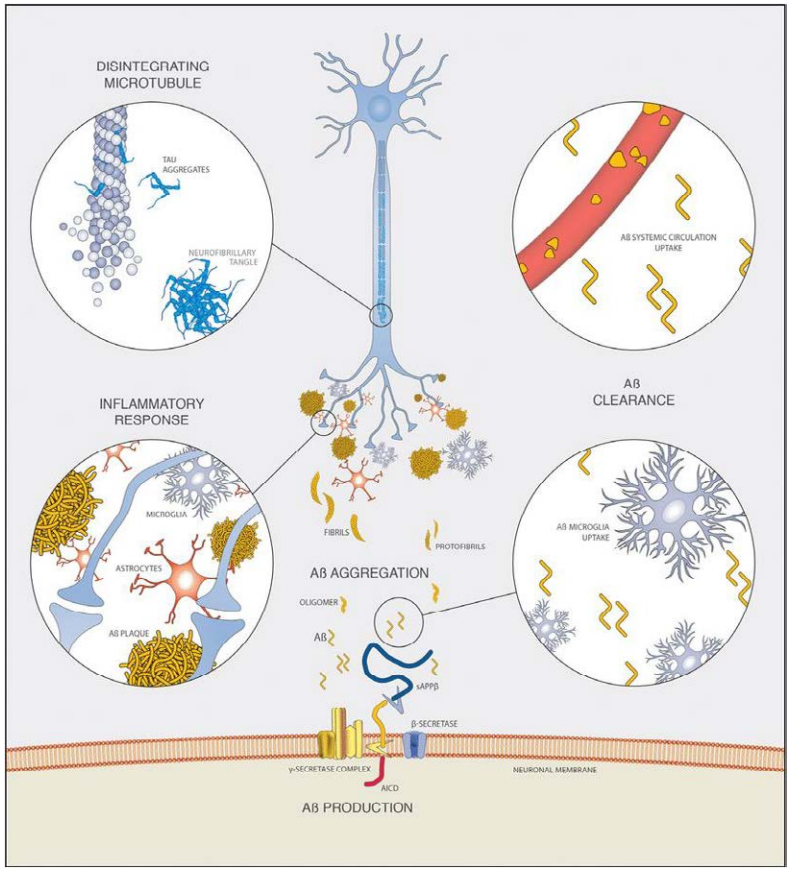

Figure 9 – Amyloid hypothesis. Visual representation of the amyloid cascade hypothesis, illustrating the key events in the development of AD: from the production and aggregation of Aβ peptides to the formation of plaques and tau-hyperphosphorylated neurofibrillary tangles (Adapted from Panza *et al*. 2019).

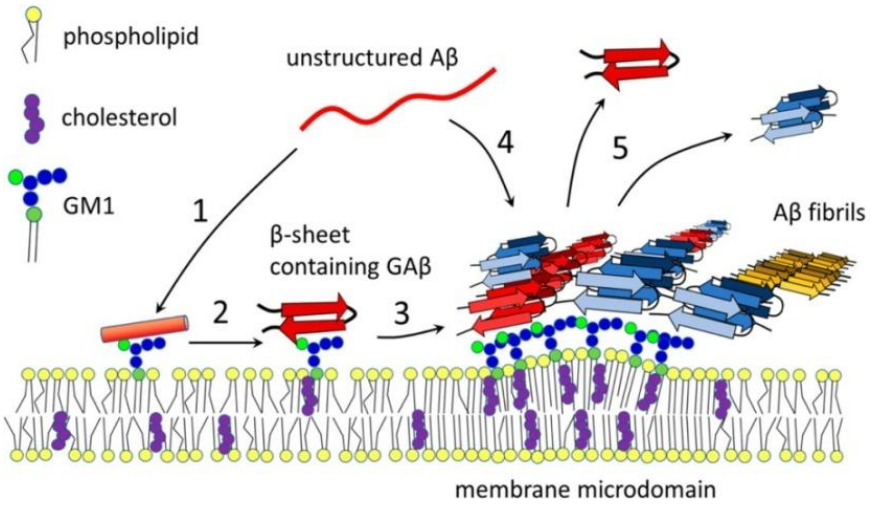

Figure 10 - Interaction Aβ/GM1. (1) α-helical conformation in Aβ is induced by not clustered. (2) Transition from α-helical to β-sheet structure induced by GM1. (3) Localized GM1 clusters in membrane microdomains are involved in increase of concentration and aggregation of Aβ peptide into higher- molecular weight aggregates. Parallel and antiparallel β structures have been found in membrane-associated amyloid fibrils. (4) Aggregation of Aβ serves as a platform for capture and binding of monomers or oligomers circulating in the intercellular space (5) (Adapted from Rudajev and Novotny 2020)

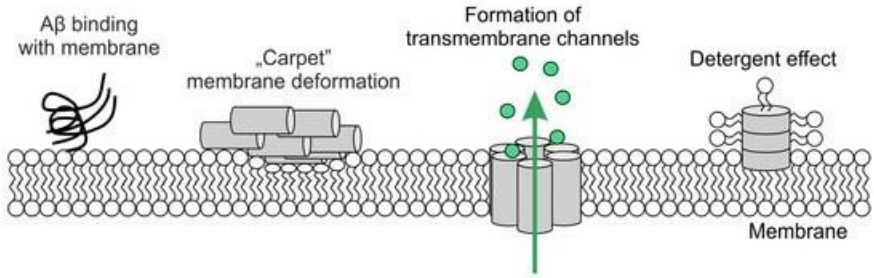

Figure 11 – Schematic representation of the Aβ-induced neurotoxicity through the formation of a transmembrane channel, via "carpet model" and the "detergent-like mechanism". (Adapted from Wiatrak *et al*. 2021).

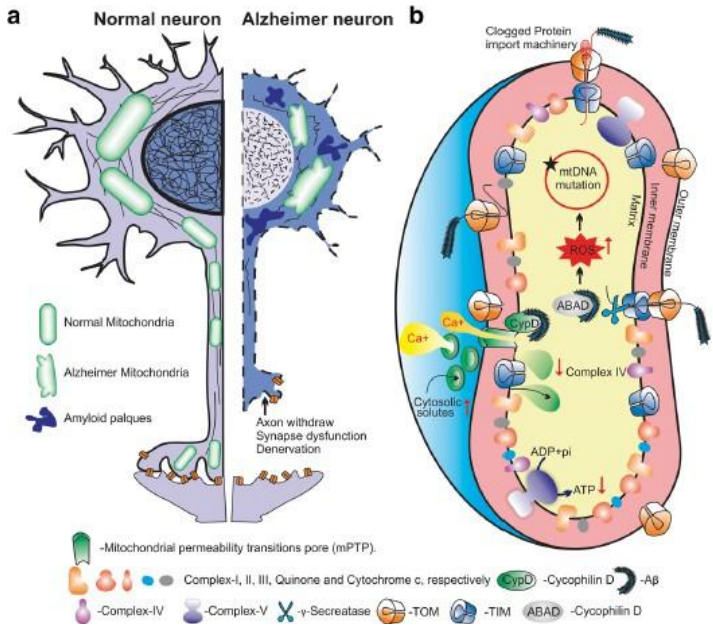

Figure 12 - Mitochondrial dysfunction in AD. A) Altered morphology of mitochondria and synaptic space and reduced level of mitochondrial axonal transport in AD neuron with respect to normal neuron. B) A detailed examination of mitochondria in a disease state reveals the translocation of Aβ into the mitochondrial matrix via the TOM/TIM complex. Following its import, Aβ disrupts mitochondrial function by: 1) impairing the activity of complex IV, 2) altering Ca^{2+} efflux, and 3) inducing mutations in mitochondrial DNA (mtDNA) (Adapted from Cadonic, Sabbir and Albensi 2016).

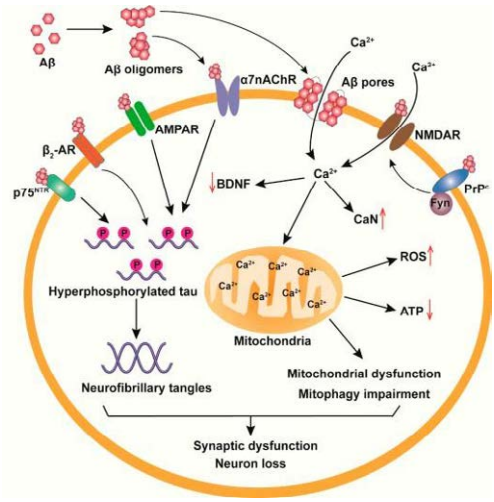

Figure 13 - Schematic diagram of neurotoxic mechanisms induced by Aβ oligomers. Aβ oligomers are found primarily at the extracellular level and can bind to multiple receptors

on the surface of the neuronal membrane, interfering with normal receptor signalling pathways. They are also able to interact directly with the membrane to form pores, leading to changes in membrane integrity and permeability. These two effects of Aβ oligomers on the cell membrane can further induce dysregulation of Ca^{2+} homeostasis, mitochondrial damage, generation of ROS, reduced ATP levels, and abnormal phosphorylation of tau, resulting in synaptic dysfunction, neuronal loss, and impaired LTP (Adapted from Huang and Liu 2020).

		Cognitive stage		
		Cognitively unimpaired	**Mild cognitive Impairment (MCI)**	**Dementia**
Biomarker profile	A-T-(N)-	Normal AD biomarkers. Cognitively unimpaired	Normal AD biomarkers with MCI	Normal AD biomarkers with dementia
	A+T-(N)-	Preclinical Alzheimer's pathologic change	Alzheimer's pathologic change with MCI	Alzheimer's pathologic change with dementia
	A+T+(N)- A+T+(N)+	Preclinical Alzheimer's disease	Preclinical Alzheimer's disease with MCI (prodromal AD)	Alzheimer's disease with dementia
	A+T-(N)+	Alzheimer's and concomitant suspected non-Alzheimer's pathologic change, cognitively unimpaired	Alzheimer's and concomitant suspected non-Alzheimer's pathologic change with MCI	Alzheimer's and concomitant suspected non-Alzheimer's pathologic change with dementia
	A-T+(N)- A-T-(N)+ A-T+(N)+	Non-Alzheimer's pathologic change, cognitively unimpaired	Non-Alzheimer's pathologic change with MCI	Non-Alzheimer's pathologic change with dementia

Table 1 – Overview of AD biomarkers continuum. Abbreviations; A, Amyloid-β; N, neurodegeneration; T, tau. Adapted from C.R.Jr., Jack, *et al*. NIA-AA research framework: toward a biological definition of Alzheimer's disease. Alzheimers Dement, 14 (4) (2018) 535-562. (Adapted from Simrén *et al.* 2023).

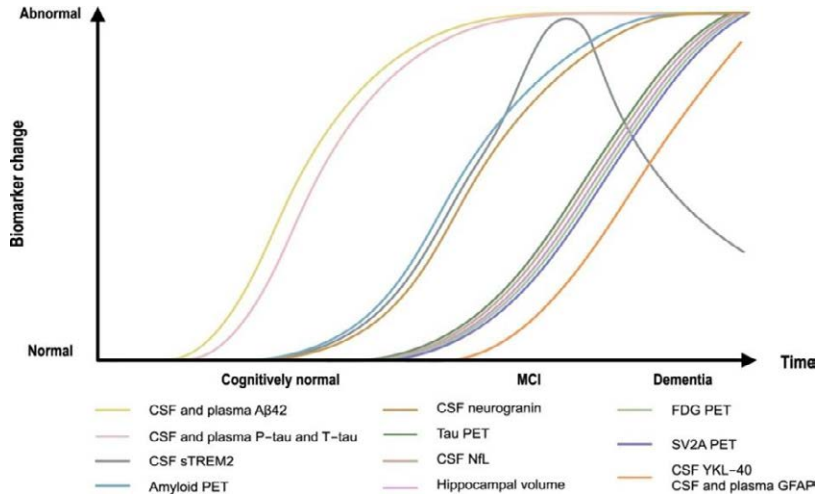

Figure 14 - A model of the temporal pattern of biomarker abnormalities for AD-related pathophysiological processes. The earliest detectable changes occur in the CSF and plasma, characterized by an altered $A\beta_{42}/A\beta_{40}$ ratio. Subsequently, amyloid plaques accumulate, becoming detectable through amyloid PET imaging. Microglial respond and secrete a soluble trigger receptor expressed on myeloid cells 2 (sTREM2), serving as a marker. sTREM2 demonstrates a characteristic peak during MCI followed by a decline upon progression to AD dementia. When tau PET becomes positive, a number of neurodegeneration and synaptic dysfunction biomarkers of function change more or less in parallel (Adapted from Zetterberg and Bendlin 2021).

SUMMARY OF ALZHEIMER DISEASE BLOOD BIOMARKERS			
	Biologic significance	**Clinical relevance**	**Limitations**
Aβ42/Aβ40[a,b]	Produced by amyloid precursor protein metabolism in brain Cleared by glymphatic system and other mechanisms Aβ42 sequestered within amyloid plaques	Reduced Aβ42 reflects brain amyloidosis Aβ42/40 ratio corrects for interindividual variation in amyloid metabolism Reduced Aβ42/40 ratio highly concordant with amyloid PET Blood and CSF Aβ42/40 highly concordant	Smaller reduction of Aβ42 in blood than CSF
Total-tau[b]	Secreted from neurons, in response to Aβ exposure or released by damaged neurons	Elevation in AD; reflects tauopathy and tangle formation Indirect marker of amyloidosis	Correlates poorly with CSF tau Does not reliably reflect tau pathology in nonAD tauopathies Elevated in stroke and CJD
Phosphorylated tau[a,b]	85 potential phosphorylation sites; several promising candidates More phosphorylation in AD	Presymptomatic elevation in AD reflects AD tauopathy and tangles Indirect marker of amyloidosis Correlates with amyloid and tau PET Blood and CSF p-tau highly concordant	Not widely available or internationally standardized
Neurofilament light[b]	Reflects rate of neurodegeneration	Reflects rate of neurodegeneration/disease progression Correlated with amyloid PET, tau PET, and MRI brain atrophy rates	Nonspecific

Abbreviations: AD, Alzheimer disease; CJD, Creutzfeldt-Jakob disease; CSF, cerebrospinal fluid; PET, positron emission tomography.
[a]Measured by immunoprecipitation mass spectrometry. [b]Measured by ultrasensitive enzyme-linked immunosorbent assay (ELISA).

Table 2- An overview of plasma biomarkers in AD. (Adapted from Zetterberg *et al*. 2020).

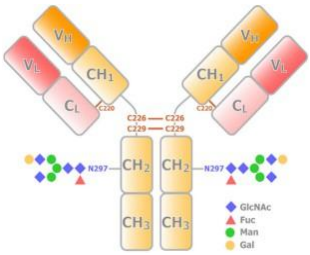

Figure 15 - Schematic representation of the structure of an IgG. IgG consist of two heavy and two light chains. Each heavy chain has VH and CH1 domains, forming the Fab portion with a light chain, and CH2-CH3 domains which are the main component of the crystallizable fragment (Fc) portion. A flexible hinge region with disulfide bridges connects Fab and Fc. The CH2 domain has an N-glycosylation site crucial for effector functions (Adapted from Tokunaga and Takeuchi 2020).

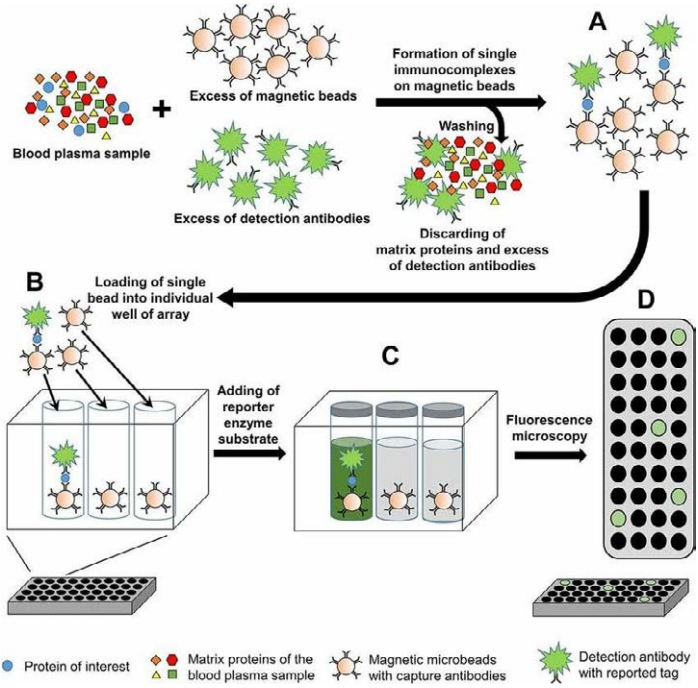

Figure 16 - The principle of SIMOA. A) A biological sample is introduced to an excess of antibody- conjugated magnetic microbeads (2.7 µm diameter), where capture and detection antibodies are immobilized on the bead surface. B) The bead-sample mixture is loaded into an array containing 50 femtoliter wells, each with dimensions of 4.5 µm diameter and 3.25 µm depth. C) Following bead loading, a reporter enzyme substrate is added, and the wells are sealed with a silicon gasket to prevent leakage and cross-contamination. D) The array is then analyzed for fluorescence signal, which corresponds to the presence and quantity of the target analyte (Adapted from Kulichikhin *et al*. 2021).

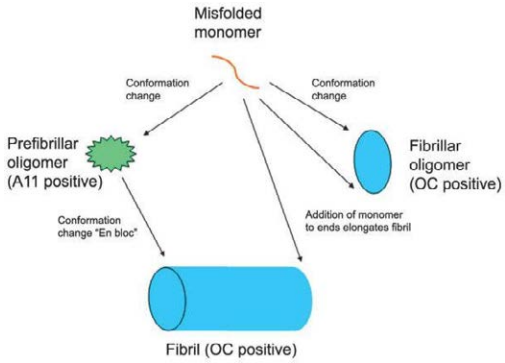

Figure 17 - Different types of amyloid oligomers and their relationships to amyloid fibrils. Amyloid aggregation involves two distinct pathways: 1) Monomers form transient prefibrillar oligomers (A11- positive, on the left) that mature into fibrils. 2) Monomers directly form fibrillar oligomers (OC-positive, on the right) serving as nuclei for fibril growth. This conformational diversity impacts our understanding of amyloid-related disease and therapeutic development (Adapted from Kayed *et al*. 2007).

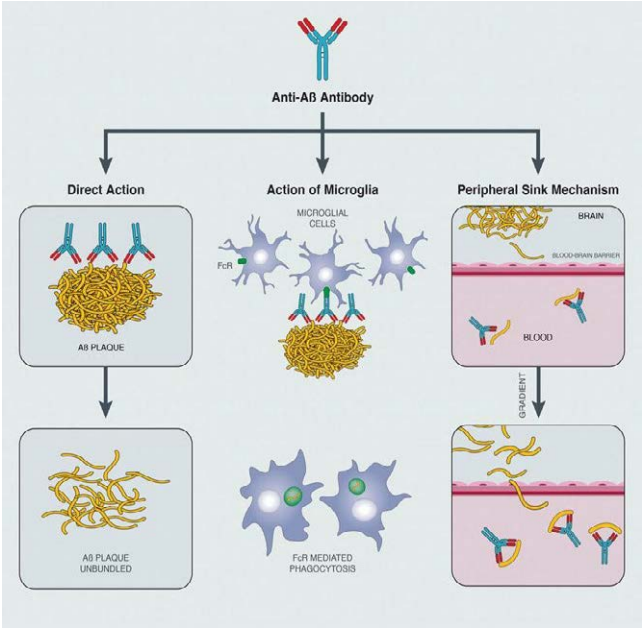

Figure 18 - Aβ removal via Aβ-specific antibodies. For the mechanism of action of anti-Aβ antibodies, there are three main hypotheses. The first is that antibody binding destabilizes different aggregate species, acting directly against Aβ plaques, fibrils, protofibrils or oligomers. The second is microglial action, leading to Fc receptor-mediated phagocytosis of Aβ. Finally, there is the hypothesis of a peripheral sink mechanism, in which the antibody

binds to Aβ present in plasma and removes it, resulting in a net efflux of Aβ from the brain to the plasma. (Adapted from Panza *et al.* 2019).

Antibody name	Antibody type	Target	Mechanism of action	Approval status	Indications	Side effects	Notes
Aducanumab (BIIB037; Aduhelm™) (Arndt et al., 2018)	Human immunoglobulin G1	Aβ aggregates	Reduction of Amyloid plaques	FDA-approved (with limitations)	Early AD (Sevigny et al., 2016)	Brain edema, brain hemorrhage (von Rosenstiel et al., 2018; Herring et al., 2021)	Discontinued by Biogen in 2024
Lecanemab (BAN2401; Leqembi) (Engund et al., 2007)	*Mouse* humanized IgG1	Aβ aggregates	Reduction of Amyloid plaques	FDA-approved (accelerated approval)	Early AD (FDA Office of the Commissioner, 2023)	Brain edema, brain hemorrhage (van Dick et al., 2023)	Ongoing clinical trials to confirm clinical efficacy
Donanemab (LY3002813; N3pG) (Tolar et al., 2020)	*Mouse* humanized IgG1	Aβ aggregates	Reduction of Amyloid plaques	FDA-approved (accelerated approval) (Eli Lilly and Company, 2023; Sims et al., 2023)	Early AD	Brain edema (ARIA), brain hemorrhage (Eli Lilly and Company, 2023; Sims et al., 2023)	Ongoing clinical trials to confirm clinical efficacy
Remternetug (LY3372993) (Alzforum, 2023)	N3pG-AB monoclonal antibody	Aβ aggregates	Reduction of Amyloid plaques	In clinical trials (Phase III)	Early AD	Under evaluation	-
Gantenerumab (RO4909832; R1450) (Ostrowitzk et al., 2012)	Fully human IgG1	Aβ aggregates	Reduction of Amyloid plaques	Failed in Phase III clinical trials	-	-	-

Table 3 – Overview of five mAbs for AD treatment.

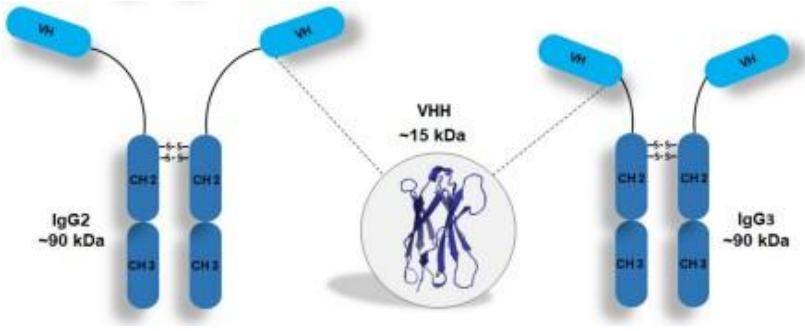

Figure 19 - Camelid antibody. The figure shows the structure of camelid antibodies: in blue are highlighted the two constant domains of the heavy chain and in light blue is highlighted the variable domain VHH (immunoglobulin G2 [IgG2] and immunoglobulin G3 [IgG3]). The three-dimensional structure of the VHH was adapted from Lesne *et al*. 2019 (Adapted from Brilhante-da-Silva *et al*. 2021).

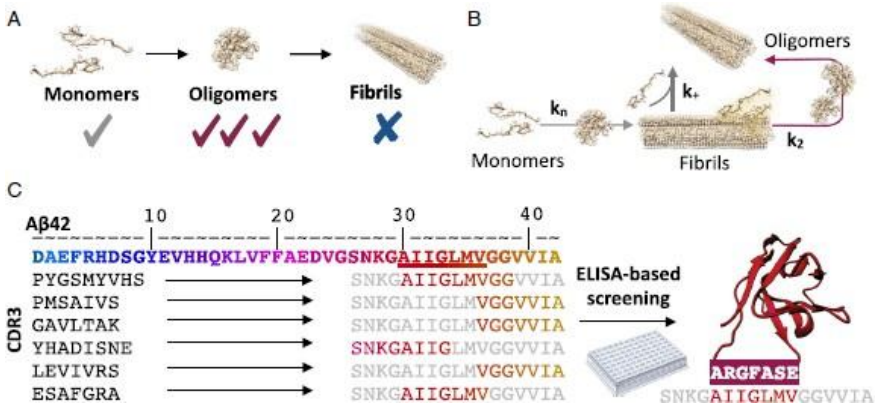

Figure 20 - Rational design of a conformation-specific antibody for $A\beta_{42}$ oligomers. A) Schematic illustration of the selections strategy to generate an antibody with selective affinity for $A\beta_{42}$ oligomers, discriminating against monomers and fibrils. B) The figure depicts the aggregation pathway of $A\beta_{42}$, including primary (k_n), secondary (k_2), and elongation (k_+) nucleation rate constants (Cohen *et al*. 2013). C) The $A\beta_{42}$ amino acid sequence is presented with a color gradient reflecting the efficacy of each residue as an oligomer binding target (red indicates high efficacy). The sequence of the complementary peptide of DesAb-O, the designed antibody exhibiting the highest affinity for Aβ oligomers, is shown in red (Adapted from Aprile *et al.* 2020).

Chapter 1
Materials and Methods

The Materials and Methods section is divided in three different sections, corresponding to the following results section.s To avoid redundancy, previously described methods will be omitted from subsequent sections.

1. First section

1.1 Patients

Between October 2020 and May 2023, we collected 52 CSF samples from patients referred to the Centre for Alzheimer's Disease and Adult Cognitive Disorders of Careggi Hospital in Florence. Patients met the following inclusion criteria: 29 patients who received a diagnosis of AD dementia according to the NIA-AA criteria (McKhann *et al*. 2011) or a diagnosis of MCI according to NIA-AA criteria (Albert *et al*. 2011).23 patients with diagnosis of other diseases affecting the CNS but without having a clear involvement of protein misfolding or aggregation (non-AD cases) have participated to this study: 19 with idiopathic normal pressure hydrocephalus (iNPH) according to international guidelines (Relkin *et al*. 2005), 1 patient with multiple sclerosis (MS), 2 with frontotemporal dementia (FTD), 1 with DLB and 1 with vascular dementia (VD), all diagnosed according to international guidelines (Thompson *et al.* 2018; Neary *et al*. 1998; McKeith *et al*. 2017; Sachdev *et al*. 2014).

1.2 Neuropsychological examination

Neuropsychological examination included global measurements of Mini-Mental State Examination (MMSE), Digit and Visuo-spatial Span forward, Rey

Liliana Napolitano, liliana98.napolitano@gmail.com, 0009-0004-3087-286X

Referee List (DOI 10.36253/fup_referee_list)
FUP Best Practice in Scholarly Publishing (DOI 10.36253/fup_best_practice)

Book References DOI 10.36253/979-12-215-0993-9.references

Auditory Verbal Learning Test, Trail Making Test A, attentional matrices, language and phonemic fluency task, constructional praxis, such as Rey-Osterrieth complex figure copy and Clock test, and executive function tests, such as Trail Making test B, Stroop Test, and Frontal Assessment Battery (Giacomucci *et al*. 2022).

1.3 CSF collection and biomarkers analysis

The CSF samples were collected by lumbar puncture, then immediately centrifuged at 200 g for 1 min, 20 °C, then at 4000 x g for 10 min at 4 °C, and the supernatant was further used for the analyses of the novel biomarkers. The pellet contained generally tiny amounts of proteins. An aliquot of the samples was stored at − 80 °C until analysis for classical biomarkers. $A\beta_{42}$ levels, $A\beta_{42}$/ $A\beta_{40}$ ratio and T-tau and P-tau levels were measured using a CLEIA analyzer LUMIPULSE G600: LumipulseG $A\beta_{40}$, LumipulseG $A\beta_{42}$, LumipulseG t-tau, and LumipulseG p-tau 181, with all reagent kits obtained from Fujirebio.

1.4 Apolipoprotein E ε4 genotyping

A standard automated method (QIA cube, QIAGEN) was used to isolate DNA from peripheral blood samples. APOE genotypes were investigated by high-resolution melting analysis (HRMA) (Sorbi *et al*. 1994). Two sets of PCR primers were designed to amplify the regions encompassing rs7412 [NC_000019.9: g[M13] [GG14] 0.45412079C > T] and rs429358 (NC_000019.9:g.45411941 T > C). The samples with known APOE genotypes, which had been validated by DNA sequencing, were used as standard references.

1.5 Bradford assay

Protein concentration of the supernatant was determined by the Bradford assay (Bradford 1976). In brief, 50 µl solutions containing increasing concentrations of bovine serum albumin (BSA, Sigma-Aldrich), ranging from 0 to 2 mg/ml, were used to develop a standard curve; 1:5 diluted Protein Assay Dye Reagent (Bio-Rad) was added to these solutions and the measured absorbance at 595 nm was then plotted versus the corresponding BSA concentration. The resulting equation was used to calculate CSF protein concentration after measuring the absorbance at 595 nm of 3 µl of CSF supernatant diluted in 47 µl of H_2O in the presence of the Protein Assay Dye Reagent.

1.6 Far-UV CD

CSF samples were analysed at 25 °C using a Jasco J-810 Spectropolarimeter equipped with a thermostated cell holder attached to a Thermo Haake C25P

water bath and using a 0.1 cm path-length cell. Far-ultraviolet circular dichroism (far-UV CD) spectra and the high tension (HT) spectra were collected over the 200-260 nm wavelength range. It was not possible to record the spectra at wavelength values lower than 200 nm, because of the high absorbance values (HT > 700 V) recorded at these wavelength values. All spectra were blank subtracted and plotted as non-normalised ellipticity (θ) values (mdeg units) versus wavelength (nm). Spectra were not normalised to mean residue ellipticity ($[\theta]_{res}$) because CSF samples are mixtures of proteins, each with a well-defined molecular weight.

1.7 DLS measurement

The size distribution profiles of CSF samples were recorded at 25 °C using a Zetasizer Nano S dynamic light scattering (DLS) device (Malvern Panalytical) thermostated with a Peltier temperature controller and using a 10 mm reduced-volume plastic cell (50 µL volume). The refractive index and viscosity were 1.45 and 0.82 cp, respectively. These values were determined from the Malvern analysis software after entering the typical CSF composition previously reported (Robertson 2010). The measurements were acquired with cell position 3.00 and attenuator index 10.

1.8 Intrinsic Tryptophan Fluorescence Assay

Intrinsic tryptophan fluorescence spectra of CSF samples were acquired at 25 °C from 300 to 500 nm after excitation at 280 nm (slits of 5 and 5, respectively), using a 0.3 × 0.3 cm black wall quartz cell (50 µl volume) on an Agilent Cary Eclipse spectrofluorometer (Agilent Technologies) equipped with a thermostated cell holder attached to an Agilent PCB 1500 water Peltier system.

1.9 Neuroblastoma cell culture

Authenticated human SH-SY5Y neuroblastoma cells were purchased from A.T.C.C. and cultured in Dulbecco's modified Eagle's medium (DMEM), F-12 Ham with 25 mM 4-(2- Hydroxyethyl) piperazine-1-ethanesulfonic acid (HEPES) and $NaHCO_3$ (1:1) supplemented with 10% fetal bovine serum (FBS), 1 mM glutamine and 1% antibiotics, as reported previously (Capitini *et al*. 2014; Bigi *et al*. 2020). Cells were maintained in a 5% CO_2 humidified atmosphere at 37 °C and grown until 80% confluence for a maximum of 20 passages.

1.10 Measurement of intracellular Ca^{2+}

SH-SY5Y cells were plated on 24-well plates containing glass coverslips at a density of 40.000 cells per well. After 24 h, they were washed with PBS and then treated for 5 h with 75 µl of CSF samples mixed 1:1 with 75 µl of cell culture medium (150 µl final volume), or for 2 h with 1 µM ionomycin in a culture

medium (75 µl) mixed 1:1 with PBS (75 µl), or with culture medium (75 µl) mixed 1:1 with PBS (75 µl) without additives (referred to as "untreated"). Cells were then washed with PBS and loaded with 4.5 µM Fluo-4 AM (Thermo Fisher Scientific) for 10 min. Following incubation, the cytosolic Ca^{2+} levels were detected after excitation at 488 nm by a TCS SP8 scanning confocal microscopy system (Leica Microsystems) equipped with an argon laser source. A series of 1-µM-thick optical sections (1024 × 1024 pixels) was taken through the cell depth for each sample using a Leica Plan Apo 63× oil immersion objective, and all sections were projected as a single composite image by superimposition. Pinhole diameters, detector gain and laser powers were optimized and settings were maintained constant. Images were analyzed using the ImageJ (NIH) software (Rasband 1997–2018). Fluorescence intensities were expressed as the percentage of that measured in untreated cells.

1.11 MTT reduction assay

SH-SY5Y cells were seeded on 96-well plates at a density of 10.000 cells per well and the MTT reduction was evaluated by the MTT assay, as reported previously (Capitini *et al*. 2014; Bigi *et al*. 2023). Briefly, cells were treated for 24 h with solutions containing CSF samples (50 µl) diluted 1:1 in complete cell culture medium (50 µl) or with culture medium (50 µl) mixed 1:1 with PBS (50 µl) without additives (referred to as "untreated"). Then, they were washed with PBS and the MTT solution was added to the culture medium for 4 h. After this time, a cell lysis buffer (20% sodium dodecyl sulfate and 50% N,N-dimethylformamide, pH 4.7) was added to each well to solubilize formazan crystalline precipitates; 1 h later,the absorbance values of blue formazan were measured at 595 nm by using an enzyme-linked immunosorbent assay plate reader (Bio-Rad). MTT reduction values were expressed as the percentage of those measured in untreated cells.

1.12 Receiver operating characteristic curve and area under the curve analysis

The values of two given parameters X and Y were plotted in a scatter plot for both non-AD and AD CSF samples. For each of the two parameters the Youden's index J was determined as:

$$J = \text{sensitivity} + \text{specificity} - 1 = q(t) + 1 - p(t) - 1 = q(t) + p(t) \qquad (1)$$

where t is a given mobile threshold, q(t) is the "sensitivity" and corresponds to the probability of a true positive, 1- p(t) is the "specificity" and correspond to the probability of a true negative. Equation 1 corresponds to:

$$J = [n_{\text{true positives}} / (n_{\text{true positives}} + n_{\text{false negatives}})] + [n_{\text{true negatives}} / (n_{\text{true negatives}} + n_{\text{false positives}})] - 1 \qquad (2)$$

where $n_{true\ positives}$ is the number of true positives and so on. The optimal threshold t* of a given parameter in a test is provided by moving t so that J is maximum:

$$J = \max_{t} [q(t) + p(t)] \quad (3)$$

The Receiver operating characteristic (ROC) curve was edited by plotting J for a moving t value in a graph of *q(t)* (sensitivity) versus *p(t)* (1-specificity), so that the diagnostic value of the analysed parameters could be evaluated, and the AUC, representing their ability to discriminate between non-AD and AD CSF samples and resulting from the area under the broken line (or polygonal chain) traced by the J values, was calculated using the GraphPad Prism 5.0 software.

1.13 Statistical analysis

Values of each parameter in non-AD and AD groups were expressed as means ± standard deviation (S.D.). An unpaired one-tailed Student t test was performed to compare non-AD versus AD values for each parameter (GraphPad Prism 5.0 software). P values lower than 0.05, 0.01 and 0.001 were considered to be statistically significant (*), highly statistically significant (**) and very highly statistically significant (***), respectively. Populations of non-AD and AD CSF samples were categorised in two groups each, on the grounds of whether their individual values for a given parameter were below or above the threshold value (t*) or occupied a given quadrant in scatter plots. This produced a total of four groups for each analysis, two for AD and two for non-AD CSF samples. The significance of the separation between non-AD and AD CSF samples was evaluated using the Fisher's exact test and the Chi-square test (GraphPad Prism 5.0 software). P values lower than 0.05, 0.01 and 0.001 were considered as above.

2. Second section

2.1 Preparation of $A\beta_{42}$ aggregates

$A\beta_{42}$ conformers were prepared as previously reported (Lambert *et al*. 1998; Dahlgren *et al*. 2002; Ladiwala *et al*. 2012). Briefly, the lyophilized peptide (Bachem) was dissolved in 100% hexafluoro-2-isopropanol (HFIP) to 1 mM and the solvent was then evaporated under nitrogen. To obtain $A\beta_{42}$ oligomers, the peptide was resuspended in 50 mM NaOH at 1 mg/ml and diluted in PBS to a final concentration of 25 μM. Then, the sample was centrifuged at 22,000 g for 30 min, the pellet discarded and the supernatant incubated at 25 °C without agitation for 1 day to obtain A+ oligomers or for 4 days to obtain A- oligomers (Ladiwala *et al*. 2012). F1 were obtained, with the same procedure, at a final concentration of 50 μM after 1 day of incubation. ADDLs were obtained by

dissolving an aliquot of the peptide in anhydrous dimethyl sulfoxide (DMSO) to 5 mM and then diluting in ice-cold F-12 medium to a final concentration of 100 μM. This solution was incubated at 4 °C for 1 day and then centrifuged at 14,000 × g for 10 min. Finally, F2 were prepared by dissolving the peptide in DMSO to 5 mM and then diluting it in 10 mM HCl to a final concentration of 100 μM. The sample was incubated at 37 °C without agitation for 1 day (Dahlgren *et al*. 2002).

2.2 CSF samples

CSF samples from human aged controls (n = 4) or AD (n = 9) samples were obtained from BioIVT (United Kingdom). Each CSF sample was received in 0.5-1 ml aliquot and stored at -80 °C. Samples were centrifuged at 4000 x g for 10 min, obtaining a pale pellet that was separated from the supernatant. The supernatant was then analyzed. Protein concentration in the supernatants of the CSF samples was determined by the Bradford colorimetric method (Bradford 1976).

2.3 DesAb-O and $DesAb_{18–24}$ purification

DesAb-O and $DesAb_{18–24}$ were purified a previously described (Aprile et al, 2017). Briefly, DesAb-O and $DesAb_{18–24}$ were expressed in Eschirichia Coli (*E.Coli*) OrigamiTM (DE3) pLysS cells (Merck Millipore), and grown for at least 15 hours at 30°C in Overnight Express Instant TB Medium (Merck Millipore) supplemented with 100 μg/ml ampicillin. Cells were collected by centrifugation, resuspended in PBS (8 mM Na_2HPO_4, 15 mM KH_2PO_4, 137 mM NaCL and 3 mM KCl, pH 7.3) with an EDTA-Free Complete Protease Inhibitor Cocktail tablet (Roche). Cells were lysed by sonication and cellular debris was removed by centrifugation. The supernatant was applied to a HisTrap HP 5 ml column (Cytiva) that has been pre-equilibrated with PBS supplemented with 15 mM imidazole. The column was then washed with several column volumes of PBS supplemented with 15 mM imidazole after which the antibody was eluted in PBS with 300 mM imidazole. The sample was then dialysed against PBS overnight at 4°C to remove imidazole, after which it was applied to a HiLoad Superdex 75 16/600 pg (Cytiva) column for size exclusion chromatography. Protein concentration was determined by measuring the absorbance at 280nm and using the molecular coefficient of DesAb-O or $DesAb_{18–24}$.

2.4 Dot-blot analysis

Dot-blot analysis was performed by spotting 2.0 μl (corresponding to 0.1 μg) of each $A\beta_{42}$ conformer onto a nitrocellulose membrane. After 30 min blocking (1.0% bovine serum albumin, BSA, in TBS/TWEEN 0.1%), $A\beta_{42}$ species were probed with 2 μM DesAb-O or with 1:15.000 human monoclonal anti-ADDLs (19.3) Ab (Creative Biolabs), or with 1:1000 rabbit polyclonal anti-oligomer

(A11) Ab (Thermo Fisher Scientific), or with 1:1000 rabbit polyclonal anti-amyloid fibrils (OC) Ab (Sigma-Aldrich, SA), or 1:1000 with mouse monoclonal anti-Aβ (6E10) Ab (Biolegend Way) and then with 1:2000 goat anti-6X His tag (Abcam), or goat anti-human (Sigma Aldrich), or goat anti-rabbit (Abcam) or rabbit anti-mouse (Abcam) the appropriate horseradish peroxidase- conjugated secondary Abs. In another set of experiments, decreasing quantities (0.1, 0.05, 0.0025, 0.001 and 0.005 μg) of $A\beta_{42}$ aggregates were spotted onto the nitrocellulose membrane, and then probed with DesAb-O and 19.3 Abs, as described above. The immunolabeled dots were detected using a Super Signal West Dura (Pierce) ImageQuant™ TL software (GE Healthcare UK Limited version 8.2).

In a set of experiments, sandwich dot-blot was performed. Briefly, 2 μl of 6E10 and DesAb-O Abs (1:500 diluted and 20 μM, respectively) were spotted onto nitrocellulose membranes. After 20 min, the blots were blocked in TBS-Tween-20 0.2% and 2.5% BSA IgG free for 40 min. The membranes were incubated with different $A\beta_{42}$ species at 1.9 μM (monomeric $A\beta_{42}$, A+ oligomers, F1 fibrils (Ladiwala *et al*. 2012) and the CSF of AD patients and control subjects at 0.1 mg/ml. Then, the membranes were probed with 1:1000 6E10 Ab overnight at 4 °C under constant shaking. The following day, the membranes were washed three times in TBS-Tween-20 0.2% and incubated with 1:3000 rabbit anti-mouse (Abcam) HRP-conjugated secondary Abs for 1 h. After three additional washes, the immunolabeled dots were detected as reported above.

2.5 ELISA assay

For indirect ELISA assay, increasing concentrations (0, 1, 5, and 10 μM, monomer equivalents) of each $A\beta_{42}$ conformer, prepared as reported above, were immobilised on a 96-well Maxisorp ELISA plate (Nunc) without shaking for 1 h at room temperature (RT). The plate was then washed three times with 20 mM Tris, pH 7.4, and 100 mM NaCl and incubated in 20 mM Tris, pH 7.4, 100 mM NaCl, and 5% BSA under constant shaking overnight at 4 °C. The day after the plate was washed six times with 20 mM Tris, pH 7.4, and 100 mM NaCl and then incubated with 40 μL solutions of 2.0 μM DesAb-O, or with 1:20.000 human monoclonal anti-oligomer (19.3) Ab (Creative Biolabs), or with 1:8000 mouse monoclonal anti-Aβ (6E10) Ab (Biolegend Way), under constant shaking for 1 h at RT. The plate was then washed six times with 20 mM Tris, pH 7.4, and 100 mM NaCl and incubated with solutions of the appropriate horseradish peroxidase-conjugated secondary Abs diluted 1:2000 goat anti-6X His tag (Abcam) for DesAb-O, 1:5000 goat anti-human (Sigma Aldrich) for 19.3 and 1:4000 rabbit anti-mouse (Abcam) for 6E10 HRP-conjugated secondary Abs, in 20 mM Tris, pH 7.4, 100 mM NaCl, and 5% BSA under shaking for 1 h at RT. Finally, the plate was washed three times with 20 mM Tris, pH 7.4, and 100 mM NaCl, then twice with 20 mM Tris, pH 7.4, 100 mM NaCl, and 0.02% Tween-20, and again three times with 20 mM Tris, pH 7.4, and 100 mM NaCl. Finally,

the amount of bound Abs was quantified by using 1-Step Ultra TMB-ELISA Substrate Solution (Thermo Fisher Scientific), according to the manufacturer's instructions, and the reaction was stopped by adding 40 µl of H_2SO_4. Then, the absorbance was measured at 450 nm by means of a CLARIOstar plate reader (BMG Labtech).

For sandwich ELISA assay, 1 µM DesAb-O or 0.5 µM $DesAb_{18–24}$ Abs were immobilised on a 96-well Maxisorp ELISA plate (Nunc) without shaking for 1 h at RT. After three washes in PBS, the plate was blocked with 5% BSA IgG free overnight at 4 °C under constant shaking. The day after, the plate was washed six times in PBS and different $A\beta_{42}$ species (M, A+ oligomers, F1 at decreasing concentrations (4500, 2250, 450, 45, 4.5 and 2.25 pg/ml for DesAb-O and 4500·103 pg/ml, 4500 pg/ml and 4.5 pg/ml for $DesAb_{18–24}$) and the CSF of AD patients (n = 9) and control subjects (n = 4) at 0.25 mg/ml were loaded into the plate overnight at 4 °C under constant shaking. In the DesAb-O plate, we loaded 4500 pg/ml of monomeric αSyn as negative control. The following day after six additional washes in PBS, the plate was incubated with 1:4000 6E10 Ab for 2 h at RT with no shaking, while αSyn was incubated with 1:4000 mouse monoclonal anti-αSyn (211) Ab (Santa Cruz Biotechnology, INC). The plate was washed six times in PBS- Tween-20 0.2% and incubated with 1:5000 rabbit anti-mouse (Abcam) HRP-conjugated secondary Ab for 1 h at RT. The plate was then washed six additional times in PBS- Tween-20 0.2% and the amount of $A\beta_{42}$ species bound was quantified as reported above.

2.6 Cell cultures

Authenticated human SH-SY5Y neuroblastoma cells were purchased and maintained as previously reported in *section 1.9*. Furthermore, Primary rat cortical neurons (Thermo Fisher Scientific) were plated in 12-well plate containing glass coverslips and maintained in neuronal basal plus medium (Thermo Fisher Scientific) supplemented with GlutaMAX (Gibco) at the concentration of 0.5 mM and 2% (v/v) B-27 serum-free complement (Gibco), in a 5% CO_2 humidified atmosphere at 37 °C (Fani *et al*. 2022). All the experiments were performed 14 days after plating (Fani *et al*. 2022).

2.7 Stimulated emission depletion (STED) microscopy

$A\beta_{42}$ assemblies were added to the culture medium of SH-SY5Y cells seeded on glass coverslips for 1 h at 3 µM (monomer equivalents). After incubation, the cells were washed with PBS, the plasma membranes were counterstained with 0.01 mg/ml tetramethylrhodamine conjugate wheat germ agglutinin (Thermo Fisher Scientific) (Cascella *et al*. 2021) for 15 min at 37 °C and cells were then fixed with 2.0% (w/v) paraformaldehyde. After washing with PBS, the plasma membranes were permeabilized with a 3.0% (v/v) glycerol solution for 5-10 min. $A\beta_{42}$ species were then detected with 4 µM DesAb-O and 1:800 FITC anti-6X tag secondary Abs (Abcam) or with 1:250 diluted human monoclonal (19.3) anti-

oligomer Ab (Creative Biolabs) and 1:1000 Alexa Fluor 488-conjugated anti-human secondary Abs or with 1:400 diluted rabbit polyclonal anti- oligomer A11 Ab (Thermo Fisher Scientific), or with 1:800 diluted rabbit polyclonal anti-amyloid fibrils OC Ab (Sigma-Aldrich), or with 1:400 diluted mouse monoclonal anti- Aβ 6E10 Abs (Biolegend Way) and 1:500 Alexa Fluor 514-conjugated anti-rabbit or anti- mouse secondary Abs (Thermo Fisher Scientific). STED xyz images (i.e., z-stacks acquired along 3 directions: x, y, and z axes) were acquired as previously reported (Cascella *et al*. 2021). In a set of experiments, SH-SY5Y cells seeded on glass coverslips were experienced for 24 h with ADDLs oligomers 3.0 μM (monomer equivalents) or CSF samples from AD patients or controls (n = 4 for both AD and control CSF samples) diluted 1:1 with cellular medium. In another set of experiments, primary rat cortical neurons were treated with CSF samples from AD patients or controls (n = 4 for both AD and control CSF samples) diluted 1:1 with cellular medium. After the incubation, the cells were counterstained and analysed by STED microscopy as reported above. In another set of experiments, A+ oligomers, F1 and a mixture containing both $A\beta_{42}$ species (1:1 molar ratio) were incubated on a glass coverslip at 25 μM in cell culture medium without cells while the CSF samples (n = 9 and n = 4 for AD and controls, respectively) were spotted at a concentration of 0.5 mg/ml. After 30 min of incubation, the samples were blocked in Casein 1X with TBS-Tween-20 0.2% for 30 min. Once washed with TBS-Tween-20 0.2%, $A\beta_{42}$ species and the CSF samples were detected with 1:800 6E10 (Biolegend Way), 2.0 μM DesAb-O or 4 μM $DesAb_{18–24}$ Ab for 1 h and then and with 1:500 Alexa Fluor 514-conjugated anti-mouse secondary Abs (Thermo Fisher Scientific) or with 1:500 FITC anti-6X tag secondary Abs (Abcam). The acquisition was performed as reported above.

2.8 Microscopy analysis of $A\beta_{42}$ aggregates bound to neuronal membranes

SH-SY5Y cells were seeded on glass coverslips and then treated for 15 min with A+ oligomers or ADDLs at a concentration of 3.0 μM (monomer equivalents), in the absence or presence of a pre-incubation with increasing molar ratio (1:0.1, 1:0.25, 1:0.5, and 1:1, monomer equivalents) between Abs and $A\beta_{42}$ species. After incubation, the cells were washed with PBS and the plasma membranes were counterstained for 15 min using 5.0 μg mL^{-1} of Alexa Fluor 633-conjugated wheat germ agglutinin (Life Technologies) (Evangelisti *et al*. 2016). Cells were fixed in 2.0% (w/v) paraformaldehyde and $A\beta_{42}$ assemblies were detected using 1:800 diluted mouse monoclonal 6E10 Ab (Biolegend Way) and then with 1:1000 diluted Alexa Fluor 488-conjugated anti-mouse secondary Abs (Thermo Fisher Scientific). To detect only the oligomers bound to the cell surface, the cellular membrane was not permeabilized, thus preventing Ab internalisation. Fluorescence emission was detected after double excitation at 633 and 488 nm by a TCS SP8 scanning confocal microscopy system (Leica Microsystems), as previously described (Bigi *et al*. 2023a). The degree of colocalization of $A\beta_{42}$ aggregates and cell membranes was estimated for regions

of interest in 30-32 cells, via the use of ImageJ (NIH, Bethesda, MD, USA) and JACOP plugin (http://rsb.info.nih.gov) software (Rasband WR).

2.9 MTT reduction inhibition assay

The cytotoxicity of the different $A\beta_{42}$ aggregates was assessed in SH-SY5Y cells seeded in 96-well plates by the MTT assay (Mosmann 1983; Evangelisti *et al.* 2014). Briefly, $A\beta_{42}$ species (monomer, A+ and A- oligomers, ADDLs, and two types of fibrils) at a concentration of 3.0 μM (monomer equivalents) were added to the culture medium of SH-SY5Y cells for 24 h following or not a pre-incubation with equimolar concentrations of DesAb-O, 19.3, A11, or OC Abs. After treatment, the culture medium was removed, cells were washed with PBS and the MTT assay was assessed as previously reported (Bigi *et al*. 2023a). Cell viability was expressed as the percentage of MTT reduction in treated cells as compared to those untreated, or to those treated with $A\beta_{42}$ species in the absence of Abs.

In a set of experiments, CSF samples (n = 4 for AD as well as controls) were added to the culture medium of SH-SY5Y cells in presence or absence of DesAb-O at 3 μM for 24 h. Treatments with CSF samples and DesAb-O were pre-incubated for 1 h at 37 °C. ADDLs oligomers at 1 μM (monomer equivalent) were used as positive control. These solutions were then added to SH-SY5Y cells for 24 h and the analysis was performed as reported above in *section 1.11.*

2.10 Measurement of cytosolic free Ca^{2+} levels

The intracellular calcium levels were measured in SH-SY5Y cells as previously described (Cascella *et al.* 2017; Bigi *et al*. 2023a). SH-SY5Y cells were treated for 5 h with ADDLs at 1 μM (monomer equivalents), or with the CSF samples (n = 4 for AD as well for controls) following or not a 1 h pre-incubation in the absence or presence of DesAb- O at 3 μM. At the end of the treatment, the cells were washed in PBS and loaded with 10 μM fluo-4 AM (Thermo Fisher Scientific) for 10 min and cytosolic Ca^{2+} levels were detected as previously described in *section 1.10*.

2.11 Measurements of calcein leakage

The intracellular calcein levels were measured in SH-SY5Y cells. Briefly, the cells were washed in PBS and loaded with 0.5 μM Calcein-AM (Thermo Fisher Scientific) for 20 min at 37 °C. Then, they were washed two additional times and treated with CSF (n = 4 for both AD and control CSF samples) and ADDLs at 1 μM (monomer equivalents; n = 4), pre-incubated for 1 h in the absence or presence of DesAb-O at 3 μM for 5 h. After fixation in 2.0% buffered paraformaldehyde for 10 min, fluorescence emission was detected after excitation at 488 nm by the TCS SP8 scanning confocal microscopy system as

previously reported (Cascella *et al.* 2021). Images were then analyzed as reported above.

2.12 Statistical analysis

Data were expressed as means ± standard deviation (S.D.), or as means ± standard error of mean (S.E.M). Comparisons between the different groups were performed by using Student t test or by one-way ANOVA followed by Bonferroni's multiple-comparison test (GraphPad Prism 5.0 software). P values lower than 0.05, 0.01 and 0.001 were considered to be statistically significant (*), highly statistically significant (**) and very highly statistically significant (***), respectively.

3.Third section

3.1 Dimeric-DesAb-O design

To design the Dimeric-DesAb-O, a flexible linker composed by a repetition of glycine (Gly) and Serine (Ser), was attached to the C-terminus of a first DesAb-O monomer and the N-terminus of a second monomer of DesAb-O, depleted of the His-tag region. Gene sequence design was carried out through the use of SnapGene software (www.snapgene.com).

3.2 Protein Expression and Purification

DesAb-O was expressed and purified as previously reported in *section 2.3*. The Dimeric-DesAb-O construct was expressed using pET28a (+) vector in *E. coli* Origami™ 2(DE3) Competent Cells (Merck Millipore), as previously described (Sormanni, Aprile and Vendruscolo 2015). Cells were grown at 37 °C in Luria–Bertani (LB) medium (MerckMillipore) supplemented with Kanamycin (50 μg /ml) under shaking at 200 rpm in a New Brunswick Innova 44R incubator shaker (Eppendorf) until reaching an OD_{600} of 0.6. Cells were then harvested by centrifugation; resuspended 20 mM phosphate buffer, pH 8.0, with the addition of one EDTA-Free Complete Protease Inhibitor Cocktail Tablet (Roche) per 500 ml of cell growth; and lysed using sonication (15s on and 45s off pulses, 40% amplitude). Cell debris was removed using centrifugation at 20,000 x *g* (JA-20 rotor, Beckman Coulter) for 45 mins. The cleared lysate was loaded onto a Ni^{2+}-NTA Superflow column (Qiagen), previously equilibrated with 20 mM phosphate buffer containing 15 mM imidazole. After washing with 20 mM phosphate buffer containing 30 mM imidazole, the His-tagged Dimeric- DesAb-O was eluted with 20 mM phosphate buffer with 300 mM imidazole and dialyzed extensively against 20 mM phosphate buffer. Dimeric-DesAb-O was finally purified using size-exclusion chromatography with a HiLoad 16/600 Superdex 75 pg column (GE Healthcare), previously equilibrated in 20 mM

phosphate buffer. Protein concentration was determined by absorbance measurement at 280 nm using theoretical extinction coefficients calculated with ExPASy ProtParam (Gill and Von Hippel 1989). Both the flow through and peak fractions were then loaded on 4–12% Bis-Tris NuPAGE gels (Thermo Fisher Scientific) to verify the sample purity.

Purification of $A\beta_{42}$ was carried out as previously described (Abelein *et al.* 2020; Vadukul *et al*. 2023). Briefly, the spider silk domain-conjugated $A\beta_{42}$ peptide, known as fusion protein (20 kDa) was expressed by heat-shock transformation in BL21 *E. coli*. Cells were grown at 37 °C in LB broth supplemented with kanamycin (50 μg/mL) with shaking at 200 rpm in a New Brunswick Innova 44R incubator shaker (Eppendorf) until an OD_{600} of 0.8 was reached. Protein expression was then induced with 1 mM IPTG, and cultures were incubated overnight at 20 °C with shaking at 200 rpm. Then, cells were collected, centrifuged, and resuspended in 20 mM Tris −HCl and 8 M urea, pH 8.0 to be sonicated on ice for 20 min (15 s on and 45 s off pulses, 20% amplitude). Following another centrifugation, the supernatant was passed through a 0.22 μm filter and loaded onto two tandem 5ml HisTrap HP columns (Cytiva), pre-equilibrated with a binding buffer (20 mM Tris−HCl and 8 M urea, pH 8, supplemented with 15 mM imidazole). After washing the columns with the same buffer to remove nonspecific binding, the fusion protein was eluted using an elution buffer 20 mM Tris-HCl, 8 M urea, pH 8.0 supplemented with 300 mM imidazole (elution buffer). 8.0), followed by concentration measurements via Nanodrop. To release the target peptide, the fusion protein was incubated with TEV protease (1:15 molar ratio) overnight at 4 °C. To ensure complete cleavage and denaturation of the spider silk domain, the sample was treated with 7 M guanidine-HCl on ice for at lease 2h. The sample was then applied on to a Superdex 75 Increase pg 10/300 column (Cytiva), previously equilibrated with 20 mM phosphate buffer, pH 8, for size-exclusion chromatography.

The monomeric peak was collected manually, and the concentration of monomeric $A\beta_{42}$ (in μM) was determined from the chromatogram using the following equation:

$$A\beta_{42}(\mu M) = \left(\frac{A_{280}/2}{0.2 * 1490}\right) * 10^6 \qquad (4)$$

Precisely, A_{280} is the absorbance at 280 nm of the elution peak of $A\beta_{42}$, 0.2 is the path length (cm) of the ATKA Pure (Cytiva) and $1490M^{-1}$ cm^{-1} is the molecular coefficient of $A\beta_{42}$.

For all cellular biology experiments and ADDLs oligomers (Lambert et al., 1998) preparation, we used $A\beta_{42}$ lyophilised peptide (Bachem) dissolved in 100% hexafluoro- 2-isopropanol (HFIP), as previously reported in *section 2.1*.

3.3 Electrospray Ionization Mass Spectrometry

Purified Dimeric-DesAb-O (~20 μM) was analysed by electrospray ionization mass spectrometry (ESI-MS) to confirm molecular weight and sample purity. The plot shows a visible a major peak at 34.270 Da, corresponding y to the molecular weight of Dimeric-DesAb-O predicted by bio-informatic softwares such as ExPASy ProtParam and Peptide Nexus (34.270 Da).

3.4 CD

Far-ultraviolet (UV) CD spectra of Dimeric-DesAb-O were acquired using a Chiroscan spectropolarimeter (Applied Photophysics) equipped with a Peltrier temperature control unit. Measurements were performed in a quartz cuvette with 1 mm path length. Samples contained 6 μM proteins in phosphate-buffered saline (PBS), pH 7.4. The far-UV CD spectra of the dimeric structure of DesAb-O were recorded from 200 to 240 nm at 20°C, and the spectrum of the buffer was subtracted from the spectra of Dimeric-DesAb-O, scanning 10 accumulations. In another set of experiments, temperature-wavelength CD spectra of 6 μM DesAb-O and Dimeric-DesAb-O were recorded between 20°C and 90°C at 5 °C intervals. A background spectrum of the sample buffer was subtracted from all sample spectra. Raw data of θ (units of mdeg) were converted to mean residue ellipticity ($[\theta]_{res}$, units deg cm^2 $dmol^{-1}$) using (Greenfield 2006):

$$[\theta]_{res} = \theta/[(n-1)*l*c] \qquad (5)$$

where θ is the raw data, n the number of amino acids, l the cuvette pathlength (cm), and c the protein concentration (M). The denaturation curves were plotted θ against temperature, and fitted using Santoro and Bolen equation (Santoro and Bolen 1988) and normalised to fraction folded (%) values:

$$[\theta]_{res} = \frac{([\theta]_{res}(F) + m(F) * T) + ([\theta]_{res}(U) + m(U) * T) * e^{\left(\frac{-\Delta G}{RT}\right)}}{\left[1 + e^{\left(\frac{-\Delta G}{RT}\right)}\right]} \qquad (6)$$

where $[\theta]_{res}$ is the measured molar residue ellipticity at temperature T (°C), $[\theta]_{res}(F)$ and $[\theta]_{res}(U)$ are the [θ]res values for the folded and unfolded states at 20 °C, respectively, m(F) and m(U) are the slopes of the folded and unfolded baselines, respectively, ΔG is the Gibbs free energy change upon unfolding and R is the universal gas constant. By fitting the data obtained with the above equation, it was possible to determine the ΔG with the temperature increase. In order to calculate the temperature of half-denaturation (Tm), we firstly determined the fraction folded with the following equation:

$$Fraction\ folded\ (\%) = \frac{([\theta]res - [\theta]res(U))}{([\theta]res(F) - [\theta]res(U))} \qquad (7)$$

The Eq. (7) works by normalizing the observed signal [θ]res against the known spectral endpoints. The denominator ([θ]res(F)-[θ]res(U)) establishes the maximum possible signal change between the fully folded ([θ]res(F)) and fully unfolded ([θ]res(U)) states. The numerator measures how far the observed signal is from the completely unfolded state, allowing the calculation of the fraction that has successfully attained the native conformation. The Tm values represent the temperature at which the protein is 50% folded and 50% unfolded (fraction folded = 50%).

3.5 Thioflavin T Fluorescence Assays

Monomeric recombinant $A\beta_{42}$ (1 μM) was incubated alone or in presence of Dimeric-DesAb-O at decreasing molar ratios (1:1, 1:0,5, 1:0,25, 1:0,125 corresponding to 1 μM, 0,5 μM, 0,25 μM, 0,125 μM Dimeric-DesAb-O concentrations) in 20 mM phosphate buffer pH 8. Samples were prepared with a final concentration of 10 μM thioflavin T (ThT) dye, gently vortexed, and pipetted into nonbinding surface black 96-well plates (Greiner Bio-One) in triplicates. The plate was read in a ClarioStar Plus microplate reader (BMG LabTech) at 37 °C. The excitation and emission wavelengths were set to 440 and 480 nm, respectively, and fluorescence intensity measurements were taken using spiral averaging (3 mm diameter). Buffer-only values were not subtracted from the sample readings but shown in the not normalized graph. Readings were taken every 2 min. To test the capability of the dimeric structure of DesAb- O compared to the monomeric sdAb, in another set of experiments monomeric $A\beta_{42}$ (1 μM) was incubated alone or in presence of 1 μM Dimeric-DesAb-O or increasing DesAb- O molar ratios (1:1, 1:2 corresponding to 1 and 2 μM DesAb-O concentrations. The data were plotted using GraphPad Prism version 9.3.1 for Windows (GraphPad Software).

To obtain $A\beta_{42}$ oligomers and perform experiments on SH-SY5Y cells, the lyophilized peptide (Bachem) was dissolved in 100% HFIP to obtain a monomeric form, followed by evaporation under nitrogen flux. Subsequently, the peptide was resuspended in PBS, resulting in a final concentration of 10 μM. For visualization of the emerging β-sheets in $A\beta_{42}$, samples were added with a final concentration of 25 μM ThT, gently vortexed and pipetted into no binding surface black 96-well plates (Grenier Bio-One) in quadruplets. The plate was read in a BioTekSynergyTM H1 Hybrid Multi-mode reader (Agilent, Santa Clara) at 37 °C. The excitation and emission wavelengths were set to 440 and 485 nm, respectively. Buffer-only values were not subtracted from the sample readings but shown in the final graph. Readings were taken every 2 min. The data were plotted using GraphPad Prism version 9.3.1 for Windows (GraphPad Software). To characterize the different type of aggregates formed during the $A\beta_{42}$ aggregation process, we collected $A\beta_{42}$ samples at various timepoints (0, 2, 4, 8, and 24 h) to conduct further experiments (see details below).

3.6 Real-Time based ELISA assay

Real-time based ELISA experiment was performed aggregating 1 μM monomeric $A\beta_{42}$ peptides in 20 mM sodium phosphate buffer (8 pH) in quiescent conditions. Twenty- microliter aliquots were taken at precise timepoints (0, 0.5, 1, 2 and 20 h) from aggregation reactions and immobilized on a 96- or 384-well Maxisorp ELISA plate (Nunc) with no shaking overnight at 4°C. $A\beta_{42}$ fibrils obtained after 4 days of incubation at 37 °C were used as a control. At the end of the incubation, the plate was then washed three times with TBS (20 mM Tris, pH 7.4, and 100 mM NaCl) and incubated in TBS supplemented with 5% bovine serum albumin (BSA) under constant shaking for 1h at RT. The plate was then washed six times with TBS and then incubated with 30 μL solutions 1 μM DesAb-O or 1 μM Dimeric-DesAb- O under constant shaking either for 1 h at RT or overnight at 4 °C. At the end of this incubation, additional six washes with TBS were performed and the plate was incubated with 30 μL solutions of rabbit polyclonal 6x His tag horseradish peroxidase (HRP) conjugated (Abcam) at a dilution of 1:4.000 in 20 mM Tris, pH 7.4, 100 mM NaCl, and 5% BSA under constant shaking for 1 h at RT. Finally, the plate was washed two times with 20 mM Tris, pH 7.4, and 100 mM NaCl, then three times with 20 mM Tris, pH 7.4, 100 mM NaCl, and 0.02% Tween- 20 and again three times with 20 mM Tris, pH 7.4, and 100 mM NaCl. Finally, the amount of bound sdAbs was quantified by using 1-Step Ultra TMB-ELISA Substrate Solution (Thermo Fisher Scientific), according to the manufacturer's instructions, and the absorbance was measured at 450 nm by means of a CLARIOstar plate reader (BMG Labtech) as previously reported (Aprile *et al*. 2020).

3.7 Transmission Electron Microscopy (TEM)

5 μM $A\beta_{42}$ samples incubated in the presence or absence of 5 μM sdAbs were aggregated in a microplate without ThT and collected after 24h of aggregation at 37°C. $A\beta_{42}$ aggregation was monitored by other replicates with ThT, allowing real-time monitoring of the reaction. Samples for TEM were then prepared spotting 4 μL onto Formvar/carbon- coated 300 mesh copper grids for 1 min. By blot dying the grid with Whatman filter, we removed excess sample were removed, allowing the grid drying for 2 min. Samples were then washed with 4 μL of water and stained with 4 μL of 2% w/v uranyl acetate (Vadukul *et al*. 2023). Grids were imaged on a T12 Spirit electron microscope (Thermo Fisher Scientific). The fibril diameter was measured using ImageJ software and all data were plotted using Excel (Version 16.89.1 (24091630)).

3.8 Dot Blot analysis

Dot blots were carried out on samples that were aggregated in the microplates without ThT at the endpoint of aggregation as previously reported (Vadukul *et al.* 2023). Samples were collected and centrifuged at max speed (~16,000g) for

30 min on a benchtop centrifuge to separate the soluble and insoluble aggregates. Prior to centrifugation, an aliquote of each sample was stored and considered as the total protein amount. At the end of the centrifuge, the supernatant was collected and the pellet was resuspended in 20 mM phosphate buffer. To analyze the proportion of soluble and insoluble $A\beta_{42}$ species and Ab fragments, three repeats of each samples were spotted onto a nitrocellulose membrane and blocked in 5% nonfat milk in 0.1% PBS-Tween for 45 min at RT (Vadukul *et al*. 2023). The membranes were then incubated overnight at 4 °C with either 1:1000 6E10 Ab for $A\beta_{42}$ detection or 1:1000 anti-6X His-tag Ab for DesAb-O and DiDesAb-O detection. The following day, the membrane were washed three times for 10 min each in 0.1% PBS-Tween. Membranes were then incubated for 1 h at RT protected from light with 1:2000 anti-mouse Alexa fluor 647 (Thermo Fisher Scientific) for 6E10 Ab and 1:1000 anti-goat anti-6X His Tag (Abcam) for the anti- 6X His Tag Ab, respectively. After three additional 10-minute washes in 0.1% PBS-Tween, the membranes were imaged with a Typhoon scanner (GE Healthcare) using the appropriate laser settings (Vadukul *et al.* 2023). The signal intensity of the supernatant was normalized to that of the total protein of the corresponding sample.

In another set of experiments, to characterize the different types of $A\beta_{42}$ aggregates formed during the $A\beta_{42}$ lyophilised peptide (Bachem) aggregation process, 2.0 µl (equivalent to 0.1 µg) of the samples at five different timepoints (0, 2, 4, 8, and 24 h) were spotted onto a nitrocellulose membrane. Following a 45-min blocking step (1.0% bovine serum albumin, BSA, in TBS-Tween 0.1%), the membrane was incubated with 1:15.000 diluted human monoclonal anti-ADDLs (19.3) Ab (Creative Biolabs), 1:1000 diluted rabbit polyclonal anti-amyloid fibrils (OC) Ab (Sigma-Aldrich) and 1:800 diluted mouse monoclonal anti-Aβ (6E10) Ab (Biolegend Way) for 1 h and 30 mins. Subsequently, the membrane was washed three times in TBS-Tween 0,1% for 10 mins each and incubated with 1:3000 diluted goat anti-6X His tag (Abcam), goat anti-human (Sigma-Aldrich), or goat anti-rabbit (Abcam) or rabbit anti-mouse (Abcam), all conjugated with horseradish peroxidase (HRP) for 1 h. After three additional washes in TBS-Tween 0,1%, the immunolabelled dots were detected using a Super-SignalWest Dura (Pierce) ImageQuant™ TL software (GE Healthcare UK Limited version 8.2) as previously reported (Bigi *et al*. 2024b).

3.9 PK Digestion

Fibrils obtained after 4 days at 37 °C under constant conditions in the presence or in the absence of sdAbs were centrifuged at max speed (~16,000g) for 1 h. The supernatant was discarded. The pellet was resuspended in 20 mM phosphate buffer and treated with increasing PK concentrations (0, 10, 25, 50 µg/ml) for 30 min at room temperature. Samples were then incubated at 95 °C for 5 min to stop the enzymatic reaction, and samples were prepared for SDS-PAGE and Western blotting analysis. 6E10 antibody diluted 1:1000 in 0.1% PBS-Tween was used as primary antibody. Data analysis was performed

assuming the band intensity at 0 μg/ml of PK of each sample as the 100%. Intensity of each 0 μg/ml of PK band was compared as well.

3.10 SDS-PAGE and Western Blotting

Fibrils from the coincubation sample were collected by centrifugation at max speed for 1h as previously reported in *section 3.9*. Samples were prepared in 4× LDS sample buffer and 10× reducing agent after which they were boiled at 95 °C for 5 min. Samples were then run on 4−12% Bis-Tris NuPAGE gels (Thermo Fisher Scientific) and transferred onto a 0.45 μm nitrocellulose membrane for 7 min at 20 V with the iBlot 2 (Thermo Fisher, Waltham). Blocking, incubation with antibodies, and detections were carried out as described above (Vadukul *et al*. 2023).

3.11 CSF samples

CSFs from human aged controls (n = 4) or AD patients (n = 4) were obtained from BioIVT, stored and processed as previously reported in *section 2.2*.

3.12 STED microscopy

$A\beta_{42}$ aggregates collected at different timepoints (0, 2, 4, 8, and 24 h) of a ThT aggregation assay were spotted and visualized by STED microscopy as described in *section 2.7*.

3.13 Confocal microscopy

To detect $A\beta_{42}$ oligomers bound to the cellular membranes and internalized into the cytosol without pre-incubating with sdAbs, we performed the experiment adding 0,5 μM $A\beta_{42}$ oligomers for 1 h to the culture medium of SH-SY5Y. The experiment was conducted as previously described in *section 2.8*. $A\beta_{42}$ species were then detected with 3 μM and 1 μM DesAb-O or Dimeric-DesAb-O and 1:800 6E10 Ab as a control. As a secondary Ab, we used diluted FITC anti-6X His-tag secondary Abs (Abcam) or Alexa Fluor 488-conjugated anti-mouse secondary Abs (Thermo Fisher Scientific). In another set of experiments, we calculate the number of $A\beta_{42}$ oligomers bound to neuronal membranes of SH-SY5Y. To perform this experiment, 0.5 μM $A\beta_{42}$ oligomers were pre- incubated or not with increasing sdAbs molar ratios (1:0.1, 1:0.25, 1:0.5, 1:1, 1:2, 1:3) corresponding to 0.25, 0.63, 1.25, 2.5, 5 and 7.5μM of sdAbs concentrations) for 1 h at 37 °C under soft shaking, and the binding experiment was then conducted as reported in *section 2.8.*

3.14 Measurement of cytosolic free Ca^{2+} levels

The intracellular calcium levels were measured in SHSY-5Y cells as previously described (Bigi *et al*. 2023; Cascella *et al.* 2017). SHSY-5Y cells were treated for 15 mins with 0,5 μM $A\beta_{42}$ oligomers previously incubated or not for 1 h at 37 °C under gentle shaking with increasing sdAbs molar ratios (1:0.1, 1:0.25, 1:0.5, 1:1, 1:2, 1:3 corresponding to 0.25, 0.63, 1.25, 2.5, 5 and 7.5μM of sdAbs concentrations). Cells were then washed in PBS and loaded with 4.5 μM Fluo-4 AM (Thermo Fisher Scientific) for 10 min and cytosolic Ca^{2+} levels were detected after excitation at 488 nm by the TCS SP8 scanning confocal microscopy system as previously reported (Bigi *et al*. 2023a; Cascella *et al*. 2021). In another set of experiments, SH-SY5Y cells were treated for 5 h with the CSFs (n = 4 for AD as well for controls) pre-incubated or not with DesAb-O or Dimeric-DesAb- O at 3 μM and 1 μM for 1 h at 37 °C under shaking. Experiments were conducted as previously described in *section 1.10*.

3.15 MTT reduction assay

To assess the cytotoxicity of $A\beta_{42}$ aggregates formed during the $A\beta_{42}$ aggregation process, a MTT reduction assay was conducted. Briefly, 1 μM $A\beta_{42}$ species collected from a ThT aggregation assay at different timepoints (0, 2, 4, 8 and 24 h) were added for 24 h to culture medium of SH-SY5Y cells. ADDLs were used as positive control. For our experiments, we decided to use $A\beta_{42}$ oligomers obtained after 8 h of incubation at 37 °C. In another set of experiments, we performed an MTT test with decreasing concentrations $A\beta_{42}$ oligomers (1 μM, 0.5 μM, 0.25 μM, 1 nM, 0.5 nM, 0.25 nM and 1 pM) in order to optimize our experimental conditions, deciding to use 0.5 μM $A\beta_{42}$ oligomers concentration for the following cellular biology experiments. In another set of experiments, $A\beta_{42}$ oligomers were pre-incubated for 1 h at 37 °C with increasing sdAbs molar ratios (1:0.1, 1:0.25, 1:0.5, 1:1, 1:2, 1:3 corresponding to 0.25, 0.63, 1.25, 2.5, 5 and 7.5 μM of sdAbs concentrations). The solutions were then added to the extracellular medium of SH-SY5Y cells. Then experiments were conducted and analyzed as reported in *section 1.11*.

3.16 Statistical analysis

Data were expressed as means ± standard error of mean (S.E.M). Comparisons between the different groups were performed by using unpaired and one-tailed Student t test or by one-way or two-way ANOVA followed by Bonferroni's multiple-comparison test (GraphPad Prism 10.3.1 software). P values lower than 0.05, 0.01, 0.001 and 0.0001 were considered to be statistically significant (*), highly statistically significant (**) and very highly statistically significant (***), and extremely statistically significant (****) respectively.

Chapter 2
First Section: Putative CSF biomarkers of Alzheimer's disease based on the novel concept of generic protein misfolding and proteotoxicity: the PRAMA cohort

1. Demographic characteristics and classical CSF biomarker distributions of the PRAMA cohort

29 patients with diagnosis of AD (AD cases) and 23 patients with diagnosis of other diseases affecting the CNS (non-AD cases) have participated to this study, for a total of 52 patients. CSF samples were collected from all patients and treated as reported in *Chapter 1- Materials and Methods*. Table 2.1 reports the mean demographic characteristics of both groups, as well as their mean values of the classical CSF biomarkers ($A\beta_{42}$/ $A\beta_{40}$ ratio and levels of t-tau and p-tau), the percentages of patients with the ε4 allele of the *APOE* gene and the mean scores of MMSE tests. Table 2.1. reports the individual values of the same parameters for all 52 patients, one by one.

The total protein concentrations of the 23 non-AD and 29 AD cases, measured using the Bradford assay, were found to have a good degree of variability, as they ranged from ca. 0.2 to ca. 1.0 mg/ml in both groups (Figure 2.1 A), in agreement with previous analyses (Dufour-Rainfray *et al*. 2013). Their mean values were 0.44 ± 0.21 and 0.44 ± 0.19, respectively, indicating similar distributions in the two groups.

The classical CSF biomarkers, namely the $A\beta_{42}$/ $A\beta_{40}$ ratio, t-tau and p-tau levels, measured with established clinical protocols as described in *Chapter 1 – Materials and Methods*, also showed a good degree of variability, but their mean values were significantly different in the two groups: 0.089 ± 0.022 and 0.053 ±

Liliana Napolitano, liliana98.napolitano@gmail.com, 0009-0004-3087-286X

Referee List (DOI 10.36253/fup_referee_list)
FUP Best Practice in Scholarly Publishing (DOI 10.36253/fup_best_practice)

Liliana Napolitano, First Section*: Putative CSF biomarkers of Alzheimer's disease based on the novel concept of generic protein misfolding and proteotoxicity: the PRAMA cohort*, © Author(s), CC BY 4.0, DOI 10.36253/979-12-215-0993-9.04, in Liliana Napolitano, *A multidisciplinary approach for the early diagnosis of Alzheimer's disease and potential therapeutic applications*, pp. 65-77, 2026, published by Firenze University Press, ISBN 979-12-215-0993-9, DOI 10.36253/979-12-215-0993-9

Book References DOI 10.36253/979-12-215-0993-9.references

0.020 for the $A\beta_{42}/A\beta_{40}$ ratio ($p<0.0001$), 306 ± 246 and 763 ± 315 for t-tau ($p<0.0001$) and 43 ± 41 and 127 ± 61 for p-tau ($p<0.0001$), in non-AD and AD groups, respectively (Figure 2.1 B,C,D). The scatter plots of $A\beta_{42}/A\beta_{40}$ *versus* t-tau and $A\beta_{42}/A\beta_{40}$ *versus* p-tau, with the optimized thresholds (t^*) derived from optimization of the Youden's indexes of the two parameters (horizontal and vertical lines, respectively), show a good separation between non-AD and AD cases, with the latter having, on average, high values of t-tau and p-tau and low values of $A\beta_{42}/A\beta_{40}$, as expected (Figure 2.2 A,C).

In particular, the three quadrants above the t^* value for t-tau (or p-tau) and below the t^* value for $A\beta_{42}/A\beta_{40}$ contain mainly AD cases and few non-AD cases, whereas the remining quadrant contains a disproportionate amount of non-AD versus AD cases ($p<0.0001$ for both Fisher's exact test and Chi-square test, for both scatter plots). The AUC in the ROC curve were found to be 0.865, 0.889 and 0.887 (>0.5) for $A\beta_{42}/A\beta_{40}$, t- tau and p-tau, respectively (Figure 2.2 B,D). Overall, the good separation of non-AD and AD cases using classical CSF biomarkers in scatter plots indicate that the two groups are good representatives of non-AD and AD cases, respectively.

2. Non-AD and AD CSFs have similar circular dichroism spectra and parameters

In order to search CSF biomarkers independent of specific protein levels and using spectroscopic methods, we started our analysis with far-UV CD spectroscopy. Far-UV CD spectra recorded for the various CSF samples displayed a good degree of variability in non-normalized mean residue ellipticity (θ), as shown for five representative non-AD and five representative AD CSF samples (Figure 2.3 A). The θ values at the wavelength of 222 nm (θ_{222}) for all 52 CSF samples ranged from ca. - 22 to ca. -162 mdeg (cell 0.1 cm) in both groups (Figure 2.3 B). Their mean values were -59 ± 36 and -57 ± 33 in non-AD and AD cases, indicating the absence of a significant difference ($p = 0.84$).

In both non-AD and AD cases, θ_{222} correlated with protein concentration measured with the Bradford assay (Figure 2.4 A,B) and with the high tension (HT) signal at 222 nm (HT_{222}), which is also a correlate of total protein concentration (Figure 2.4 C,D). This indicates that the variability of CD spectra resulted from the variability in protein concentration. That HT_{222} is a correlate of the concentration of CSF proteins rather than other compounds present in the CSF samples and possibly contributing to the optical absorption, is shown by the correlation between HT_{222} and protein concentration measured with the Bradford assay in the two groups of patients (Figure 2.4 E,F).

In all CD spectra, negative peaks at ca. 208 and 222 nm were observed indicating that the spectra are dominated by proteins with substantial α-helical structure (Figure 2.3 A). This occurs because the all-α human serum albumin (HSA) is by far the most abundant protein in CSF and only one of the first ten most abundant proteins of the CSF is all-β, with the other nine being either mixed α

/β or all-α proteins (Lardinois *et al*. 2014). When other CD parameters were evaluated, including wavelength of the first or second peak, θ at any given wavelength, ratios of θ at two given wavelengths, θ normalized for protein concentration, etc., no significant differences were found between the non-AD and AD groups.

3. Non-AD and AD CSFs have different wavelengths of maximum fluorescence emission

We then compared the various CSF samples by recording their intrinsic tryptophan fluorescence spectra, which also appeared to be highly variable in terms of overall fluorescence intensity, as shown for the same representative five non-AD and five AD CSF samples (Figure 2.3 C). The values of fluorescence intensity at the wavelength of maximum emission (λ_{max}) ranged from ca. 160 a.u. to ca. 1200 a.u. in both groups and their mean values were 595 ± 260 and 502 ± 150 in non-AD and AD cases (Figure 2.3 D), indicating the absence of a significant difference, although a trend seems to be present ($p = 0.11$, Student *t* test). Subtle variations of the λ_{max} value was found in the various fluorescence spectra (Figure 2.3 E). In particular, the λ_{max} values ranged from 338 to 344 nm in non-AD cases and from 338 to 349 nm in AD cases, with a few AD cases having very high λ_{max} values, producing an extended tail out of the Gaussian distribution (Figure 2.3 E). The mean values in the two groups were 340.9 ± 1.4 nm and 341.9 ± 2.7 nm, respectively (Figure 2.3 E), indicating the absence of a significant difference, although a trend seems again to be present ($p = 0.11$). The λmax of the intrinsic fluorescence spectrum of a protein correlate positively with the solvent exposure of its tryptophan residues, which are hydrophobic and generally buried within the hydrophobic cores of native proteins (with lower λmax values), but become solvent exposed in case of partial or total unfolding or misfolding (with higher λ_{max} values). The anomalously high λ_{max} values of some AD cases indicate that, on average, their CSF proteins have a higher extent of partially unfolded or misfolded proteins.

4. Non-AD and AD CSFs have different quantities of protein aggregates

Size distributions of the particles present in CSF samples were acquired with dynamic light scattering (DLS), as shown here for the same representative five non-AD and five AD cases (Figure 2.5 A,B). In both cases, a peak of small species having an apparent hydrodynamic diameter (D_h) of ca. 10 nm is evident, which arises from the dominant largest CSF proteins, such as HSA. However, large species arising from protein aggregates are also present in both groups, all having D_h values around or higher than 100 nm (Figure 2.5 A,B). The light scattering intensity (*LSI*) arising from small species (D_h~ 10 nm) and large species (D_h> 30 nm) is higher in non-AD and AD cases, respectively, indicating a larger proportion of protein aggregates in the latter group (Figure 2.5 A,B). This

difference remains evident when considering all 23 non-AD and 29 AD cases, with large species accounting for 57 ± 20% and 67 ± 25% of *LSI* in the two groups, respectively (Figure 2.5 C). The difference is not yet significant but indicates again a trend ($p = 0.12$).

To interpret these data, we need to consider that *LSI* scales with the square and sixth power of the mass and *Dh* of the particles present in the sample, respectively. Therefore, the percentage of aggregate-derived *LSI* is a large overestimate of the percent population of these species in a CSF sample. When the size distributions are converted into light scattering volume (%) rather than *LSI* (%), the smaller species become dominant (data not shown). However, it is just because of this relationship between LSI and *Dh* that the DLS technique is very sensitive to protein aggregates, allowing to unravel and compare CSF samples with subtle differences in aggregate populations.

Another relevant DLS parameter is the light scattering count rate (LSCR), which corresponds to the total number of photons scattered by the sample per time unit, in units of kilocounts per second (kcps), and correlating again with the size of CSF particles. The LSCR ranges from ca. 30 to ca. 650 kcps and from ca. 50 to ca. 1200 Kcps in the two groups, respectively, with means of 248 ± 206 and 322 ± 258 kcps, respectively (Figure 2.5 D). This difference is not significant, however ($p = 0.27$).

5. Non-AD and AD CSFs have different abilities to destabilize cell membranes.

It is well known that protein aggregates have the ability to bind to and destabilize biological membranes and, when added to the extracellular medium of cell cultures, they destabilize the cell membrane and cause an influx of Ca^{2+} ions from the medium into the cytosol (Bigi *et al*. 2020; Cascella *et al.* 2021; Fani *et al*. 2021; Fani *et al*. 2022; Bigi *et al.* 2023a). We therefore tested the 23 non-AD and 29 AD CSF samples to cultured SH- SY5Y neuroblastoma cells by adding them to the extracellular medium (1:1) and measuring the intracellular Ca^{2+} levels after 5 h, using the Fluo-4 AM probe and confocal fluorescence microscopy. Cells left untreated (negative control) and treated with 1 μM ionomycin for 2 h (positive control) had very low (100%) and very high (677%) intracellular Ca^{2+} levels (Figure 2.6 A). Cells treated with CSF samples had variable increases of intracellular Ca^{2+} levels, as shown for the representative five non-AD and five AD samples (Figure 2.6 A). The Ca^{2+} levels ranged from ca. 110% to ca. 250% in non-AD cases (with the exception of one outlier sample) and from ca. 140 to ca. 340% in AD patients, relative to untreated cells (Figure 2.6 B). The mean values in the two groups were 181 ± 54% and 229 ± 53%, respectively, relative to untreated cells (Figure 2.6 B) and the difference is highly significant ($p = 0.0021$).

We also evaluated the ability of the various CSF samples to impair mitochondrial function of SH-SY5Y cells using the MTT reduction test, which measures the ability of the mitochondria to reduce the tetrazolium due MTT to formazan after 24 h of treatment (Cascella *et al*. 2021; Fani *et al.* 2021; Cascella *et al*. 2022; Bigi *et al*. 2023a). Both non- AD and AD cases caused, on average, small

decreases of MTT reduction relative to untreated cells, with values from ca. 77 to ca. 103% and from ca. 79 to ca. 105% in the two groups, respectively (Figure 2.6 C). However, the two groups were found to behave similarly with values of 93.5 ± 6.3% and 92.0 ± 7.7%, respectively ($p = 0.45$). The MTT reduction assay may fail to reveal differences between the two groups relative to the Ca^{2+} assay, both because of its lower sensitivity and because mitochondrial dysfunction is a downstream process in a complex cascade of events that start with aggregate-induced membrane destabilization as its earliest event when aggregates are added extracellularly (Kayed *et al*. 2004; Demuro *et al*. 2005; Zampagni *et al*. 2011; Cascella *et al*. 2021; Fani *et al*. 2022). For this reason, the Ca^{2+} assay distinguishes directly and with higher sensitivity the presence of potentially toxic aggregates in the CSF samples.

6. Evidence for fluorescence, DLS, and toxicity parameters as potential AD biomarkers

The analysis presented so far indicates that AD CSF samples are characterized by higher values of (i) λ_{max} values in intrinsic tryptophan fluorescence spectra, (ii) *LSI* from large protein species in the DLS analysis and (iii) cytosolic Ca^{2+} ion levels induced in cultured cells. This finding has a rationale in the presence of higher amounts of (i) misfolded proteins exposing tryptophan residues, (ii) large protein particles and (iii) misfolded protein oligomers inducing Ca^{2+} dyshomeostasis in cells, respectively.

The scatter plot of *LSI* from large protein species versus λ_{max} with the thresholds (t^*) derived from optimization of the Youden's indexes of the two parameters (horizontal and vertical lines, respectively), indicates a separation between non-AD and AD cases (Figure 2.7 A). The three quadrants above one or both t^* values contain mainly AD cases and few non-AD cases, whereas the only quadrant below both t^* values contains a disproportionate amount of non-AD versus AD cases ($p = 0.011$, Fisher's exact test; $p = 0.0075$, Chi-square test). A diagnosis of AD based on the CSF parameters occupying one of the three quadrants above at least one t^* value has a modest sensitivity but fairly good specificity (medium probability of false negatives but low probability of false positives). The AUC values in the ROC curve were found to be 0.648 and 0.560 (>0.5) for *LSI* and λ_{max}, respectively, indicating a fairly good accuracy of a test based on the two parameters separately (Figure 2.7 B).

The scatter plot for intracellular Ca^{2+} levels versus λ_{max} indicates a better separation between non-AD and AD cases (Figure 2.7 C). The three quadrants above one or both t^* values contain nearly all AD cases but also a non-negligible amount of non-AD cases, whereas the quadrant below both t^* values contain very few AD cases and a large amount of non-AD cases ($p = 0.0016$, Fisher's exact test; $p = 0.0009$, Chi-square test). Consequently, a diagnosis of AD based on these two CSF parameters occupying one of the three quadrants above at least one t^* value has a high sensitivity and medium specificity (very low probability

of false negatives but medium probability of false positives). The AUC values in the ROC curve were found to be 0.780 and 0.560 (>0.5) for Ca^{2+} levels and λ_{max}, respectively, indicating again a good accuracy of a test based on the two parameters separately (Figure 2.7 D).

The scatter plot for intracellular Ca^{2+} levels versus *LSI* also indicates a good separation between non-AD and AD cases (Figure 2.7 E), similarly to the previous analysis ($p = 0.0006$, Fisher's exact test; $p = 0.0003$, Chi-square test), reporting again a high sensitivity and medium specificity. The AUC values in the ROC curve were found to be 0.780 and 0.648 (>0.5) for Ca^{2+} levels and *LSI*, respectively, indicating again a good accuracy of a test based on the two parameters separately (Figure 2.7 F).

7. Comparison between novel and classical biomarkers.

As a next step in our analysis, we combined three classical and well-established CSF biomarkers ($A\beta_{42}/A\beta_{40}$ ratio, t-tau levels and p-tau levels) with the three novel putative biomarkers identified here (intrinsic fluorescence λ_{max}, *LSI* from large protein species in DLS and cytosolic Ca^{2+} levels in cells). The scatter plots for all possible pairs are shown in Figure 2.8. The scatter plots for each of three novel biomarkers versus $A\beta_{42}/A\beta_{40}$ ratio all show a good separation between non-AD and AD cases (Figure 2.8 A,C), with non-AD and AD cases crowding the bottom-right and three remaining quadrants, respectively ($p<0.0001$, Fisher's exact and Chi-square tests for the plot with λ_{max}; $p<0.0001$, Fisher's exact and Chi-square tests for the plot with *LSI*; $p = 0.001$, Fisher's exact test, and $p = 0.0007$, Chi-square test for the plot with Ca^{2+} levels). The scatter plots for each of three novel biomarkers versus either T-tau levels (Figure 2.8 D,F) or P-tau levels (Figure 2.8 G,I) also show a good separation with non-AD and AD cases occupying, in all cases, the bottom-left and three remaining quadrants, respectively ($p<0.0001$, Fisher's exact and Chi-square tests for λ_{max}; $p<0.0001$, Fisher's exact and Chi-square tests for *LSI*; $p = 0.0004$, Fisher's exact test, and $p = 0.0003$, Chi-square test for Ca^{2+} levels). In all nine scatter plots we obtained a similarly high sensitivity but a higher specificity relative to the analyses obtained with pairs of novel biomarkers, indicating that combined analyses with established and novel biomarkers improve the overall accuracy.

Since the Ca^{2+} levels and the three classical biomarkers ($A\beta_{42}/A\beta_{40}$ ratio and levels of t-tau and p-tau) separate very well the two AD and non-AD populations, the best level of diagnosis in terms of both sensitivity and specificity is achieved when considering AD cases only in one quadrant, which is the top-left for Ca^{2+} levels versus $A\beta_{42}/A\beta_{40}$ ratio (Figure 2.8 C) and the top-right for Ca^{2+} levels versus t-tau (Figure 2.8 F) and p-tau (Figure 2.8 I). The number of false positives and false negatives are only 1-3 out of 23 cases and 2-3 out of 29 cases, respectively ($p<0.0001$ with both statistical tests). The comparison between scatter plots built with pairs of classical biomarkers (Figure 2.2 A,C) and mixed classical and novel biomarkers (Figure 2.8) indicate good separations with $p<0.0001$ in all

cases, using both the Fisher's exact and Chi-square tests. This observation legitimates the use of the three novel CSF parameters analyzed here for AD diagnosis.

The comparison between scatter plots built solely with pairs of novel biomarkers (Figure 2.7) and those built solely with classical biomarkers (Figure 2.2 A,C) also indicate good separations in all cases, provided Ca^{2+} levels is utilized as one of the novel biomarkers ($p<0.002$ in all cases, using both statistical tests). The scatter plot using intrinsic fluorescence λ_{max} and *LSI* from large species yields the least satisfactory performance.

8. Chapter 2: figures and tables

	ApoE ε4+ [a]	Age at CSF collection	p-tau (pg/ml)	t-tau (pg/ml)	$A\beta_{42}$ (pg/ml)	$A\beta_{42}$ /$A\beta_{40}$	MMSE score [b]
Non - AD	18.2% (n=22)	71.8 ± 7.0 (n=21)	42.6 ± 40.5 (n=23)	305.7 ± 246.0 (n= 23)	708.0 ± 389.1 (n=23)	0.089 ± 0.022 (n=23)	26.4 ± 4.3 (n=5)
AD	40.7% (n=27)	70.2 ± 7.3 (n=29)	126.9 ± 60.6 (n=29)	763.1 ± 315.0 (n=29)	675.0 ± 295.9 (n=29)	0.053 ± 0.020 (n=29)	19.7 ± 5.7 (n=25)

Table 2.1 - Mean genetic, demographic and clinical characteristics and biomarkers distribution of the studied non-AD and AD patients. [a] All patients underwent *APOE* genotyping: *APOE* genotype was coded as *APOE* ε4- (no *APOE* ε4alleles) and *APOE* ε4+ (presence of one or two *APOE* ε4 alleles). The column reports the percentage of *APOE* ε4+ genotype and the number of patients analysed (n). [b] The MMSE score ranges for any patient from 0 to 30, with 30 indicating high brain performance. The n value of non-AD cases is low because there was no clinical indication to perform a MMSE test in many cases.

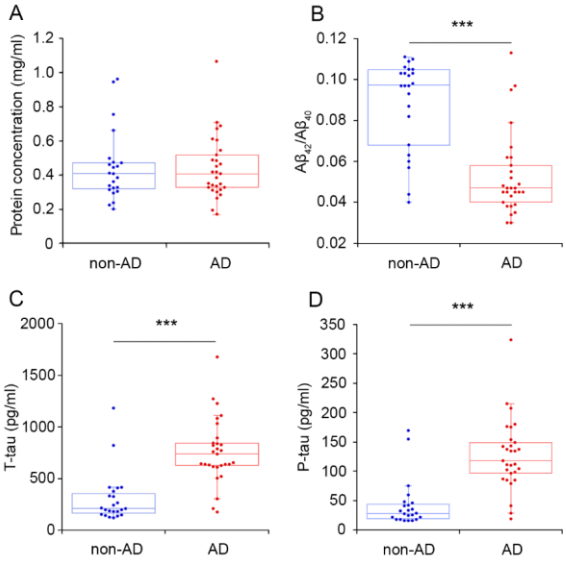

Figure 2.1 - Box plots reporting the protein concentration determined with the Bradford assay (A), the $A\beta_{42}/A\beta_{40}$ ratio (B), T-tau levels (C) and P-tau levels (D) in all CSF samples

of non-AD and AD patients. The boxes, horizontal lines, whiskers and individual dots have the same meaning as in Figure 2a. The two populations were compared with the Student *t* test in all plots (*** $p < 0.001$).

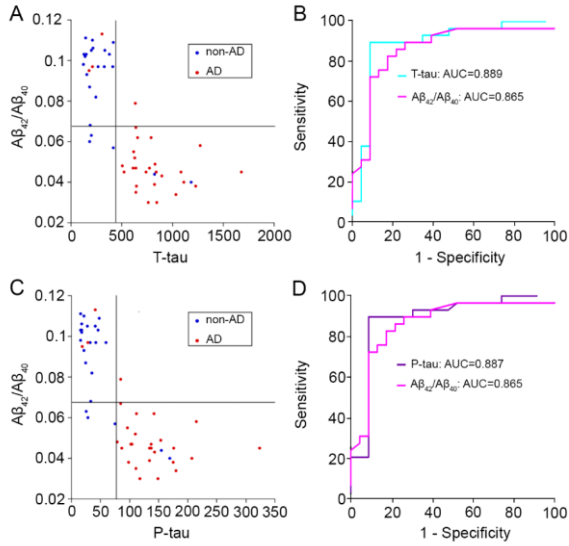

Figure 2.2 - (A,C) Scatter plots for the $A\beta_{42}/A\beta_{40}$ ratio versus T-tau (A) and P-tau (C). (B,D) ROC curves of the $A\beta_{42}/A\beta_{40}$ ratio and T-tau (B) and of the $A\beta_{42}/ A\beta_{40}$ ratio and P-tau (D). AUC values are indicated for each parameter. Non-AD (blue) and AD (red) CSF samples categorized to occupy the top-left quadrant or the remaining three quadrants provide a good separation between non-AD and AD patients.

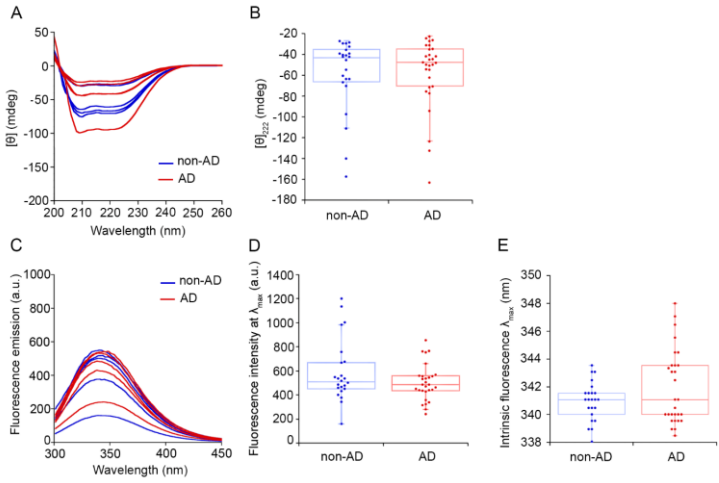

Figure 2.3 - Non-AD and AD CSFs have similar circular dichroism spectra and parameters. A) Far-UV CD spectra of five representative non-AD and five representative AD CSF

samples. B) Box plots reporting the ellipticity (θ) at 222 nm in all non-AD and AD CSF samples. C) Intrinsic fluorescence spectra of five representative non-AD and five representative AD CSF samples. D) Box plots reporting the fluorescence intensity at *λmax* in all non-AD and AD CSF samples. E) Box plots reporting the wavelength of maximum intrinsic fluorescence (*λmax*) in all non-AD and AD CSF samples. In panels B,D,E the boxes represent the central distributions of the individual points (from 25th to 75th percentile), the horizontal lines within the boxes are the median values, the whiskers are the range of values from the minimum to the maximum, excluding outliers, and the dots are individual experimental points.

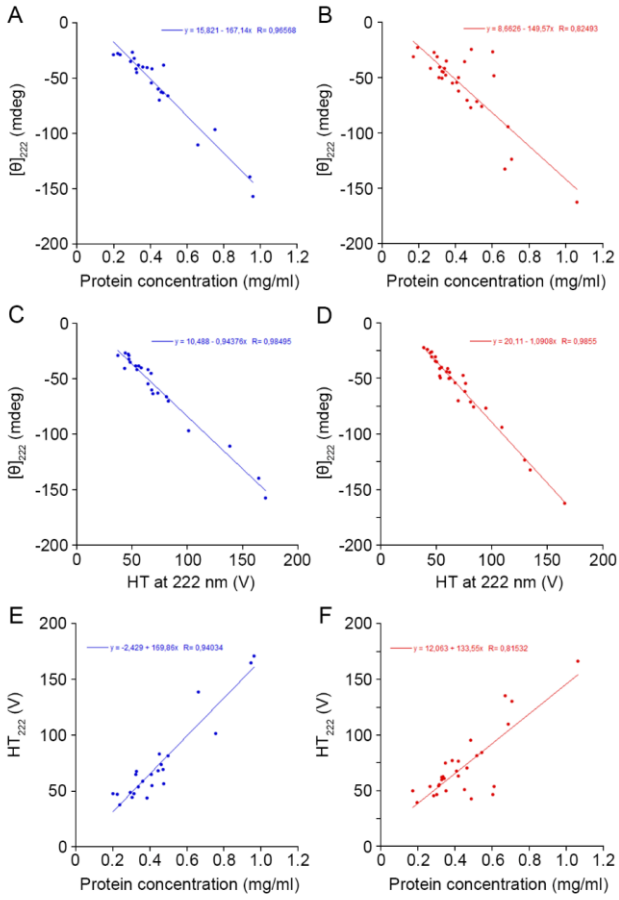

Figure 2.4 - Scatter plots reporting the dependence of θ_{222} on protein concentration, the dependence of θ_{222} on HT_{222} and the dependence of HT_{222} on protein concentration measured with the Bradford assay in non-AD and AD CSF samples. A-B) Scatter plots reporting the dependence of θ_{222} on protein concentration in non-AD A) and AD B) CSF samples. C-D) Scatter plots reporting the dependence of θ_{222} on HT_{222} in non- AD C) and AD D) CSF samples. D-E) Scatter plots reporting the dependence of HT_{222} on protein concentration measured with the Bradford assay in non-AD E) and AD F) CSF samples.

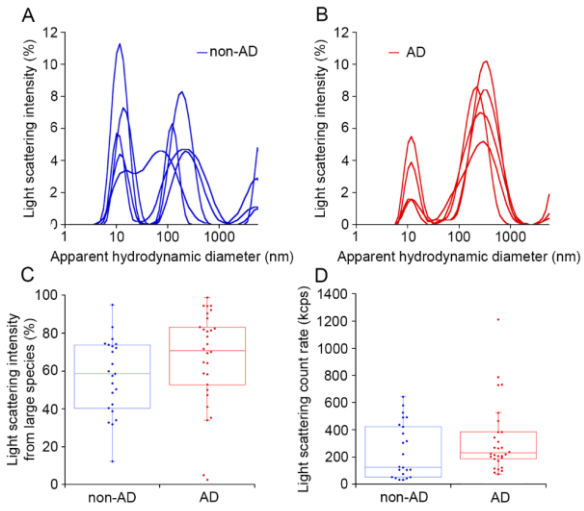

Figure 2.5 - Non-AD and AD CSFs have different quantities of protein aggregates. A-B) Size distributions by light scattering intensity (*LSI*) of particles present in five representative non-AD A) and five representative AD B) CSF samples acquired with DLS. C) Box plots reporting the *LSI* values from large species in all non-AD and AD CSF samples. D) Box plots reporting the light scattering count rate (*LSCR*) in all non-AD and AD CSF samples. The boxes, horizontal lines, whiskers and individual dots have the same meaning as in Figure 2a.

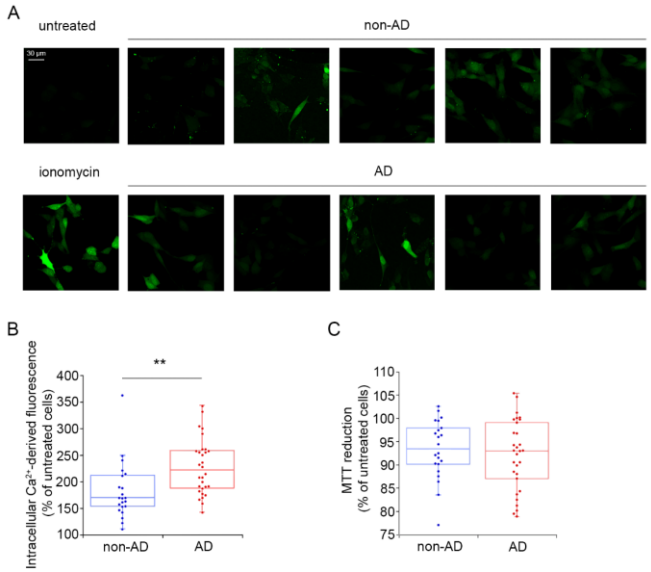

Figure 2.6 - Non-AD and AD CSFs have different abilities to destabilize cell membranes. A) Representative confocal microscope images showing the intracellular Ca^{2+} levels in SH-

SY5Y cells treated for 5 h with CSF samples of five non-AD and five AD patients. Untreated cells and cells treated with 1 μM ionomycin for 2 h are also shown as negative and positive controls, respectively. B) Box plots reporting the semi-quantitative analysis of all the Ca^{2+}-derived fluorescence values. C) Box plots reporting the MTT reduction values in SH-SY5Y cells treated for 24 h with CSF samples of all non-AD and all AD patients. The boxes, horizontal lines, whiskers and individual dots have the same meaning as in Figure 2a. The two populations were compared with the Student *t* test (** $p < 0.01$).

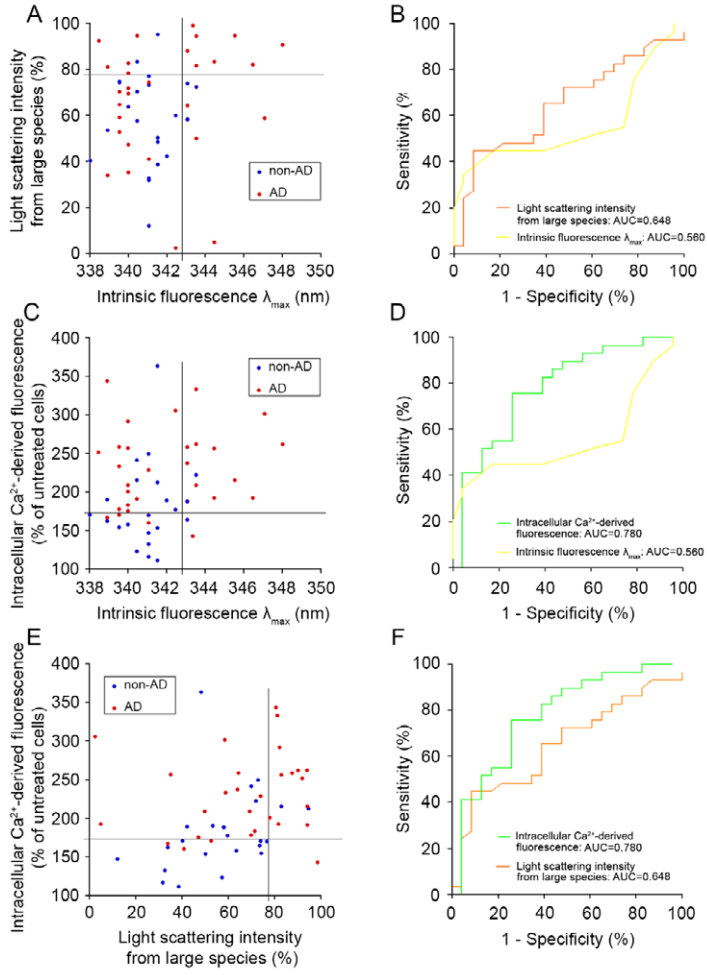

Figure 2.7 - Evidence for fluorescence, DLS, and toxicity parameters as potential AD biomarkers. A) Scatter plot for *LSI* from large protein species versus intrinsic fluorescence *λmax* with the optimized thresholds (*t**) derived from optimization of the Youden's indexes of the two parameters (horizontal and vertical lines, respectively). B) Corresponding ROC curves of the two parameters. AUC values are indicated for each parameter. C) Scatter plot for intracellular Ca^{2+} levels versus intrinsic fluorescence λ_{max} with the optimized thresholds (*t**) as horizontal and vertical lines, respectively. D)

Corresponding ROC curves of the two parameters. AUC values are indicated for each parameter. E) Scatter plot for intracellular Ca^{2+} levels versus *LSI* from large species with the optimized thresholds (t^*) as horizontal and vertical lines, respectively. F) Corresponding ROC curves of the two parameters. AUC values are indicated for each parameter. Non-AD (blue) and AD (red) CSF samples categorized to occupy the first quadrant (below both t^* values) or the remaining three quadrants (above at least one t^* value) provide a good separation between non-AD and AD patients.

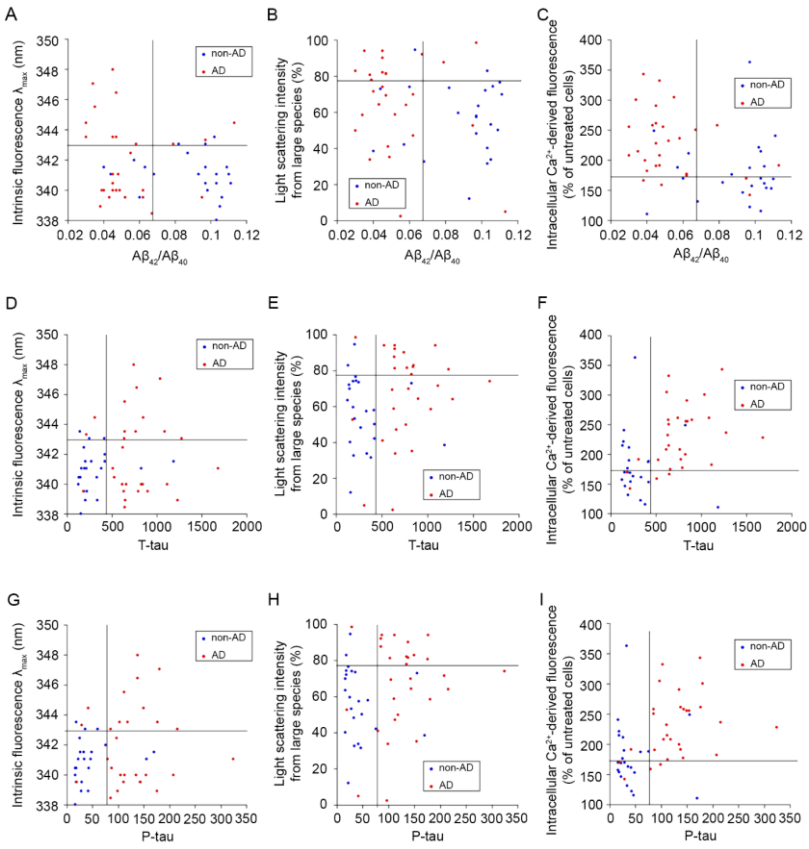

Figure 2. 8 - Comparison between novel and classical biomarkers. A,B,C) Scatter plots for intrinsic fluorescence *λmax* (A), *LSI* from large species (B) and intracellular Ca^{2+}-derived fluorescence (C) versus $A\beta_{42}/A\beta_{40}$ ratio. D,E,F) Scatter plots for intrinsic fluorescence *λmax* (D), *LSI* from large species (E) and intracellular Ca^{2+}-derived fluorescence (F) versus T-tau. G,H,I) Scatter plots for intrinsic fluorescence *λmax* (G), *LSI* from large species (H) and intracellular Ca^{2+}-derived fluorescence (I) versus P-tau. In all cases, the optimized thresholds (t^*) derived from optimization of the Youden's indexes of each couple of parameters are represented as horizontal and vertical lines, respectively. Non-AD (blue) and AD (red) CSF samples categorized to occupy the bottom-right quadrant or the remaining three quadrants (A-C), or the bottom-left quadrant or the remaining three quadrants (D-I) provide a good separation between non-AD and AD patients

Chapter 3
Second Section: A single domain antibody detects and neutralises toxic $A\beta_{42}$ oligomers in the Alzheimer's disease CSF

1. DesAb-O selectively detects synthetic $A\beta_{42}$ oligomers *in vitro*

We firstly evaluated the specificity of DesAb-O against different $A\beta_{42}$ conformers by dot- blot analysis. $A\beta_{42}$ conformers were assembled *in vitro* according to well-defined protocols. Thus, toxic A+ and nontoxic A- oligomers (Ladiwala *et al.* 2012), toxic $A\beta_{42}$ ADDLs (Lambert *et al*. 1998) and two types of fibrils, namely F1 (Ladiwala *et al.* 2012) and F2 (Dahlgren *et al*. 2002) were formed and their identities were confirmed by routinely analysing them by atomic force microscopy (AFM) and dot-blots using their respective conformation-sensitive Abs, as previously reported (Banchelli *et al.* 2020). The various $A\beta_{42}$ species were then deposited (2 µl, corresponding to 0.1 µg) onto a nitrocellulose membrane and detected with the different Abs. As controls, we used the 19.3 Ab, specific for amyloid β-derived diffusible ligands (ADDLs) (Savage *et al*. 2014), A11 Ab, recognizing toxic oligomers from various proteins, but not their monomeric or fibrillar conformations (Kayed *et al.* 2003), and OC Ab, specifically raised against fibrillar aggregates (Kayed *et al.* 2007).

DesAb-O was found to selectively target toxic A+ oligomers and ADDLs, with a minor cross-reaction with nontoxic A- oligomers (Figure 3.1 A). As expected, each of the above mentioned control Abs bound to their targeted conformers according to previous reports (Kayed *et al.* 2003; Kayed *et al.* 2007; Ladiwala *et al.* 2012; Savage *et al*. 2014; Bigi *et a.*, 2020). Proper loading of each $A\beta_{42}$ species was confirmed by the sequence-specific 6E10 Ab which targets the N-terminus of $A\beta_{42}$ (Kim *et al*. 1990; Kayed *et al*. 2003; Kayed *et al*. 2007;

Liliana Napolitano, liliana98.napolitano@gmail.com, 0009-0004-3087-286X

Referee List (DOI 10.36253/fup_referee_list)
FUP Best Practice in Scholarly Publishing (DOI 10.36253/fup_best_practice)

Liliana Napolitano, Second Section*: A single domain antibody detects and neutralises toxic $A\beta_{42}$ oligomers in the Alzheimer's disease CSF*, © Author(s), CC BY 4.0, DOI 10.36253/979-12-215-0993-9.05, in Liliana Napolitano, *A multidisciplinary approach for the early diagnosis of Alzheimer's disease and potential therapeutic applications*, pp. 79-93, 2026, published by Firenze University Press, ISBN 979-12-215-0993-9, DOI 10.36253/979-12-215-0993-9

Book References DOI 10.36253/979-12-215-0993-9.references

Baghallab *et al*. 2018), which bound all the analysed $A\beta_{42}$ species, independently of their aggregation state (Figure 3.1 A).

We then assessed the sensitivity of DesAb-O by evaluating its ability to probe decreasing amounts of $A\beta_{42}$ conformers (0.10, 0.05, 0.025, 0.01 and 0.005 μg), previously deposited onto a nitrocellulose membrane (Figure 3.1 B). DesAb-O was found to detect A+ oligomers and ADDLs down to 0.01 μg, which when compared to the control 19.3 Ab, appeared more sensitive (Figure 3.1 B).

The reactivity of DesAb-O against $A\beta_{42}$ species was also quantified by performing an indirect ELISA assay. Briefly, we coated the wells of the ELISA plates with increasing concentrations of $A\beta_{42}$ conformers (0, 1, 5 and 10 μM). We then incubated the plates with DesAb-O and subsequently with the appropriate secondary Abs. Our results showed that DesAb-O clearly recognized toxic A+ oligomers and ADDLs at 5 and 10 μM, with a specificity that increased with aggregate concentration (Figure 3.1 C), revealing no affinity for the monomeric or fibrillar forms even at high concentrations (Figure 3.1 C). The 19.3 Ab was also assessed for a relative comparison, revealing high affinity for A+ oligomers and ADDLs, even at 1 μM for the former species, but showing a minor specificity for $A\beta_{42}$ monomers (Figure 3.1 D). As expected, the 6E10 Ab, was found to detect all the analysed $A\beta_{42}$ conformers in a dose-dependent manner (Figure 3.2), as the $A\beta_{42}$ N-terminus is solvent-exposed regardless of the aggregated state of the peptide (De *et al*. 2019). Overall, dot-blot and ELISA results demonstrate the ability of DesAb-O to selectively discriminate $A\beta_{42}$ conformers, in agreement with previously established work (Aprile *et al*. 2017; Aprile *et a*. 2020). Moreover, the affinity of DesAb- O against $A\beta_{42}$ oligomers and its selectivity for the oligomeric species with respect to the monomers and fibrils do not seem to be any worse than those observed with commercially available Abs, providing the platform for further applications.

2. DesAb-O detects synthetic $A\beta_{42}$ oligomers bound to neuronal membrane and internalized into the cytosol

To analyse whether or not the ability of DesAb-O to selectively detect $A\beta_{42}$ oligomers *in vitro* are also reflected in cultured cells, human neuroblastoma SH-SY5Y cells were exposed for 1 h to different types of $A\beta_{42}$ species at 3.0 μM (monomer equivalents) and then the plasma membrane (red channel) and $A\beta_{42}$ aggregates (green channel) were counterstained and analysed by the super-resolution stimulated emission depletion (STED) microscope (Cascella *et al.* 2021) (Figure 3.3 and 3.4). DesAb-O was found to detect toxic A+ oligomers and ADDLs (Figure 3.4 A), showing an increase of the green fluorescent signal by 1362 ± 46% and 1010 ± 45%, respectively, with respect to the untreated cells, taken as 100% (Figure 3.4 B). In particular, by analysing different optical sections (apical, median and basal planes to the coverslip) DesAb-O can identify these oligomers bound to the neuronal membranes and penetrating into the cells

(Figure 3.3).

Similar results were obtained with the 19.3 Ab (1010 ± 99% and 1235 ± 39%) and to a lower extent with the A11 one (680 ± 66% and 633 ± 97%) (Figure 3.4 A,B). Interestingly, the 19.3 and A11 antibodies exhibited a green fluorescence signal in foci, in contrast to the diffused green fluorescence observed in DesAb-O. Indeed, this variation can be attributed to the small dimensions and the high sensitivity of the sdAb for oligomeric conformers, which facilitates binding to a higher number of epitopes on the oligomer surface. OC Ab specifically recognized both types of fibrillar conformers (F1 and F2), which appeared predominantly bound to the plasma membranes, and the green fluorescent signal increased by 557 ± 55% and 562 ± 57% for the former type of fibril (Ladiwala *et al*. 2012) and the latter type of fibril (Dahlgren *et al.* 2002), respectively (Figure 3.4 A,B). As expected, the sequence-specific 6E10 Ab detected both A+ oligomers and ADDLs and F1 and F2 fibrils on neuronal cells (Figure 3.4 A,B). None of the Abs detected nontoxic A- oligomers, that evoked a very low and undetectable fluorescent signal because they are known to weakly interact with neuronal membranes (Ladiwala *et al.* 2012; Banchelli *et al*. 2020; Bigi *et al*. 2020).

Overall, in our experimental conditions DesAb-O selectively discriminated toxic $A\beta_{42}$ oligomers with respect to monomeric and fibrillar forms of the peptide, at least similarly to the other commercially available conformation-sensitive Abs, suggesting a very promising potential for the detection of harmful $A\beta_{42}$ species in biological fluids.

3. DesAb-O inhibits the interaction of $A\beta_{42}$ oligomers with neuronal membranes preventing mitochondrial dysfunction

We further evaluated whether DesAb-O was also able to capture $A\beta_{42}$ oligomers, preventing their detrimental effects on neuronal cells. To this purpose, A+ oligomers and ADDLs were pre-incubated for 1 h with DesAb-O or the A11 Abs at increasing molar ratios between oligomers and Abs (from 1:0.1 to 1:1), and these solutions were then added to the cell culture medium of SH-SY5Y cells for 15 min. Unlike previous experiments, the oligomers were added to cultured cells only after pre-incubation with DesAb-O. To detect only the oligomers bound to the cell surface, the cellular membrane was not permeabilized at this stage, thus preventing antibody internalization. The binding affinity of the aggregates for cellular membranes was assessed by confocal microscopy using the 6E10 Ab as a probe. Our results showed a strong colocalization of $A\beta_{42}$ A+ oligomers and ADDLs with the neuronal membranes in the absence of the pre-incubation with Abs (Figure 3.5 A), confirming previously reported data (Schengrund 2010; Evangelisti *et al.* 2013; Bigi *et al*. 2020). Notably, the binding of both types of $A\beta_{42}$ aggregates was significantly reduced in the presence of DesAb-O up to 1:0.1 molar ratio (by 40 ± 3% and 36 ± 2%, respectively) (Figure 3.5 A,C). The same analysis was performed with the A11 Ab, which was found to prevent the

interaction of the oligomers with the membrane only at 1:1 molar ratio (by 44 ± 5% and 48 ± 7%, respectively) (Figure 3.5 B,D). These results again suggested a great affinity of DesAb-O for the oligomers, at least equal to that of a traditional conformation-sensitive Ab.

We then evaluated whether DesAb-O was also able to prevent the neurotoxic effects evoked by $A\beta_{42}$ aggregates, by analysing their mitochondrial status with the MTT reduction test. $A\beta_{42}$ species (3.0 μM) were incubated in the absence or presence of an equimolar concentration of DesAb-O for 1 h, and then these solutions were added to the culture medium of SH-SY5Y cells for 24 h. Our results showed that A+ oligomers and ADDLs significantly reduced (by 31 ± 3% and 35 ± 3%, respectively) the mitochondrial activity of SH-SY5Y cells as compared to untreated cells (Figure 3.5 E), as previously shown (Kayed *et al*. 2003; Ladiwala *et al*. 2012; Evangelisti *et al*. 2016; Cascella *et al*. 2017; Bigi *et al.* 2020). Both types of fibrils were also found to be significantly toxic, even if to a lesser extent with respect to the oligomeric species (the reduction of cell viability was 21 ± 2% and 17 ± 2% for F1 and F2, respectively, as reported in Figure 3.5 E), confirming previous data (Dahlgren *et al*. 2002; Ladiwala *et al*. 2012; Bigi *et al*. 2020). When A+ oligomers and ADDLs were pre-incubated for 1 h in the presence of DesAb-O, we observed a significant improvement of mitochondrial function (by 18 ± 4% and 11 ± 3%, respectively, with respect to cells treated with the same species in the absence of DesAb-O), whereas the fibrils-induced neurotoxicity was not affected by DesAb-O (Figure 3.5 E), confirming again its high specificity in the targeting of $A\beta_{42}$ oligomeric conformations. The same analysis was performed with the 19.3 and A11 Abs, that were found to significantly prevent the cytotoxicity induced by A+ oligomers (increase of MTT reduction by 15 ± 5% and 18 ± 4%, respectively) and ADDLs (by 13 ± 3% and 22 ± 3%, respectively), whereas the OC Ab markedly suppressed the cytotoxicity of fibrillar conformations (by 16 ± 4% and 16 ± 5%, respectively), as already shown (Bigi *et al*. 2020). Of note, DesAb-O did not affect neuronal viability when added alone to the cell culture medium, thus making it an excellent tool for future tentative therapeutic applications.

4. DesAb-O detects $A\beta_{42}$ oligomers in the CSF of AD patients *in vitro*

Considering the encouraging data obtained with DesAb-O both *in vitro* and in cultured cells, we then assessed its ability to identify $A\beta_{42}$ species that are present in the CSF of AD patients with respect to the CSF of age-matched control subjects. We performed a series of proof-of-concept experiments on a small set of clinical samples of CSF (n = 9 from AD and n = 4 from controls) to explore whether our assays could detect differences between the two groups. We first performed a sandwich dot-blot analysis by spotting 2 μl of the capture Abs 6E10 and DesAb-O (corresponding to 0.01 mg/ml and 10 μM, respectively) onto a nitrocellulose membrane that was then incubated with 1.5 ml of $A\beta_{42}$ species at 2 μM or CSF from AD patients and controls at 0.1 mg/ml. The membranes were

then revealed with the 6E10 Ab. This approach, which is different from the classical dot-blot employed in Figure 3.1 A,B, is useful in a context in which the amount of oligomers we expected to have in the CSF of AD patients was very low. The 6E10 Ab, as expected, showed positive signal with all samples, including the CSFs (Figure 3.6 A). Despite the improved sensitivity in the recognition of oligomeric species, that gave rise to a high signal (Figure 3.6 A), DesAb-O was also found to generate a slight cross- reaction with monomers and to a minor extent with fibrils. Interestingly, an intense spot was observed following the incubation of DesAb-O with AD CSF and only a weak signal with the control CSF (Figure 3.6 A).

To further demonstrate the capability of DesAb-O to identify $A\beta_{42}$ oligomers in the CSF of AD patients with respect to control individuals, we performed a sandwich indirect ELISA assay, again to improve specificity and sensitivity. Briefly, we coated the ELISA plate with 1 μM DesAb-O and incubated with decreasing concentrations (4500, 2250, 450, 45, 4,5 and 2,25 pg/ml) of $A\beta_{42}$ species ($A\beta_{42}$ monomer (M), A+ oligomers, and fibrils (F1) prepared according to Ladiwala *et al*. 2012), the CSF from AD patients (n = 9) and that from control subjects (n = 4) at the concentration of 0.25 mg/ml. The plates were then probed with 6E10 as detection Ab. We found that DesAb-O significantly recognized A+ oligomers (Figure 3.6 B, orange bars) down to 2.25 pg/ml with respect to the monomeric and fibrillar forms of $A\beta_{42}$ (Figure 3.6 B, blue and grey bars, respectively), showing a lower affinity for these forms only at the highest concentration. As a control, we used monomeric αSyn, which was not recognized by DesAb-O, demonstrating again its high specificity for $A\beta_{42}$ (Figure 3.6 B, yellow bar). Notably, DesAb-O generated a high signal with the CSFs of AD patients (Figure 3.6 B, magenta bar) that appeared significantly different from that obtained with those of control subjects (Figure 3.6 B, green bar).

The ability of DesAb-O to detect $A\beta_{42}$ oligomers in the CSFs of AD patients was also exploited by super-resolution STED microscopy (Cascella *et al*. 2021). $A\beta_{42}$ species (25 μM) and CSFs from AD patients and controls (0.5 mg/ml) were deposited on a glass coverslip and labelled with 6E10 and DesAb-O Abs. As expected, the 6E10 Ab clearly recognized both preformed A+ oligomers and fibrils, even in a 1:1 mixture between oligomeric and fibrillar species (Figure 3.6 C). In particular, A+ oligomers exhibited green-fluorescent punctae, which appeared to be small and globular at the very high magnifications allowed by STED microscopy, whereas F1 appeared fibrillar in morphology (Figure 3.6 C, bottom box magnifications). Monomeric $A\beta_{42}$ is difficult to detect (Figure 3.6 C), in agreement with the results obtained in a cellular context (Figure 3.6 A,B). For this reason, the 6E10 Ab did not detect Aβ species in control CSF AD samples, whereas it did with AD CSFs, recognizing green fluorescent punctae, globular in shape, some of which apparently larger than oligomeric species (Figure 3.6 C, bottom box magnifications). In contrast, DesAb-O clearly recognizes A+ oligomers rather than fibrils, revealing the presence of small globular green fluorescent punctae in the solutions containing 1:1 mixture (Figure 3.6 C, bottom box magnifications). We then evaluated the CSFs, observing that DesAb-O can

selectively detect small, globular and round species compatible with $A\beta_{42}$ oligomers in the CSFs of AD patients, displaying no signal in the control ones (Figure 3.6 C, bottom box magnifications).

To validate our experimental approach, we tested another sdAb named $DesAb_{18–24,}$ which has been rationally designed to target $A\beta_{42}$ fibrils, specifically the region VFFAEDVG (De *et al*. 2019; Aprile *et al*. 2017). We thus performed a sandwich indirect ELISA assay by coating the wells with 0.5 μM $DesAb_{18–24}$ and then performing the test as described above. Our results showed that $DesAb_{18–24}$ clearly recognizes $A\beta_{42}$ fibrils down to 4.5 pg/ml, with low affinity for monomeric $A\beta_{42}$ down to 4500 pg/ml and no binding for A+ oligomers, except at the highest concentration (Figure 3.7 A). Notably, $DesAb_{18–24}$ was found to generate a higher absorbance value from the control CSFs with respect to that observed from AD patients, because of the high cross-reaction with the monomers (Figure 3.7 A), confirming the difference in terms of total $A\beta_{42}$ between patients and controls reported in literature.

The specificity of $DesAb_{18–24}$ was also evaluated by STED microscopy, showing a clear detection of preformed $A\beta_{42}$ fibrils, without any signal for both CSFs as the monomeric protein is difficult to reveal in this experimental condition (Figure 3.7 B).

5. DesAb-O detects $A\beta_{42}$ oligomers present in AD CSFs upon their interaction with neuronal cells

To further evaluate the ability of DesAb-O to target $A\beta_{42}$ oligomers present in the CSFs of AD patients, we applied high resolution STED microscopy to SH-SY5Y cells exposed to ADDLs, or to the CSFs of AD patients and age-matched control subjects (without pre- incubation with Abs). Following the administration for 5 h of ADDLs at 3.0 μM (monomer equivalents) or CSFs diluted 1:1 with the extracellular medium, the $A\beta_{42}$ aggregates (green channel) were counterstained with DesAb-O or 6E10 Abs and cell membrane (red channel) with wheat germ agglutinin (WGA, Figure 3.8 A,B). Cells exposed to ADDLs exhibited green-fluorescent punctae, which appeared to be small and globular at the very high magnifications allowed by STED microscopy (Figure 3.8 A,B, bottom image magnification). The DesAb-O derived green-fluorescent signals were consistent with the results obtained with the 6E10 Ab. In particular, the semi-quantitative analysis revealed that the oligomeric species are localised both intracellularly and extracellularly. Notably, DesAb-O can recognize a number of small and globular intracellular and extracellular $A\beta_{42}$ species in the CSFs of AD patients, with a morphology that resembles that of the oligomeric species (Figure 3.8 A, bottom image magnification). In addition to the small oligomeric species, the 6E10 Ab can also recognize larger aggregates in the CSFs of AD patients that, at high magnification, appeared round in morphology (Figure 3.8 B, bottom image magnification). In contrast, cells treated with the CSFs of control subjects and counterstained with both DesAb-O and 6E10 showed the presence of few $A\beta_{42}$

aggregates outside the cells or attached to the membrane, which probably represent nontoxic oligomers that are not able to permeabilize the cell membrane or low amounts of toxic oligomers that do not manifest their toxicity due to their small quantity (Figure 3.8 A,B, bottom image magnification).

Similar results were obtained in primary rat cortical neurons exposed to AD and control CSFs and labelled with DesAb-O (Figure 3.8 C).

6. DesAb-O prevents neuronal dysfunction induced by the CSFs of AD patients.

We finally evaluated whether DesAb-O can also neutralise the cytotoxicity of oligomers present in the CSFs of AD patients. A relatively high volume (ml of sample) is required to perform these experiments, so they were performed on 4 AD and 4 age-matched control CSFs. We first monitored the dysregulation of cytosolic Ca^{2+} homeostasis, which is an early upstream event evoked by extracellular $A\beta_{42}$ oligomers both in cultured neuronal cells and in relevant mouse AD models, where Ca^{2+} ions flow from the extracellular space to the cytosol (Demuro *et al*. 2005; Arbel-Ornath *et al*. 2017; Cascella *et al*. 2021; Fani *et al*. 2022; Bigi *et al*. 2023a; Bigi *et al*. 2023b). SH-SY5Y cells were treated for 5 h with the CSFs from AD patients and control subjects diluted 1:1 with the cell culture medium, following or not a 1 h pre-incubation with DesAb-O at 3 μM. The CSFs of AD patients caused a significant influx of Ca^{2+} ions (by 230 ± 11%) relative to untreated cells (Figure 3.9 A), whereas the CSFs of control subjects generated only a slight and non- significant alteration of Ca^{2+} homeostasis (Figure 3.9 A). A 1 h pre-incubation with DesAb-O significantly reduced the effect induced by the CSFs of AD patients (by 77 ± 20%), without affecting that observed in cells treated with the control ones (Figure 3.9 A). As a positive control, ADDLs were found to generate an extensive Ca^{2+} influx (by 405 ± 15%, Figure 3.9 A), that markedly decreased (by 250 ± 26%) following a 1 h pre-incubation with DesAb-O. Similar results were obtained in primary rat cortical neurons exposed for 2.5 h to the CSFs of AD patients and control subjects following or not a 1 h pre-incubation with DesAb-O at 3 μM (Figure 3.9 B). These results confirm the high specificity of DesAb-O in the targeting of neurotoxic $A\beta_{42}$ conformers present in AD CSFs.

The protective effect of DesAb-O was also observed from the analysis of the alteration of membrane permeability induced by $A\beta_{42}$ oligomers, monitoring the release of the fluorescent probe calcein-acetoxymethyl (AM), previously loaded into the cells (Cascella *et al*. 2017). SH-SY5Y cells, pre-loaded with calcein-AM, were treated with the CSFs of AD patients and controls diluted 1:1 with the extracellular medium for 5 h following or not a 1 h pre-incubation with DesAb-O at 3 μM. Unlike control CSFs, the AD ones caused a significant permeabilization of the cellular membrane relative to untreated cells, albeit to a lesser extent than ADDLs used as a positive control (Figure 3.9 C). Interestingly, DesAb-O can significantly prevent the membrane permeabilization induced by AD CSFs causing

an increase of intracellular calcein-derived fluorescence (by 23 ± 9%), although to a minor extent with respect to that evoked by ADDLs (by 41 ± 11%) (Figure 3.9 C). We also carried out an MTT reduction test following the administration of CSFs diluted 1:1 with the extracellular medium for 24 h. Unlike the control CSFs, those derived from AD patients caused a modest reduction of the mitochondrial activity of cells (by 19 ± 1%) that was reduced by the 1 h pre-incubation with 3 µM DesAb-O, evident as an improvement of mitochondrial function of 11 ± 2% (Figure 3.9 D). ADDLs caused a significant reduction of cell viability (by 36 ± 4%), that was prevented by DesAb-O, evident as an improvement of mitochondrial function of 15 ± 7% (Figure 3.9 D), confirming previous results shown in Figure 3.5 E.

Overall, these results confirmed the selective ability of DesAb-O to bind and neutralise both *in vitro* synthesised and patient-derived $A\beta_{42}$ oligomers, representing a promising tool for a future diagnostic, therapeutic and prognostic application in AD.

7 Chapter 3: figures and tables

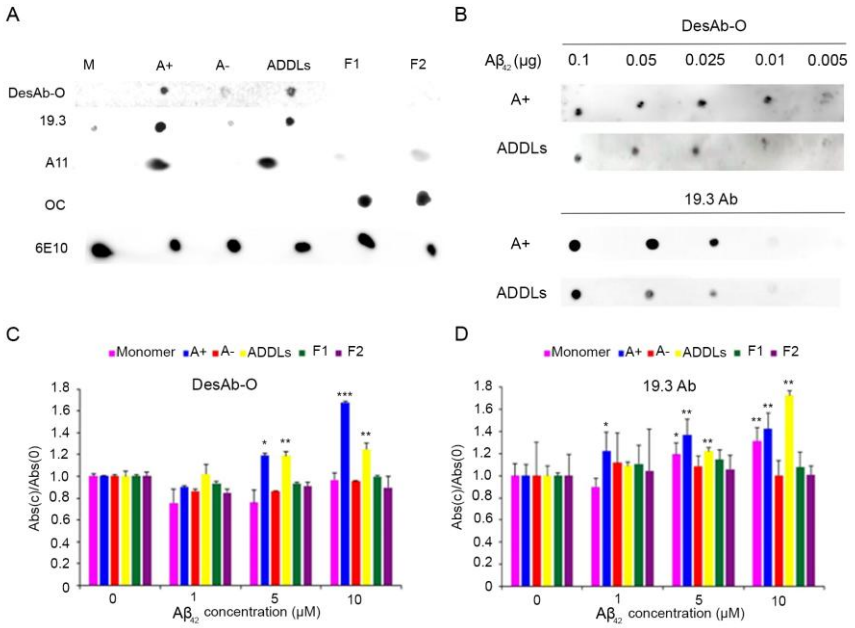

Figure 3.1 - DesAb-O selectively detects synthetic $A\beta_{42}$ oligomers *in vitro*. A-B) Dot-blot analysis of Aβ42 species. (A) Samples of monomeric $A\beta_{42}$ (M), oligomeric (A+,A- and ADDLs) and two type of fibrillar species (F1 from Ladiwala *et al.*, 2012 and F2 from Dahlgren *et al*., 2002) were deposited (2 µl/spot, corresponding to 0.1 µg) onto a nitrocellulose membrane and detected with the indicated Abs. (B) Samples of A+ oligomers and ADDLs at various amounts (0.25, 0.10, 0.05, 0.025, 0.01, 0.005 µg) were probed with DesAb-O (top) and 19.3 (bottom) Abs. C-D) ELISA measurements taken at increasing

concentration of $A\beta_{42}$ species using DesAb-O (C) and 19.3 (D) Abs. Data were normalized for the corresponding average value at concentration 0 μM. Experimental errors are S.D. (n = 3). Samples were analysed by Student t test relative to 0 μM (*P<0.05, ** P<0.01 and ***P<0.001).

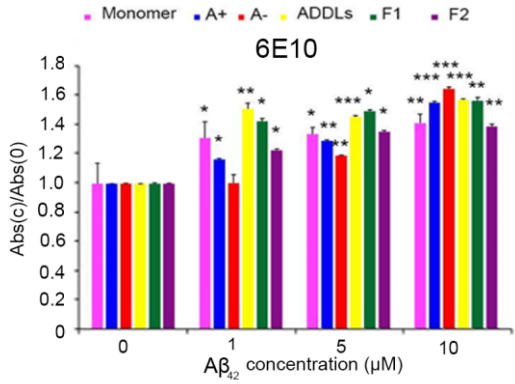

Figure 3.2 - 6E10 Ab detects all $A\beta_{42}$ species in a dose-dependent manner. Indirect ELISA measurements taken at increasing concentration of $A\beta_{42}$ species using the 6E10 Ab. Data were normalised for the corresponding average value at concentration 0 μM. Experimental errors are S.D. (n = 3). Samples were analysed by Student *t* test relative to 0 μM (*P<0.05, ** P<0.01 and ***P<0.001).

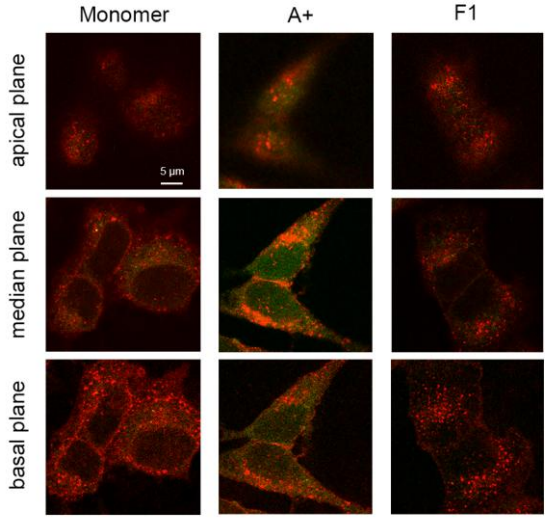

Figure 3.3 - DesAb-O detects $A\beta_{42}$ oligomers bound to the neuronal membrane and internalized into the cytosol. Representative STED microscopy images showing the basal, median, and apical sections of SH-SY5Y cells treated for 1 h with the indicated $A\beta_{42}$

species at 3.0 μM (monomer equivalents). Red and green fluorescence indicates respectively the cell membranes and the $A\beta_{42}$ species, detected with wheat germ agglutinin (WGA) and DesAb-O Ab.

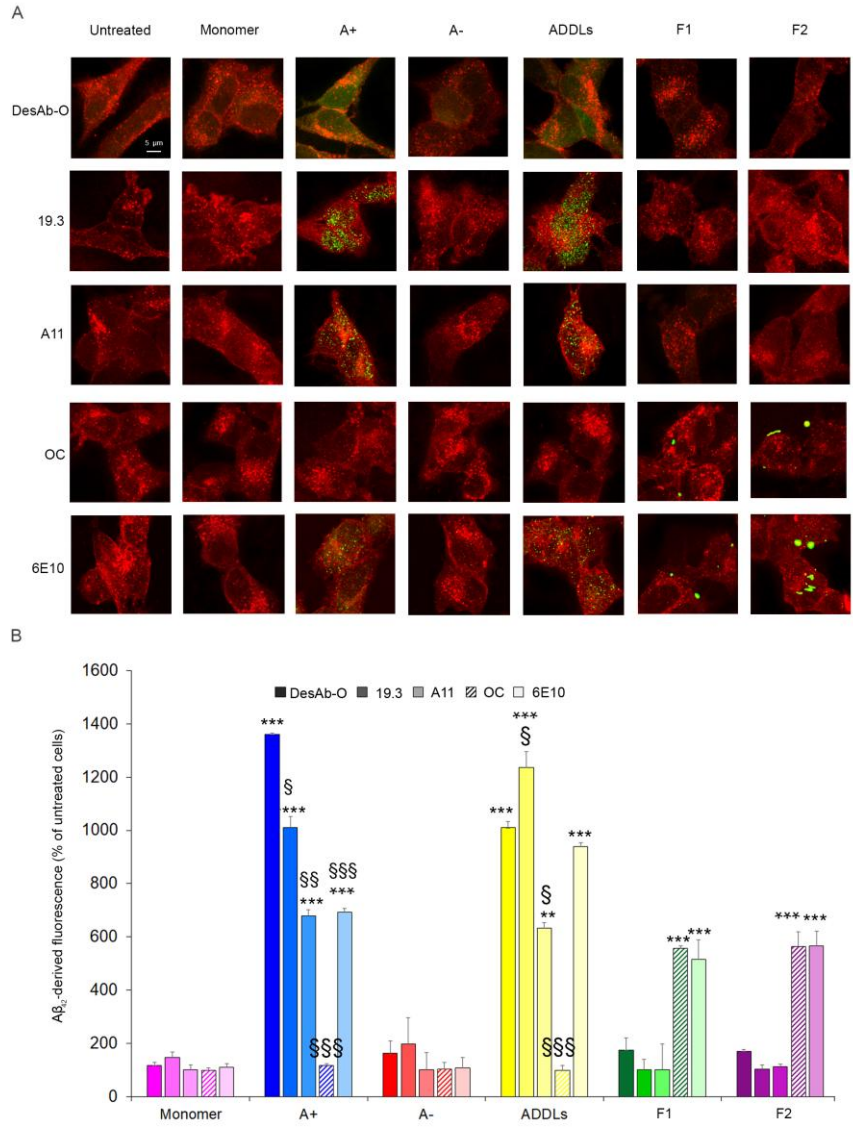

Figure 3.4 - DesAb-O detects synthetic $A\beta_{42}$ oligomers interacting with neuronal cells. A) Representative STED microscopy images of SH-SY5Y cells treated with the indicated Aβ42 species at 3.0 μM (monomer equivalents) for 1 h. Red and green fluorescence indicates respectively the cell membranes and the $A\beta_{42}$ species, detected with the indicated Abs. B) The results of a semi-quantitative analysis of the green fluorescent signal.

Experimental errors are S.E.M. (n = 3). Samples were analysed by Student *t* test relative to untreated cells (**P<0.01, and ***P<0.001), or to cells treated with the same $A\beta_{42}$ species and detected with DesAb-O (§P<0.05, §§P<0.01, §§§P P<0.001).

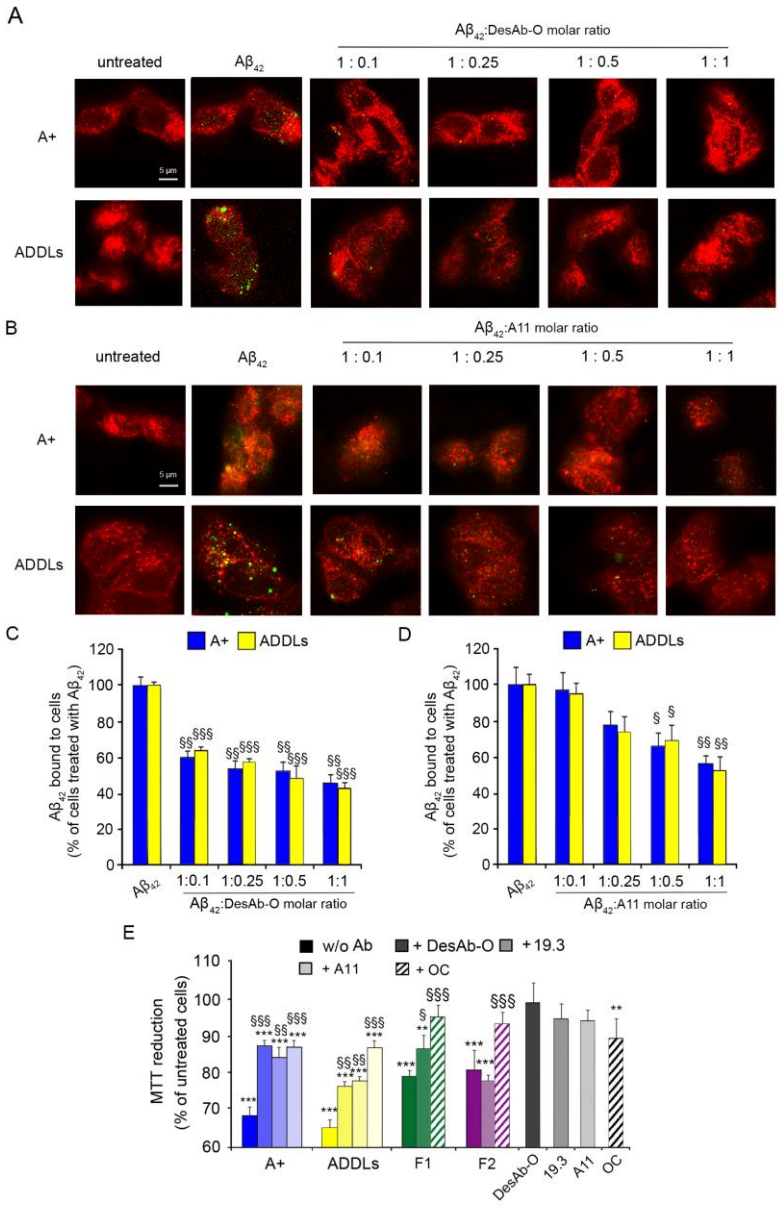

Figure 3.5 - DesAb-O inhibits the binding of $A\beta_{42}$ oligomers to the neuronal membrane

preventing their induced mitochondrial dysfunction. A-B). Representative confocal microscopy images of SH- SY5Y cells treated with 3.0 μM (monomer equivalents) A+ oligomers and ADDLs following 1 h pre- incubation in the absence or presence of DesAb-O (A) or A11 (B) Abs at the indicated $A\beta_{42}$:Abs molar ratios, where molar ratios refer to monomer equivalents. Red and green fluorescence indicates the cell membranes and $A\beta_{42}$ oligomers detected with the 6E10 Ab. C-D). Degree of membrane binding of A+ oligomers and ADDLs measured following incubation under the conditions represented in panels A and B, determined by using the ImageJ (NIH, Bethesda, MD, USA) and JACOP plugin (rsb.info.nih.gov) software. C) MTT reduction in SH-SY5Y cells treated for 24 h with the indicated $A\beta_{42}$ aggregates at a concentration of 3.0 μM (monomer equivalents) following a 1 h pre-incubation in the absence or presence of the indicated Abs. Abs alone were also tested as a control. Experimental errors are S.E.M. (n = 4). Samples were analysed by one-way ANOVA followed by Bonferroni's multiple-comparison test relative to untreated cells (*P<0.05, **P<0.01, and ***P<0.001), or to cells treated with the same $A\beta_{42}$ species without any Ab (§P<0.05, §§P<0.01, §§§P P<0.001). 200-250 (A-D) and 250,000-300,000 (E) cells were analysed per condition.

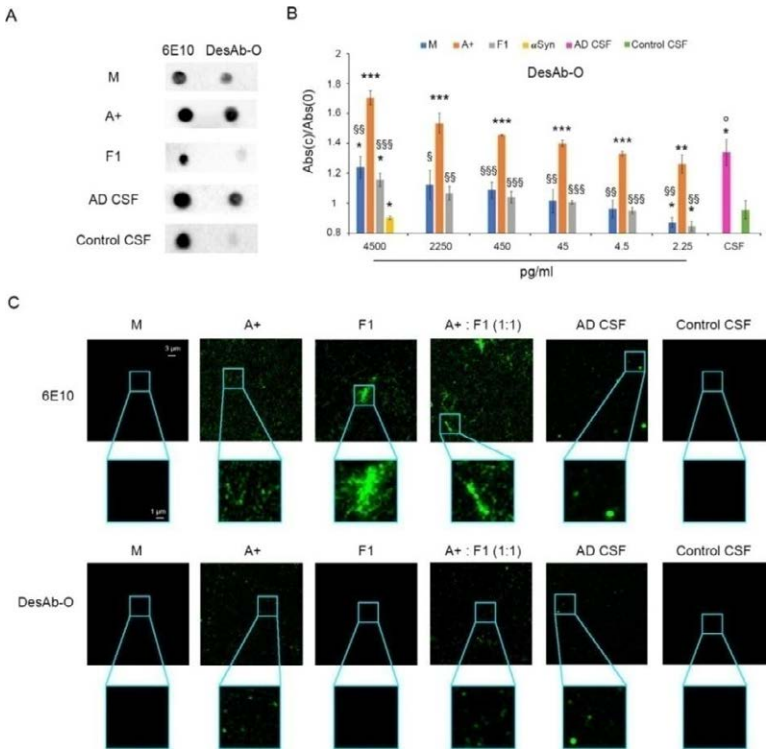

Figure 3.6 - DesAb-O detects $A\beta_{42}$ oligomers in the CSFs of AD patients *in vitro*. A) Representative sandwich dot-blot analysis of $A\beta_{42}$ species and CSFs. The capture Abs, 6E10 and DesAb-O, were spotted onto nitrocellulose membranes (2 μl corresponding to 1:100 and 10 μM). The membranes were incubated with solutions containing different $A\beta_{42}$ species (monomeric $A\beta_{42}$ (M), A+ oligomers, fibrils (F1) at 0.01 mg/ml, the CSF

from a representative AD patient (n = 9) and that from a representative control subject (n = 4) at 0.1 mg/ml. Finally, the membranes were probed with the detection 6E10 Ab. B) Sandwich indirect ELISA. 0.25 mg/ml of CSFs from AD patients and control subjects were adsorbed and quantified by using DesAb-O at 1 µM. Standard curve was obtained with decreasing concentration of $A\beta_{42}$ species formed *in vitro*. α-Synuclein monomeric protein was used as a negative control. Data were normalised for the corresponding average value at concentration 0 pg/ml. Experimental errors are S.E.M (n = 4 for synthetic samples and control CSFs and n = 9 for AD CSFs). Samples were analysed by Student *t* test relative to 0 pg/ml (* P<0.05, **P<0.01, *** P<0.001) or to A+ (§ P<0.05, §§ P<0.01, §§§P<0.001) or to control CSF (° P<0.05).C) Representative STED images showing $A\beta_{42}$ species (M, A+, F1, a mixture containing A+ and F1 at 1:1 molar ratio) and CSFs collected from AD patients and controls spotted in a glass coverslip at 25 µM and 0.5 mg/ml, respectively (n = 4 for synthetic samples and control CSFs and n = 9 for AD CSFs). The green fluorescent signals arise from the staining with 1:800 6E10 and 2 µM DesAb-O Abs. Higher magnifications of the $A\beta_{42}$ species are shown in the boxed areas.

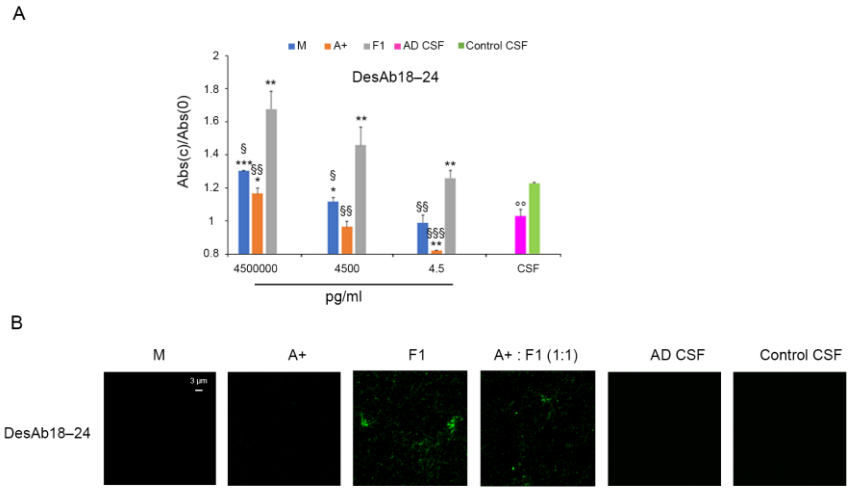

Figure 3.7 - $DesAb_{18–24}$ detects $A\beta_{42}$ fibrils and shows a non-specific signal in the CSF samples. A) Sandwich ELISA assay. 0.25 mg/ml of CSF samples from AD patients and control subjects were adsorbed and quantified using $DesAb_{18–24}$ at 0.5 µM. Standard curve was obtained with decreasing concentration of $A\beta_{42}$ species formed *in vitro*. Data were normalized for the corresponding average value at concentration 0 pg/ml). Experimental errors are S.E.M. (n = 4). Samples were analysed by Student *t* test relative to 0 pg/ml (* P<0.05, **P<0.01, *** P<0.001) or to F1 (§ P<0.05, §§ P<0.01, §§§P<0.001) or to control CSF (°° P<0.01). B) Representative STED images showing $A\beta_{42}$ species (M, A+ oligomers, F1, and a mixture containing both A+ and F1 at 1:1 molar ratio) and CSF samples collected from AD patients and controls (n = 4) spotted in a glass coverslip at 25 µM and 0.5 mg/ml, respectively. The green fluorescent signals arise from the staining with 4 µM $DesAb_{18–24}$.

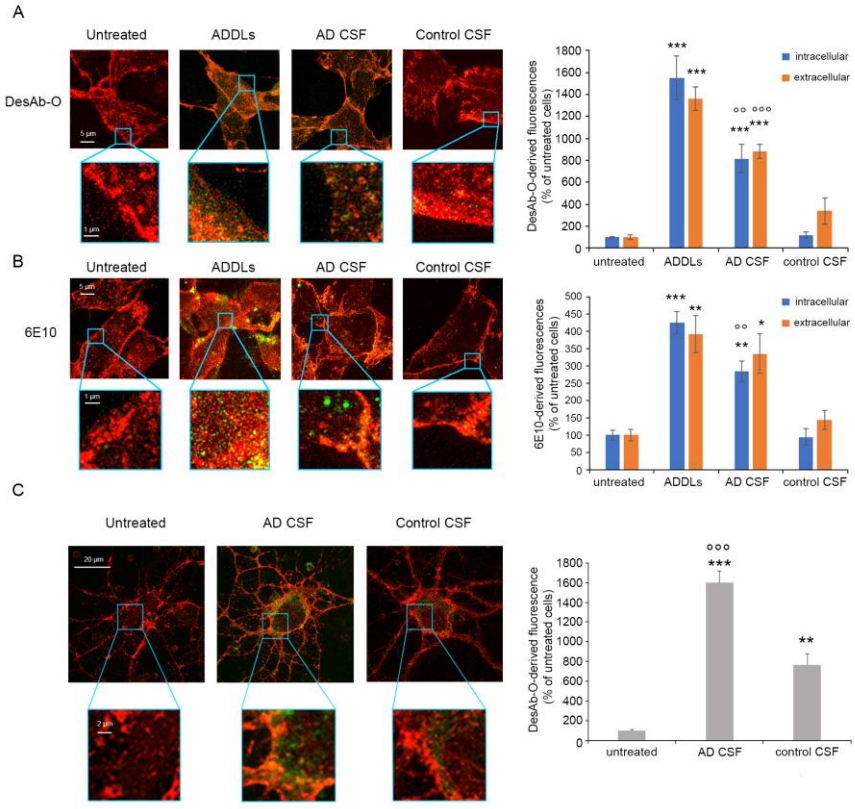

Figure 3.8 - DesAb-O detects $A\beta_{42}$ oligomers present in CSFs of AD patients upon their interaction with neuronal cells. A-B) Representative STED microscopy images of SH-SY5Y cells treated with ADDLs at 3.0 μM (monomer equivalents) or CSFs from AD patients and age-matched controls diluted 1:1 with the extracellular medium, for 5 h. Red and green fluorescence indicates the cell membranes and the $A\beta_{42}$ species detected with DesAb-O (A) and 6E10 (B), respectively. Higher magnifications of the $A\beta_{42}$ species are shown in the boxed areas. The histograms represent the results of a semi-quantitative analysis of the green fluorescent signal. C) Representative STED microscopy images of primary rat cortical neurons treated with AD and control CSFs, as reported in A-B. Red and green fluorescence indicates the cell membranes and the $A\beta_{42}$ species detected with DesAb-O, respectively. Higher magnifications of the $A\beta_{42}$ species are shown in the boxed areas. Experimental errors are S.E.M. (n = 4 for synthetic samples and control CSFs and n = 9 for AD CSFs). 200-250 cells were analysed per condition. Samples were analysed by Student *t* test relative to untreated cells (**P<0.01 and ***P<0.001), or to cells treated with control CSFs (°°P<0.01 and °°°P<0.001).

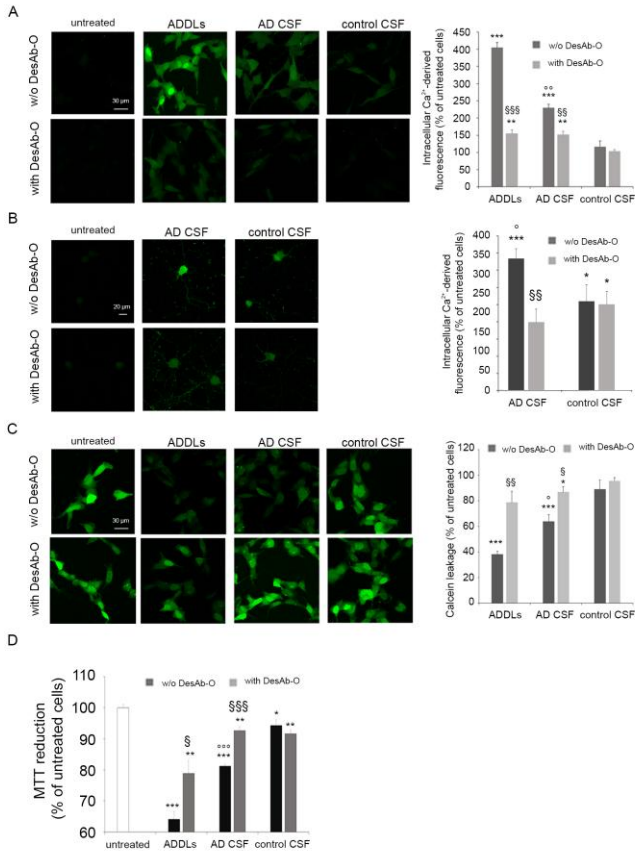

Figure 3.9 - DesAb-O prevents neuronal dysfunction induced by the CSFs of AD patients. A) Intracellular Ca^{2+}-derived fluorescence in SH-SY5Y untreated cells or treated for 5 h with ADDLs at 1 µM (monomer equivalents), or with CSFs from AD patients and age-matched control subjects (n = 4) following or not a 1 h pre-incubation in the absence or presence of DesAb-O at 3 µM. B) Intracellular Ca^{2+}-derived fluorescence in primary rat cortical neurons untreated or treated for 2.5 h with CSFs from AD patients and control subjects (n = 4) following or not a 1 h pre-incubation in the absence or presence of DesAb-O at 3 µM. C) Intracellular calcein-derived fluorescence in SH-SY5Y cells untreated or treated for 5 h with ADDLs at 1 µM (monomer equivalents), or with CSFs from AD patients and control subjects (n = 4) following or not a 1 h pre-incubation in the absence or presence of DesAb-O at 3 µM. D) MTT reduction in SH-SY5Y cells treated for 24 h with ADDLs at 1 µM (monomer equivalents), or with CSFs from AD patients and control subjects (n = 4) following or not a 1 h pre-incubation with DesAb-O at 3 µM. Experimental errors are S.E.M. Samples were analysed by Student *t* test relative to untreated cells (* P<0.05, ** P<0.01 and ***P<0.001) or to cells treated with samples without DesAb-O (§P<0.05, §§P<0.01 and §§§P<0.001) or to cells treated with control CSFs (°P<0.05, °°P<0.01 and °°°P<0.001). 200-250 (A,C),80-150 (B) and 250.000-300.000 (D) cells were analysed per condition.

Chapter 4
Third Section: Design of a dimeric-nanobody specific for $A\beta_{42}$ oligomers: the Dimeric-DesAb-O

1. Dimeric-DesAb-O design

The rationale behind the engineering of DesAb-O was to design a dimeric sdAb able to bind $A\beta_{42}$ oligomers with a higher binding avidity and specificity. It is conceivable that the dimer may be capable of binding to multiple exposed binding sites within the oligomeric structure, rather than binding to a single exposed monomeric binding site. This could result in an enhanced binding avidity and specificity for oligomeric structures, rather than a stronger affinity. However, it is challenging to distinguish between an increased avidity or affinity. Consequently, we evaluated them as a whole, rather than analysing them individually.

To obtain a dimeric structure of this sdAb, a flexible linker $(GGGGS)_3$, consisting of a repetition of glycine (Gly) and serine (Ser) residues over a length of 15 amino acids (Huston *et al*. 1988), was attached to the C-terminus of the first monomer and the N- terminus of the second monomer, cleaved from its His-tagged region, as reported in Figure 4.1. In particular, the N-terminus of DesAb-O presents a solvent-exposed loop region composed of approximately 34 amino acids, mainly composed of Ser and Gly, as the flexible linker described above, as well as threonine (Thr), proline (Pro), aspartic acid (Asp), lysine (Lys), glutamine (Gln) and alanine (Ala), which have been suggested as preferred linker elements by Argos (Argos 1990; Chen, Zaro and Shen 2013). Together, these features represent a good composition for a *partial natural linker*, composed by the flexible $(GGGGS)_3$ linker and the loop region of the second monomer, for a total length of 39 amino acids (Figure 4.1). The length of the linker guarantees a wide range of movement of both domains and the possibility of binding antigen sites

Liliana Napolitano, liliana98.napolitano@gmail.com, 0009-0004-3087-286X

Referee List (DOI 10.36253/fup_referee_list)
FUP Best Practice in Scholarly Publishing (DOI 10.36253/fup_best_practice)

Liliana Napolitano, Third Section*: Design of a dimeric-nanobody specific for $A\beta_{42}$ oligomers: the Dimeric-DesAb-O*, © Author(s), CC BY 4.0, DOI 10.36253/979-12-215-0993-9.06, in Liliana Napolitano, *A multidisciplinary approach for the early diagnosis of Alzheimer's disease and potential therapeutic applications*, pp. 95-115, 2026, published by Firenze University Press, ISBN 979-12-215-0993-9, DOI 10.36253/979-12-215-0993-9

Book References DOI 10.36253/979-12-215-0993-9.references

distance between them (Chen, Zaro and Shen 2013; Yusakul *et al*. 2016) The gene sequence was modified using software SnapGene (www.snapgene.com).

2. Structural characterization of the Dimeric-DesAb-O

The Dimeric-DesAb-O was expressed in *E. coli* and purified, as detailed in Figure 4.2. Thereafter, the secondary structure, molecular weight and thermal stability were characterised by CD and ESI-MS, as reported in Figure 4.3. CD spectroscopy demonstrated that the dimeric structure of DesAb-O exhibits a predominant β-sheet secondary structure, similar to that observed for the monomer (Figure 4.3 A). To provide a more accurate interpretation of the CD spectra of these sdAbs, the BestSel software (v1.3.230210; Micsonai *et al*. 2018) was employed (Table 4.1).

BestSel analysis revealed an increased proportion of antiparallel β-sheet secondary structure for the Dimeric-DesAb-O compared to DesAb-O (61% and 57%, respectively). Notably, DesAb-O comprises 7% parallel β-sheet, an element that is entirely absent from the dimeric structure profile. Conversely, the dimeric sdAb exhibits a 3% α-helix, likely attributable to the presence of the linker, which is absent in the BestSel results for DesAb- O, as reported in Table 4.1.

To evaluate the molecular weight of the engineered DesAb-O, we employed the use of ESI-MS, as represented in Figure 4.3 B. From the ESI-MS spectrum, the mass of the Dimeric-DesAb-O construct was determined to be 34.270 Da. The experimental value was found to be in complete agreement with the theoretical measurements obtained with with ExPASy ProtParam (Gill and Von Hippel 1989) (34.269 Da), which were used to derive the molecular weight.

To assess whether the new dimeric construct had similar structural stability as the monomeric DesAb-O, we performed a thermal denaturation experiment to determine the temperature of half-denaturation (*Tm*) (Figure 4.3 C). CD spectra were recorded between 20 °C and 90 °C to monitor the thermal unfolding of the protein (Figure 4.3 C). The sdAbs concentration was 6 μM in PBS pH 7.4. The molar residue ellipticity per residue ($[\theta]_{res}$) at a 210 nm was extracted from each CD spectrum and plotted as a function of temperature (Figure 4.3 D). The resulting thermal denaturation curves were fitted with a two-state model and normalised to fraction folded (%) values. The sdAbs share very close thermal denaturation points as the Dimeric-DesAb-O had a *Tm* of 72.7 °C, whereas the value for DesAb-O was 74.6 °C (Figure 4.3 D). This structural characterisation showed how the engineering of DesAb-O and the addition of a flexible linker resulted in a stable dimeric sdAb that shared the secondary structure and a *Tm* close to the monomeric sdAb

3. The Dimeric-DesAb-O slows down $A\beta_{42}$ aggregation in a dose-dependent manner

To assess the ability of the Dimeric-DesAb-O to interfere on the $A\beta_{42}$ aggregation process, we performed ThT assays on solutions containing 1 μM

monomeric $A\beta_{42}$ in the presence of decreasing $A\beta_{42}$ monomeric:Dimeric-DesAb-O molar ratios (1:1, 1:0,5, 1:0,25, 1:0,125), as reported in Figure 4.4 A. Interestingly, the Dimeric-DesAb-O massively reduced the $A\beta_{42}$ aggregation process at the 1:1 molar ratio, increasing the aggregation half-time (t_{50}) approximately 2-fold compared to $A\beta_{42}$ alone (3.2 ± 1.1 h and 1.5 ± 0.4, respectively). Furthermore, the t_{50} of the co-incubated $A\beta_{42}$ and Dimeric-DesAb-O samples decreased proportionally with decreasing Dimeric-DesAb-O concentration (2 ± 0.4 h for 1:0.5; 1.8 ± 0.3 for 1:0.25; 1.7 ± 0.3 h for 1:0.125; $A\beta_{42}$ monomeric:Dimeric-DesAb-O respectively), demonstrating the remarkable ability of the Dimeric-DesAb-O to interfere with the $A\beta_{42}$ aggregation process even at low concentrations (Figure 4.4 A).

To evaluate the improvement of the dimeric sdAb with respect to DesAb-O, we tested increasing molar ratios of $A\beta_{42}$ monomeric:DesAb-O (1:1, 1:2) as represented in Figure 4.4 B. The aggregation profile obtained with increasing DesAb-O molar ratios slightly increased the t_{50} (1.8 ± 0,6 h for 1:2, 1.7 ± 0.4 h for 1:1, 1.5 ± 0.4 h $A\beta_{42}$ monomeric:DesAb-O respectively) slowing down the $A\beta_{42}$ aggregation process. Despite this interference, DesAb-O did not slow the aggregation process to the same extent as the Dimeric-DesAb- O, increasing the t_{50} only 1.3-fold at 1:2 $A\beta_{42}$ monomer:sdAb molar ratio. Notably, the dimeric form of DesAb-O exhibited a comparable inhibitory effect at a significantly lower molar ratio of 1:0.25 (by 1.8 ± 0.5 h) indicating a substantially greater potency in interfering with the aggregation process of the $A\beta_{42}$.

4. Dimeric-DesAb-O has improved specificity of binding for $A\beta_{42}$ oligomers

With the aim of investigating the specificity and selectivity of the Dimeric-DesAb-O for $A\beta_{42}$ oligomeric conformers, we performed a Real-Time Based ELISA assay using DesAb-O as control. To do so, we prepared solutions of 1 μM $A\beta_{42}$,and we monitored the aggregation of $A\beta_{42}$ by ThT (Figure 4.4 C). The aggregation reaction was stopped at different timepoints (0, 0.5, 1, 2, 22 h) to collect $A\beta_{42}$ samples to adsorb in an ELISA plate overnight. The following day, 1 μM DesAb-O or 1 μM Dimeric-DesAb-O were used as primary antibodies. The absorbance signals were all compared against the timepoint 0 h. Our experiments showed that after 0.5 h, the Dimeric-DesAb-O slightly increased the absorbance signal probably due to the initial formation of low molecular weight aggregates, exhibiting a statistically difference with DesAb-O at the same time (Figure 4.4 D). As the time-course continues, our experiments revealed a significant increase in absorbance signal for both sdAbs, especially after 1 and 2 h from the begging of the aggregation, approximately close to the half-time of aggregation as determined by ThT (Figure 4.4 C,D), where oligomers are at their maximum amount. At these timepoints, the Dimeric-DesAb-O exhibited the highest absorbance being approximately 2-fold higher than that initial aggregation time point, showing a significant difference compared to DesAb-O at the same time. After 20 hours of aggregation, the Dimeric- DesAb-O still showed an absorbance

approximately 1.3-fold higher than time 0, indicating the binding to $A\beta_{42}$ species, while DesAb-O returned to similar absorbance levels as the initial ones, as previously reported (Aprile *et al*. 2020). In order to understand whether the dimeric form of DesAb-O was recognising $A\beta_{42}$ oligomers or $A\beta_{42}$ fibrillar conformers, we used $A\beta_{42}$ fibrils obtained after 4 days of incubation at 37 °C as a control, as represented in Figure 4.4 D. Interestingly, neither sdAbs recognised these $A\beta_{42}$ fibrils, resulting in an absorbance signal well below timepoint 0. From this evidence, we can assess that the Dimeric-DesAb-O is able to recognise $A\beta_{42}$ oligomers at very low concentrations, with high specificity and affinity, representing a successful improvement of the previous outstanding DesAb-O specificity for $A\beta_{42}$ oligomers.

5. Dimeric-DesAb-O induces morphological and structural changes in $A\beta_{42}$ fibrils

To further investigate the impact of the Dimeric-DesAb-O on the $A\beta_{42}$ aggregation, we analysed the structural and morphological changes induced in $A\beta_{42}$ fibrils upon incubation with this dimeric sdAb. To do so, 5 μM $A\beta_{42}$ samples obtained in the absence or in the presence of equimolar concentration of DesAb-O or Dimeric-DesAb-O at the end of a ThT aggregation assay were visualized by taking advantage of Transmission Electron Microscopy (TEM) (Figure 4.5 A). From our analysis, the $A\beta_{42}$ fibrillar structures obtained in the absence of sdAbs showed a dense network of connections (Figure 4.5 A, first column), presenting a diameter of approximately 11.5 ± 0.1 nm, as represented in Figure 4.5 B. On the contrary, $A\beta_{42}$ fibrils obtained from co- incubation with DesAb-O showed a reduced ability to form connections and a tendency to fracture, as indicated by the symbol * (Figure 4.5 A, second column). Furthermore, these $A\beta_{42}$ fibrils exhibited a reduced diameter width with respect to $A\beta_{42}$ fibrils obtained in the absence of sdAbs, averaging 10 ± 1 nm (Figure 4.5 B). Interestingly, a striking change in the morphology of $A\beta_{42}$ fibrils occurs when monomeric $A\beta_{42}$ is co-incubated with the Dimeric-DesAb-O. In fact, fibrils have shown jagged appearance with the presence of globular structures on their surface (Figure 4.5 A, third column). In addition, from TEM images background we can observe the presence of electrodense short fragments suggesting that fibrils may be breaking or degrading due to increased structural weakness. Furthermore, these $A\beta_{42}$ fibrils exhibited a further reduction in diameter compared to those formed in the presence of DesAb-O resulting exceptionally thin, with an average (7.4 ± 0.6 nm), and suggesting a more potent inhibitory effect of the dimeric sdAb on fibril assembly (Figure 4.5 B).

In order to investigate the increased $A\beta_{42}$ fibrils fragility induced by the sdAbs co- incubation with $A\beta_{42}$ monomer in ThT aggregation assays, we performed a Dot Blot assay. Briefly, samples were collected at the end of a ThT experiment and centrifuged at max speed (~17,000*g*) for 30 min on a benchtop

centrifuge to separate the soluble and insoluble aggregates, as previously reported (Vadukul *et al.* 2023). Prior to centrifugation, an aliquot of each sample was reserved and considered as the total protein amount. To analyze the distribution of $A\beta_{42}$ and sdAbs, samples were spotted onto nitrocellulose membrane and incubated with 6E10 Abs for $A\beta_{42}$ detection or anti-6X His-tag Abs for sdAbs detection. The signal intensity in the supernatant was normalized to the total protein content of the corresponding sample. Quantifications of $A\beta_{42}$ fibrils and sdAbs deposited into the pellet are represented in Figure 4.6.

Our results showed that samples of $A\beta_{42}$ fibrils obtained in the absence of sdAbs showed a low presence in the supernatant (14 ± 3%) and high amount (88 ± 5%) in the pellet, respectively (Figure 4.7 A). This might indicate a high strength and robustness of the fibrils, which do not tend to break or resuspend in the supernatant. Conversely, samples obtained in the presence of DesAb-O and Dimeric-DesAb-O displayed an increased occurrence of fibrillar material in the supernatant (22 ± 2% and 36 ± 2%; respectively) and only partial deposition in the pellet (79 ± 5% and 68 ± 5%; respectively), as represented in Figure 4.7 A. This suggests an increase in fibril fragility and a heightened tendency for fragmentation. Moreover, the presence of smaller fragments in the supernatant, likely due to their reduced ability to sediment effectively during centrifugation, further supports this observation.

This fragmentation also explains the presence of material in the background of the TEM images, as noted earlier. Even more surprisingly, our results showed that DesAb-O was predominantly adhered to the $A\beta_{42}$ fibrils deposited in the pellet (17% ± 2% and 84% ± 4%; for supernatant and pellet respectively), whereas in contrast, the Dimeric-DesAb-O was more adhered to the fragments found in the supernatant of the samples (58% ± 9% and 50% ± 3%, for supernatant and pellet respectively) (Figure 4.7 B). The observation that $A\beta_{42}$ forms thinner and more fragile fibrils in the presence of the Dimeric-DesAb-O, with a greater occurrence of this sdAb in the fragments, suggests that the dimeric form of DesAb-O may interfere with $A\beta_{42}$ assembly, promoting its fragmentation. Furthermore, the dimeric sdAb may bind to $A\beta_{42}$ oligomers, stabilizing them and preventing their aggregation.

We further investigate the ability of sdAbs to modify the structure of $A\beta_{42}$ fibrils. Thus, we carried out a proteinase K (PK) digestion assay (Figure 4.7 C) to determine whether sdAbs co-incubation could influence the PK digestion sensitivity due to the generation of structural modifications in $A\beta_{42}$ fibrils. Briefly, fibrils were collected from the co-incubation sample with sdAbs at the end of aggregation by centrifugation at max speed (~17,000*g*) for 1 h, resuspended in PBS and treated with 0, 10, 25, 50 μg/mL PK for 30 mins. Samples were then incubated at 95 °C for 5 min to stop the enzymatic reaction and loaded on SDS-PAGE for a Western blotting analysis as previously reported (Vadukul *et al*. 2023). Bands intensity at each concentration were normalized on the 0 μg/mL correspondent band. Our results showed that $A\beta_{42}$ fibrils obtained in the presence of DesAb-O displayed an increased resistance to PK digestion at low

PK concentrations (10 μg/mL) while samples obtained in the absence of sdAbs and in the presence of the Dimeric-DesAb-O followed a similar trend, shared by samples co-incubated with DesAb- O at increased PK concentrations, as represented in Figure 4.7 E.

These results demonstrate that the co-incubation with sdAbs during the $A\beta_{42}$aggregation process induces important and fundamental changes in the structure of $A\beta_{42}$ fibrils. Furthermore, the co-incubation with the Dimeric-DesAb-O, as evidenced by dot blot and TEM microscopy, resulted in impressive changes, leading to a reduction in fiber diameter, increased fragility and a greater tendency to form stabilized aggregate structures. Taken together, this evidence indicates the strong tendency of this dimeric sdAb to interfere with $A\beta_{42}$ aggregation.

6. Characterisation of $A\beta_{42}$ aggregates with ThT assay, dot blot assay and STED microscopy

With the aim of obtaining transient $A\beta_{42}$ aggregates for cell biology experiments, we used the $A\beta_{42}$ synthetic peptide. Initially, we characterised the $A\beta_{42}$ aggregation by ThT assay, confirming that the synthetic $A\beta_{42}$ peptide aggregation occurs in a manner comparable to the recombinant peptide. Precisely, samples of synthetic $A\beta_{42}$ monomers at 10 µM was mixed with 25µM ThT, incubated at 37 °C and ThT fluorescence was monitored at 482 nm over a span of 24 h. The progressive increase of the ThT fluorescent signal provides insight into β-sheets formation. Concomitantly, we collected aliquots of the reaction solution at different timepoints (0, 2, 4, 8 and 24 h) in order to characterise the reactive properties and the morphology of the species formed during the aggregation process (Figure 4.8). We took advantage of dot blot assay and super resolution STED microscopy coupled with conformation-sensitives Abs able to distinguish specific $A\beta_{42}$ aggregate conformations. In particular, we used the anti-ADDLs 19.3 Ab (Savage *et al*. 2014) and the anti-amyloid fibrils OC Ab (Kayed *et al.* 2007). As controls, we used the 6E10 Ab, which binds to the N-terminus of $A\beta_{42}$ peptides without distinguishing between different conformations. At 0 h we found a higher ThT signal compared to the buffer-only samples, called control in Figure 4.8 A, with only a minimal positivity for 19.3 Ab and none for OC Ab in the dot blot assay and STED images (Figure 4.8 B,C,D,E). After 2 h of incubation, we observed an increase in ThT fluorescence, indicating the formation of aggregated species (Figure 4.8 A), that appeared positive for 19.3 Ab and to a lesser extent for OC Ab (Figure 4.8 C,D). At T2, the ThT fluorescent signal further increased (Figure 4.8 A), as well as the positivity for 19.3 Ab and only a minor signal for OC Ab (Figure 4.8 C,D). After 8 h, we found the exponential phase of the sigmoidal curve and a sharp increase in ThT fluorescent signal (Figure 4.8 A). Concurrently, strong positivity with 19.3 Ab and the presence of numerous small, globular species in STED images (Figure 4.8 C,E) indicated the highest concentration of oligomers. We also noticed a positivity for OC Ab (Figure 4.8 D,E), indicating the formation of few fibrillary species. At the end of the

aggregation reaction, the ThT curve reached a plateau (Figure 4.8 A), suggesting the presence of $A\beta_{42}$ fibrils and the end of new aggregate formation. Dot blot assays and STED images showed positivity for OC Ab together with the presence of fibrillary elongated species and only a minor presence of oligomers (Figure 4.8 D,E). As control, 6E10 Ab exhibited positivity for each type of species (Figure 4.8 B,E), indicating the proper loading and the progressive maturation of $A\beta_{42}$ fibrils. Overall, STED imaging and Dot blot analyses reveals that after 8 hours of incubation, the $A\beta_{42}$ solution becomes heterogeneous, comprising a mixture of oligomers, pre-fibrillar aggregates, and low molecular weight fibrils.

7. $A\beta_{42}$ oligomeric species obtained after 8 hours of incubation exhibit high toxicity

Then, we investigated the toxicity of the various $A\beta_{42}$ aggregates generated during the $A\beta_{42}$ aggregation process, taking advantage of the MTT reduction test. In this experiment, $A\beta_{42}$ species collected at different timepoints (0, 2, 4, 8 and 24 h) were added to the extracellular medium of SH-SY5Y cells for 24 h. Our findings revealed that $A\beta_{42}$ species formed at the beginning of the aggregation process (0 h), mostly composed of the monomeric form, did not significantly reduce cell mitochondrial activity (16 ± 6%) as compared to untreated cells, taken as 100 % (Figure 4.9 A). In contrast, starting from 2 h of aggregation we observed a progressive reduction of cell viability (34 ± 4%) which became significant after 4 h (50 ± 2%) and reached its peak after 8 h (58 ± 3%), in which the solution mostly consists of oligomeric species. Finally, after 24 h, we observed a minor toxicity with respect to the timepoints collected after 4 and 8 h, even if $A\beta_{42}$ conformers still generated a significant reduction of cell viability (41 ± 4%), probably due to the presence of residual $A\beta_{42}$ oligomers and $A\beta_{42}$ fibrils (Figure 4.9 A). These findings suggest that after 8 h of incubation, we have the highest amount of $A\beta_{42}$ oligomers due to the half-time of aggregation as determined by ThT and evidenced by dot blot and STED images. For this reason, $A\beta_{42}$ transient oligomers obtained after 8 h of aggregation performed the highest toxicity.

Therefore, to investigate more into their ability to induce toxicity, we conducted a dose-dependent MTT assay (Figure 4.9 B). Increasing concentrations (ranging from 0.5 pM to 1 μM) of the aggregates formed after 8 h of aggregation were added to the extracellular medium of SH-SY5Y cells for 24 h. Figure 4.9 B illustrates that oligomers caused significant mitochondrial dysfunction only at 0.5 and 1 μM (reduction of 33 ± 3% and 51 ± 2%, respectively).

8. The Dimeric-DesAb-O detects $A\beta_{42}$ oligomers interacting with cellular membranes and internalized into the cytoplasm

For cell biology experiments, we used the $A\beta_{42}$ synthetic peptide from which we characterised the $A\beta_{42}$ aggregation by ThT assay, confirming that the synthetic $A\beta_{42}$ peptide aggregation occurs in a manner comparable to the

recombinant peptide. Furthermore, we characterized aggregates obtained at different timepoints, taking advantage of Dot Blot assay and STED microscopy (Figure 4.8) and we characterized their toxicity by MTT assay (Figure 4.9). Given the great ability of DesAb-O to selectively detect $A\beta_{42}$ in cultured cells as previously reported in Bigi *et al*. 2024b, we investigate the capability of the Dimeric-DesAb-O to detect $A\beta_{42}$ oligomers in cells model and whether the engineering had resulted in an increased ability DesAb-O to detect $A\beta_{42}$ oligomeric conformers. Briefly, human neuroblastoma SH-SY5Y cells were exposed to 0.5 μM $A\beta_{42}$ oligomers for 1 h. Plasma membrane (red channel) and $A\beta_{42}$ aggregates (green channel) were counterstained and analysed by confocal microscopy, as previously reported (Bigi *et al*. 2024b). Two different concentrations, 3 μM and 1 μM, were tested for DesAb-O and the Dimeric-DesAb-O as primary antibodies. 6E10 Ab were used as control. Our results showed that at 3 μM both sdAbs highly recognize $A\beta_{42}$ oligomers interacting with neuronal membranes and internalized into the cells (Figure 4.10 A), showing an increase of the green fluorescent signal by 172 ± 13% and 205 ± 18%, for DesAb-O and its dimeric form respectively, with respect to the untreated cells, taken as 100% (Figure 4.10 B). On the contrary, at 1 μM, DesAb-O did not recognize $A\beta_{42}$ oligomers in a statistically significant manner, increasing the green fluorescent signal by 140 ± 17%, while the Dimeric-DesAb-O was still able to recognize $A\beta_{42}$ oligomeric conformers inducing an increase of the green signal by 173 ± 14% (Figure 4.10 B). Furthermore, a heterogeneous aggregate solution including high molecular weight aggregates and small fibrils as previously characterized was used for the cell experiments in this project (Figure 4.10 A). The sdAbs were only able to recognise the oligomeric species with respect to high molecular weight structures, which were recognised by 6E10 Ab (Figure 4.10 A) representing further evidence of their specificity for $A\beta_{42}$ oligomers. Overall, in our experimental conditions, the Dimeric-DesAb-O selectively recognized toxic $A\beta_{42}$ oligomers interacting with cellular membranes even at lower concentrations than DesAb-O, showing a higher sensitivity than the monomeric sdAb and suggesting a very promising potential for the detection of harmful $A\beta_{42}$ species in biological fluids.

9. The Dimeric-DesAb-O inhibits the interaction of $A\beta_{42}$ oligomers with neuronal membranes preventing $A\beta_{42}$-induced neurotoxicity

We then evaluated whether the Dimeric-DesAb-O was able to capture $A\beta_{42}$ oligomers, preventing their interaction with neuronal membranes and the following detrimental effects. With this aim, $A\beta_{42}$ oligomers at 0.5 μM were pre-incubated for 1 h with DesAb- O and the Dimeric-DesAb-O at increasing molar ratios between $A\beta_{42}$ oligomers and sdAbs (1:0.1, 1:0.25, 1:0.5, 1:1, 1:2, 1:3), and these solutions were added to the cell culture medium of SH-SY5Y cells for 15 mins, as previously reported (Bigi *et al*. 2024b). To detect only the oligomers bound to the cell surface, the cellular membrane was not permeabilized at this

stage, thus preventing Ab internalization. The binding affinity of the aggregates for cellular membranes was assessed by confocal microscopy using the 6E10 Ab as a probe. $A\beta_{42}$ oligomers showed to be colocalized with cellular membranes in the absence of pre-incubation with sdAb (Figure 4.11 A) as previously reported (Schengrud 2010; Evangelist *et al*. 2013; Bigi *et al*. 2020; Bigi *et al*. 2024b). Following the pre-incubation with sdAb, the interaction between $A\beta_{42}$ oligomers and the neuronal membranes showed to be significantly reduced. In particular, Dimeric-DesAb-O massively reduce this interaction up to 1:0.1 $A\beta_{42}$ oligomers:sdAb molar ratio (by 810 ± 63%), while DesAb-O and was found to prevent the interaction of the oligomers with the membrane up to 1:0.5 $A\beta_{42}$ oligomers:sdAb molar ratio (by 896 ± 62%) (Figure 4.11 B). These results again suggest the increased avidity of the Dimeric-DesAb-O with respect to DesAb-O for $A\beta_{42}$ oligomers, representing another evidence of the successful engineering of the monomeric sdAb.

10. The Dimeric-DesAb-O prevent from the dysregulation of cytosolic Ca^{2+} homeostasis and the mitochondrial dysfunction induced by $A\beta_{42}$ oligomers

We then evaluated the ability of the Dimeric-DesAb-O to prevent the detrimental effects induced by $A\beta_{42}$ oligomers, such as the increase of intracellular Ca^{2+} levels and the mitochondrial dysfunction. Firstly, we monitored the disruption of cytosolic Ca^{2+} homeostasis, an early upstream event induced by extracellular $A\beta_{42}$, both in cultured neurons and in relevant mouse AD model, in which Ca^{2+} ions flow from the extracellular space into the cytosol (Bigi *et al*. 2023; Fani *et al*. 2022; Demuro *et al*. 2005; Cascella *et al*. 2021). Briefly, SH-SY5Y cells were treated for 15 min with increasing $A\beta_{42}$ oligomers:sdAbs molar ratio, following or not 1 h of pre-incubation. sdAbs were tested alone as controls. Our results showed that $A\beta_{42}$ oligomers caused an extensive Ca^{2+} influx (by 280 ± 2%) relative to untreated cells taken as 100% (Figure 4.12 A,B). Following 1 h of pre-incubation, the Dimeric-DesAb-O markedly reduced the intracellular free Ca^{2+} levels up to 1:0.1 $A\beta_{42}$ oligomers:Dimeric-DesAb-O molar ratio (by 179 ± 3%) showing a higher protective effect compared to DesAb-O that prevents the Ca^{2+} intracellular increase up to 1:0.25 $A\beta_{42}$ oligomers:DesAb-O molar ratio (by 209 ± 5%), as visualized in Figure 4.12 A and quantified in Figure 4.12 B. Of note, both sdAbs does not affect neuronal viability when added alone to the cell medium. From this evidence, the Dimeric-DesAb-O showed an increased protective effect compared to DesAb-O and representing a successful engineering of the initial sdAb.

The protective effect of the Dimeric-DesAb-O was also evaluated by analyzing the mitochondrial status of cultured cells treated with $A\beta_{42}$ oligomers by MTT reduction test (Figure 4.12 C). $A\beta_{42}$ oligomeric species at 0.5 μM were incubated in the absence or presence of increasing $A\beta_{42}$ oligomers:sdAbs molar ratios (1:0.1, 1:0.25, 1:0.5, 1:1, 1:2, 1:3) for 1 h, and then these solutions were

added to the culture medium of SH-SY5Y cells for 24 h. Our results showed that $A\beta_{42}$ oligomers significantly reduced (by 35 ± 2%) the mitochondrial activity of SH-SY5Y cells as compared to untreated cells, taken as 100%, as previously shown (Evangelisti *et al*. 2016; Cascella *et al*. 2017; Bigi *et al*. 2020; Bigi *et al*. 2024b) (Figure 4.12 C). When $A\beta_{42}$ oligomers were pre- incubated for 1 h with decreasing molar ratios of Dimeric-DesAb-O, we observed a significant recover of the mitochondrial functionality up to 1:0.5 $A\beta_{42}$ oligomers:Dimeric- DesAb-O molar ratios (by 24 ± 2%) and reaching its maximum restore at 1:2 $A\beta_{42}$ oligomers:Dimeric-DesAb-O molar ratio (by 19 ± 3%), whereas DesAb-O was able to prevent the mitochondrial impairment only at 1:3 $A\beta_{42}$ oligomers:DesAb-O molar ratio (by 22 ± 1%). At 1:3 molar ratio, we can observe a slightly decreased ability of the Dimeric-DesAb-O to prevent the mitochondrial dysfunction induced by $A\beta_{42}$ oligomers, with respect to the 1:2 molar ratio (by 22 ± 1% and 19 ± 3%, respectively) that it is not observed in other experiments, as reported in Figure 4.12 C. This behavior could be justified by the concentration of the sdAb and the treatment length. Indeed, it is likely that the high concentration of the Dimeric-DesAb-O could lead to increasing interactions between sdAbs domains and the following release of the $A\beta_{42}$ oligomers. Nevertheless, the dimeric structure of DesAb-O still significantly prevents the mitochondrial dysfunction sharing a similar action with DesAb-O at the same molar ratio (Figure 4.12 C).

Considering these results together, we can confirm the increased ability of the Dimeric-DesAb-O to prevent $A\beta_{42}$ oligomers-induced toxicity, representing a promising tool for a future application in AD treatment.

11. The Dimeric-DesAb-O prevents toxic effects induced by the CSFs of AD patients

Considering the encouraging data obtained with the Dimeric-DesAb-O both *in vitro* and in cultured cells and given the previously reported ability of DesAb-O to selectively detect $A\beta_{42}$ oligomers in cultured cells exposed to CSFs of AD patients (Bigi *et al*. 2024b), we performed a proof-of concept experiment on a small set of clinical samples of CSF (n = 4 from AD and from controls subjects). We aimed to evaluate whether the Dimeric-DesAb-O was able to neutralize the cytotoxicity induced by $A\beta_{42}$ oligomeric species present in CSFs derived from AD patients and whether the engineering resulted in improved performance of DesAb-O (Figure 4.13 A,B). Thus, we monitored the dysregulation of cytosolic Ca^{2+} homeostasis in SH-SY5Y treated for 5 h with the CSFs from AD patients and control subjects diluted 1:1 with the cell culture medium, following or not a 1 h pre-incubation with 3 μM or 1 μM sdAbs, as previously reported (Bigi *et al*. 2024b). The CSFs of AD patients significantly increased the intracellular Ca^{2+} concentration (by 190 ± 7%) relative to untreated cells (Figure 4.13 A,B), while the CSFs of control subjects only slightly increased the intracellular Ca^{2+} free levels (by 140 ± 5%). After 1 h of pre-incubation with 3 μM both DesAb-O and

Dimeric-DesAb-O completely reduced the Ca^{2+} dyshomeostasis induced by CSFs derived from AD patients (by 93 ± 3% and 84 ± 5%, respectively) and CSFs from control-subjects (by 96 ± 5% and 95 ± 6%, respectively) both showing a massive protective effect, as represented in Figure 4.13 B. However, decreasing the sdAbs concentration to 1 μM, we observed a reduced ability of DesAb-O to prevent the cytotoxic effects induced by AD CSFs (by 150 ± 6%) whereas the Dimeric-DesAb-O continued to abolish the Ca^{2+} dyshomeostasis induced by these biological fluids derived from AD patients (by 99 ± 5%) (Figure 4.13 B). Moreover, at 1 μM both sdAbs showed a total preservation of the Ca^{2+} dyshomeostasis in cells treated with CSFs derived from control- subjects (by 102 ± 6% and 84 ± 5% for DesAb-O and Dimeric-DesAb-O, respectively) (Figure 4.13 B).

Taken together, these data demonstrate the ability of the Dimeric-DesAb-O to selectively detect and neutralize toxic species present in the CSFs of AD patients. Our data also indicate that the engineering of DesAb-O has led to the production of a promising tool for future potential application in the diagnosis, therapy and prognosis of AD, improving on the previous excellent ability of DesAb-O.

12. Chapter 4: figures and tables

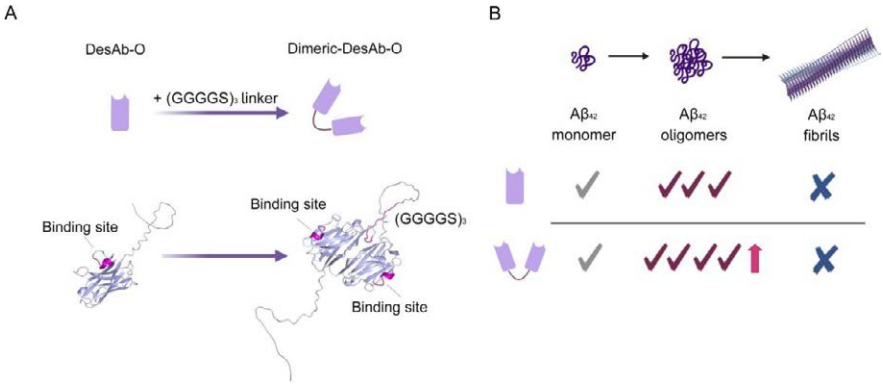

Figure 4.1 - Dimeric-DesAb-O design. A Schematic representation of the ingeneration of DesAb-O (left) to obtain the Dimeric-DesAb-O (right). A) Representative binding sites and loop region highlighted in bright purple. 3D reconstruction was obtained Alphaphold Colab 2. B) Schematic representation of the aim of the study. We designed a dimeric structure of DesAb-O to obtain an enhanced specificity and affinity for $A\beta_{42}$ oligomers, while avoiding increased binding to $A\beta_{42}$ monomers or fibrils.

	DesAb-O (%)	Dimeric-DesAb-O (%)
Helix 1 (regular)	0.0	0.0
Helix 2 (distorted)	0.0	2.6
Anti-parallel 1 (left-twisted)	6.4	8.8
Anti-parallel 2 (relaxed)	34.7	29.9
Anti-parallel 3 (right-twisted)	15.5	21.9
Parallel	6.9	0.0
Turn	8.8	10.4
Others	27.7	26.3

Table 4.1 - Estimated secondary structure content (%) obtained with Best Sell software between the wavelength range of 195 and 250 nm. The total antiparallel β-sheet secondary structure was determined by summing all values relative to each type of antiparallel structure (left twisted, relaxed and right twisted), which was 56.6% for DesAb-O and 60.7% for the Dimeric-DesAb-O. The dimeric sdAb exhibits a 2.6% α-helix, likely attributable to the presence of the linker.

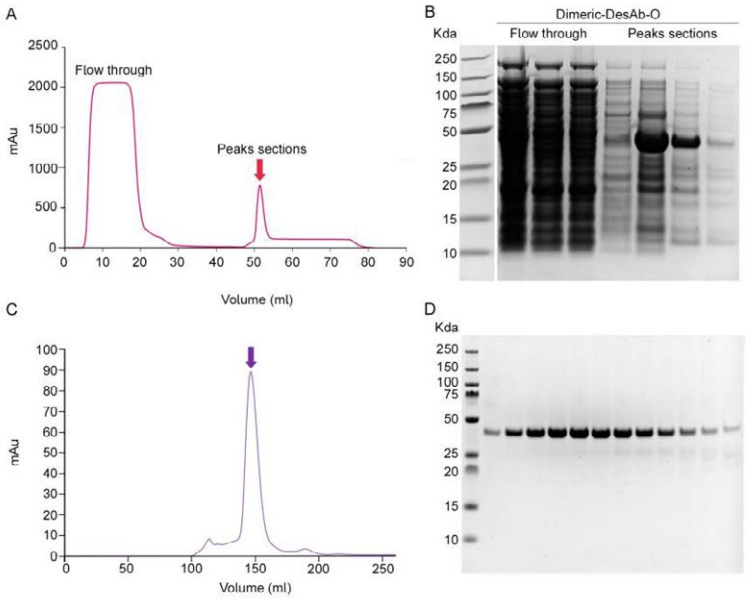

Figure 4.2 - Dimeric-DesAb-O expression and purification. A) Nickel-affinity chromatogram of the Dimeric-DesAb-O. Data were plotted using Excel (Version 16.89.1)

B) SDS-PAGE of samples taken after Nickel-affinity; flow through (lanes 1-3), peak sections (lane 4-7). The Dimeric-DesAb-O lane is indicated by the red arrow. C) SEC chromatogram of the Dimeric-DesAb-O. Data were plotted using Excel (Version 16.89.1). The peak relative to our protein is evidenced by the purple arrow. D) SDS-PAGE of Dimeric- DesAb-O peak sections taken after SEC to verify the sample purity.

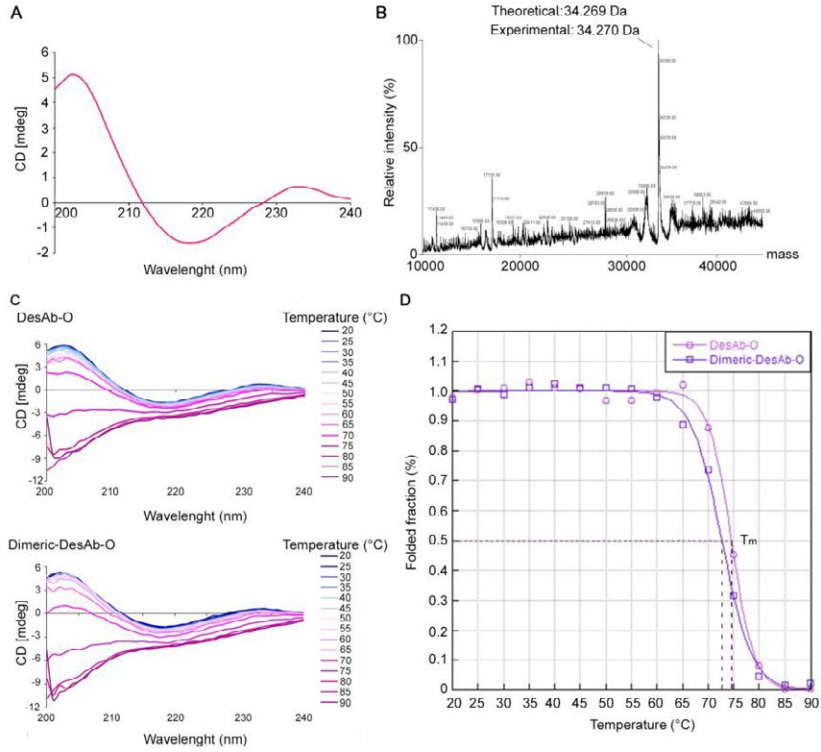

Figure 4.3 - Structural characterization of the Dimeric-DesAb-O. A) CD spectrum of the Dimeric- DesAb-O. The presence of peaks at 202 nm and 218 nm evidence the predominant β-sheet secondary structure of the dimeric sdAb. B) ESI-MS spectrum. Theoretical molecular weight was determined by ExPASy ProtParam software (34.269 Da) being perfectly in line with the mass observed by ESI-MS (34.270 Da). ESI-MS was performed by Lisa Haigh using the Chemistry Mass Spectrometry facilities available at the Molecular Sciences Research Hub, Department of Chemistry, Imperial College London. C) CD spectra of DesAb-O and the Dimeric-DesAb-O between 20 °C and 90 °C. D) DesAb-O and Dimeric- DesAb-O denaturation curves were obtained using the CD signal at 210 nm plotted against temperature, fitted with the Santoro and Bolen equation and normalized to fraction folded (%) values. Dimeric-DesAb- O had a temperature of half-denaturation (*Tm*) of 72.7 °C, while the value for DesAb-O was 74.6°C.

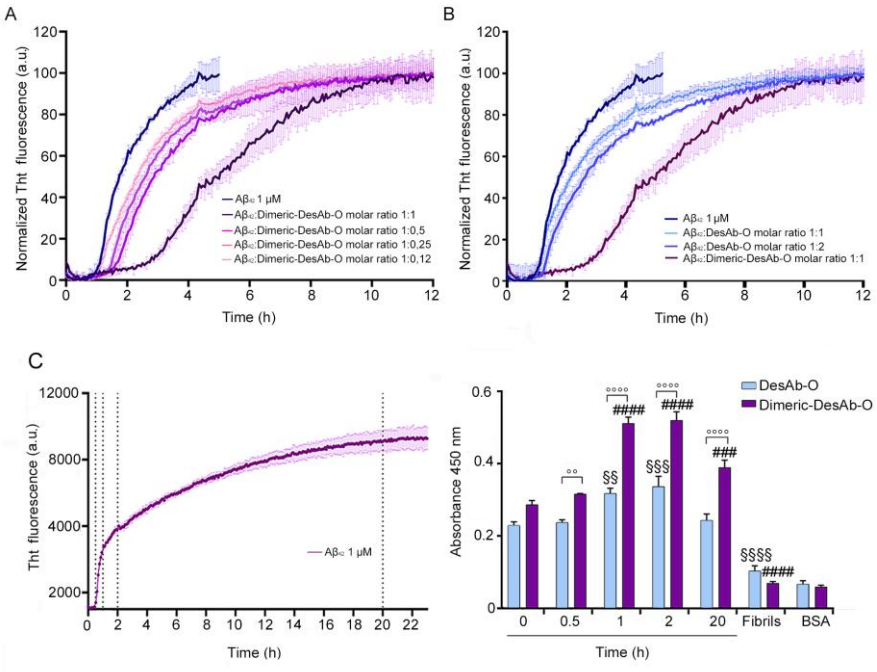

Figure 4.4 - The Dimeric-DesAb-O markedly interfere with $A\beta_{42}$ aggregation process and recognize with high specificity and sensitivity $A\beta_{42}$ oligomers. A) Representative ThT fluorescence assay of decreasing $A\beta_{42}$:Dimeric-DesAb-O molar ratios. 1 μM $A\beta_{42}$ (blue) was incubated with different Dimeric- DesAb-O molar ratios: 1:1 (dark purple), 1:0,5 (bright purple), 1:0,25 (dark pink) and 1:0,1 (pink). B) Representative ThT fluorescence assay of 1:1 $A\beta_{42}$:Dimeric-DesAb-O molar ratio and increasing $A\beta_{42}$:DesAb-O molar ratios as controls. 1 μM $A\beta_{42}$ (blue) was incubated with two DesAb-O molar ratios: 1:1 (bright light blue) and 1:2 (light blue). For the t_{50} quantification, we averaged three ThT aggregation assays. C) ThT-based *in vitro* aggregation assay of 1 μM Aβ42 (average of three replicates is shown). The black dashed lines indicate the time at which samples were collected from the aggregation reaction to perform the ELISA experiment. D) ELISA experiment performed on samples collected from the aggregation reaction shown in C, using DesAb-O and the Dimeric-DesAb-O as primary antibodies. $A\beta_{42}$ fibrils obtained after 4 days of incubation at 37 °C were used as a control. BSA signal represents the background absorbance values. The bar corresponding to DesAb-O is colored light blue while the one corresponding to the Dimeric-DesAb-O is purple. Error bars are representative of the S.E.M. Statistical analysis was performed by ANOVA with multiple comparison. Samples (n = 4) were analysed by Two-way ANOVA multiple comparison test comparing the absorbance of DesAb-O and Dimeric DesAb-O at the same times (°°P <0,01 and °°°°P<0,0001) and VS their respective time 0' (§§P <0,01, §§§P <0,005 and §§§§P<0,0001 for DesAb-O and ###P < 0,005, ####P < 0,0001 for Dimeric-DesAb-O).

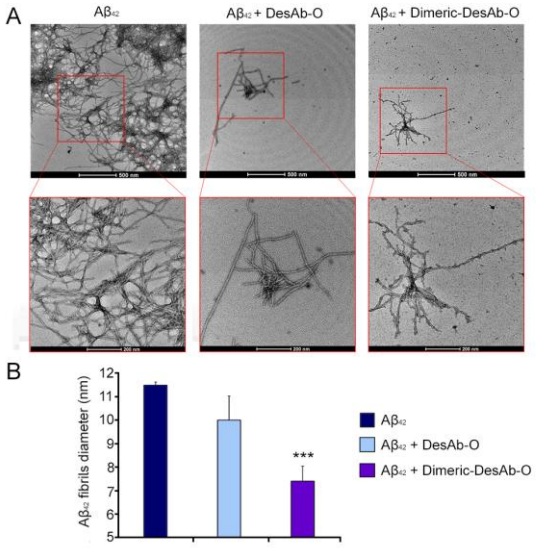

Figure 4.5 - $A\beta_{42}$ fibrils visualization and diameter quantification. A) TEM images of $A\beta_{42}$ fibrils obtained in the absence or in the presence of sdAbs at the end of a ThT aggregation assay. Higher magnifications of $A\beta_{42}$ fibrils are showed in the box area. B) $A\beta_{42}$ fibrils diameter quantification performed with ImageJ. Error bars are representative of the S.E.M (n = 3). For each TEM image, 15 to 25 diameter values were obtained and averaged. The mean value displayed in the graph represents the mean value of all the images for each condition. Measures were analysed by One-tailed t-test comparing the diameter width of the $A\beta_{42}$ fibrils obtained in the presence of the sdAbs VS the diameter width of the $A\beta_{42}$ fibrils obtained in absence of sdAbs (***P < 0,005 VS Dimeric-DesAb-O).

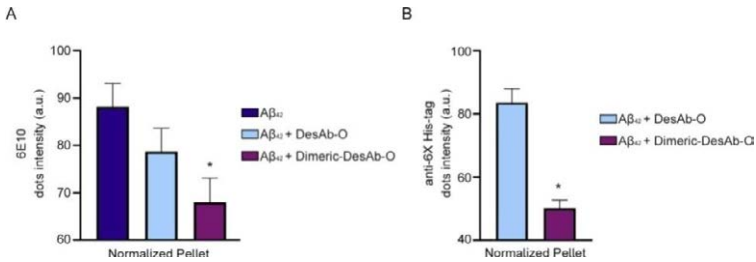

Figure 4.6 - Quantification of $A\beta_{42}$ fibrils and sdAbs deposited into the pellet. A) Pellet quantification of $A\beta_{42}$ fibrils obtained in the presence or absence of sdAbs normalized on total proteins signal. Error bars are representative of the S.E.M (n = 3). Samples were analyzed by One-Tailed Student t- test relative to Aβ fibrils obtained without antibody VS Aβ fibrils obtained in the presence of the Dimeric- DesAb-O (*P < 0.05) B) Pellet quantification of sdAbs deposited into the pellet normalized on total proteins signal. $A\beta_{42}$ signal was subtracted as background. Error bars are representative of the S.E.M (n = 2). Samples were analyzed by One-Tailed Student t-test to compare the presence of DesAb-O in the pellet compared to the Dimeric-DesAb-O (* P < 0.05)

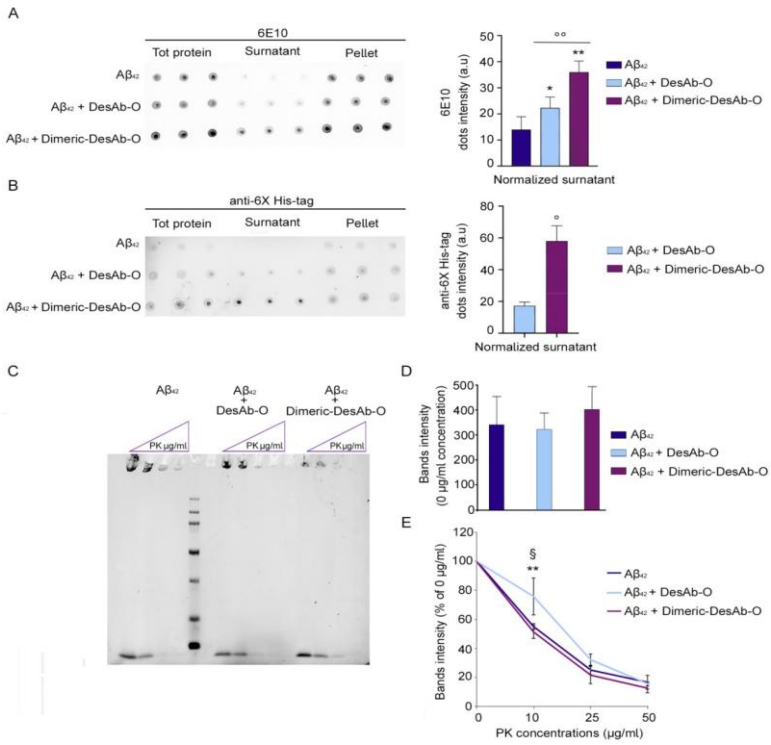

Figure 4.7 - Evaluation of $A\beta_{42}$ fibrils fragility and morphological changes induced by co-incubation with sdAbs. A,B) Dot Blot of total protein, surnatant and pellet of centrifuged Aβ42 fibrils samples obtained in co-incubation or not with sdAbs. The membranes were incubated with 6E10 (A) and anti-6X His-tag (B) as primary Abs for the quantification of $A\beta_{42}$ and sdAbs, respectively. $A\beta_{42}$ signal was subtracted as background. Error bars are representative of the S.E.M (n = 3 for 6E10 Ab and n = 2 for anti- 6X His-tag Ab). Samples were analyzed by One-Tailed Student t-test relative to $A\beta_{42}$ fibrils obtained without antibody VS $A\beta_{42}$ fibrils obtained in the presence of sdAbs (* $P < 0.05$ VS DesAb-O and ** $P < 0.01$ VS Dimeric-DesAb-O, respectively) or to $A\beta_{42}$ fibrils obtained in the presence of DesAb-O compared to $A\beta_{42}$ aggregates obtained in the presence of the Dimeric-DesAb-O (°° $P < 0.01$) or in panel B to compare the presence of DesAb-O in the supernatant compared to the Dimeric-DesAb-O (° $P < 0.05$). C) Representative Western Blot of $A\beta_{42}$ fibrils obtained in co-incubation with sdAbs or not treated with increasing PK concentrations (0, 10, 25, 50 μg/mL) for 30 mins. D) Quantification of 0 μg/mL bands intensity (n = 3) for each treatment. We can assess that all fibrils obtained in different conditions share a similar bands intensity at 0 μg/mL, demonstrating a consistent baseline across different treatment conditions, enabling reliable normalization of bands obtained at higher PK concentrations. E) Evaluation of $A\beta_{42}$ fibrils resistance to the PK digestion at increasing PK concentrations (0, 10, 25, 50 μg/mL). $A\beta_{42}$ fibrils obtained in the presence of DesAb-O showed a slightly increased resistance to the PK digestion at 10μg/mL. Experimental errors are S.E.M. (n = 3). Samples were analyzed by one-tailed Student t-test relative to Aβ fibrils obtained without antibody VS Aβ fibrils obtained in the presence of

DesAb-O (§ $P < 0.05$), or to Aβ fibrils obtained in the presence of Dimeric- DesAb-O compared to Aβ aggregates obtained in the presence of DesAb-O (** $P < 0.01$).

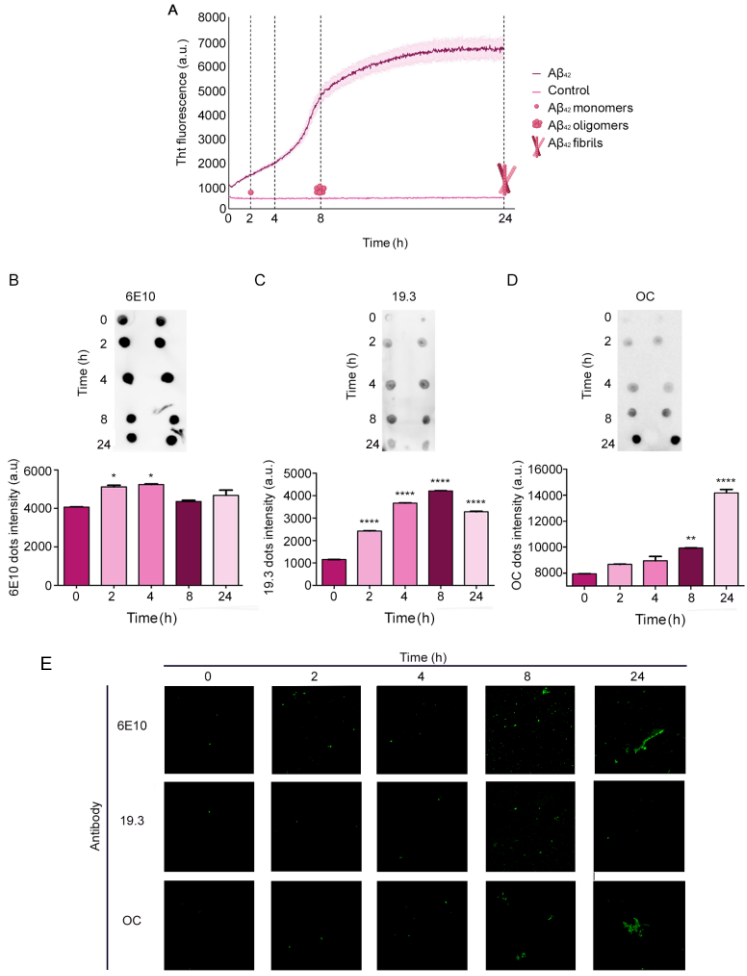

Figure 4.8 - Characterisation of $A\beta_{42}$ aggregates starting from the synthetic peptide. A) Monomeric $A\beta_{42}$ was incubated in PBS at 10 µM with 25 µM ThT dye. The plate was read in a BioTekSynergy^{TM}H1 Hybrid Multi-mode reader (Agilent, Santa Clara, United States) at 37 °C. Data were plotted using GraphPad Prism version 5.00 for Windows (GraphPad Software). Time points were collected at 0, 2, 4, 8 and 24 h to perform a characterization of $A\beta_{42}$ aggregates. B-D) Dot blot analysis and quantification of $A\beta_{42}$ samples collected at different timepoints. Samples of different $A\beta_{42}$ species were deposited (2 µl/spot) onto a nitrocellulose membrane and detected with the indicated antibodies (Abs). Membranes were incubated with 6E10 (B), 19.3 (C) and OC (D) primary Abs. The dot blot incubated with the 19.3 Ab showed the presence of oligomeric species since the early stage of the aggregation (2 h and 4 h) with the maximum amount reached at 8 h, consistent with the ThT assay showing the exponential phase at 8 h. From the dot blot obtained with the OC

Ab, we can see an increase of the dots intensity at 24 h, in line with the aggregation assay showing the reaching of the plateau due to the fibrils formation. Experimental errors are S.E.M. (n = 2). Samples were analysed by one-tailed Student t-test relative to their respective time 0 h (*P < 0,05, **P < 0.01, and ****P < 0.0001). E) STED microscopy images and visualisation of $A\beta_{42}$ samples collected at different timepoints. Samples of different $A\beta_{42}$ species were immunolabeled with 6E10, 19.3 and OC Abs. The STED microscopy images are perfectly in line with the dot blot assay results, showing the presence of oligomers since the initial stage of the aggregation $A\beta_{42}$ process as represented in 0, 2 and 4 h of 19.3 Abs images. After 24 h, the presence of fibrils is proved by the OC Abs signal confirming the aggregation assay and dot blot assay results.

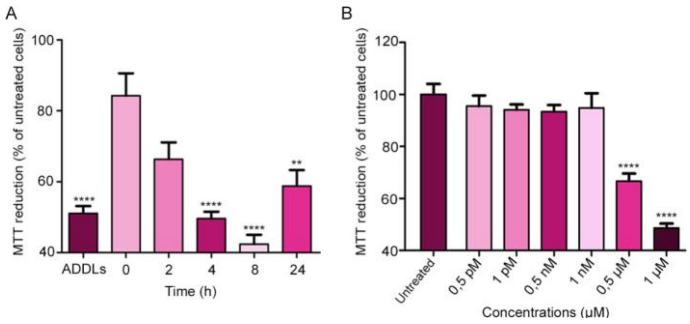

Figure 4.9 - $A\beta_{42}$ oligomeric species obtained after 8 h of incubation exhibit high toxicity. A) MTT reduction in SH-SY5Y cells treated for 24 h with various $A\beta_{42}$ aggregates (1 µM) obtained at different timepoints (0, 2, 4, 8 and 24 h) during aggregation (n = 2). ADDLs were used as a positive control. B) MTT reduction in SH-SY5Y cells treated for 24 h with $A\beta_{42}$ aggregates obtained after 8 h of aggregation in a dose-dependent manner. Experimental errors are S.E.M. (n = 3). Samples were analysed by One-way ANOVA followed by Bonferroni's multiple comparison test relative to untreated cells (**P<0.01 and ****P<0.0001).

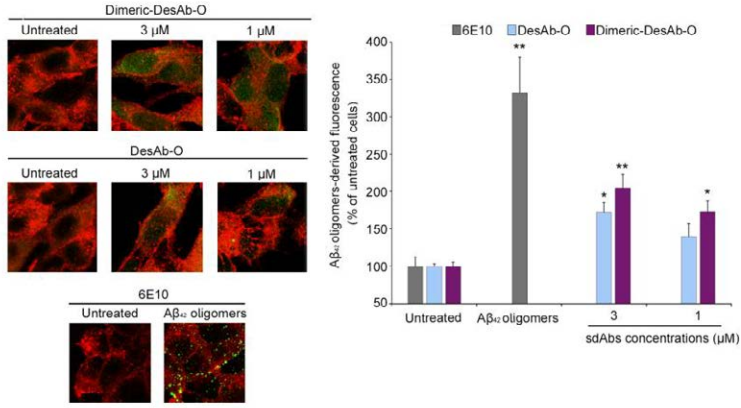

Figure 4.10 - The Dimeric-DesAb-O detects $A\beta_{42}$ oligomers interacting with neuronal cells at lower concentrations than DesAb-O. A) Representative confocal microscopy

images of SH-SY5Y cells treated with $A\beta_{42}$ species at 0.5μM for 1 h. Red and green fluorescence indicates respectively the cell membranes and the $A\beta_{42}$oligomers, detected respectively with wheat germ agglutinin (WGA) and sdAbs at two different concentrations of (3 μM or 1 μM). B) The histograms represent the results of a semi-quantitative analysis of the green fluorescent signal. Experimental errors are S.E.M. (n = 3). Samples were analyzed by one-tailed Student t-test to their respective untreated cells (*$P < 0.05$ and **$P < 0.01$). 200–250 cells were analyzed per condition.

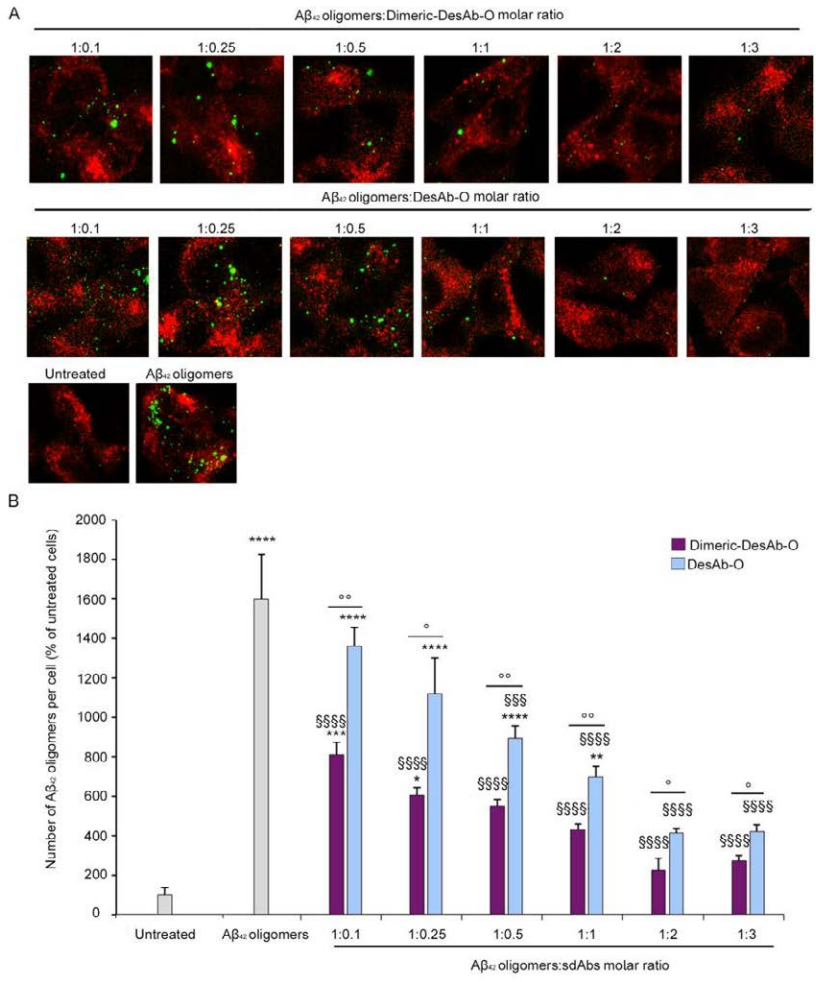

Figure 4.11 - The Dimeric-DesAb-O inhibits the binding of $A\beta_{42}$ oligomers to the neuronal membrane in a greater extent respect to DesAb-O. A) Representative confocal microscopy images of SH-SY5Y cells treated with 0.5 μM $A\beta_{42}$ oligomers following 1 h pre-incubation in the absence or in the presence of Dimeric-DesAb-O (first row) or DesAb-O (second row) at the indicated $A\beta_{42}$:sdAbs molar ratios. Red and green fluorescence indicates the cell membranes and $A\beta_{42}$ oligomers detected with WGA and 6E10 Ab, respectively. B) Count of $A\beta_{42}$ oligomers bound to the cellular membrane

measured following incubation under the conditions represented in panels A. Error bars indicate S.E.M. Statistical analysis was performed by ANOVA with multiple comparisons. Samples (n = 3) were analysed by one-way ANOVA followed by Bonferroni's multiple-comparison test to untreated cells (**$P < 0.05$, **$P < 0.01$, ***$P < 0.001$ and ****$P < 0.0001$), or to cells treated with $A\beta_{42}$ oligomers only (§§§§ $P < 0.001$ and §§§§ $P < 0.0001$) or to compare sdAbs at the same molar ratio (° $P < 0.05$ and °° $P < 0.01$).

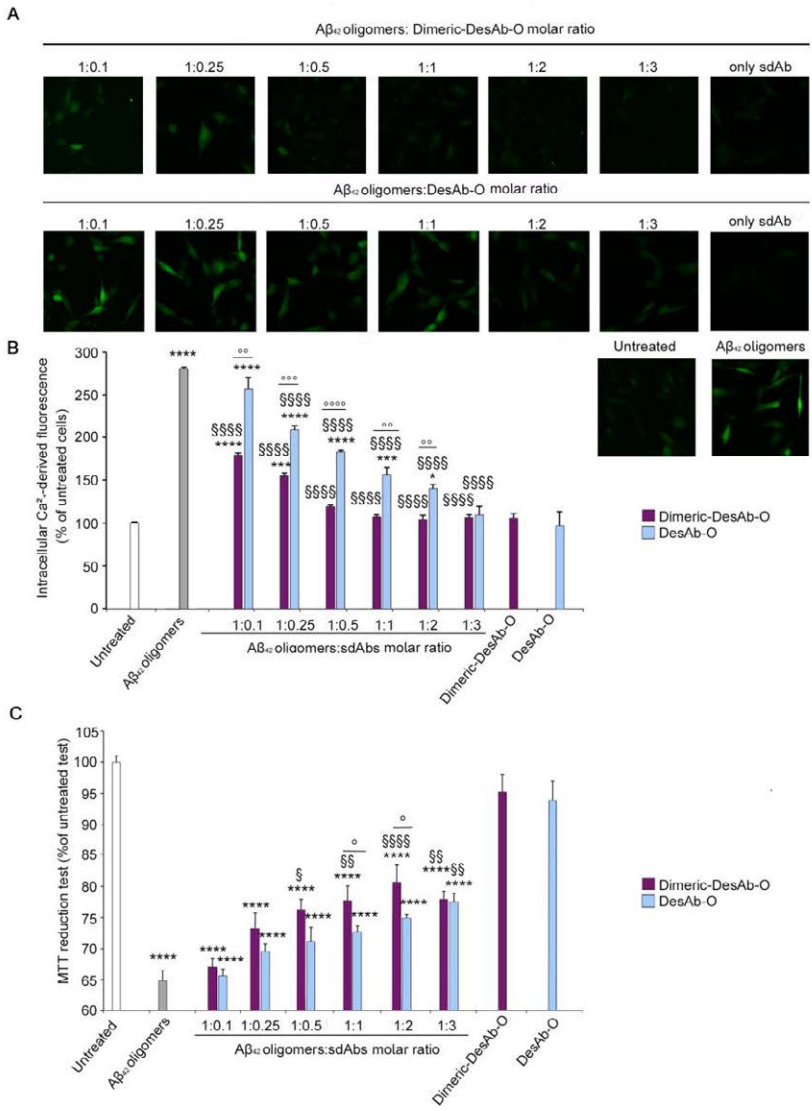

Figure 4.12 - The Dimeric-DesAb-O strongly prevents the neurotoxicity induced by $A\beta_{42}$ oligomers. A) Representative confocal microscopy images showing the Ca^{2+}- derived fluorescence in SH-SY5Y cells treated for 15 mins with 0.5 μM $A\beta_{42}$ oligomers with

increasing molar ratios (1:0.1, 1:0.25, 1:0.5, 1:1, 1:2, 1:3) of Dimeric-DesAb-O or DesAb-O. Cells were then loaded with the Fluo-4AM probe as described in the Methods section. B) Semi-quantitative analyses of the Ca^{2+}- derived fluorescence expressed as the percentage of the values for untreated cells. C) MTT reduction in SH-SY5Y cells treated for 24 h with increasing $A\beta_{42}$ oligomers:sdAbs molar ratios (1:0.1, 1:0.25, 1:0.5, 1:1, 1:2, 1:3). Errors are S.E.M. (n = 3 for confocal experiment and n = 4 for MTT). Samples were analyzed by One-way ANOVA followed by Bonferroni's multiple-comparison test to untreated cells (****P < 0.0001), or to cells treated with $A\beta_{42}$ oligomers (§ P < 0.05, §§ P < 0.01 and §§§§ P < 0.0001) or to compare sdAbs at the same molar ratio (° P < 0.05).

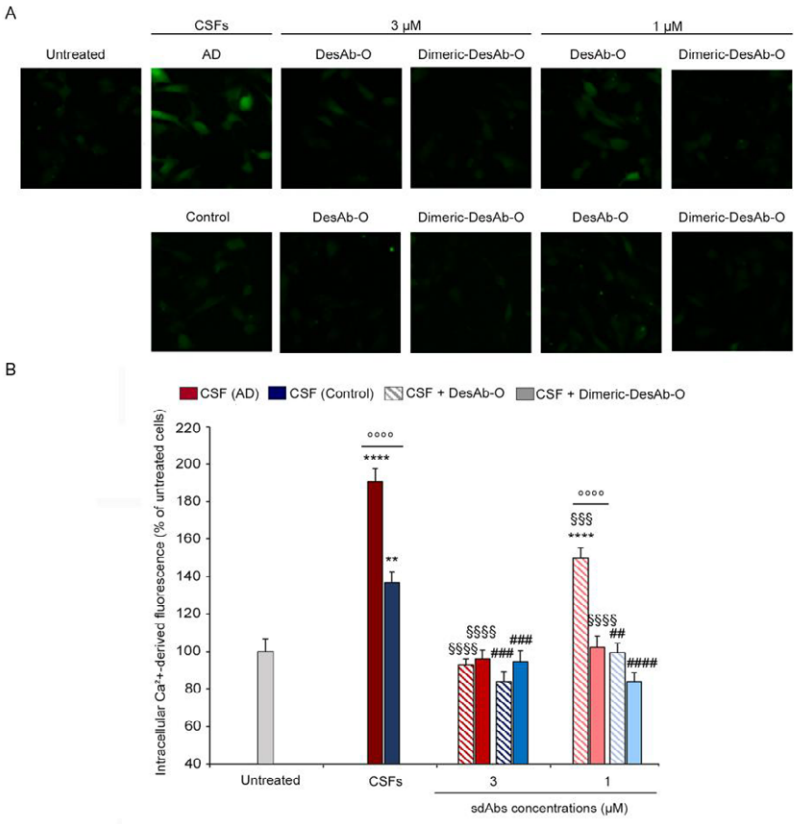

Figure 4.13 - The Dimeric-DesAb-O significantly reduce the Ca^{2+} dyshomeostasis induced by CSFs derived from AD patients. Intracellular Ca^{2+}-derived fluorescence in SH-SY5Y cells treated for 5 h with CSFs from AD patients and age-matched control subjects (n = 4), diluted 1:1 with the extracellular medium, following 1 h pre-incubation in the absence or in the presence of Dimeric-DesAb-O and DesAb-O at 3 µM or 1 µM. Experimental errors are S.E.M. Samples were analysed by One-way ANOVA relative to untreated cells (**P < 0.01 and ****P < 0.0001) or to cells treated with samples without DesAb-O (§§§ P < 0.001 and §§§§ P < 0.0001) or to compare the sdAbs at the same ratio (°°°° P < 0.0001).

Chapter 5
Discussion

AD accounts for 60-70% of cases of dementia worldwide (https://www.alz.org). The NIA-AA have proposed a research framework based on a biomarker-grounded biological, rather than syndromal, definition of AD, where the disease has to be regarded as a continuum (Jack *et al*. 2018). In this spectrum, seven biomarkers have attained widely recognized diagnostic relevance. These include the low levels of the $A\beta_{42}$ peptide and the high concentration of t-tau and p-tau in the CSF. They also include the high cortical amyloid deposition and cortical tau deposition measured with PET, poor brain glucose metabolism measured with FDG PET, and significant brain atrophy imaged with magnetic resonance imaging. The availability of this group of CSF-based and imaging-based biomarkers has led to the introduction of the AT(N) system for a biological characterization and staging of the disease (Jack *et al*. 2018).

The study and identification of novel biomarkers are important to enrich the aforementioned research framework, but also as diagnostic tools for supporting the existing biomarkers that often produce uncertain diagnoses in early AD, to address the pathological complexity and heterogeneity of the disease, and to enrich our biomarker list with others with more prognostic value (Hampel *et al*. 2021a).
All the classical protein-based biomarkers reveal the soluble and aggregation states of specific proteins, such as $A\beta_{42}$, t-tau and p-tau. However, it is recognized that protein misfolding diseases, including AD, are characterized by a generic failure of the PN, which physiologically maintains proteins in a soluble non-aggregated state (Labbadia and Morimoto 2015). In a compromised PN status a great number of proteins lose solubility and gain a propensity to misfold and aggregate (Hipp, Park and Hartl 2014). Accumulation of protein aggregates is both an effect and a cause of PN decline, driving a vicious cycle that ultimately leads to its collapse (Hipp, Park and Hartl 2014; Labbadia and Morimoto 2015).

Liliana Napolitano, liliana98.napolitano@gmail.com, 0009-0004-3087-286X

Referee List (DOI 10.36253/fup_referee_list)
FUP Best Practice in Scholarly Publishing (DOI 10.36253/fup_best_practice)

Liliana Napolitano, *Discussion*, © Author(s), CC BY 4.0, DOI 10.36253/979-12-215-0993-9.07, in Liliana Napolitano, *A multidisciplinary approach for the early diagnosis of Alzheimer's disease and potential therapeutic applications*, pp. 117-125, 2026, published by Firenze University Press, ISBN 979-12-215-0993-9, DOI 10.36253/979-12-215-0993-9

Book References DOI 10.36253/979-12-215-0993-9.references

Consistently, in all neurodegenerative disease the main characterizing protein deposits are often associated with those of other proteins.

Building on this idea, in this work we compared CSFs extracted from AD and non-AD cases in a novel Italian study named PRAMA and we sought the presence of aggregated protein species, detectable with biophysical methods, and proteotoxicity, in the form of misfolded protein oligomers able to cause cell dysfunction to cultured cells using cell viability assays. This idea is based on the detection of misfolded proteins not just of the $A\beta_{42}$ and tau proteins, that represent a very small fraction of the protein population composing the CSF, but of the overall CSF proteome.

29 patients with fin al clinical diagnosis of AD (AD cases) and 20 patients with final clinical diagnosis of other diseases affecting the CNS (non-AD cases) were recruited. Their CSF samples were collected and treated as reported in *section 1.1* in *Chapter 1*. At the time of CSF collection and analysis, the diagnosis was uncertain and was ascertained only after following clinical examination. None of the final diagnoses were post-mortem. In this work, we reported the mean and individual demographic characteristics of both groups, values of the classical CSF biomarkers ($A\beta_{42}/A\beta_{40}$ ratio and levels of t-tau and p-tau), percentages of patients with the ε4 allele of the *APOE* gene and scores of MMSE tests.

The total protein concentrations of the CSFs, measured using the Bradford assay, ranged from *ca.* 0.2 to 1.0 mg/ml in both groups, indicating similar distributions in the two groups in agreement with previous analyses (Dufour-Rainfray *et al.* 2013). Scatter plots of $A\beta_{42}/A\beta_{40}$ *versus* t-tau and $A\beta_{42}/A\beta_{40}$ *versus* p-tau, with the thresholds (t^*) derived from optimization of the Youden's indexes of the two parameters, show a good separation between non-AD and AD cases. This analysis validates our cohort as it indicates that the two groups are good representatives of non-AD and AD cases, respectively.

Once observed that our cohort was representative of non-AD and AD cases, CSFs were first compared by recording the size distributions of their particles with DLS, for five representative non-AD and five representative AD CSFs. In both cases, a peak of small species having an apparent hydrodynamic diameter (D_h) of *ca.* 10 nm is evident, which arises from the dominant largest CSF proteins, such as human serum albumin. This occurs because the all-α human serum albumin (HSA) is by far the most abundant protein in CSF and only one of the first ten most abundant proteins of the CSF is all-β, with the other nine being either mixed α/β or all-α proteins, as previously reported (Lardinois *et al*. 2014). However, large species arising from protein aggregates are also present in both groups, all having D_h values around or higher than 100 nm. The *LSI* arising from large species (D_h> 30 nm) is higher in AD cases, indicating a larger proportion of protein aggregates in this group. In 2019, De and co-workers analysed the size and morphology of aggregates present in CSF samples using a newly developed super-resolution technique called AD-PAINT (AD-PAINT) and measured the size of individual aggregates, which ranged from 20 nm to 300 nm (De *et al.*

2019).To examine the aggregate morphologies, they compared the size distribution of protein aggregates in the CSF of control, MCI, and AD subjects. Analysis of the aggregate size histograms revealed a statistically significant (99% confidence) increase in smaller aggregates (< 50 nm) in MCI CSF compared to controls. In line with our results, they demonstrated that AD CSF showed a ten-fold increase in the proportion of larger, mature aggregates (~ 40 to 200 nm) relative to controls. Furthermore, their finding suggests a potential link between smaller aggregates and increased membrane permeability observed in MCI (Kremer *et al.* 2000, De *et al.* 2019). Indeed, since protein aggregates added to the extracellular medium of cultured cells have the ability to bind and destabilize biological membranes and cause an influx of Ca^{2+} ions into the cytosol (Bigi *et al.* 2020; Cascella *et al.* 2021; Fani *et al*. 2021; Fani *et al*. 2022; Bigi *et al*. 2023a), the levels of intracellular Ca^{2+} ions of cultured cells exposed to CSF samples are a good indicator of CSF proteotoxicity (Fani *et al*. 2022). We therefore added the CSFs to the extracellular medium of SH-SY5Y neuroblastoma cells (1:1) and measured the intracellular Ca^{2+} levels after 5 h, using the Fluo-4 AM probe and confocal fluorescence microscopy. From our study, cells treated with AD CSFs showed higher Ca^{2+} levels compared to cells treated with non-AD CSFs (except one outlier sample) in agreement with others findings (Yerbury and Wilson 2010; Bigi *et al*. 2024b). To sum up, AD CSFs are characterized by higher values of *LSI* from large protein species in the DLS distributions and higher ability to induce high cytosolic Ca^{2+} levels when added to the medium of cultured cells. These findings have a rationale in the presence of higher amounts of large protein particles and misfolded protein oligomers inducing Ca^{2+} dyshomeostasis in cells, respectively.

We then combined the three classical CSF biomarkers ($A\beta_{42}/A\beta_{40}$, t-tau, p-tau) with the two novel putative biomarkers identified here (*LSI*, Ca^{2+} levels). The comparison between scatter plots built with pairs of classical biomarkers and mixed classical and novel biomarkers indicate good separations with $p<0.0001$ in all cases, using both the Fisher's exact and Chi-square tests. This observation legitimates the use of the two novel CSF parameters analyzed here for AD diagnosis. In this context, many efforts have been made to find new biomarkers and combine them with traditional biomarkers to study their application in the early and differential diagnosis of AD (Westin *et al*. 2012, Sutphen *et al*. 2015, Lusardi *et al*. 2017, Wiedrick *et al*. 2019). In line with our results, in 2023, Liu and coworkers performed an analysis of CSF and blood serum revealing distinct protein profiles in individuals with AD compared to controls. AD patients exhibited altered levels of multiple proteins, with 8 increased and 60 decreased in CSF, and 55 increased and 10 decreased in serum. These findings highlight a systemic dysregulation of protein expression associated with AD, affecting both the central nervous system and peripheral blood. Among the 8 proteins over-expressed in the CSF, 3 of them, the sodium-/potassium-transporting ATPase subunit beta-1 (AT1B1), serglycin (SRGN) and thioredoxin-dependent peroxide reductase mitochondrial (PRDX3), were found to highly differentiate AD subjects from controls subjects with an AUC lower but close to those of CSF $A\beta_{42}$, t-tau,

and p-tau (Liu *et al*. 2023).

These results showed that although the AD/non-AD segregation using novel biomarkers is not as high as that obtained with classical biomarkers, it is very highly significant. In the broader context of AD, the possibility to distinguish AD and non-AD cases based on the novel biomarkers identified here reinforces the view that PN is compromised in AD leading to an aggregated and proteotoxic status of Aβ and tau, and many other proteins of the entire proteome. With the aim of recognizing aggregated toxic species for the development of possible treatment for AD or research purposes, major efforts have been made over the years to design conformational Abs raised by different investigators against independently generated Aβ oligomers, detected in AD brains unlike age-matched healthy individuals (Kayed *et al*. 2003; Gong *et al*. 2003; Kayed *et al*. 2007; Hillen *et al*. 2010). Indeed, considerable attention was invested in the development of robust assays to characterize and quantify oligomers, discriminating them from the monomeric form (Hefti *et al*. 2013; Savage *et al.* 2014; De *et al*. 2019). In all the ELISA-based methods, a significant overlap in the total mass of Aβ oligomers between patients and controls has been observed, although a small increase in the oligomeric mass has been reported for some cohorts (Jekel *et al*. 2015; Savage *et al*. 2014). However, due to the lack of suitable sensitive methods, the detection, quantification and isolation of these soluble neurotoxic species from biological fluids remain difficult, because of their heterogeneity, transient nature and very low concentration.

Nanobodies or sdAbs have been recently proposed as promising tools for basic research and potential candidates for diagnostic and therapeutic applications in a range of pathological conditions, thanks to their high target specificity and affinity, as well as low immunogenic potential (Muyldermans 2013, Zheng *et al*. 2022). In particular, the rational design of sdAbs that selectively target specific Aβ conformers neutralising their neurotoxicity has a great potential of diagnostic and therapeutic value for AD (Zameer *et al*. 2008; Lafaye *et al*. 2009; Kasturirangan *et al*. 2012; David, Jones and Tayebi 2014; Aprile *et al*. 2020; Zheng *et al*. 2022). A dozen of sdAbs have shown their therapeutic or diagnostic potential value for AD *in vitro* (Bélanger *et al*. 2019), and two of them, namely R3VQ and A2, have reached *in vivo* imaging as they bind brain Aβ deposits and tau inclusions, respectively (Li *et al*. 2016).

In this work, we examined the potential role of a sdAb, named DesAb-O, targeting a conformational epitope formed by residues 29-36 of $A\beta_{42}$ and exposed by the oligomeric species (Aprile *et al.* 2020), to selectively detect and neutralise $A\beta_{42}$ oligomers both from synthetic origin and present in AD CSFs. We first characterised its ability to detect a range of pathologically relevant, highly stable and well-characterised $A\beta_{42}$ aggregates (A+ and A- oligomers, ADDLs, and two type of fibrils) (Lambert *et al*. 1998; Dahlgren *et al*. 2002; Ladiwala *et al*. 2012), taking advantage of a panel of commercially available conformation-sensitive Abs, as controls. The immunoassays analysis revealed a high affinity and selectivity of DesAb-O for $A\beta_{42}$ oligomers, at least equal to that of the A11 and 19.3 Abs,

raised against prefibrillar oligomers and ADDLs, respectively (Kayed *et al*. 2003; Savage *et al*. 2014), with only a minor cross-reaction with the monomeric protein, nontoxic oligomers, and fibrillar conformers. We also evaluated the ability of DesAb-O to selectively detect $A\beta_{42}$ oligomers in cultured cells, demonstrating a great performance also in a more physiological condition.

We then revealed that the pre-incubation of DesAb-O with $A\beta_{42}$ oligomers strongly reduces their interaction with neuronal membranes in a dose-dependent manner, and this protective effect appears more evident for DesAb-O than the A11 Ab, at least at low $A\beta_{42}$:Abs molar ratios. This suggests that DesAb-O can detect the key epitopes normally exposed on the surface of toxic oligomers and responsible for the interaction with the membrane more effectively than the A11 Ab, presumably because of its smaller size, that enables a more precise targeting of critical epitopes. Our results are consistent with those obtained with conformation-sensitive Abs, such as ACU-954 and A-887755, specifically raised against Aβ oligomers, namely ADDLs and globulomers, respectively, that were found to prevent their binding to neurons (Shughrue *et al.* 2010; Hillen *et al.* 2010), rescuing the impaired synaptic transmission (Hillen *et al.* 2010). The capture of $A\beta_{42}$ oligomers by DesAb-O was also found to prevent their induced mitochondrial dysfunction, in agreement with large body of evidence supporting the protective effects of Abs, such as A11, OC, AUC-954, A-887755, and PMN310, against neuronal dysfunction (Kayed *et al.* 2003; Kayed *et al.* 2007; Hillen *et al*. 2010; Shughrue *et al*. 2010; Gibbs *et al*. 2019; Bigi *et al*. 2020). Notably, DesAb-O showed no inherent toxicity when added alone to the cell culture medium, thus making it an excellent tool for future tentative therapeutic applications.

Other sdAbs have been reported to target pathologically relevant $A\beta_{42}$ oligomers. For example, the V31-1 was able to recognize intraneuronal oligomers in human brain slices and to inhibit fibril formation preventing their induced neurotoxicity (Lafaye *et al.* 2009), suggesting a great potential for the detection and diagnosis of Aβ oligomers in AD patients (Pain, Dumont and Dumoulin 2015). In addition, two sdAbs, namely PrioAD12 against anti-$A\beta_{40}$ and PrioAD13 against $A\beta_{42}$ (David, Jones and Tayebi 2014) can detect Aβ oligomers simultaneously in the blood and retina of APP/PS1 mice before their appearance in the brain, with respect to age-matched wild-type mice controls (Habiba *et al*. 2021).

When we moved our approach to CSFs, we revealed a remarkable ability of DesAb-O to selectively identify $A\beta_{42}$ oligomers also in a biological fluid from AD patients compared to age-matched control subjects. Previous studies detected $A\beta_{42}$ oligomers in AD CSFs by using two-site ELISA assay and the couple 19.3/82E1 Abs (Savage *et al.* 2014), or homotypic ELISA using 82E1 Ab (Hölttä *et al*. 2013) or BAN50 Ab (Herskovits *et al*. 2013). Even if these reported assays used different oligomer standards, a trend has emerged suggesting that a sub-pg/ml sensitivity is required to detect CSF oligomers (Georganopoulou *et al.* 2005; Hölttä *et al*. 2013; Savage *et al*. 2014). Indeed, in our assay we have been

able to measure an average oligomer concentration of c.a. 4.5 pg/ml, in good agreement with previous findings (Hölttä *et al.* 2013; Savage *et al.* 2014;Yang *et al*. 2015). It is important to clarify that some studies reported a lack of significant change in total aggregates between AD and controls, using both a sdAbs, named Nb3, and a mAb, named Bapineuzimab (Yang *et al.* 2015; Drews *et al.* 2017). This suggests that the total amount of the aggregates is not a critical factor in AD CSFs, but it is rather the nature of these aggregates and their effects to be important.

Further analyses were conducted in this work on neuroblastoma cells to test the possible therapeutic potential of DesAb-O against the neurotoxic $A\beta_{42}$ oligomers present in the CSFs of AD patients. We first demonstrated that the CSFs of AD patients caused significant Ca^{2+} influx, membrane permeabilization and mitochondrial dysfunction, in agreement with previous findings (Walsh *et al.* 2002; Klyubin *et al*. 2008; Yerbury and Wilson 2017) and suggesting that the AD CSF contains neurotoxic species. Notably, DesAb-O was found to prevent neuronal dysfunction caused by Aβ oligomers present in the CSFs of AD patients, in agreement with other studies using Nb3 and other Abs against Aβ (Walsh *et al.* 2002; Klyubin *et al*. 2008), or extracellular chaperones (Yerbury and Wilson 2010). It is well known that the shielding of toxic hydrophobic regions exposed on the oligomer surface by either polyclonal or monoclonal Abs, extracellular chaperones and even other proteins present in biological fluids such as transthyretin, appears to be an effective method to suppress the toxicity of misfolded $A\beta_{42}$ oligomers (Keyed *et al.* 2003; Savage *et al*. 2014; Cascella *et al.* 2013a; Cascella *et al*. 2013b), but the high sensitivity and selectivity of DesAb-O and possibly other sdAbs relative to other Abs and chaperones could offer a remarkable potential of these biotechnological tools against AD particularly in its early stages.

In this context and with the aim of improving the DesAb-O specificity and affinity for $A\beta_{42}$ oligomers, we design the Dimeric-DesAb-O. The dimeric structure was obtained connecting two monomers with a flexible $(GGGGS)_3$ linker and removing the His-tag region from the N-terminus of the second monomer. Together, the loop region of DesAb- O and the flexible GS linker compose a *partial natural linker* of 39 aa length. We then characterize the structure of Dimeric-DesAb-O investigating the secondary structure, molecular weight and thermal stability by CD and ESI-MS. We found that the dimeric sdAb shared the same structure and, surprisingly, a close temperature of half-denaturation with its monomer (Klement *et al*. 2015).

Thereafter, we tested the ability of the Dimeric-DesAb-O to interfere with the $A\beta_{42}$ aggregation process performing ThT assays and whether it showed an increased specificity and affinity for $A\beta_{42}$oligomers with respect to the monomeric sdAb, performing a Real-Time Based ELISA assay. Interestingly, the Dimeric-DesAb-O showed a massive interference in the $A\beta_{42}$ aggregation at an equimolar concentration with the $A\beta_{42}$ monomer and in a dose dependence manner decreasing the sdAb concentration. We also tested DesAb-O as a control

observing that it can interfere with $A\beta_{42}$ aggregation at a lower extent compared to the dimeric sdAb, which demonstrates a substantially enhanced potency. Furthermore, our results showed a higher ability of the Dimeric-DesAb-O in recognizing $A\beta_{42}$ oligomers with respect to the monomeric sdAb. Indeed, the highest absorbance values, as determined by ThT assay, was observed approximately close to the half-time of aggregation, time in which oligomeric species reach their maximum amount.

A significant difference was obtained compared to DesAb-O at the same time of aggregation, suggesting that the engineering of DesAb-O sharply improved the previous outstanding affinity and specificity for $A\beta_{42}$ oligomers.

In literature, the engineering of sdAbs through the application of a flexible linker was extensively used over the past years with the aim of increase the binding avidity and specificity for their antigen. In 2011, Hultberg and coworkers obtained multivalent constructs against the Respiratory Syncytial Virus fusion protein (RSV F), the highly pathogenic avian influenza virus A (H5N1 HA) and Rabies G protein. Surprisingly, a bivalent protein composed of two identical anti-F VHHs extremely increased the RSV neutralizing ability by 4000-fold. Similarly, multivalent constructs against influenza H5N1 and vesicular stomatitis virus (VSV) also showed significantly increased potency. They observed that the optimal length of the linker connecting the VHHs, ranging between 9 and 35 aa, varied depending on the virus and specific antibody combination, highlighting the need for case-by-case optimization. For instance, a shorter linker worked better for trivalent anti-influenza constructs, while linker length did not significantly impact on bivalent anti-RSV constructs (Hultberg *et al*. 2011). Later in 2014, Cardoso and colleagues fused two identical anti-influenza neuraminidases (NA) VHHs using the llama IgG2c hinge as a flexible linker. Similar to the study mentioned above, the antiviral potency of the bivalent format was found to be significantly enhanced (Cardoso *et al*. 2014). These studies support the possibility that the addition of a flexible linker is a successful method for the optimization of the binding avidity and affinity of sdAbs for their antigen and that the linker length optimized case-by-case ensures wide range of movement of both domains and the ability to bind antigenic sites spaced between them. We further investigated the impact of the Dimeric-DesAb-O on the $A\beta_{42}$ aggregation, by using TEM. Our data revealed that the co-incubation of $A\beta_{42}$ monomer with sdAbs induced morphological and structural changes in $A\beta_{42}$ fibrils. In particular, in the presence of the dimeric DesAb-O we observed a reduction in width fibrils dimeter, a jagged appearance and a highly increased fragility. Similar results have been reported with other nanobodies, also known as Nbs, such as, V31-1 (Lafaye *et al.* 2009), A4 and E1 (Kasturirangan *et al*. 2012), able to selectively recognize low-molecular-weight Aβ42oligomers and inhibit fibrils formation (Lafaye *et al.* 2009, Kasturirangan *et al*. 2012). In 2022, another Nbs was developed to specifically binds the PHF6 sequence, located in the core structure of au aggregation, inhibiting this process (Danis *et al*. 2022).

Further evidences of the inhibition of $A\beta_{42}$aggregation have been observed with anti-Aβ single chain fragment variable antibodies (scFvs), that are composed by the heavy and light variable chain variable regions of an entire immunoglobulin (Bird *et al*. 1989), sharing a similar structure with the dimeric form of DesAb-O that differs from an scFv only for the presence of two identical variable heavy domains as recognition sites. In 2011, Marín-Argany and colleagues tested the conformational changes induced in $A\beta_{42}$oligomers by scFv-h3D6 binding. This scFv was able to induce nontoxic conformational changes in $A\beta_{42}$ oligomeric species, abolishing their detrimental effects (Marín-Argany *et al.* 2011). Our results agreed with a large body of evidence supporting the morphological and structural changes in $A\beta_{42}$ fibrils by scFv binding, such as the scFv59 (Fukuchi *et al*. 2006a; Fukuchi *et al*. 2006b), scFv B6 (Yoshihara *et al.* 2008), and scFv-1E8 (Nisbet *et al*. 2013).

We then evaluate the ability of the Dimeric-DesAb-O to selectively detect $A\beta_{42}$ in cultured cells, as previously reported (Bigi *et al*. 2024b). The pre-incubation of the dimeric sdAb with $A\beta_{42}$ oligomers caused a massive reduction of their interaction with neuronal membranes in a dose-dependent manner, in agreement with another scFv, called NUsc1, able to prevent the interaction of $A\beta_{42}$ oligomers in mature rat hippocampal cultures (Selles *et al*. 2022). Furthermore, we observed a decreased alteration of intracellular Ca^{2+}free levels and an increased prevention of the mitochondrial dysfunction at lower $A\beta_{42}$ oligomers:sdAb molar ratios compared to DesAb-O, suggesting that the presence of two cooperative binding sites for $A\beta_{42}$ oligomers enhances the detection of key epitopes exposed by toxic oligomers, thus preventing the interaction with neuronal membranes more efficiently than DesAb-O.

These results appear to be consistent with those obtained with other scFv, such as A4- scFv (Zameer *et al*. 2008), scFv-1E8 (Nisbet *et al*. 2013), and HCDR3 (Manoutcharian *et al*. 2004) able to capture $A\beta_{42}$ oligomers and prevent detrimental effects, such as mitochondrial dysfunction. Indeed, Zameer and coworkers performed a lactate dehydrogenase (LDH) release assay on human SH-SY5Y neuroblastoma cells, observing that the treatment with $A\beta_{42}$ monomer in the presence of scFv for 96 h determined no signs of toxicity. Taking advance of the AFM, they observed morphological changes in $A\beta_{42}$ aggregates formed in the presence of scFv (Zameer *et al*. 2008). In line with our results, this data was further confirmed using an MTT assay and evaluating the mitochondrial dysfunction induced by $A\beta_{42}$ oligomers (Zameer *et al*. 2008). In agreement, Nisbet and colleagues performed a cell counting Kit-8 assay (CCK-8) and LDH assay on primary cortical neuronal cultures treated with $A\beta_{42}$ oligomers in the absence or in the presence of scFv-1E8. In both analyses, the co-incubation with the scFv significantly restored the cell viability, suggesting the ability of this scFv to prevent the detrimental effects induced by $A\beta_{42}$ oligomers on cultured cells (Nisbet *et al*. 2013). With a different approach, Manoutcharian and coworkers obtained two new anti-$A\beta_{42}$ phage- displayed scFvs Abs. They focused on a specific part of the Ab called the heavy chain complementarity-determining

region 3 (HCDR3), a crucial part that directly interacts with the antigen and created two small synthetic peptides, N44 and C44, that mimicked the HCDR3 region of the scFv with the highest $A\beta_{42}$ oligomers affinity. They studied the effect of HCDR3-derived synthetic peptides on hippocampal cultures that were exposed to $A\beta_{42}$ peptide in the absence or in the presence of the synthetic peptides N44 and C44, by the MTT assay. Their results showed that the co-incubation with N44 did not prevent the mitochondrial dysfunction induced by the $A\beta_{42}$ peptide, whereas C44, in its linear form, significantly prevented the $A\beta_{42}$ toxicity (Manoutcharian *et al.* 2004), appearing perfectly in line with our results. Further evidence was obtained in mice models where a scFv, called W20, was found to prevent the neuropathology induced by the accumulation of αSyn and mutant huntingtin protein aggregates (Zha *et al*. 2016).

This work also included a proof-of-concept analysis on the therapeutic potential of Dimeric-DesAb-O against neurotoxic $A\beta_{42}$ oligomers present in the CSF samples of AD patients. Firstly, we demonstrated that the administration of AD CSFs to human SH- SY5Y neuroblastoma cells caused significant Ca^{2+} influx, in agreement with previous findings (Walsh *et al*. 2002, Klyubin *et al.* 2008, Yerbury and Wilson 2017, Bigi *et al*. 2024b) and suggesting that the AD CSF contains neurotoxic species. Notably, the Dimeric-DesAb-O was found to prevent neuronal dysfunction caused by $A\beta_{42}$ oligomers present in the CSFs of AD patients at lower concentrations than DesAb- O, demonstrating again the increased specificity for $A\beta_{42}$ oligomers and its ability to detect these toxic aggregates in complex biological fluid, such as the CSF extracted from AD patients.

While further studies in larger cohorts of AD patients and controls are needed, our data support the idea that engineering sdAbs directed against $A\beta_{42}$ oligomers greatly improves the performance of nanobodies. Furthermore, they may represent a new biotechnological tool for the diagnosis of AD at a very early stage of pathology due to their high specificity for $A\beta_{42}$ oligomers and their ability to detect them in complex biological fluids.

Chapter 6
Conclusions and future perspectives

In conclusion, in this thesis are reported significant contributions to the field of AD research on two fronts. Firstly, this research has explored the potential of the identification of large protein aggregates in the CSFs of AD patients and the evaluation of their ability to induce an increase of intracellular Ca^{2+} levels as novel biomarkers for an early diagnosis of AD. Through rigorous biochemical, biophysical and cellular analyses, this study provided compelling evidence for these two novel biomarkers to be able to discriminate CSFs derived from AD patients from control subjects, legitimating their use for AD diagnosis, also in combination with classical biomarkers, to improve their diagnostic accuracy. Secondly, this study underlies the importance of sdAbs raised against Aβ oligomers as promising tools for the early diagnosis and therapy of AD. By meticulously characterizing their binding properties, demonstrating their efficacy in mitigating Aβ-induced toxicity *in vitro* and their ability to discriminate between AD CSFs and CSFs derived from age-matched control subjects, this work lays a strong foundation for the advancement of sdAb-based diagnosis and therapy.
Despite these promising results, these studies have some limitations. Indeed, it will be important to apply all the studies reported in this thesis to larger and/or other cohorts to corroborate our experimental evidence. It will also be important to assess whether these two novel biomarkers are extendable to plasma samples, usable as prognostic tools, in addition to diagnostic. Finally, it will be important to assess whether they are exploitable for early diagnosis in the preclinical phase of AD, on the grounds that a defective PN is an early event in protein misfolding diseases and a cause of the formation of amyloid plaques and neurofibrillary tangles detectable with classical biomarkers. Additional studies are also required for sdAbs, that should be again tested for their ability to detect Aβ oligomers in larger cohorts of AD patients, as previously reported. Further investigation

Liliana Napolitano, liliana98.napolitano@gmail.com, 0009-0004-3087-286X

Referee List (DOI 10.36253/fup_referee_list)
FUP Best Practice in Scholarly Publishing (DOI 10.36253/fup_best_practice)

Liliana Napolitano, *Conclusion and Future Perspectives*, © Author(s), CC BY 4.0, DOI 10.36253/979-12-215-0993-9.08, in Liliana Napolitano, *A multidisciplinary approach for the early diagnosis of Alzheimer's disease and potential therapeutic applications*, pp. 127-128, 2026, published by Firenze University Press, ISBN 979-12-215-0993-9, DOI 10.36253/979-12-215-0993-9

Book References DOI 10.36253/979-12-215-0993-9.references

utilizing animal models or human-relevant cellular models, such as induced pluripotent stem cells (iPSCs), is also crucial. These models offer the distinct advantage of retaining patient-specific genetic backgrounds, enabling the evaluation of these sdAbs in a context that closely mirrors the complexities of human brain cells and facilitates translationally relevant insights.

Altogether, these studies on the research of new putative biomarkers and the testing and engineering of sdAbs as promising tools for an early diagnosis and therapy of AD, represent a crucial step towards a future in which this devastating disease for patients and families, will be only a distant fading nightmare.

References

2021 Alzheimer's disease facts and figures. (2021). *Alzheimer's & Dementia: The Journal of the Alzheimer's Association*, *17*(3), 327–406. https://doi.org/10.1002/alz.12328

2023 Alzheimer's disease facts and figures. (2023). *Alzheimer's & Dementia: The Journal of the Alzheimer's Association*, *19*(4), 1598–695. https://doi.org/10.1002/alz.13016

Abelein, A., Chen, G., Kitoka, K., Aleksis, R., Oleskovs, F., Sarr, M., Landreh, M., Pahnke, J., Nordling, K., Kronqvist, N., Jaudzems, K., Rising, A., Johansson, J., & Biverstål, H. (2020). High-yield Production of Amyloid-β Peptide Enabled by a Customized Spider Silk Domain. *Scientific Reports*, *10*(1), 235. https://doi.org/10.1038/s41598-019-57143-x

Ackaert, C., Smiejkowska, N., Xavier, C., Sterckx, Y. G. J., Denies, S., Stijlemans, B., Elkrim, Y., Devoogdt, N., Caveliers, V., Lahoutte, T., Muyldermans, S., Breckpot, K., & Keyaerts, M. (2021). Immunogenicity Risk Profile of Nanobodies. *Frontier in Immunology*, *12*, 632687. https://doi.org/10.3389/fimmu.2021.632687

Ahmed M., Davis, J., Aucoin, D., Sato, T., Ahuja, S., Aimoto, S., Elliott, J. I., Van Nostrand, W. E., Smith, S. O. (2010). Structural conversion of neurotoxic amyloid-beta(1-42) oligomers to fibrils. Nat Struct Mol Biol. May;17(5):561-7. doi: 10.1038/nsmb.1799. Epub 2010 Apr 11. PMID: 20383142; PMCID: PMC2922021.

Albert, M. S., DeKosky, S. T., Dickson, D., Dubois, B., Feldman, H. H., Fox, N. C., Gamst, A., Holtzman, D. M., Jagust, W. J., Petersen, R. C., Snyder, P. J., Carrillo, M. C., Thies, B., & Phelps, C. H. (2011). The diagnosis of mild cognitive impairment due to Alzheimer's disease: Recommendations from the National Institute on Aging-Alzheimer's Association workgroups on diagnostic guidelines for Alzheimer's disease. *Alzheimer's & Dementia: The Journal of the Alzheimer's Association*, *7*(3), 270–79.

Referee List (DOI 10.36253/fup_referee_list)
FUP Best Practice in Scholarly Publishing (DOI 10.36253/fup_best_practice)

https://doi.org/10.1016/j.jalz.2011.03.008

Alonso, A. D., Cohen, L. S., Corbo, C., Morozova, V., ElIdrissi, A., Phillips, G., & Kleiman, F. E. (2018). Hyperphosphorylation of Tau Associates with Changes in Its Function Beyond Microtubule Stability. *Frontiers in Cellular Neuroscience*, *12*, 338. https://doi.org/10.3389/fncel.2018.00338

Alzforum. 2023. Remternetug [cited 26 Apr 2023]. https:// www. alzfo rum. org/ therapeuti cs/ remternetug.

Alzheimer Europe. Dementia in Europe Yearbook 2019: estimating the prevalence of dementia in Europe. (2020).

Alzheimer, A., Stelzmann, R. A., Schnitzlein, H. N., & Murtagh, F. R. (1995). An English translation of Alzheimer's 1907 paper, 'Uber eineeigenartigeErkankung der Hirnrinde'. *Clinical Anatomy (New York, N.Y.)*, *8*(6), 429–31. https://doi.org/10.1002/ca.980080612

Alzheimer's Disease and Dementia. Aducanumab Discontinued as an Alzheimer's Treatment. (n.d.). *Alzheimer's Disease and Dementia*. Retrieved 4 December 2024, from https://alz.org/alzheimers-dementia/treatments/aducanumab

Amador-Ortiz, C., Lin, W.-L., Ahmed, Z., Personett, D., Davies, P., Duara, R., Graff- Radford, N. R., Hutton, M. L., & Dickson, D. W. (2007). TDP-43 immunoreactivity in hippocampal sclerosis and Alzheimer's disease. *Annals of Neurology*, *61*(5), 435–45. https://doi.org/10.1002/ana.21154

Amm, I., Sommer, T., & Wolf, D. H. (2014). Protein quality control and elimination of protein waste: The role of the ubiquitin-proteasome system. *Biochimica Et Biophysica Acta*, *1843*(1), 182–96. https://doi.org/10.1016/j.bbamcr.2013.06.031

An, Y., Varma, V. R., Varma, S., Casanova, R., Dammer, E., Pletnikova, O., Chia, C. W., Egan, J. M., Ferrucci, L., Troncoso, J., Levey, A. I., Lah, J., Seyfried, N. T., Legido-Quigley, C., O'Brien, R., &Thambisetty, M. (2018). Evidence for brain glucose dysregulation in Alzheimer's disease. *Alzheimer's & Dementia: The Journal of the Alzheimer's Association*, *14*(3), 318–29. https://doi.org/10.1016/j.jalz.2017.09.011

Andrews, S. J., Renton, A. E., Fulton-Howard, B., Podlesny-Drabiniok, A., Marcora, E., & Goate, A. M. (2023). The complex genetic architecture of Alzheimer's disease: Novel insights and future directions. *EBioMedicine*, *90*, 104511. https://doi.org/10.1016/j.ebiom.2023.104511

Angelova, P. R., & Abramov, A. Y. (2018). Role of mitochondrial ROS in the brain: From physiology to neurodegeneration. *FEBS Letters*, *592*(5), 692–702. https://doi.org/10.1002/1873-3468.12964

Antonell, A., Mansilla, A., Rami, L., Lladó, A., Iranzo, A., Olives, J., Balasa, M., Sánchez-Valle, R., & Molinuevo, J. L. (2014). Cerebrospinal fluid level of YKL-40 protein in preclinical and prodromal Alzheimer's disease. *Journal of Alzheimer's Disease: JAD*, *42*(3), 901–8. https://doi.org/10.3233/JAD-140624

Aprile, F. A., Sormanni, P., Perni, M., Arosio, P., Linse, S., Knowles, T. P. J., Dobson, C. M., & Vendruscolo, M. (2017). Selective targeting of primary and secondary nucleation pathways in Aβ42 aggregation using a rational antibody

scanning method. *Science Advances*, *3*(6), e1700488. https://doi.org/10.1126/sciadv.1700488

Aprile, F. A., Sormanni, P., Podpolny, M., Chhangur, S., Needham, L.-M., Ruggeri, F. S., Perni, M., Limbocker, R., Heller, G. T., Sneideris, T., Scheidt, T., Mannini, B., Habchi, J., Lee, S. F., Salinas, P. C., Knowles, T. P. J., Dobson, C. M., & Vendruscolo, M. (2020). Rational design of a conformation-specific antibody for the quantification of Aβ oligomers. *Proceedings of the National Academy of Sciences of the United States of America*, *117*(24), 13509–18. https://doi.org/10.1073/pnas.1919464117

Arbel-Ornath, M., Hudry, E., Boivin, J. R., Hashimoto, T., Takeda, S., Kuchibhotla, K. V., Hou, S., Lattarulo, C. R., Belcher, A. M., Shakerdge, N., Trujillo, P. B., Muzikansky, A., Betensky, R. A., Hyman, B. T., &Bacskai, B. J. (2017). Soluble oligomeric amyloid-β induces calcium dyshomeostasis that precedes synapse loss in the living mouse brain. *Molecular Neurodegeneration*, *12*(1), 27. https://doi.org/10.1186/s13024-017-0169-9

Argos, P. (1990). An investigation of oligopeptides linking domains in protein tertiary structures and possible candidates for general gene fusion. *Journal of Molecular Biology*, *211*(4), 943–58. https://doi.org/10.1016/0022-2836(90)90085-Z

Ariga, T., Kobayashi, K., Hasegawa, A., Kiso, M., Ishida, H., &Miyatake, T. (2001). Characterization of high-affinity binding between gangliosides and amyloid beta- protein. *Archives of Biochemistry and Biophysics*, *388*(2), 225–30. https://doi.org/10.1006/abbi.2001.2304

Arispe, N., Diaz, J. C., & Simakova, O. (2007). Abeta ion channels. Prospects for treating Alzheimer's disease with Abeta channel blockers. *Biochimica Et Biophysica Acta*, *1768*(8), 1952–65. https://doi.org/10.1016/j.bbamem.2007.03.014

Arndt, J. W., Qian, F., Smith, B. A., Quan, C., Kilambi, K. P., Bush, M. W., Walz, T., Pepinsky, R. B., Bussière, T., Hamann, S., Cameron, T. O., &Weinreb, P. H. (2018). Structural and kinetic basis for the selectivity of aducanumab for aggregated forms of amyloid-β. *Scientific Reports*, *8*(1), 6412. https://doi.org/10.1038/s41598-018-24501-0

Ashton, N. J., Pascoal, T. A., Karikari, T. K., Benedet, A. L., Lantero-Rodriguez, J., Brinkmalm, G., Snellman, A., Schöll, M., Troakes, C., Hye, A., Gauthier, S., Vanmechelen, E., Zetterberg, H., Rosa-Neto, P., & Blennow, K. (2021). Plasma p-tau231: A new biomarker for incipient Alzheimer's disease pathology. *Acta Neuropathologica*, *141*(5), 709–24. https://doi.org/10.1007/s00401-021-02275-6

Bäckman, L., Jones, S., Berger, A.-K., Laukka, E. J., & Small, B. J. (2005). Cognitive impairment in preclinical Alzheimer's disease: A meta-analysis. *Neuropsychology*, *19*(4), 520–31. https://doi.org/10.1037/0894-4105.19.4.520

Baghallab, I., Reyes-Ruiz, J. M., Abulnaja, K., Huwait, E., & Glabe, C. (2018). Epitomic Characterization of the Specificity of the Anti-Amyloid Aβ Monoclonal Antibodies 6E10 and 4G8. *Journal of Alzheimer's Disease: JAD*, *66*(3), 1235– 44. https://doi.org/10.3233/JAD-180582

Balchin, D., Hayer-Hartl, M., & Hartl, F. U. (2016). In vivo aspects of protein folding and quality control. *Science (New York, N.Y.)*, *353*(6294), aac4354. https://doi.org/10.1126/science.aac4354

Banchelli, M., Cascella, R., D'Andrea, C., Cabaj, L., Osticioli, I., Ciofini, D., Li, M. S., Skupień, K., de Angelis, M., Siano, S., Cecchi, C., Pini, R., La Penna, G., Chiti, F., & Matteini, P. (2020). Nanoscopic insights into the surface conformation of neurotoxic amyloid β oligomers. *RSC Advances*, *10*(37), 21907–13. https://doi.org/10.1039/d0ra03799k

Barenholz, Y. (2004). Sphingomyelin and cholesterol: From membrane biophysics and rafts to potential medical applications. *Sub-Cellular Biochemistry*, *37*, 167–215. https://doi.org/10.1007/978-1-4757-5806-1_5

Barrera, N. P., Zhou, M., & Robinson, C. V. (2013). The role of lipids in defining membrane protein interactions: Insights from mass spectrometry. *Trends in Cell Biology*, *23*(1), 1–8. https://doi.org/10.1016/j.tcb.2012.08.007

Bateman, R. J., Xiong, C., Benzinger, T. L. S., Fagan, A. M., Goate, A., Fox, N. C., Marcus, D. S., Cairns, N. J., Xie, X., Blazey, T. M., Holtzman, D. M., Santacruz, A., Buckles, V., Oliver, A., Moulder, K., Aisen, P. S., Ghetti, B., Klunk, W. E., McDade, E., … Dominantly Inherited Alzheimer Network. (2012). Clinical and biomarker changes in dominantly inherited Alzheimer's disease. *The New England Journal of Medicine*, *367*(9), 795–804. https://doi.org/10.1056/NEJMoa1202753

Batko, J., Antosz, K., Miśków, W., Pszczołowska, M., Walczak, K., & Leszek, J. (2024). Chaperones-A New Class of Potential Therapeutic Targets in Alzheimer's Disease. *International Journal of Molecular Sciences*, *25*(6), 3401. https://doi.org/10.3390/ijms25063401

Bélanger, K., Iqbal, U., Tanha, J., MacKenzie, R., Moreno, M., & Stanimirovic, D. (2019). Single-Domain Antibodies as Therapeutic and Imaging Agents for the Treatment of CNS Diseases. *Antibodies (Basel, Switzerland)*, *8*(2), 27. https://doi.org/10.3390/antib8020027.

Bellomo, G., Toja, A., Paolini Paoletti, F., Ma, Y., Farris, C. M., Gaetani, L., Salvadori, N., Chiasserini, D., Wojdała, A. L., Concha-Marambio, L., & Parnetti, L. (2024). Investigating alpha-synuclein co-pathology in Alzheimer's disease by means of cerebrospinal fluid alpha-synuclein seed amplification assay. *Alzheimer's & Dementia*, *20*(4), 2444–52. https://doi.org/10.1002/alz.13658

Benedet, A. L., Brum, W. S., Hansson, O., Alzheimer's Disease Neuroimaging Initiative, Karikari, T. K., Zimmer, E. R., Zetterberg, H., Blennow, K., & Ashton, N. J. (2022). The accuracy and robustness of plasma biomarker models for amyloid PET positivity. *Alzheimer's Research & Therapy*, *14*(1), 26. https://doi.org/10.1186/s13195-021-00942-0

Benilova, I., Karran, E., & De Strooper, B. (2012). The toxic Aβ oligomer and Alzheimer's disease: An emperor in need of clothes. *Nature Neuroscience*, *15*(3), 349–57. https://doi.org/10.1038/nn.3028

Bento, C. F., Renna, M., Ghislat, G., Puri, C., Ashkenazi, A., Vicinanza, M., Menzies, F. M., & Rubinsztein, D. C. (2016). Mammalian Autophagy: How

Does It Work? *Annual Review of Biochemistry*, *85*, 685–713. https://doi.org/10.1146/annurev- biochem-060815-014556

Berridge, M. J. (1998). Neuronal calcium signaling. *Neuron*, *21*(1), 13–26. https://doi.org/10.1016/s0896-6273(00)80510-3

Berridge, M. J., Lipp, P., & Bootman, M. D. (2000). The versatility and universality of calcium signalling. *Nature Reviews. Molecular Cell Biology*, *1*(1), 11–21. https://doi.org/10.1038/35036035

Bhatia, S., Rawal, R., Sharma, P., Singh, T., Singh, M., & Singh, V. (2022). Mitochondrial Dysfunction in Alzheimer's Disease: Opportunities for Drug Development. *Current Neuropharmacology*, *20*(4), 675–92. https://doi.org/10.2174/1570159X19666210517114016

Bigi, A., Cascella, R., Fani, G., Bernacchioni, C., Cencetti, F., Bruni, P., Chiti, F., Donati, C., & Cecchi, C. (2023a). Sphingosine 1-phosphate attenuates neuronal dysfunction induced by amyloid-β oligomers through endocytic internalization of NMDA receptors. *The FEBS Journal*, *290*(1), 112–33. https://doi.org/10.1111/febs.16579

Bigi, A., Fani, G., Bessi, V., Napolitano, L., Bagnoli, S., Ingannato, A., Neri, L., Cascella, R., Matteini, P., Sorbi, S., Nacmias, B., Cecchi, C., & Chiti, F. (2024a). Putative novel CSF biomarkers of Alzheimer's disease based on the novel concept of generic protein misfolding and proteotoxicity: The PRAMA cohort. *TranslationalNeurodegeneration*, *13*(1), 14. https://doi.org/10.1186/s40035-024-00405-0

Bigi, A., Loffredo, G., Cascella, R., & Cecchi, C. (2020). Targeting Pathological Amyloid Aggregates with Conformation-Sensitive Antibodies. *Current Alzheimer Research*, *17*(8), 722–34. https://doi.org/10.2174/1567205017666201109093848

Bigi, A., Lombardo, E., Cascella, R., & Cecchi, C. (2023b). The Toxicity of Protein Aggregates: New Insights into the Mechanisms. *International Journal of Molecular Sciences*, *24*(9), 7974. https://doi.org/10.3390/ijms24097974

Bigi, A., Napolitano, L., Vadukul, D. M., Chiti, F., Cecchi, C., Aprile, F. A., & Cascella, R. (2024b). A single-domain antibody detects and neutralises toxic Aβ42 oligomers in the Alzheimer's disease CSF. *Alzheimer's Research & Therapy*, *16*(1), 13. https://doi.org/10.1186/s13195-023-01361-z

Biomarkers Definitions Working Group. (2001). Biomarkers and surrogate endpoints: Preferred definitions and conceptual framework. *Clinical Pharmacology and Therapeutics*, *69*(3), 89–95. https://doi.org/10.1067/mcp.2001.113989

Bird, R. E., Hardman, K. D., Jacobson, J. W., Johnson, S., Kaufman, B. M., Lee, S. M., Lee, T., Pope, S. H., Riordan, G. S., & Whitlow, M. (1988). Single-chain antigen- binding proteins. *Science (New York, N.Y.)*, *242*(4877), 423–26. https://doi.org/10.1126/science.3140379

Bitan, G., Kirkitadze, M. D., Lomakin, A., Vollers, S. S., Benedek, G. B., & Teplow, D. B. (2003). Amyloid beta -protein (Abeta) assembly: Abeta 40 and Abeta 42 oligomerize through distinct pathways. *Proceedings of the National Academy of Sciences of the United States of America*, *100*(1), 330–35.

https://doi.org/10.1073/pnas.222681699

Blennow, K., Wallin, A., Agren, H., Spenger, C., Siegfried, J., & Vanmechelen, E. (1995). Tau protein in cerebrospinal fluid: A biochemical marker for axonal degeneration in Alzheimer disease? *Molecular and Chemical Neuropathology*, *26*(3), 231–45. https://doi.org/10.1007/BF02815140

Blessed, G., Tomlinson, B. E., & Roth, M. (1968). The association between quantitative measures of dementia and of senile change in the cerebral grey matter of elderly subjects. *The British Journal of Psychiatry: The Journal of Mental Science*, *114*(512), 797–811. https://doi.org/10.1192/bjp.114.512.797

Bode, D. C., Freeley M., Nield J., Palma M., Viles J.H. (2019). Amyloid-β oligomers have a profound detergent-like effect on lipid membrane bilayers, imaged by atomic force and electron microscopy. *J Biol Chem. 294(19):7566-72.* doi: 10.1074/jbc.AC118.007195.

Boess, F., Sakaoka, S., Abi-Saab, D., Scelsi, M., delmar, P., Hofmann, C., Klein, G., Baudler, M., Doody, R., & Kerchner, G. (2021). Graduation study design: Evaluation of once-weekly subcutaneous administration of gantenerumab on brain amyloid load. *Alzheimer's & Dementia*, *17*. https://doi.org/10.1002/alz.052060

Bondi, M. W., Edmonds, E. C., & Salmon, D. P. (2017). Alzheimer's Disease: Past, Present, and Future. *Journal of the International Neuropsychological Society: JINS*, *23*(9–10), 818–31. https://doi.org/10.1017/S135561771700100X

Bondi, M. W., Monsch, A. U., Galasko, D., Butters, N., Salmon, D. P., & Delis, D. C. (1994). Preclinical cognitive markers of dementia of the Alzheimer type. *Neuropsychology*, *8*(3), 374–84. https://doi.org/10.1037/0894-4105.8.3.374

Braak, H., & Braak, E. (1994). Morphological criteria for the recognition of Alzheimer's disease and the distribution pattern of cortical changes related to this disorder. *Neurobiology of Aging*, *15*(3), 355–56; discussion 379-80. https://doi.org/10.1016/0197-4580(94)90032-9

Bradford, M. M. (1976). A rapid and sensitive method for the quantitation of microgram quantities of protein utilizing the principle of protein-dye binding. *Analytical Biochemistry*, *72*, 248–54. https://doi.org/10.1006/abio.1976.9999

Brehme, M., Voisine, C., Rolland, T., Wachi, S., Soper, J. H., Zhu, Y., Orton, K., Villella, A., Garza, D., Vidal, M., Ge, H., & Morimoto, R. I. (2014). A chaperome subnetwork safeguards proteostasis in aging and neurodegenerative disease. *Cell Reports*, *9*(3), 1135–50. https://doi.org/10.1016/j.celrep.2014.09.042

Brilhante-da-Silva, N., de Oliveira Sousa, R. M., Arruda, A., Dos Santos, E. L., Marinho, A. C. M., Stabeli, R. G., Fernandes, C. F. C., & Pereira, S. D. S. (2021). Camelid Single-Domain Antibodies for the Development of Potent Diagnosis Platforms. *Molecular Diagnosis & Therapy*, *25*(4), 439–56. https://doi.org/10.1007/s40291-021-00533-7

Brodaty, H., Heffernan, M., Kochan, N. A., Draper, B., Trollor, J. N., Reppermund, S., Slavin, M. J., & Sachdev, P. S. (2013). Mild cognitive

impairment in a community sample: The Sydney Memory and Ageing Study. *Alzheimer's & Dementia: The Journal of the Alzheimer's Association*, *9*(3), 310-17.e1. https://doi.org/10.1016/j.jalz.2011.11.010

Brooks, W. H. (2024). Polyamine Dysregulation and Nucleolar Disruption in Alzheimer's Disease. *Journal of Alzheimer's Disease*, *98*(3), 837. https://doi.org/10.3233/JAD-231184

Buchhave, P., Minthon, L., Zetterberg, H., Wallin, A. K., Blennow, K., & Hansson, O. (2012). Cerebrospinal fluid levels of β-amyloid 1-42, but not of tau, are fully changed already 5 to 10 years before the onset of Alzheimer dementia. *Archives of General Psychiatry*, *69*(1), 98–106. https://doi.org/10.1001/archgenpsychiatry.2011.155

Budd Haeberlein, S., Aisen, P. S., Barkhof, F., Chalkias, S., Chen, T., Cohen, S., Dent, G., Hansson, O., Harrison, K., von Hehn, C., Iwatsubo, T., Mallinckrodt, C., Mummery, C. J., Muralidharan, K. K., Nestorov, I., Nisenbaum, L., Rajagovindan, R., Skordos, L., Tian, Y., … Sandrock, A. (2022). Two Randomized Phase 3 Studies of Aducanumab in Early Alzheimer's Disease. *The Journal of Prevention of Alzheimer's Disease*, *9*(2), 197–210. https://doi.org/10.14283/jpad.2022.30

Butterfield, D. A., & Halliwell, B. (2019). Oxidative stress, dysfunctional glucose metabolism, and Alzheimer disease. *Nature Reviews. Neuroscience*, *20*(3), 148. https://doi.org/10.1038/s41583-019-0132-6

Cadonic, C., Sabbir, M. G., & Albensi, B. C. (2016). Mechanisms of Mitochondrial Dysfunction in Alzheimer's Disease. *Molecular Neurobiology*, *53*(9), 6078– 90. https://doi.org/10.1007/s12035-015-9515-5

Caillé, I., Allinquant, B., Dupont, E., Bouillot, C., Langer, A., Müller, U., & Prochiantz, A. (2004). Soluble form of amyloid precursor protein regulates proliferation of progenitors in the adult subventricular zone. *Development (Cambridge, England)*, *131*(9), 2173–81. https://doi.org/10.1242/dev.01103

Camberg, J., Doyle, S., Johnston, D.,Wickner, S. (2013). Molecular Chaperones. 10.1016/B978-0-12-374984-0.00221-7.

Canevari, L., Clark, J. B., & Bates, T. E. (1999). Beta-Amyloid fragment 25-35 selectively decreases complex IV activity in isolated mitochondria. *FEBS Letters*, *457*(1), 131–34. https://doi.org/10.1016/s0014-5793(99)01028-5

Capitini, C., Conti, S., Perni, M., Guidi, F., Cascella, R., De Poli, A., Penco, A., Relini, A., Cecchi, C., & Chiti, F. (2014). TDP-43 inclusion bodies formed in bacteria are structurally amorphous, non-amyloid and inherently toxic to neuroblastoma cells. *PloS One*, *9*(1), e86720. https://doi.org/10.1371/journal.pone.0086720

Cardoso, F. M., Ibañez, L. I., Van den Hoecke, S., De Baets, S., Smet, A., Roose, K., Schepens, B., Descamps, F. J., Fiers, W., Muyldermans, S., Depicker, A., &Saelens, X. (2014). Single-domain antibodies targeting neuraminidase protect against an H5N1 influenza virus challenge. *Journal of Virology*, *88*(15), 8278–96. https://doi.org/10.1128/JVI.03178-13

Carmona, S., Hardy, J., & Guerreiro, R. (2018). The genetic landscape of Alzheimer disease. *Handbook of Clinical Neurology*, *148*, 395–408. https://doi.org/10.1016/B978-0-444-64076-5.00026-0

Caroli, A., & Frisoni, G. B. (2010). The dynamics of Alzheimer's disease biomarkers in the Alzheimer's Disease Neuroimaging Initiative cohort. Neurobiol Aging. Aug;31(8):1263-74. doi: 10.1016/j.neurobiolaging.2010.04.024. Epub 2010 Jun 11. PMID: 20538373; PMCID: PMC3467365.

Cascella, R., & Cecchi, C. (2021). Calcium Dyshomeostasis in Alzheimer's Disease Pathogenesis. *International Journal of Molecular Sciences*, *22*(9), 4914. https://doi.org/10.3390/ijms22094914

Cascella, R., Bigi, A., Riffert, D. G., Gagliani, M. C., Ermini, E., Moretti, M., Cortese, K., Cecchi, C., & Chiti, F. (2022). A quantitative biology approach correlates neuronal toxicity with the largest inclusions of TDP-43. *Science Advances*, *8*(30), eabm6376. https://doi.org/10.1126/sciadv.abm6376

Cascella, R., Chen, S. W., Bigi, A., Camino, J. D., Xu, C. K., Dobson, C. M., Chiti, F., Cremades, N., & Cecchi, C. (2021). The release of toxic oligomers from α- synuclein fibrils induces dysfunction in neuronal cells. *Nature Communications*, *12*(1), 1814. https://doi.org/10.1038/s41467-021-21937-3.

Cascella, R., Conti, S., Mannini, B., Li, X., Buxbaum, J. N., Tiribilli, B., Chiti, F., & Cecchi, C. (2013a). Transthyretin suppresses the toxicity of oligomers formed by misfolded proteins in vitro. *Biochimica Et Biophysica Acta*, *1832*(12), 2302–14. https://doi.org/10.1016/j.bbadis.2013.09.011

Cascella, R., Conti, S., Tatini, F., Evangelisti, E., Scartabelli, T., Casamenti, F., Wilson, M. R., Chiti, F., & Cecchi, C. (2013b). Extracellular chaperones prevent Aβ42- induced toxicity in rat brains. *Biochimica Et Biophysica Acta*, *1832*(8), 1217–26. https://doi.org/10.1016/j.bbadis.2013.04.012

Cascella, R., Evangelisti, E., Bigi, A., Becatti, M., Fiorillo, C., Stefani, M., Chiti, F., & Cecchi, C. (2017). Soluble Oligomers Require a Ganglioside to Trigger Neuronal Calcium Overload. *Journal of Alzheimer'sDisease: JAD*, *60*(3), 923–38. https://doi.org/10.3233/JAD-170340

Cecchi, C., Nichino, D., Zampagni, M., Bernacchioni, C., Evangelisti, E., Pensalfini, A., Liguri, G., Gliozzi, A., Stefani, M., & Relini, A. (2009). A protective role for lipid raft cholesterol against amyloid-induced membrane damage in human neuroblastoma cells. *Biochimica Et Biophysica Acta*, *1788*(10), 2204–16. https://doi.org/10.1016/j.bbamem.2009.07.019

Chasseigneaux, S., & Allinquant, B. (2012). Functions of Aβ, sAPPα and sAPPβ: Similarities and differences. *Journal of Neurochemistry*, *120 Suppl 1*, 99–108. https://doi.org/10.1111/j.1471-4159.2011.07584.x

Chatani, E., Yuzu, K., Ohhashi, Y., & Goto, Y. (2021). Current Understanding of the Structure, Stability and Dynamic Properties of Amyloid Fibrils. *International Journal of Molecular Sciences*, *22*(9), 4349. https://doi.org/10.3390/ijms22094349

Chatziefstathiou, A., Canaslan, S., Kanata, E., Vekrellis, K., Constantinides, V. C., Paraskevas, G. P., Kapaki, E., Schmitz, M., Zerr, I., Xanthopoulos, K.,

Sklaviadis, T., & Dafou, D. (2024). SIMOA Diagnostics on Alzheimer's Disease and Frontotemporal

Cheignon, C., Tomas, M., Bonnefont-Rousselot, D., Faller, P., Hureau, C., & Collin, F. (2018). Oxidative stress and the amyloid beta peptide in Alzheimer's disease. *Redox Biology*, *14*, 450–64. https://doi.org/10.1016/j.redox.2017.10.014

Chen, T., O'Gorman, J., Castrillo-Viguera, C., Rajagovindan, R., Curiale, G. G., Tian, Y., Patel, D., von Rosenstiel, P., von Hehn, C., Salloway, S., Hock, C., Nitsch, R. M., Haeberlein, S. B., Sandrock, A., & Singhal, P. (2024). Results from the long- term extension of PRIME: A randomized Phase 1b trial of aducanumab. *Alzheimer's & Dementia: The Journal of the Alzheimer's Association*, *20*(5), 3406–15. https://doi.org/10.1002/alz.13755

Chen, X., Zaro, J. L., & Shen, W.-C. (2013). Fusion protein linkers: Property, design and functionality. *Advanced Drug Delivery Reviews*, *65*(10), 1357–69. https://doi.org/10.1016/j.addr.2012.09.039

Chen, Y.R., & Glabe, C. G. (2006). Distinct early folding and aggregation properties of Alzheimer amyloid-beta peptides Abeta40 and Abeta42: Stable trimer or tetramer formation by Abeta42. *The Journal of Biological Chemistry*, *281*(34), 24414–22. https://doi.org/10.1074/jbc.M602363200

Cheng, B., Gong, H., Xiao, H., Petersen, R.B., Zheng, L., Huang, K. (2013). Inhibiting Toxic Aggregation of Amyloidogenic Proteins: A Therapeutic Strategy for Protein Misfolding Diseases. *Biochim. Biophys. Acta (BBA), 1830, 4860–71.*

Chételat, G., Arbizu, J., Barthel, H., Garibotto, V., Law, I., Morbelli, S., van de Giessen, E., Agosta, F., Barkhof, F., Brooks, D. J., Carrillo, M. C., Dubois, B., Fjell, A.M., Frisoni, G. B., Hansson, O., Herholz, K., Hutton, B. F., Jack, C. R., Lammertsma, A. A., … Drzezga, A. (2020). Amyloid-PET and 18F-FDG-PET in the diagnostic investigation of Alzheimer's disease and other dementias. *The Lancet. Neurology*, *19*(11), 951–62. https://doi.org/10.1016/S1474-4422(20)30314-8

Chiti, F., & Dobson, C. M. (2006). Protein misfolding, functional amyloid, and human disease. *Annual Review of Biochemistry*, *75*, 333–66. https://doi.org/10.1146/annurev.biochem.75.101304.123901

Chiti, F., & Dobson, C. M. (2017). Protein Misfolding, Amyloid Formation, and Human Disease: A Summary of Progress Over the Last Decade. *Annual Review of Biochemistry*, *86*, 27–68. https://doi.org/10.1146/annurev-biochem-061516-045115.

Ciechanover, A., & Brundin, P. (2003). The ubiquitin proteasome system in neurodegenerative diseases: Sometimes the chicken, sometimes the egg. *Neuron*, *40*(2), 427–46. https://doi.org/10.1016/s0896-6273(03)00606-8

Cinquanta, L., Fontana, D. E., & Bizzaro, N. (2017). Chemiluminescent immunoassay technology: What does it change in autoantibody detection? *Auto- Immunity Highlights*, *8*(1), 9. https://doi.org/10.1007/s13317-017-0097-2

Clapham, D. E. (2007). Calciumsignaling. *Cell*, *131*(6), 1047–58.

https://doi.org/10.1016/j.cell.2007.11.028

Cline, E. N., Bicca, M. A., Viola, K. L., & Klein, W. L. (2018). The Amyloid-β Oligomer Hypothesis: Beginning of the Third Decade. *Journal of Alzheimer's Disease: JAD*, *64*(s1), S567–S610. https://doi.org/10.3233/JAD-179941

Cohen, S. I. A., Linse, S., Luheshi, L. M., Hellstrand, E., White, D. A., Rajah, L., Otzen, D. E., Vendruscolo, M., Dobson, C. M., & Knowles, T. P. J. (2013). Proliferation of amyloid-β42 aggregates occurs through a secondary nucleation mechanism. *Proceedings of the National Academy of Sciences of the United States of America*, *110*(24), 9758–63. https://doi.org/10.1073/pnas.1218402110

Colom-Cadena, M., Gelpi, E., Charif, S., Belbin, O., Blesa, R., Martí, M. J., Clarimón, J., & Lleó, A. (2013). Confluence of α-synuclein, tau, and β-amyloid pathologies in dementia with Lewy bodies. *Journal of Neuropathology and Experimental Neurology*, *72*(12), 1203–12. https://doi.org/10.1097/NEN.0000000000000018

Colvin, M. T., Silvers, R., Ni, Q. Z., Can, T. V., Sergeyev, I., Rosay, M., Donovan, K. J., Michael, B., Wall, J., Linse, S., Griffin, R. G. (2016). Atomic Resolution Structure of Monomorphic Aβ42 Amyloid Fibrils. J Am Chem Soc.138(30):9663-74. doi: 10.1021/jacs.6b05129. Epub 2016 Jul 14. PMID: 27355699; PMCID: PMC5389415.

Congdon, E. E., & Sigurdsson, E. M. (2018). Tau-targeting therapies for Alzheimer disease. *Nature Reviews. Neurology*, *14*(7), 399–415. https://doi.org/10.1038/s41582-018-0013-z

Corey-Bloom, J. (2002). The ABC of Alzheimer's disease: Cognitive changes and their management in Alzheimer's disease and related dementias. *International Psychogeriatrics*, *14 Supp 1*, 51–75. https://doi.org/10.1017/s1041610203008664

Cummings, J., Osse, A. M. L., Cammann, D., Powell, J., & Chen, J. (2024). Anti-Amyloid Monoclonal Antibodies for the Treatment of Alzheimer's Disease. *BioDrugs*, *38*(1), 5–22. https://doi.org/10.1007/s40259-023-00633-2

Dahlgren, K. N., Manelli, A. M., Stine, W. B., Baker, L. K., Krafft, G. A., & LaDu, M. J. (2002). Oligomeric and fibrillar species of amyloid-beta peptides differentially affect neuronal viability. *The Journal of Biological Chemistry*, *277*(35), 32046–53. https://doi.org/10.1074/jbc.M201750200

Danis, C., Dupré, E., Zejneli, O., Caillierez, R., Arrial, A., Bégard, S., Mortelecque, J., Eddarkaoui, S., Loyens, A., Cantrelle, F.-X., Hanoulle, X., Rain, J.-C., Colin, M., Buée, L., & Landrieu, I. (2022). Inhibition of Tau seeding by targeting Tau nucleation core within neurons with a single domain antibody fragment. *Molecular Therapy: The Journal of the American Society of Gene Therapy*, *30*(4), 1484–99. https://doi.org/10.1016/j.ymthe.2022.01.009

David, M. A., Jones, D. R., Tayebi, M. Potential candidate camelid antibodies for the treatment of protein-misfolding diseases. (2014). J Neuroimmunol. 272(1-2):76-85. doi: 10.1016/j.jneuroim.2014.05.001. Epub 2014 May 10. PMID: 24864011.

de la Monte, S. M., Tong M. Brain metabolic dysfunction at the core of

Alzheimer's disease. (2014). Biochem Pharmacol. 88(4):548-59. doi: 10.1016/j.bcp.2013.12.012.

De Strooper, B. (2003). Aph-1, Pen-2, and Nicastrin with Presenilin generate an active gamma-Secretase complex. *Neuron*, *38*(1), 9–12. https://doi.org/10.1016/s0896-6273(03)00205-8

De Strooper, B., & Karran, E. (2016). The Cellular Phase of Alzheimer's Disease. *Cell*, *164*(4), 603–15. https://doi.org/10.1016/j.cell.2015.12.056

De, S., Whiten, D. R., Ruggeri, F. S., Hughes, C., Rodrigues, M., Sideris, D. I., Taylor, C. G., Aprile, F. A., Muyldermans, S., Knowles, T. P. J., Vendruscolo, M., Bryant, C., Blennow, K., Skoog, I., Kern, S., Zetterberg, H., & Klenerman, D. (2019). Soluble aggregates present in cerebrospinal fluid change in size and mechanism of toxicity during Alzheimer's disease progression. *Acta Neuropathologica Communications*, *7*(1), 120. https://doi.org/10.1186/s40478-019-0777-4

Demattos, R. B., Lu, J., Tang, Y., Racke, M. M., Delong, C. A., Tzaferis, J. A., Hole, J. T., Forster, B. M., McDonnell, P. C., Liu, F., Kinley, R. D., Jordan, W. H., & Hutton, M. L. (2012). A plaque-specific antibody clears existing β-amyloid plaques in Alzheimer's disease mice. *Neuron*, *76*(5), 908–20. https://doi.org/10.1016/j.neuron.2012.10.029

Demuro, A., Mina, E., Kayed, R., Milton, S. C., Parker, I., &Glabe, C. G. (2005). Calcium dysregulation and membrane disruption as a ubiquitous neurotoxic mechanism of soluble amyloid oligomers. *The Journal of Biological Chemistry*, *280*(17), 17294–300. https://doi.org/10.1074/jbc.M500997200

Deng, J., Habib, A., Obregon, D. F., Barger, S. W., Giunta, B., Wang, Y.-J., Hou, H., Sawmiller, D., & Tan, J. (2015). Soluble amyloid precursor protein alpha inhibits tau phosphorylation through modulation of GSK3β signaling pathway. *Journal of Neurochemistry*, *135*(3), 630–37. https://doi.org/10.1111/jnc.13351

Dickerson, B. C., Wolk, D. A.; Alzheimer's Disease Neuroimaging Initiative. MRI cortical thickness biomarker predicts AD-like CSF and cognitive decline in normal adults. Neurology. (2012). Jan 10;78(2):84-90. doi: 10.1212/WNL.0b013e31823efc6c. Epub 2011 Dec 21. PMID: 22189451; PMCID: PMC3466670.

Dickey, C. A., Koren, J., Zhang, Y.-J., Xu, Y.-F., Jinwal, U. K., Birnbaum, M. J., Monks, B., Sun, M., Cheng, J. Q., Patterson, C., Bailey, R. M., Dunmore, J., Soresh, S., Leon, C., Morgan, D., &Petrucelli, L. (2008). Akt and CHIP coregulate tau degradation through coordinated interactions. *Proceedings of the National Academy of Sciences of the United States of America*, *105*(9), 3622–27. https://doi.org/10.1073/pnas.0709180105

Ding, Q., Markesbery, W. R., Chen, Q., Li, F., & Keller, J. N. (2005). Ribosome dysfunction is an early event in Alzheimer's disease. *The Journal of Neuroscience: The Official Journal of the Society for Neuroscience*, *25*(40), 9171–75. https://doi.org/10.1523/JNEUROSCI.3040-05.2005

Drews, A., De, S., Flagmeier, P., Wirthensohn, D. C., Chen, W.-H., Whiten, D. R., Rodrigues, M., Vincke, C., Muyldermans, S., Paterson, R. W., Slattery, C. F., Fox, N. C., Schott, J. M., Zetterberg, H., Dobson, C. M., Gandhi, S.,

&Klenerman, D. (2017). Inhibiting the Ca2+ Influx Induced by Human CSF. *Cell Reports*, *21*(11), 3310–16. https://doi.org/10.1016/j.celrep.2017.11.057

Dufour-Rainfray, D., Beaufils, E., Vourc'h, P., Vierron, E., Mereghetti, L., Gendrot, C., Hommet, C., Andres, C. R., Guilloteau, D., &Mondon, K. (2013). Total protein level in cerebrospinal fluid is stable in elderly adults. *Journal of the American Geriatrics Society*, *61*(10), 1819–21. https://doi.org/10.1111/jgs.12489

Edelman, G. M. (1970). The structure and function of antibodies. *Scientific American*, *223*(2), 34–42. https://doi.org/10.1038/scientificamerican0870-34

Eisenberg, D., & Jucker, M. (2012). The amyloid state of proteins in human diseases. *Cell*, *148*(6), 1188–1203. https://doi.org/10.1016/j.cell.2012.02.022

Eli Lilly and Company. Lilly—News Release. (2023). Lilly's Donanemab Significantly Slowed Cognitive and Functional Decline in Phase 3 Study of Early Alzheimer's Disease. https:// inves tor. lilly. com/ news- releases/ news-relea se- detai ls/ lillys- donanemab- significantly- slowed- cognitive- and-functional.

Engelman, D. M. (2005). Membranes are more mosaic than fluid. *Nature*, *438*(7068), 578–80. https://doi.org/10.1038/nature04394

Englund, H,, Sehlin, D., Johansson, A. S., Nilsson, L. N., Gellerfors, P., Paulie, S., Lannfelt, L., Pettersson, F. E. (2007). Sensitive ELISA detection of amyloid-beta protofibrils in biological samples. J Neurochem.103(1):334-45. doi: 10.1111/j.1471-4159.2007.04759.x.Epub 2007 Jul 10. PMID: 17623042.

Esteves, A., Arduíno, D., Silva, D. F., Martins-Branco, D., Oliveira, C., & Cardoso, S. (2009). *MITOCHONDRIAL METABOLISM IN AGE-RELATED NEURODEGENERATIVE DISORDERS:ALZHEIMER'S AND PARKINSON'S REVISITED* (pp. 187–244).

Evangelisti, E., Cascella, R., Becatti, M., Marrazza, G., Dobson, C. M., Chiti, F., Stefani, M., & Cecchi, C. (2016). Binding affinity of amyloid oligomers to cellular membranes is a generic indicator of cellular dysfunction in protein misfolding diseases. *Scientific Reports*, *6*, 32721. https://doi.org/10.1038/srep32721

Evangelisti, E., Wright, D., Zampagni, M., Cascella, R., Fiorillo, C., Bagnoli, S., Relini, A., Nichino, D., Scartabelli, T., Nacmias, B., Sorbi, S., Cecchi, C. (2013) Lipid rafts mediate amyloid-induced calcium dyshomeostasis and oxidative stress in Alzheimer's disease. Curr Alzheimer Res. Feb; 10(2):143-53. doi: 10.2174/1567205011310020004. PMID: 22950913.

Evangelisti, E., Zampagni, M., Cascella, R., Becatti, M., Fiorillo, C., Caselli, A., Bagnoli, S., Nacmias, B., Cecchi, C. (2014) Plasma membrane injury depends on bilayer lipid composition in Alzheimer's disease. J Alzheimers Dis.41(1):289-300. doi: 10.3233/JAD-131406. PMID: 24614900.

Ewers, M., Mattsson, N., Minthon, L., Molinuevo, J. L., Antonell, A., Popp, J., Jessen, F., Herukka, S.-K., Soininen, H., Maetzler, W., Leyhe, T., Bürger, K., Taniguchi, M., Urakami, K., Lista, S., Dubois, B., Blennow, K., & Hampel, H. (2015). CSF biomarkers for the differential diagnosis of Alzheimer's disease: A large-scale international multicenter study. *Alzheimer's &*

Dementia: The Journal of the Alzheimer's Association, *11*(11), 1306–15. https://doi.org/10.1016/j.jalz.2014.12.006

Fabiani, C., & Antollini, S. S. (2019). Alzheimer's Disease as a Membrane Disorder: Spatial Cross-Talk Among Beta-Amyloid Peptides, Nicotinic Acetylcholine Receptors and Lipid Rafts. *Frontiers in Cellular Neuroscience*, *13*, 309. https://doi.org/10.3389/fncel.2019.00309

Fagan, A. M., Mintun, M. A., Shah, A. R., Aldea, P., Roe, C. M., Mach, R. H., Marcus, D., Morris, J. C., & Holtzman, D. M. (2009). Cerebrospinal fluid tau and ptau(181) increase with cortical amyloid deposition in cognitively normal individuals: Implications for future clinical trials of Alzheimer's disease. *EMBO Molecular Medicine*, *1*(8–9), 371–80. https://doi.org/10.1002/emmm.200900048

Fani, G., La Torre, C. E., Cascella, R., Cecchi, C., Vendruscolo, M., & Chiti, F. (2022). Misfolded protein oligomers induce an increase of intracellular Ca2+ causing an escalation of reactive oxidative species. *Cellular and Molecular Life Sciences: CMLS*, *79*(9), 500. https://doi.org/10.1007/s00018-022-04513-w

Fani, G., Mannini, B., Vecchi, G., Cascella, R., Cecchi, C., Dobson, C. M., Vendruscolo, M., & Chiti, F. (2021). Aβ Oligomers Dysregulate Calcium Homeostasis by Mechanosensitive Activation of AMPA and NMDA Receptors. *ACS Chemical Neuroscience*, *12*(4), 766-81. https://doi.org/10.1021/acschemneuro.0c00811

FDA Office of the Commissioner. FDA. (2023) [cited 31 May 2023]. FDA Grants Accelerated Approval for Alzheimer's Disease Treatment. https:// www. fda. gov/ news- events/ press- announcements/ fda- grants- accel erated- approval- alzheimers- disea se- treat ment.

Ferrer, I. (2002). Differential expression of phosphorylated translation initiation factor 2 alpha in Alzheimer's disease and Creutzfeldt-Jakob's disease. *Neuropathology and Applied Neurobiology*, *28*(6), 441–51. https://doi.org/10.1046/j.1365- 2990.2002.t01-1-00410.x

Ferrer, I., Blanco, R., Carmona, M., Puig, B., Barrachina, M., Gómez, C., & Ambrosio, S. (2001). Active, phosphorylation-dependent mitogen-activated protein kinase (MAPK/ERK), stress-activated protein kinase/c-Jun N-terminal kinase (SAPK/JNK), and p38 kinase expression in Parkinson's disease and Dementia with Lewy bodies. *Journal of Neural Transmission (Vienna, Austria: 1996)*, *108*(12), 1383–96. https://doi.org/10.1007/s007020100015

Finder, V. H., Vodopivec, I., Nitsch, R. M., & Glockshuber, R. (2010). The recombinant amyloid-beta peptide Abeta1-42 aggregates faster and is more neurotoxic than synthetic Abeta1-42. *Journal of Molecular Biology*, *396*(1), 9–18. https://doi.org/10.1016/j.jmb.2009.12.016

Fitzpatrick, A. W. P., Debelouchina, G. T., Bayro, M. J., Clare, D. K., Caporini, M. A., Bajaj, V. S., Jaroniec, C. P., Wang, L., Ladizhansky, V., Müller, S. A., MacPhee, C. E., Waudby, C. A., Mott, H. R., De Simone, A., Knowles, T. P. J., Saibil, H. R., Vendruscolo, M., Orlova, E. V., Griffin, R. G., & Dobson, C. M. (2013). Atomic structure and hierarchical assembly of a cross-β amyloid

fibril. *Proceedings of the National Academy of Sciences of the United States of America*, *110*(14), 5468–73. https://doi.org/10.1073/pnas.1219476110

Fleisher, A. S., Chen, K., Quiroz, Y. T., Jakimovich, L. J., Gomez, M. G., Langois, C. M., Langbaum, J. B., Ayutyanont, N., Roontiva, A., Thiyyagura, P., Lee, W., Mo, H., Lopez, L., Moreno, S., Acosta-Baena, N., Giraldo, M., Garcia, G., Reiman, R. A., Huentelman, M. J., Kosik, K. S., Tariot, P. N., Lopera, F., Reiman, E. M. (2012). Florbetapir PET analysis of amyloid-β deposition in the presenilin 1 E280A autosomal dominant Alzheimer's disease kindred: a cross-sectional study. Lancet Neurol.11(12):1057-65. doi: 10.1016/S1474-4422(12)70227-2. Epub 2012 Nov 6. PMID: 23137949; PMCID: PMC3515078.

Fletcher, J. (2023). *Lilly's Donanemab Significantly Slowed Cognitive and Functional Decline in Phase 3 Study of Early Alzheimer's Disease*.

Förster, S., Grimmer, T., Miederer, I., Henriksen, G., Yousefi, B. H., Graner, P., Wester, H.-J., Förstl, H., Kurz, A., Dickerson, B. C., Bartenstein, P., &Drzezga, A. (2012). Regional expansion of hypometabolism in Alzheimer's disease follows amyloid deposition with temporal delay. *Biological Psychiatry*, *71*(9), 792–97. https://doi.org/10.1016/j.biopsych.2011.04.023

Friede, R. L., & Samorajski, T. (1970). Axon caliber related to neurofilaments and microtubules in sciatic nerve fibers of rats and mice. *The Anatomical Record*, *167*(4), 379–87. https://doi.org/10.1002/ar.1091670402

Frisoni, G. B., Fox, N. C., Jack, C. R., Scheltens, P., & Thompson, P. M. (2010). The clinical use of structural MRI in Alzheimer disease. *Nature Reviews. Neurology*, *6*(2), 67–77. https://doi.org/10.1038/nrneurol.2009.215

Frost, D., Gorman, P. M., Yip, C. M., & Chakrabartty, A. (2003). Co-incorporation of A beta 40 and A beta 42 to form mixed pre-fibrillar aggregates. *European Journal of Biochemistry*, *270*(4), 654–63. https://doi.org/10.1046/j.1432- 1033.2003.03415.x

Fukuchi, K., Accavitti-Loper, M. A., Kim, H.-D., Tahara, K., Cao, Y., Lewis, T. L., Caughey, R. C., Kim, H., & Lalonde, R. (2006a). Amelioration of amyloid load by anti-Abeta single-chain antibody in Alzheimer mouse model. *Biochemical and Biophysical Research Communications*, *344*(1), 79–86. https://doi.org/10.1016/j.bbrc.2006.03.145

Fukuchi, K., Tahara, K., Kim, H.-D., Maxwell, J. A., Lewis, T. L., Accavitti-Loper, M. A., Kim, H., Ponnazhagan, S., & Lalonde, R. (2006b). Anti-Abeta single-chain antibody delivery via adeno-associated virus for treatment of Alzheimer's disease. *Neurobiology of Disease*, *23*(3), 502–11. https://doi.org/10.1016/j.nbd.2006.04.012

Fukumoto, H., Tokuda, T., Kasai, T., Ishigami, N., Hidaka, H., Kondo, M., Allsop, D., & Nakagawa, M. (2010). High-molecular-weight beta-amyloid oligomers are elevated in cerebrospinal fluid of Alzheimer patients. *FASEB Journal: Official Publication of the Federation of American Societies for Experimental Biology*, *24*(8), 2716–26. https://doi.org/10.1096/fj.09-150359

Fukunaga, S., Ueno, H., Yamaguchi, T., Yano, Y., Hoshino, M., & Matsuzaki, K. (2012). GM1 cluster mediates formation of toxic Aβ fibrils by providing

hydrophobic environments. *Biochemistry*, *51*(41), 8125–31. https://doi.org/10.1021/bi300839u

Georganopoulou, D. G., Chang, L., Nam, J.-M., Thaxton, C. S., Mufson, E. J., Klein, W. L., & Mirkin, C. A. (2005). Nanoparticle-based detection in cerebral spinal fluid of a soluble pathogenic biomarker for Alzheimer's disease. *Proceedings of the National Academy of Sciences of the United States of America*, *102*(7), 2273– 76. https://doi.org/10.1073/pnas.0409336102

Giacomucci, G., Mazzeo, S., Bagnoli, S., Ingannato, A., Leccese, D., Berti, V., Padiglioni, S., Galdo, G., Ferrari, C., Sorbi, S., Bessi, V., & Nacmias, B. (2022). Plasma neurofilament light chain as a biomarker of Alzheimer's disease in Subjective Cognitive Decline and Mild Cognitive Impairment. *Journal of Neurology*, *269*(8), 4270–80. https://doi.org/10.1007/s00415-022-11055-5

Gibbs, E., Silverman, J. M., Zhao, B., Peng, X., Wang, J., Wellington, C. L., Mackenzie, I. R., Plotkin, S. S., Kaplan, J. M., & Cashman, N. R. (2019). A Rationally Designed Humanized Antibody Selective for Amyloid Beta Oligomers in Alzheimer's Disease. *Scientifi Reports*, *9*(1), 9870. https://doi.org/10.1038/s41598-019-46306-5

Gill, S. C., & von Hippel, P. H. (1989). Calculation of protein extinction coefficients from amino acid sequence data. *Analytical Biochemistry*, *182*(2), 319–26. https://doi.org/10.1016/0003-2697(89)90602-7

Ginsberg, S. D., Galvin, J. E., Chiu, T. S., Lee, V. M., Masliah, E., Trojanowski, J. Q. (1998). RNA sequestration to pathological lesions of neurodegenerative diseases. Acta Neuropathol. 1998 Nov;96(5):487-94. doi: 10.1007/s004010050923. PMID: 9829812.

Gisslén, M., Price, R. W., Andreasson, U., Norgren, N., Nilsson, S., Hagberg, L., Fuchs, D., Spudich, S., Blennow, K., & Zetterberg, H. (2016). Plasma Concentration of the Neurofilament Light Protein (NFL) is a Biomarker of CNS Injury in HIV Infection: A Cross-Sectional Study. *EBioMedicine*, *3*, 135–40. https://doi.org/10.1016/j.ebiom.2015.11.036

Glenner, G. G., & Wong, C. W. (1984). Alzheimer's disease and Down's syndrome: Sharing of a unique cerebrovascular amyloid fibril protein. *Biochemical and Biophysical Research Communications*, *122*(3), 1131–35. https://doi.org/10.1016/0006-291x(84)91209-9

Goedert M, Masuda-Suzukake M, Falcon B. (2017) Like prions: the propagation of aggregated tau and α-synuclein in neurodegeneration. Brain. 140(2):266-78. doi: 10.1093/brain/aww230. Epub 2016 Sep 21. PMID: 27658420.

Golde, T. E., Eckman, C. B., & Younkin, S. G. (2000). Biochemical detection of Abeta isoforms: Implications for pathogenesis, diagnosis, and treatment of Alzheimer's disease. *Biochimica Et Biophysica Acta*, *1502*(1), 172–87. https://doi.org/10.1016/s0925-4439(00)00043-0

Gong, Y., Chang, L., Viola, K. L., Lacor, P. N., Lambert, M. P., Finch, C. E., Krafft, G. A., & Klein, W. L. (2003). Alzheimer's disease-affected brain: Presence of oligomeric A beta ligands (ADDLs) suggests a molecular basis for reversible memory loss. *Proceedings of the National Academy of Sciences*

of the United States of America, *100*(18), 10417–22. https://doi.org/10.1073/pnas.1834302100

Gorantla, N. V., & Chinnathambi, S. (2018). Tau Protein Squired by Molecular Chaperones During Alzheimer's Disease. *Journal of Molecular Neuroscience: MN*, *66*(3), 356–68. https://doi.org/10.1007/s12031-018-1174-3

Greenfield NJ. (2006). Using circular dichroism spectra to estimate protein secondary structure. *Nat Protoc*. 1(6):2876-90. doi: 10.1038/nprot.2006.202. PMID: 17406547; PMCID: PMC2728378

Greenough, M. A., Camakaris, J., & Bush, A. I. (2013). Metal dyshomeostasis and oxidative stress in Alzheimer's disease. *Neurochemistry International*, *62*(5), 540–55. https://doi.org/10.1016/j.neuint.2012.08.014

Guerreiro, R. J., Gustafson, D. R., & Hardy, J. (2012). The genetic architecture of Alzheimer's disease: Beyond APP, PSENs and APOE. *Neurobiology of Aging*, *33*(3), 437–56. https://doi.org/10.1016/j.neurobiolaging.2010.03.025

Guo, T., Zhang, D., Zeng, Y., Huang, T. Y., Xu, H., & Zhao, Y. (2020). Molecular and cellular mechanisms underlying the pathogenesis of Alzheimer's disease. *Molecular Neurodegeneration*, *15*(1), 40. https://doi.org/10.1186/s13024-020-00391-7

Habiba, U., Descallar, J., Kreilaus, F., Adhikari, U. K., Kumar, S., Morley, J. W., Bui, B. V., Koronyo-Hamaoui, M., & Tayebi, M. (2021). Detection of retinal and blood Aβ oligomers with nanobodies. *Alzheimer's & Dementia (Amsterdam, Netherlands)*, *13*(1), e12193. https://doi.org/10.1002/dad2.12193

Halliwell, B., & Gutteridge, J. M. C. (2015). *Free Radicals in Biology and Medicine*. Oxford University Press.

Hamers-Casterman, C., Atarhouch, T., Muyldermans, S., Robinson, G., Hamers, C., Songa, E. B., Bendahman, N., & Hamers, R. (1993). Naturally occurring antibodies devoid of light chains. *Nature*, *363*(6428), 446–48. https://doi.org/10.1038/363446a0

Hampel, H., Cummings, J., Blennow, K., Gao, P., Jack, C. R., &Vergallo, A. (2021a). Developing the ATX(N) classification for use across the Alzheimer disease continuum. *Nature Reviews. Neurology*, *17*(9), 580–89. https://doi.org/10.1038/s41582-021-00520-w

Hampel, H., Hardy, J., Blennow, K., Chen, C., Perry, G., Kim, S. H., Villemagne, V. L., Aisen, P., Vendruscolo, M., Iwatsubo, T., Masters, C. L., Cho, M., Lannfelt, L., Cummings, J. L., &Vergallo, A. (2021b). The Amyloid-β Pathway in Alzheimer's Disease. *Molecular Psychiatry*, *26*(10), 5481–503. https://doi.org/10.1038/s41380-021-01249-0

Hansen, D. V., Hanson, J. E., and Sheng, M. (2018). Microglia in Alzheimer's disease. J *Cell Biol.* 217(2):459-472. doi: 10.1083/jcb.201709069. Epub 2017 Dec 1. PMID: 29196460; PMCID: PMC5800817.

Hansson, O., Janelidze, S., Hall, S., Magdalinou, N., Lees, A. J., Andreasson, U., Norgren, N., Linder, J., Forsgren, L., Constantinescu, R., Zetterberg, H., Blennow, K., & Swedish BioFINDER study. (2017). Blood-based NfL: A biomarker for differential diagnosis of parkinsonian disorder. *Neurology*, *88*(10), 930–37. https://doi.org/10.1212/WNL.0000000000003680

Hansson, O., Lehmann, S., Otto, M., Zetterberg, H., & Lewczuk, P. (2019). Advantages and disadvantages of the use of the CSF Amyloid β (Aβ) 42/40 ratio in the diagnosis of Alzheimer's Disease. *Alzheimer's Research & Therapy*, *11*(1), 34. https://doi.org/10.1186/s13195-019-0485-0

Hardy, J., & Allsop, D. (1991). Amyloid deposition as the central event in the aetiology of Alzheimer's disease. *Trends in Pharmacological Sciences*, *12*(10), 383–88. https://doi.org/10.1016/0165-6147(91)90609-v

Hardy, J., & Selkoe, D. J. (2002). The amyloid hypothesis of Alzheimer's disease: Progress and problems on the road to therapeutics. *Science (New York, N.Y.)*, *297*(5580), 353–56. https://doi.org/10.1126/science.1072994

Hashimoto, M., Rockenstein, E., Crews, L., & Masliah, E. (2003). Role of protein aggregation in mitochondrial dysfunction and neurodegeneration in Alzheimer's and Parkinson's diseases. *Neuromolecular Medicine*, *4*(1–2), 21–36. https://doi.org/10.1385/NMM:4:1-2:21

Hebda, J.A. & Miranker, A.D. (2009). The Interplay of Catalysis and Toxicity by Amyloid Intermediates on Lipid Bilayers: Insights from Type II Diabetes. *Annu. Rev. Biophys. 2009, 38, 125–52.*

Hefti, F., Goure, W. F., Jerecic, J., Iverson, K. S., Walicke, P. A., &Krafft, G. A. (2013). The case for soluble Aβ oligomers as a drug target in Alzheimer's disease. *Trends in Pharmacological Sciences*, *34*(5), 261–66. https://doi.org/10.1016/j.tips.2013.03.002

Heneka, M. T., Carson, M. J., El Khoury, J., Landreth, G. E., Brosseron, F., Feinstein, D. L., Jacobs, A. H., Wyss-Coray, T., Vitorica, J., Ransohoff, R. M., Herrup, K., Frautschy, S. A., Finsen, B., Brown, G. C., Verkhratsky, A., Yamanaka, K., Koistinaho, J., Latz, E., Halle, A., … Kummer, M. P. (2015). Neuroinflammation in Alzheimer's disease. *The Lancet. Neurology*, *14*(4), 388–405. https://doi.org/10.1016/S1474-4422(15)70016-5

Hepp, D. H., Vergoossen, D. L. E., Huisman, E., Lemstra, A. W., Netherlands Brain Bank, Berendse, H. W., Rozemuller, A. J., Foncke, E. M. J., & van de Berg, W. D. J. (2016). Distribution and Load of Amyloid-β Pathology in Parkinson Disease and Dementia with Lewy Bodies. *Journal of Neuropathology and Experimental Neurology*, *75*(10), 936–45. https://doi.org/10.1093/jnen/nlw070

Hernández-Ortega, K., Garcia-Esparcia, P., Gil, L., Lucas, J. J., & Ferrer, I. (2016). Altered Machinery of Protein Synthesis in Alzheimer's: From the Nucleolus to the Ribosome. *Brain Pathology (Zurich, Switzerland)*, *26*(5), 593–605. https://doi.org/10.1111/bpa.12335

Herring, W. L., Gould, I. G., Fillit, H., Lindgren, P., Forrestal, F., Thompson, R., & Pemberton-Ross, P. (2021). Predicted Lifetime Health Outcomes for Aducanumab in Patients with Early Alzheimer's Disease. *Neurology and Therapy*, *10*(2), 919–40. https://doi.org/10.1007/s40120-021-00273-0

Hershko, A., & Ciechanover, A. (1998). The ubiquitin system. *Annual Review of Biochemistry*, *67*, 425–79. https://doi.org/10.1146/annurev.biochem.67.1.425

Herskovits, A. Z., Locascio, J. J., Peskind, E. R., Li, G., & Hyman, B. T. (2013). A Luminex assay detects amyloid β oligomers in Alzheimer's disease

cerebrospinal fluid. *PloS One*, *8*(7), e67898. https://doi.org/10.1371/journal.pone.0067898

Heyman, A., Peterson, B., Fillenbaum, G., & Pieper, C. (1996). The consortium to establish a registry for Alzheimer's disease (CERAD). Part XIV: Demographic and clinical predictors of survival in patients with Alzheimer's disease. *Neurology*, *46*(3), 656–60. https://doi.org/10.1212/wnl.46.3.656

Hillen, H., Barghorn, S., Striebinger, A., Labkovsky, B., Müller, R., Nimmrich, V., Nolte, M. W., Perez-Cruz, C., van der Auwera, I., van Leuven, F., van Gaalen, M., Bespalov, A. Y., Schoemaker, H., Sullivan, J. P., & Ebert, U. (2010). Generation and therapeutic efficacy of highly oligomer-specific beta-amyloid antibodies. *The Journal of Neuroscience: The Official Journal of the Society for Neuroscience*, *30*(31), 10369–79. https://doi.org/10.1523/JNEUROSCI.5721-09.2010

Hipp, M. S., Park, S.-H., & Hartl, F. U. (2014). Proteostasis impairment in protein- misfolding and -aggregation diseases. *Trends in Cell Biology*, *24*(9), 506–14. https://doi.org/10.1016/j.tcb.2014.05.003

Hodges, J. R., Graham, N., & Patterson, K. (1995). Charting the progression in semantic dementia: Implications for the organisation of semantic memory. *Memory (Hove, England)*, *3*(3–4), 463–95. https://doi.org/10.1080/09658219508253161

Hof, P. R., Vogt, B. A., Bouras, C., & Morrison, J. H. (1997). Atypical form of Alzheimer's disease with prominent posterior cortical atrophy: A review of lesion distribution and circuit disconnection in cortical visual pathways. *Vision Research*, *37*(24), 3609–25. https://doi.org/10.1016/S0042-6989(96)00240-4

Hölttä, M., Hansson, O., Andreasson, U., Hertze, J., Minthon, L., Nägga, K., Andreasen, N., Zetterberg, H., & Blennow, K. (2013). Evaluating amyloid-β oligomers in cerebrospinal fluid as a biomarker for Alzheimer's disease. *PloS One*, *8*(6), e66381. https://doi.org/10.1371/journal.pone.0066381

Hong, S., Beja-Glasser, V. F., Nfonoyim, B. M., Frouin, A., Li, S., Ramakrishnan, S., Merry, K. M., Shi, Q., Rosenthal, A., Barres, B. A., Lemere, C. A., Selkoe, D. J., Stevens, B. (2016). Complement and microglia mediate early synapse loss in Alzheimer mouse models. *Science*. 352(6286):712-716. doi: 10.1126/science.aad8373.

Hong, S., Ostaszewski, B. L., Yang, T., O'Malley, T. T., Jin, M., Yanagisawa, K., Li, S., Bartels, T., & Selkoe, D. J. (2014). Soluble Aβ oligomers are rapidly sequestered from brain ISF in vivo and bind GM1 ganglioside on cellular membranes. *Neuron*, *82*(2), 308–19. https://doi.org/10.1016/j.neuron.2014.02.027

Huang, W.-J., Zhang, X., & Chen, W.-W. (2016). Role of oxidative stress in Alzheimer's disease. *Biomedical Reports*, *4*(5), 519–22. https://doi.org/10.3892/br.2016.630

Huang, Y.R., & Liu, R.-T. (2020). The Toxicity and Polymorphism of β-Amyloid Oligomers. *International Journal of Molecular Sciences*, *21*(12), 4477. https://doi.org/10.3390/ijms21124477

Hubin, E., van Nuland, N. a. J., Broersen, K., & Pauwels, K. (2014). Transient dynamics of Aβ contribute to toxicity in Alzheimer's disease. *Cellular and Molecular Life Sciences: CMLS*, *71*(18), 3507–21. https://doi.org/10.1007/s00018-014-1634-z

Hultberg, A., Temperton, N. J., Rosseels, V., Koenders, M., Gonzalez-Pajuelo, M., Schepens, B., Ibañez, L. I., Vanlandschoot, P., Schillemans, J., Saunders, M., Weiss, R. A., Saelens, X., Melero, J. A., Verrips, C. T., Van Gucht, S., & de Haard, H. J. (2011). Llama-derived single domain antibodies to build multivalent, superpotent and broadened neutralizing anti-viral molecules. *PloS One*, *6*(4), e17665. https://doi.org/10.1371/journal.pone.0017665

Huston, J. S., Levinson, D., Mudgett-Hunter, M., Tai, M. S., Novotný, J., Margolies, M. N., Ridge, R. J., Bruccoleri, R. E., Haber, E., &Crea, R. (1988). Protein engineering of antibody binding sites: Recovery of specific activity in an anti- digoxin single-chain Fv analogue produced in Escherichia coli. *Proceedings of the National Academy of Sciences*, *85*(16), 5879–83. https://doi.org/10.1073/pnas.85.16.5879

Hyman, B. T., Van Hoesen, G. W., Damasio, A. R., & Barnes, C. L. (1984). Alzheimer's disease: Cell-specific pathology isolates the hippocampal formation. *Science (New York, N.Y.)*, *225*(4667), 1168–70. https://doi.org/10.1126/science.6474172

Iadecola C. (2017). The Neurovascular Unit Coming of Age: A Journey through Neurovascular Coupling in Health and Disease. Neuron. 96(1):17-42. doi: 10.1016/j.neuron.2017.07.030. PMID: 28957666; PMCID: PMC5657612.

Jack, C. R., & Holtzman, D. M. (2013). Biomarker modeling of Alzheimer's disease. *Neuron*, *80*(6), 1347–58. https://doi.org/10.1016/j.neuron.2013.12.003

Jack, C. R., Bennett, D. A., Blennow, K., Carrillo, M. C., Dunn, B., Haeberlein, S. B., Holtzman, D. M., Jagust, W., Jessen, F., Karlawish, J., Liu, E., Molinuevo, J. L., Montine, T., Phelps, C., Rankin, K. P., Rowe, C. C., Scheltens, P., Siemers, E., Snyder, H. M., … Contributors. (2018). NIA-AA Research Framework: Toward a biological definition of Alzheimer's disease. *Alzheimer's & Dementia: The Journal of the Alzheimer's Association*, *14*(4), 535–62. https://doi.org/10.1016/j.jalz.2018.02.018

Jack, C. R., Dickson, D. W., Parisi, J. E., Xu, Y. C., Cha, R. H., O'Brien, P. C., Edland, S. D., Smith, G. E., Boeve, B. F., Tangalos, E. G., Kokmen, E., & Petersen, R. C. (2002). Antemortem MRI findings correlate with hippocampal neuropathology in typical aging and dementia. *Neurology*, *58*(5), 750–57. https://doi.org/10.1212/wnl.58.5.750

Jack, C. R., Knopman, D. S., Jagust, W. J., Petersen, R. C., Weiner, M. W., Aisen, P. S., Shaw, L. M., Vemuri, P., Wiste, H. J., Weigand, S. D., Lesnick, T. G., Pankratz, V. S., Donohue, M. C., &Trojanowski, J. Q. (2013b). Tracking pathophysiological processes in Alzheimer's disease: An updated hypothetical model of dynamic biomarkers. *The Lancet. Neurology*, *12*(2), 207–16. https://doi.org/10.1016/S1474-4422(12)70291-0

Jack, C. R., Knopman, D. S., Jagust, W. J., Shaw, L. M., Aisen, P. S., Weiner, M.

W., Petersen, R. C., &Trojanowski, J. Q. (2010a). Hypothetical model of dynamic biomarkers of the Alzheimer's pathological cascade. *The Lancet. Neurology*, *9*(1), 119–28. https://doi.org/10.1016/S1474-4422(09)70299-6

Jack, C. R., Lowe, V. J., Senjem, M. L., Weigand, S. D., Kemp, B. J., Shiung, M. M., Knopman, D. S., Boeve, B. F., Klunk, W. E., Mathis, C. A., & Petersen, R. C. (2008). 11C PiB and structural MRI provide complementary information in imaging of Alzheimer's disease and amnestic mild cognitive impairment. *Brain: A Journal of Neurology*, *131*(Pt 3), 665–80. https://doi.org/10.1093/brain/awm336

Jack, C. R., Lowe, V. J., Weigand, S. D., Wiste, H. J., Senjem, M. L., Knopman, D. S., Shiung, M. M., Gunter, J. L., Boeve, B. F., Kemp, B. J., Weiner, M., Petersen, R. C., & Alzheimer's Disease Neuroimaging Initiative. (2009). Serial PIB and MRI in normal, mild cognitive impairment and Alzheimer's disease: Implications for sequence of pathological events in Alzheimer's disease. *Brain: A Journal of Neurology*, *132*(Pt 5), 1355–65. https://doi.org/10.1093/brain/awp062

Jack, C. R., Vemuri, P., Wiste, H. J., Weigand, S. D., Lesnick, T. G., Lowe, V., Kantarci, K., Bernstein, M. A., Senjem, M. L., Gunter, J. L., Boeve, B. F., Trojanowski, J. Q., Shaw, L. M., Aisen, P. S., Weiner, M. W., Petersen, R. C., Knopman, D. S., & Alzheimer's Disease Neuroimaging Initiative. (2012). Shapes of the trajectories of 5 major biomarkers of Alzheimer disease. *Archives of Neurology*, *69*(7), 856– 67. https://doi.org/10.1001/archneurol.2011.3405

Jack, C. R., Wiste, H. J., Vemuri, P., Weigand, S. D., Senjem, M. L., Zeng, G., Bernstein, M. A., Gunter, J. L., Pankratz, V. S., Aisen, P. S., Weiner, M. W., Petersen, R. C., Shaw, L. M., Trojanowski, J. Q., Knopman, D. S., & Alzheimer's Disease Neuroimaging Initiative. (2010b). Brain beta-amyloid measures and magnetic resonance imaging atrophy both predict time-to-progression from mild cognitive impairment to Alzheimer's disease. *Brain: A Journal of Neurology*, *133*(11), 3336–48. https://doi.org/10.1093/brain/awq277

Jackson, R. J., Hellen, C. U. T., & Pestova, T. V. (2010). The mechanism of eukaryotic translation initiation and principles of its regulation. *Nature Reviews. Molecular Cell Biology*, *11*(2), 113–27. https://doi.org/10.1038/nrm2838

Jagust, W. J. (2010). Amyloid imaging: Coming to a PET scanner near you. *Annals of Neurology*, *68*(3), 277–78. https://doi.org/10.1002/ana.22144

Jakob-Roetne, R., & Jacobsen, H. (2009). Alzheimer's disease: From pathology to therapeutic approaches. *AngewandteChemie (International Ed. in English)*, *48*(17), 3030–59. https://doi.org/10.1002/anie.200802808

Janelidze, S., Mattsson, N., Palmqvist, S., Smith, R., Beach, T. G., Serrano, G. E., Chai, X., Proctor, N. K., Eichenlaub, U., Zetterberg, H., Blennow, K., Reiman, E. M., Stomrud, E., Dage, J. L., & Hansson, O. (2020). Plasma P-tau181 in Alzheimer's disease: Relationship to other biomarkers, differential diagnosis, neuropathology and longitudinal progression to Alzheimer's

dementia. *Nature Medicine*, *26*(3), 379–86. https://doi.org/10.1038/s41591-020-0755-1

Janelidze, S., Stomrud, E., Palmqvist, S., Zetterberg, H., van Westen, D., Jeromin, A., Song, L., Hanlon, D., Tan Hehir, C. A., Baker, D., Blennow, K., & Hansson, O. (2016). Plasma β-amyloid in Alzheimer's disease and vascular disease. *Scientific Reports*, *6*, 26801. https://doi.org/10.1038/srep26801

Jansen, W. J., Ossenkoppele, R., Knol, D. L., Tijms, B. M., Scheltens, P., Verhey, F. R. J., Visser, P. J., Amyloid Biomarker Study Group, Aalten, P., Aarsland, D., Alcolea, D., Alexander, M., Almdahl, I. S., Arnold, S. E., Baldeiras, I., Barthel, H., van Berckel, B. N. M., Bibeau, K., Blennow, K., … Zetterberg, H. (2015). Prevalence of cerebral amyloid pathology in persons without dementia: A meta- analysis. *JAMA*, *313*(19), 1924–38. https://doi.org/10.1001/jama.2015.4668

Jarrett, J. T., Berger, E. P., & Lansbury, P. T. (1993). The carboxy terminus of the beta amyloid protein is critical for the seeding of amyloid formation: Implications for the pathogenesis of Alzheimer's disease. *Biochemistry*, *32*(18), 4693–97. https://doi.org/10.1021/bi00069a001

Jekel, K., Damian, M., Wattmo, C., Hausner, L., Bullock, R., Connelly, P. J., Dubois, B., Eriksdotter, M., Ewers, M., Graessel, E., Kramberger, M. G., Law, E., Mecocci, P., Molinuevo, J. L., Nygård, L., Olde-Rikkert, M. G., Orgogozo, J.-M., Pasquier, F., Peres, K., … Frölich, L. (2015). Mild cognitive impairment and deficits in instrumental activities of daily living: A systematic review. *Alzheimer's Research & Therapy*, *7*(1), 17. https://doi.org/10.1186/s13195-015-0099-0

Ji, S.R., Wu, Y., & Sui, S. (2002). Cholesterol is an important factor affecting the membrane insertion of beta-amyloid peptide (A beta 1-40), which may potentially inhibit the fibril formation. *The Journal of Biological Chemistry*, *277*(8), 6273–79. https://doi.org/10.1074/jbc.M104146200

Jinwal, U. K., Trotter, J. H., Abisambra, J. F., Koren, J., Lawson, L. Y., Vestal, G. D., O'Leary, J. C., Johnson, A. G., Jin, Y., Jones, J. R., Li, Q., Weeber, E. J., & Dickey, C. A. (2011). The Hsp90 kinase co-chaperone Cdc37 regulates tau stability and phosphorylation dynamics. *The Journal of Biological Chemistry*, *286*(19), 16976-83. https://doi.org/10.1074/jbc.M110.182493

Johnson, J. K., Head, E., Kim, R., Starr, A., & Cotman, C. W. (1999). Clinical and pathological evidence for a frontal variant of Alzheimer disease. *Archives of Neurology*, *56*(10), 1233–39. https://doi.org/10.1001/archneur.56.10.1233

Kagan, B. L., Azimov, R., & Azimova, R. (2004). Amyloid peptide channels. *The Journal of Membrane Biology*, *202*(1), 1–10. https://doi.org/10.1007/s00232-004-0709-4

Kakio, A., Nishimoto, S. I., Yanagisawa, K., Kozutsumi, Y., & Matsuzaki, K. (2001). Cholesterol-dependent formation of GM1 ganglioside-bound amyloid beta- protein, an endogenous seed for Alzheimer amyloid. *The Journal of Biological Chemistry*, *276*(27), 24985–90. https://doi.org/10.1074/jbc.M100252200

Kakio, A., Nishimoto, S., Yanagisawa, K., Kozutsumi, Y., & Matsuzaki, K.

(2002). Interactions of amyloid beta-protein with various gangliosides in raft-like membranes: Importance of GM1 ganglioside-bound form as an endogenous seed for Alzheimer amyloid. *Biochemistry*, *41*(23), 7385–90. https://doi.org/10.1021/bi0255874

Kamat, P. K., Kalani, A., Rai, S., Swarnkar, S., Tota, S., Nath, C., & Tyagi, N. (2016). Mechanism of Oxidative Stress and Synapse Dysfunction in the Pathogenesis of Alzheimer's Disease: Understanding the Therapeutics Strategies. *Molecular Neurobiology*, *53*(1), 648–61. https://doi.org/10.1007/s12035-014-9053-6

Kaneko, M., Koike, H., Saito, R., Kitamura, Y., Okuma, Y., & Nomura, Y. (2010). Loss of HRD1-mediated protein degradation causes amyloid precursor protein accumulation and amyloid-beta generation. *The Journal of Neuroscience: The Official Journal of the Society for Neuroscience*, *30*(11), 3924–32. https://doi.org/10.1523/JNEUROSCI.2422-09.2010

Kaneko, M., Saito, R., Okuma, Y., & Nomura, Y. (2012). Possible involvement of ubiquitin ligase HRD1 insolubilization in amyloid β generation. *Biological & Pharmaceutical Bulletin*, *35*(2), 269–72. https://doi.org/10.1248/bpb.35.269

Kapasi A., DeCarli C., Schneider J. A. (2017). Impact of multiple pathologies on the threshold for clinically overt dementia. *Acta Neuropathol*. 134:171–86. doi: 10.1007/s00401-017-1717-7.

Karch, C. M., Cruchaga, C., & Goate, A. M. (2014). Alzheimer's disease genetics: From the bench to the clinic. *Neuron*, *83*(1), 11–26. https://doi.org/10.1016/j.neuron.2014.05.041

Karikari, T. K., Pascoal, T. A., Ashton, N. J., Janelidze, S., Benedet, A. L., Rodriguez, J. L., Chamoun, M., Savard, M., Kang, M. S., Therriault, J., Schöll, M., Massarweh, G., Soucy, J.-P., Höglund, K., Brinkmalm, G., Mattsson, N., Palmqvist, S., Gauthier, S., Stomrud, E., … Blennow, K. (2020). Blood phosphorylated tau 181 as a biomarker for Alzheimer's disease: A diagnostic performance and prediction modelling study using data from four prospective cohorts. *The Lancet. Neurology*, *19*(5), 422–33. https://doi.org/10.1016/S1474- 4422(20)30071-5

Karran, E., & De Strooper, B. (2022). The amyloid hypothesis in Alzheimer disease: New insights from new therapeutics. *Nature Reviews. Drug Discovery*, *21*(4), 306–18. https://doi.org/10.1038/s41573-022-00391-w

Kasturirangan, S., Li, L., Emadi, S., Boddapati, S., Schulz, P., &Sierks, M. R. (2012). Nanobody specific for oligomeric β-amyloid stabilizes nontoxic form. *Neurobiology of Aging*, *33*(7), 1320–28. https://doi.org/10.1016/j.neurobiolaging.2010.09.020

Kaushik, S., Cuervo A.M. Proteostasis and aging. Nat Med. 2015 Dec;21(12):1406-15. doi: 10.1038/nm.4001. PMID: 26646497.

Kayed, R., Head, E., Sarsoza, F., Saing, T., Cotman, C. W., Necula, M., Margol, L., Wu, J., Breydo, L., Thompson, J. L., Rasool, S., Gurlo, T., Butler, P., & Glabe, C. G. (2007). Fibril specific, conformation dependent antibodies recognize a generic epitope common to amyloid fibrils and fibrillar oligomers that is absent in prefibrillar oligomers. *Molecular Neurodegeneration*, *2*, 18.

https://doi.org/10.1186/1750-1326-2-18
Kayed, R., Head, E., Thompson, J. L., McIntire, T. M., Milton, S. C., Cotman, C. W., & Glabe, C. G. (2003). Common structure of soluble amyloid oligomers implies common mechanism of pathogenesis. *Science (New York, N.Y.)*, *300*(5618), 486–89. https://doi.org/10.1126/science.1079469
Kayed, R., Sokolov, Y., Edmonds, B., McIntire, T. M., Milton, S. C., Hall, J. E., & Glabe, C. G. (2004). Permeabilization of lipid bilayers is a common conformation- dependent activity of soluble amyloid oligomers in protein misfolding diseases. *The Journal of Biological Chemistry*, *279*(45), 46363–66. https://doi.org/10.1074/jbc.C400260200
Keck, S., Nitsch, R., Grune, T., & Ullrich, O. (2003). Proteasome inhibition by paired helical filament-tau in brains of patients with Alzheimer's disease. *Journal of Neurochemistry*, *85*(1), 115–22. https://doi.org/10.1046/j.1471-4159.2003.01642.x
Khachaturian, Z. S. (1989). The role of calcium regulation in brain aging: Reexamination of a hypothesis. *Aging (Milan, Italy)*, *1*(1), 17–34. https://doi.org/10.1007/BF03323872
Kim, K. S., Wen, GY., Bancher, C., Chen, CMJ, Sapienza, V., Hong, H., Wisniewski HM. (1990) Detection and quantification of amyloid β-peptide with two mono- clonal antibodies. *Neurosci Res Comm*, 7:113–22.
Kim, S., Sharma, C., Jung, U. J., & Kim, S. R. (2023). Pathophysiological Role of Microglial Activation Induced by Blood-Borne Proteins in Alzheimer's Disease. *Biomedicines*, *11*(5), 1383. https://doi.org/10.3390/biomedicines11051383
Kim, S.I., Yi, J.S., & Ko, Y.G. (2006). Amyloid beta oligomerization is induced by brain lipid rafts. *Journal of Cellular Biochemistry*, *99*(3), 878–89. https://doi.org/10.1002/jcb.20978
Kim, Y. E., Hipp, M. S., Bracher, A., Hayer-Hartl, M., & Hartl, F. U. (2013). Molecular chaperone functions in protein folding and proteostasis. *Annual Review of Biochemistry*, *82*, 323–55. https://doi.org/10.1146/annurev-biochem-060208-092442
Kinger, S., Jagtap, Y. A., Kumar, P., Choudhary, A., Prasad, A., Prajapati, V. K., Kumar, A., Mehta, G., & Mishra, A. (2024). Proteostasis in neurodegenerative diseases. *Advances in Clinical Chemistry*, *121*, 270–333. https://doi.org/10.1016/bs.acc.2024.04.002
Kish, S. J. (1997). Brain energy metabolizing enzymes in Alzheimer's disease: Alpha- ketoglutarate dehydrogenase complex and cytochrome oxidase. *Annals of the New York Academy of Sciences*, *826*, 218–28. https://doi.org/10.1111/j.1749- 6632.1997.tb48473.x
Kleiger, G., & Mayor, T. (2014). Perilous journey: A tour of the ubiquitin-proteasome system. *Trends in Cell Biology*, *24*(6), 352–59. https://doi.org/10.1016/j.tcb.2013.12.003
Klement, M., Liu, C., Loo, B. L. W., Choo, A. B.-H., Ow, D. S.-W., & Lee, D.-Y. (2015). Effect of linker flexibility and length on the functionality of a cytotoxic engineered antibody fragment. *Journal of Biotechnology*, *199*, 90–

97. https://doi.org/10.1016/j.jbiotec.2015.02.008

Klyubin, I., Betts, V., Welzel, A. T., Blennow, K., Zetterberg, H., Wallin, A., Lemere, C. A., Cullen, W. K., Peng, Y., Wisniewski, T., Selkoe, D. J., Anwyl, R., Walsh, D. M., & Rowan, M. J. (2008). Amyloid beta protein dimer-containing human CSF disrupts synaptic plasticity: Prevention by systemic passive immunization. *The Journal of Neuroscience: The Official Journal of the Society for Neuroscience*, *28*(16), 4231–37. https://doi.org/10.1523/JNEUROSCI.5161-07.2008

Knopman, D. S., Amieva, H., Petersen, R. C., Chételat, G., Holtzman, D. M., Hyman, B. T., Nixon, R. A., & Jones, D. T. (2021). Alzheimer disease. *Nature Reviews. Disease Primers*, *7*(1), 33. https://doi.org/10.1038/s41572-021-00269-y

Kollmer, M., Close, W., Funk, L., Rasmussen, J., Bsoul, A., Schierhorn, A., Schmidt, M., Sigurdson, C. J., Jucker, M., &Fändrich, M. (2019). Cryo-EM structure and polymorphism of Aβ amyloid fibrils purified from Alzheimer's brain tissue. *Nature Communications*, *10*(1), 4760. https://doi.org/10.1038/s41467-019-12683-8

Kosik, K. S., Joachim, C. L., & Selkoe, D. J. (1986). Microtubule-associated protein tau (tau) is a major antigenic component of paired helical filaments in Alzheimer disease. *Proceedings of the National Academy of Sciences of the United States of America*, *83*(11), 4044–48. https://doi.org/10.1073/pnas.83.11.4044

Kravats, A.N.,Wickner, S.,Camberg, J.L. (2022). Molecular Chaperones. *Ref. Modul. Life Sci.*

Kremer, J. J., Pallitto, M. M., Sklansky, D. J., & Murphy, R. M. (2000). Correlation of beta-amyloid aggregate size and hydrophobicity with decreased bilayer fluidity of model membranes. *Biochemistry*, *39*(33), 10309–18. https://doi.org/10.1021/bi0001980

Kulichikhin, K. Y., Fedotov, S. A., Rubel, M. S., Zalutskaya, N. M., Zobnina, A. E., Malikova, O. A., Neznanov, N. G., Chernoff, Y. O., & Rubel, A. A. (2021). Development of molecular tools for diagnosis of Alzheimer's disease that are based on detection of amyloidogenic proteins. *Prion*, *15*(1), 56–69. https://doi.org/10.1080/19336896.2021.1917289

Labbadia, J., & Morimoto, R. I. (2015). The biology of proteostasis in aging and disease. *Annual Review of Biochemistry*, *84*, 435–64. https://doi.org/10.1146/annurev- biochem-060614-033955

Ladiwala, A. R. A., Litt, J., Kane, R. S., Aucoin, D. S., Smith, S. O., Ranjan, S., Davis, J., Van Nostrand, W. E., & Tessier, P. M. (2012). Conformational differences between two amyloid β oligomers of similar size and dissimilar toxicity. *The Journal of Biological Chemistry*, *287*(29), 24765–73. https://doi.org/10.1074/jbc.M111.329763

Lafaye, P., Achour, I., England, P., Duyckaerts, C., &Rougeon, F. (2009). Single-domain antibodies recognize selectively small oligomeric forms of amyloid beta, prevent Abeta-induced neurotoxicity and inhibit fibril formation. *Molecular Immunology*, *46*(4), 695–704.

https://doi.org/10.1016/j.molimm.2008.09.008

LaFerla, F. M., Green, K. N., & Oddo, S. (2007). Intracellular amyloid-beta in Alzheimer's disease. *Nature Reviews. Neuroscience*, *8*(7), 499–509. https://doi.org/10.1038/nrn2168

Lafleche, G., & Albert, M. S. (1995). Executive function deficits in mild Alzheimer's disease. *Neuropsychology*, *9*(3), 313–20. https://doi.org/10.1037/0894-4105.9.3.313

Lambert, M. P., Barlow, A. K., Chromy, B. A., Edwards, C., Freed, R., Liosatos, M., Morgan, T. E., Rozovsky, I., Trommer, B., Viola, K. L., Wals, P., Zhang, C., Finch, C. E., Krafft, G. A., & Klein, W. L. (1998). Diffusible, nonfibrillar ligands derived from Abeta1-42 are potent central nervous system neurotoxins. *Proceedings of the National Academy of Sciences of the United States of America*, *95*(11), 6448–53. https://doi.org/10.1073/pnas.95.11.6448

Lambert, M. P., Viola, K. L., Chromy, B. A., Chang, L., Morgan, T. E., Yu, J., Venton, D. L., Krafft, G. A., Finch, C. E., & Klein, W. L. (2001). Vaccination with soluble Abeta oligomers generates toxicity-neutralizing antibodies. *Journal of Neurochemistry*, *79*(3), 595–605. https://doi.org/10.1046/j.1471-4159.2001.00592.x

Landau, S. M., Mintun, M. A., Joshi, A. D., Koeppe, R. A., Petersen, R. C., Aisen, P. S., Weiner, M. W., Jagust, W. J., & Alzheimer's Disease Neuroimaging Initiative. (2012). Amyloid deposition, hypometabolism, and longitudinal cognitive decline. *Annals of Neurology*, *72*(4), 578–86. https://doi.org/10.1002/ana.23650

Lardinois, O., Kirby, P. J., Morgan, D. L., Sills, R. C., Tomer, K. B., &Deterding, L. J. (2014). Mass spectrometric analysis of rat cerebrospinal fluid proteins following exposure to the neurotoxicant carbonyl sulfide. *Rapid Communications in Mass Spectrometry: RCM*, *28*(23), 2531–38. https://doi.org/10.1002/rcm.7046

Le Bastard, N., Coart, E., Vanderstichele, H., Vanmechelen, E., Martin, J. J., Engelborghs, S. (2013). Comparison of two analytical platforms for the clinical qualification of Alzheimer's disease biomarkers in pathologically-confirmed dementia. J Alzheimers Dis.33(1):117-31. doi: 10.3233/JAD-2012-121246. PMID: 22936010.

Lee, A. G. (2003). Lipid-protein interactions in biological membranes: A structural perspective. *Biochimica Et Biophysica Acta*, *1612*(1), 1–40. https://doi.org/10.1016/s0005-2736(03)00056-7

Lee, J.-H., Yu, W. H., Kumar, A., Lee, S., Mohan, P. S., Peterhoff, C. M., Wolfe, D. M., Martinez-Vicente, M., Massey, A. C., Sovak, G., Uchiyama, Y., Westaway, D., Cuervo, A. M., & Nixon, R. A. (2010). Lysosomal proteolysis and autophagy require presenilin 1 and are disrupted by Alzheimer-related PS1 mutations. *Cell*, *141*(7), 1146–58. https://doi.org/10.1016/j.cell.2010.05.008

Lesne, J., Chang, HJ., De Visch, A. *et al.* Structural basis for chemically-induced homodimerization of a single domain antibody. (2019). *Sci Rep* 9, 1840. https://doi.org/10.1038/s41598-019-38752-y

Leuzy, A., Mattsson-Carlgren, N., Palmqvist, S., Janelidze, S., Dage, J. L., & Hansson, O. (2022). Blood-based biomarkers for Alzheimer's disease. *EMBO Molecular Medicine*, *14*(1), e14408. https://doi.org/10.15252/emmm.202114408

Lewczuk P., Matzen, A., Blennow, K., Parnetti, L., Molinuevo, J. L., Eusebi, P., Kornhuber, J., Morris, J. C., Fagan, A. M. (2017). Cerebrospinal Fluid Aβ42/40 Corresponds Better than Aβ42 to Amyloid PET in Alzheimer's Disease. J Alzheimers Dis. 55(2):813-22. doi: 10.3233/JAD-160722. PMID: 27792012; PMCID: PMC5147502.

Li, G., Bien-Ly, N., Andrews-Zwilling, Y., Xu, Q., Bernardo, A., Ring, K., Halabisky, B., Deng, C., Mahley, R. W., & Huang, Y. (2009). GABAergic interneuron dysfunction impairs hippocampal neurogenesis in adult apolipoprotein E4 knockin mice. *Cell Stem Cell*, *5*(6), 634–45. https://doi.org/10.1016/j.stem.2009.10.015

Li, S., Hong, S., Shepardson, N. E., Walsh, D. M., Shankar, G. M., & Selkoe, D. (2009). Soluble oligomers of amyloid Beta protein facilitate hippocampal long-term depression by disrupting neuronal glutamate uptake. *Neuron*, *62*(6), 788–801. https://doi.org/10.1016/j.neuron.2009.05.012

Li, T., Vandesquille, M., Koukouli, F., Dudeffant, C., Youssef, I., Lenormand, P., Ganneau, C., Maskos, U., Czech, C., Grueninger, F., Duyckaerts, C., Dhenain, M., Bay, S., Delatour, B., & Lafaye, P. (2016). Camelid single-domain antibodies: A versatile tool for in vivo imaging of extracellular and intracellular brain targets. *Journal of Controlled Release: Official Journal of the Controlled Release Society*, *243*, 1–10. https://doi.org/10.1016/j.jconrel.2016.09.019

Li, X., An, W.-L., Alafuzoff, I., Soininen, H., Winblad, B., & Pei, J.-J. (2004). Phosphorylated eukaryotic translation factor 4E is elevated in Alzheimer brain. *Neuroreport*, *15*(14), 2237–40. https://doi.org/10.1097/00001756-200410050-00019

Lin, H., Bhatia, R., & Lal, R. (2001). Amyloid beta protein forms ion channels: Implications for Alzheimer's disease pathophysiology. *FASEB Journal: Official Publication of the Federation of American Societies for Experimental Biology*, *15*(13), 2433–44. https://doi.org/10.1096/fj.01-0377com

Lin, M.S., Chen, L.Y., Wang, S. S. S., Chang, Y., & Chen, W.Y. (2008). Examining the levels of ganglioside and cholesterol in cell membrane on attenuation the cytotoxicity of beta-amyloid peptide. *Colloids and Surfaces. B, Biointerfaces*, *65*(2), 172–77. https://doi.org/10.1016/j.colsurfb.2008.03.012

Liu, C.C., Liu, C.C., Kanekiyo, T., Xu, H., & Bu, G. (2013). Apolipoprotein E and Alzheimer disease: Risk, mechanisms and therapy. *Nature Reviews. Neurology*, *9*(2), 106–18. https://doi.org/10.1038/nrneurol.2012.263

Liu, P., Li, L., He, F., Meng, F., Liu, X., Su, Y., Su, X., Luo, B., & Peng, G. (2023). Identification of Candidate Biomarkers of Alzheimer's Disease via Multiplex Cerebrospinal Fluid and Serum Proteomics. *International Journal of Molecular Sciences*, *24*(18), 14225. https://doi.org/10.3390/ijms241814225

Lo, R. Y., Hubbard, A. E., Shaw, L. M., Trojanowski, J. Q., Petersen, R. C., Aisen, P. S., Weiner, M. W., Jagust, W. J., & Alzheimer's Disease Neuroimaging

Initiative. (2011). Longitudinal change of biomarkers in cognitive decline. *Archives of Neurology*, *68*(10), 1257–66. https://doi.org/10.1001/archneurol.2011.123

Lopez Salon, M., Pasquini, L., Besio Moreno, M., Pasquini, J. M., & Soto, E. (2003). Relationship between beta-amyloid degradation and the 26S proteasome in neural cells. *Experimental Neurology*, *180*(2), 131–43. https://doi.org/10.1016/s0014-4886(02)00060-2

Löppönen, M., Räihä, I., Isoaho, R., Vahlberg, T., & Kivelä, S.-L. (2003). Diagnosing cognitive impairment and dementia in primary health care—A more active pproach is needed. *Age and Ageing*, *32*(6), 606–12. https://doi.org/10.1093/ageing/afg097

Love S. & Miners J. S. Cerebrovascular disease in ageing and Alzheimer's disease. (2016). *Acta Neuropathol*. 2016;131:645–58. doi: 10.1007/s00401-015-1522-0

Lu, R. C., Tan, M. S., Wang, H., Xie, A. M., Yu, J. T., & Tan, L. (2014). Heat shock protein 70 in Alzheimer's disease. *BioMed Research International*, *2014*, 435203. https://doi.org/10.1155/2014/435203

Lusardi, T. A., Phillips, J. I., Wiedrick, J. T., Harrington, C. A., Lind, B., Lapidus, J. A., Quinn, J. F., & Saugstad, J. A. (2017). MicroRNAs in Human Cerebrospinal Fluid as Biomarkers for Alzheimer's Disease. *Journal of Alzheimer's Disease: JAD*, *55*(3), 1223–33. https://doi.org/10.3233/JAD-160835

Manoutcharian, K., Acero, G., Munguia, M. E., Becerril, B., Massieu, L., Govezensky, T., Ortiz, E., Marks, J. D., Cao, C., Ugen, K., & Gevorkian, G. (2004). Human single chain Fv antibodies and a complementarity determining region-derived peptide binding to amyloid-beta 1-42. *Neurobiology of Disease*, *17*(1), 114–21. https://doi.org/10.1016/j.nbd.2004.06.005

Marín-Argany, M., Rivera-Hernández, G., Martí, J., & Villegas, S. (2011). An anti-Aβ (amyloid β) single-chain variable fragment prevents amyloid fibril formation and cytotoxicity by withdrawing Aβ oligomers from the amyloid pathway. *The Biochemical Journal*, *437*(1), 25–34. https://doi.org/10.1042/BJ20101712

Martinez-Lopez, N., Athonvarangkul, D., & Singh, R. (2015). Autophagy and aging. *Advances in Experimental Medicine and Biology*, *847*, 73–87. https://doi.org/10.1007/978-1-4939-2404-2_3

Mason, R. P., Shoemaker, W. J., Shajenko, L., Chambers, T. E., & Herbette, L. G. (1992). Evidence for changes in the Alzheimer's disease brain cortical membrane structure mediated by cholesterol. *Neurobiology of Aging*, *13*(3), 413–19. https://doi.org/10.1016/0197-4580(92)90116-f

Mastrogiacoma, F., Lindsay, J. G., Bettendorff, L., Rice, J., & Kish, S. J. (1996). Brain protein and alpha-ketoglutarate dehydrogenase complex activity in Alzheimer's disease. *Annals of Neurology*, *39*(5), 592–98. https://doi.org/10.1002/ana.410390508

Matsuzaki, K. (2007). Physicochemical interactions of amyloid beta-peptide with lipid bilayers. *Biochimica Et Biophysica Acta*, *1768*(8), 1935–42. https://doi.org/10.1016/j.bbamem.2007.02.009

Matsuzaki, K., Kato, K., & Yanagisawa, K. (2010). Abeta polymerization through interaction with membrane gangliosides. *Biochimica Et Biophysica Acta*, *1801*(8), 868–77. https://doi.org/10.1016/j.bbalip.2010.01.008

Mattson, M. P. (2004). Pathways towards and away from Alzheimer's disease. *Nature*, *430*(7000), 631–39. https://doi.org/10.1038/nature02621

Mattson, M. P., Cheng, B., Davis, D., Bryant, K., Lieberburg, I., &Rydel, R. E. (1992). Beta-Amyloid peptides destabilize calcium homeostasis and render human cortical neurons vulnerable to excitotoxicity. *The Journal of Neuroscience: The Official Journal of the Society for Neuroscience*, *12*(2), 376–89. https://doi.org/10.1523/JNEUROSCI.12-02-00376.1992

Mattsson, N., Zetterberg, H., Hansson, O., Andreasen, N., Parnetti, L., Jonsson, M., Herukka, S.-K., van der Flier, W. M., Blankenstein, M. A., Ewers, M., Rich, K., Kaiser, E., Verbeek, M., Tsolaki, M., Mulugeta, E., Rosén, E., Aarsland, D., Visser, P. J., Schröder, J., … Blennow, K. (2009). CSF biomarkers and incipient Alzheimer disease in patients with mild cognitive impairment. *JAMA*, *302*(4), 385–93. https://doi.org/10.1001/jama.2009.1064

McKeith, I.G., Boeve, B.F., Dickson, D.W., Halliday, G., Taylor, J.P., Weintraub, D., Aarsland, D., Galvin, J., Attems, J., Ballard, C. G., Bayston, A., Beach, T. G., Blanc, F., Bohnen, N., Bonanni, L., Bras, J., Brundin, P., Burn, D., et al. (2017). Diagnosis and management of dementia with Lewy bodies: Fourth consensus report of the DLB Consortium. Neurology. 2017 Jul 4;89(1):88-100. doi: 10.1212/WNL.0000000000004058. Epub 2017 Jun 7. PMID: 28592453; PMCID: PMC5496518.

McKhann, G. M., Knopman, D. S., Chertkow, H., Hyman, B. T., Jack, C. R. Jr, Kawas, C. H., Klunk, W. E., Koroshetz, W. J., Manly, J. J., Mayeux, R., Mohs, R. C., Morris, J. C., Rossor, M. N., Scheltens, P., Carrillo, M. C., Thies, B., Weintraub, S., Phelps, C. H. (2011), The diagnosis of dementia due to Alzheimer's disease: recommendations from the National Institute on Aging-Alzheimer's Association workgroups on diagnostic guidelines for Alzheimer's disease. Alzheimers Dement. May;7(3):263-9. doi: 10.1016/j.jalz.2011.03.005. Epub 2011 Apr 21. PMID: 21514250; PMCID: PMC3312024.

McKinnon, C., & Tabrizi, S. J. (2014). The ubiquitin-proteasome system in neurodegeneration. *Antioxidants & Redox Signaling*, *21*(17), 2302-21. https://doi.org/10.1089/ars.2013.5802

McLaurin, J., Franklin, T., Fraser, P. E., & Chakrabartty, A. (1998). Structural transitions associated with the interaction of Alzheimer beta-amyloid peptides with gangliosides. *The Journal of Biological Chemistry*, *273*(8), 4506–15. https://doi.org/10.1074/jbc.273.8.4506

Mendez, M. F. (2017). Early-Onset Alzheimer Disease. *Neurologic Clinics*, *35*(2), 263–81. https://doi.org/10.1016/j.ncl.2017.01.005.

Miao, J., Ma, H., Yang, Y., Liao, Y., Lin, C., Zheng, J., Yu, M., & Lan, J. (2023).

Microglia in Alzheimer's disease: Pathogenesis, mechanisms, and therapeutic potentials. *Frontier in Aging Neuroscience*, *15*. https://www.frontiersin.org/journals/aging-neuroscience/articles/10.3389/fnagi.2023.1201982

Miao, W. (2008). Electrogenerated chemiluminescence and its biorelated applications. *Chemical Reviews*, *108*(7), 2506–53. https://doi.org/10.1021/cr068083a

Micsonai, A., Wien, F., Bulyáki, É., Kun, J., Moussong, É., Lee, Y.-H., Goto, Y., Réfrégiers, M., &Kardos, J. (2018). BeStSel: A web server for accurate protein secondary structure prediction and fold recognition from the circular dichroism spectra. *Nucleic Acids Research*, *46*(W1), W315–W322. https://doi.org/10.1093/nar/gky497

Mielke, M. M., & Fowler, N. R. (2024). Alzheimer disease blood biomarkers: Considerations for population-level use. *Nature Reviews. Neurology*, *20*(8), 495–504. https://doi.org/10.1038/s41582-024-00989-1

Milstein, C. (1980). Monoclonal antibodies. *Scientific American*, *243*(4), 66–74. https://doi.org/10.1038/scientificamerican1080-66

Mormino, E. C., Kluth, J. T., Madison, C. M., Rabinovici, G. D., Baker, S. L., Miller, B. L., Koeppe, R. A., Mathis, C. A., Weiner, M. W., Jagust, W. J., & Alzheimer's Disease Neuroimaging Initiative. (2009). Episodic memory loss is related to hippocampal-mediated beta-amyloid deposition in elderly subjects. *Brain: A Journal of Neurology*, *132*(Pt 5), 1310–23. https://doi.org/10.1093/brain/awn320

Mosmann, T. (1983). Rapid colorimetric assay for cellular growth and survival: Application to proliferation and cytotoxicity assays. *Journal of Immunological Methods*, *65*(1–2), 55–63. https://doi.org/10.1016/0022-1759(83)90303-4

Murakami, K. (2014). Conformation-specific antibodies to target amyloid β oligomers and their application to immunotherapy for Alzheimer's disease. *Bioscience, Biotechnology, and Biochemistry*, *78*(8), 1293–1305. https://doi.org/10.1080/09168451.2014.940275

Muyldermans, S. (2013). Nanobodies: Natural single-domain antibodies. *Annual Review of Biochemistry*, *82*, 775–97. https://doi.org/10.1146/annurev-biochem-063011-092449

Nakashima-Yasuda, H., Uryu, K., Robinson, J., Xie, S. X., Hurtig, H., Duda, J. E., Arnold, S. E., Siderowf, A., Grossman, M., Leverenz, J. B., Woltjer, R., Lopez, O. L., Hamilton, R., Tsuang, D. W., Galasko, D., Masliah, E., Kaye, J., Clark, C. M., Montine, T. J., … Trojanowski, J. Q. (2007). Co-morbidity of TDP-43 proteinopathy in Lewy body related diseases. *Acta Neuropathologica*, *114*(3), 221–29. https://doi.org/10.1007/s00401-007-0261-2

Nalivaeva, N. N., & Turner, A. J. (2013). The amyloid precursor protein: A biochemical enigma in brain development, function and disease. *FEBS Letters*, *587*(13), 2046–54. https://doi.org/10.1016/j.febslet.2013.05.010

Neary, D., Snowden, J. S., Gustafson, L., Passant, U., Stuss, D., Black, S., Freedman, M., Kertesz, A., Robert, P. H., Albert, M., Boone, K., Miller, B. L.,

Cummings, J., & Benson, D. F. (1998). Frontotemporal lobar degeneration: A consensus on clinical diagnostic criteria. *Neurology*, *51*(6), 1546–54. https://doi.org/10.1212/wnl.51.6.1546

Nebes, R. D. (1989). Semantic memory in Alzheimer's disease. *Psychological Bulletin*, *106*(3), 377–94. https://doi.org/10.1037/0033-2909.106.3.377

Nicolson, G. L. (2014). The Fluid-Mosaic Model of Membrane Structure: Still relevant to understanding the structure, function and dynamics of biological membranes after more than 40 years. *Biochimica Et Biophysica Acta*, *1838*(6), 1451–66. https://doi.org/10.1016/j.bbamem.2013.10.019

Nikolaev, A., McLaughlin, T., O'Leary, D. D. M., & Tessier-Lavigne, M. (2009). APP binds DR6 to trigger axon pruning and neuron death via distinct caspases. *Nature*, *457*(7232), 981–89. https://doi.org/10.1038/nature07767

Nisbet, R. M., Nigro, J., Breheney, K., Caine, J., Hattarki, M. K., & Nuttall, S. D. (2013). Central amyloid-β-specific single chain variable fragment ameliorates Aβ aggregation and neurotoxicity. *Protein Engineering, Design & Selection: PEDS*, *26*(10), 571–80. https://doi.org/10.1093/protein/gzt025

Nonaka, T., Masuda-Suzukake, M., & Hasegawa, M. (2018). Molecular mechanisms of the co-deposition of multiple pathological proteins in neurodegenerative diseases. *Neuropathology: Official Journal of the Japanese Society of Neuropathology*, *38*(1), 64–71. https://doi.org/10.1111/neup.12427

Nunomura, A., Perry, G., Aliev, G., Hirai, K., Takeda, A., Balraj, E. K., Jones, P. K., Ghanbari, H., Wataya, T., Shimohama, S., Chiba, S., Atwood, C. S., Petersen, R. B., & Smith, M. A. (2001). Oxidative damage is the earliest event in Alzheimer disease. *Journal of Neuropathology and Experimental Neurology*, *60*(8), 759– 67. https://doi.org/10.1093/jnen/60.8.759

Nyhus, C., Pihl, M., Hyttel, P., & Hall, V. (2019). Evidence for nucleolar dysfunction in Alzheimer's disease. *Reviews in the Neurosciences*, *30*, 685–700. https://doi.org/10.1515/revneuro-2018-0104

O'Connor, A., Karikari, T. K., Poole, T., Ashton, N. J., Lantero Rodriguez, J., Khatun, A., Swift, I., Heslegrave, A. J., Abel, E., Chung, E., Weston, P. S. J., Pavisic, I. M., Ryan, N. S., Barker, S., Rossor, M. N., Polke, J. M., Frost, C., Mead, S., Blennow, K., … Fox, N. C. (2021). Plasma phospho-tau181 in presymptomatic and symptomatic familial Alzheimer's disease: A longitudinal cohort study. *Molecular Psychiatry*, *26*(10), 5967–76. https://doi.org/10.1038/s41380-020- 0838-x

Obregon, D., Hou, H., Deng, J., Giunta, B., Tian, J., Darlington, D., Shahaduzzaman, M., Zhu, Y., Mori, T., Mattson, M. P., & Tan, J. (2012). Soluble amyloid precursor protein-α modulates β-secretase activity and amyloid-β generation. *Nature Communications*, *3*, 777. https://doi.org/10.1038/ncomms1781

Olsson, B., Alberg, L., Cullen, N. C., Michael, E., Wahlgren, L., Kroksmark, A.-K., Rostasy, K., Blennow, K., Zetterberg, H., & Tulinius, M. (2019). NFL is a marker of treatment response in children with SMA treated with nusinersen. *Journal of Neurology*, *266*(9), 2129–36. https://doi.org/10.1007/s00415-019-09389-8

Olsson, B., Lautner, R., Andreasson, U., Öhrfelt, A., Portelius, E., Bjerke, M., Hölttä, M., Rosén, C., Olsson, C., Strobel, G., Wu, E., Dakin, K., Petzold, M., Blennow, K., & Zetterberg, H. (2016). CSF and blood biomarkers for the diagnosis of Alzheimer's disease: A systematic review and meta-analysis. *The Lancet. Neurology*, *15*(7), 673–84. https://doi.org/10.1016/S1474-4422(16)00070-3

Ossenkoppele, R., Rabinovici, G. D., Smith, R., Cho, H., Schöll, M., Strandberg, O., Palmqvist, S., Mattsson, N., Janelidze, S., Santillo, A., Ohlsson, T., Jögi, J., Tsai, R., La Joie, R., Kramer, J., Boxer, A. L., Gorno-Tempini, M. L., Miller, B. L., Choi, J. Y., … Hansson, O. (2018). Discriminative Accuracy of [18F]flortaucipir Positron Emission Tomography for Alzheimer Disease vs Other Neurodegenerative Disorders. *JAMA*, *320*(11), 1151–62. https://doi.org/10.1001/jama.2018.12917

Ostrowitzki, S., Bittner, T., Sink, K. M., Mackey, H., Rabe, C., Honig, L. S., Cassetta, E., Woodward, M., Boada, M., van Dyck, C. H., Grimmer, T., Selkoe, D. J., Schneider, A., Blondeau, K., Hu, N., Quartino, A., Clayton, D., Dolton, M., Dang, Y., … Doody, R. S. (2022). Evaluating the Safety and Efficacy of Crenezumab vs Placebo in Adults With Early Alzheimer Disease: Two Phase 3 Randomized Placebo-Controlled Trials. *JAMA Neurology*, *79*(11), 1113–21. https://doi.org/10.1001/jamaneurol.2022.2909

Ostrowitzki, S., Deptula, D., Thurfjell, L., Barkhof, F., Bohrmann, B., Brooks, D. J., Klunk, W. E., Ashford, E., Yoo, K., Xu, Z. X., Loetscher, H., Santarelli, L. (2012) Mechanism of amyloid removal in patients with Alzheimer disease treated with gantenerumab. Arch Neurol. Feb;69(2):198-207. doi: 10.1001/archneurol.2011.1538. Epub 2011 Oct 10. PMID: 21987394.

Ovod, V., Ramsey, K. N., Mawuenyega, K. G., Bollinger, J. G., Hicks, T., Schneider, T., Sullivan, M., Paumier, K., Holtzman, D. M., Morris, J. C., Benzinger, T., Fagan, A. M., Patterson, B. W., & Bateman, R. J. (2017). Amyloid β concentrations and stable isotope labeling kinetics of human plasma specific to central nervous system amyloidosis. *Alzheimer's & Dementia: The Journal of the Alzheimer's Association*, *13*(8), 841–49. https://doi.org/10.1016/j.jalz.2017.06.2266

Pain, C., Dumont, J., & Dumoulin, M. (2015). Camelid single-domain antibody fragments: Uses and prospects to investigate protein misfolding and aggregation, and to treat diseases associated with these phenomena. *Biochimie*, *111*, 82–106. https://doi.org/10.1016/j.biochi.2015.01.012

Palmqvist, S., Janelidze, S., Quiroz, Y. T., Zetterberg, H., Lopera, F., Stomrud, E., Su, Y., Chen, Y., Serrano, G. E., Leuzy, A., Mattsson-Carlgren, N., Strandberg, O., Smith, R., Villegas, A., Sepulveda-Falla, D., Chai, X., Proctor, N. K., Beach, T. G., Blennow, K., … Hansson, O. (2020). Discriminative Accuracy of Plasma Phospho-tau217 for Alzheimer Disease vs Other Neurodegenerative Disorders. *JAMA*, *324*(8), 772–81. https://doi.org/10.1001/jama.2020.12134

Pannee, J., Shaw, L. M., Korecka, M., Waligorska, T., Teunissen, C. E., Stoops, E., Vanderstichele, H. M. J., Mauroo, K., Verberk, I. M. W., Keshavan, A.,

Pesini, P., Sarasa, L., Pascual-Lucas, M., Fandos, N., Allué, J.-A., Portelius, E., Andreasson, U., Yoda, R., Nakamura, A., … Zetterberg, H. (2021). The global Alzheimer's Association round robin study on plasma amyloid β methods. *Alzheimer's&Dementia (Amsterdam, Netherlands)*, *13*(1), e12242. https://doi.org/10.1002/dad2.12242

Panza, F., Lozupone, M., Seripa, D., & Imbimbo, B. P. (2019). Amyloid-β immunotherapy for alzheimer disease: Is it now a long shot? *Annals of Neurology*, *85*(3), 303–315. https://doi.org/10.1002/ana.25410

Paravastu, A. K., Leapman, R. D., Yau, W.-M., & Tycko, R. (2008). Molecular structural basis for polymorphism in Alzheimer's beta-amyloid fibrils. *Proceedings of the National Academy of Sciences of the United States of America*, *105*(47), 18349–54. https://doi.org/10.1073/pnas.0806270105

Parker, W. D., Filley, C. M., & Parks, J. K. (1990). Cytochrome oxidase deficiency in Alzheimer's disease. *Neurology*, *40*(8), 1302–3. https://doi.org/10.1212/wnl.40.8.1302

Perchiacca, J. M., Ladiwala, A. R. A., Bhattacharya, M., & Tessier, P. M. (2012). Structure-based design of conformation- and sequence-specific antibodies against amyloid β. *Proceedings of the National Academy of Sciences of the United States of America*, *109*(1), 84–89. https://doi.org/10.1073/pnas.1111232108

Pereira, C., Santos, M. S., & Oliveira, C. (1998). Mitochondrial function impairment induced by amyloid beta-peptide on PC12 cells. *Neuroreport*, *9*(8), 1749–55. https://doi.org/10.1097/00001756-199806010-00015

Perrin, R. J., Fagan, A. M., & Holtzman, D. M. (2009). Multimodal techniques for diagnosis and prognosis of Alzheimer's disease. *Nature*, *461*(7266), 916–22. https://doi.org/10.1038/nature08538

Perry, R. J., & Hodges, J. R. (1999). Attention and executive deficits in Alzheimer's disease. A critical review. *Brain: A Journal of Neurology*, *122 (Pt 3)*, 383–404. https://doi.org/10.1093/brain/122.3.383

Peters, C., Espinoza, M. P., Gallegos, S., Opazo, C., & Aguayo, L. G. (2015). Alzheimer's Aβ interacts with cellular prion protein inducing neuronal membrane damage and synaptotoxicity. *Neurobiology of Aging*, *36*(3), 1369–77. https://doi.org/10.1016/j.neurobiolaging.2014.11.019

Pickford, F., Masliah, E., Britschgi, M., Lucin, K., Narasimhan, R., Jaeger, P. A., Small, S., Spencer, B., Rockenstein, E., Levine, B., & Wyss-Coray, T. (2008). The autophagy-related protein beclin 1 shows reduced expression in early Alzheimer disease and regulates amyloid beta accumulation in mice. *The Journal of Clinical Investigation*, *118*(6), 2190–99. https://doi.org/10.1172/JCI33585.

Pietrzak, M., Rempala, G., Nelson, P. T., Zheng, J.-J., & Hetman, M. (2011). Epigenetic silencing of nucleolar rRNA genes in Alzheimer's disease. *PloS One*, *6*(7), e22585. https://doi.org/10.1371/journal.pone.0022585

Pollard, H.B., Rojas, E., Arispe, N. (1993). A New Hypothesis for the Mechanism of Amyloid Toxicity, Based on the Calcium Channel Activity of Amyloid Protein (A P) in Phospholipid Bilayer Membranes. *Ann. N. Y. Acad. Sci. 695,*

165–168

Popugaeva, E., Pchitskaya, E., & Bezprozvanny, I. (2018). Dysregulation of Intracellular Calcium Signaling in Alzheimer's Disease. *Antioxidants & Redox Signaling*, *29*(12), 1176–88. https://doi.org/10.1089/ars.2018.7506

Praticò, D. (2008). Oxidative stress hypothesis in Alzheimer's disease: A reappraisal. *Trends in Pharmacological Sciences*, *29*(12), 609–15. https://doi.org/10.1016/j.tips.2008.09.001

Rabinovici, G. D. (2019). Late-onset Alzheimer Disease. *Continuum (Minneapolis, Minn.)*, *25*(1), 14–33. https://doi.org/10.1212/CON.0000000000000700

Rai, S. N., Singh, C., Singh, A., Singh, M. P., & Singh, B. K. (2020). Mitochondrial Dysfunction: A Potential Therapeutic Target to Treat Alzheimer's Disease. *Molecular Neurobiology*, *57*(7), 3075-88. https://doi.org/10.1007/s12035-020- 01945-y

Rasmussen, M. K., Mestre, H., & Nedergaard, M. (2018). The glymphatic pathway in neurological disorders. *The Lancet. Neurology*, *17*(11), 1016–24. https://doi.org/10.1016/S1474-4422(18)30318-1

Reed, B. R., Mungas, D., Farias, S. T., Harvey, D., Beckett, L., Widaman, K., Hinton, L., & DeCarli, C. (2010). Measuring cognitive reserve based on the decomposition of episodic memory variance. *Brain: A Journal of Neurology*, *133*(Pt 8), 2196–209. https://doi.org/10.1093/brain/awq154

Reese, L.C., Taglialatela, G. A. (2011). Role for calcineurin in Alzheimer's disease. *Curr. Neuropharmacol. 9, 685–92.*

Reiman, E. M., Quiroz, Y. T., Fleisher, A. S., Chen, K., Velez-Pardo, C., Jimenez-Del- Rio, M., Fagan, A. M., Shah, A. R., Alvarez, S., Arbelaez, A., Giraldo, M., Acosta-Baena, N., Sperling, R. A., Dickerson, B., Stern, C. E., Tirado, V., Munoz, C., Reiman, R. A., Huentelman, M. J., … Lopera, F. (2012). Brain imaging and fluid biomarker analysis in young adults at genetic risk for autosomal dominant Alzheimer's disease in the presenilin 1 E280A kindred: A case-control study. *The Lancet. Neurology*, *11*(12), 1048–56. https://doi.org/10.1016/S1474-4422(12)70228-4

Reiss, A. B., Arain, H. A., Stecker, M. M., Siegart, N. M., & Kasselman, L. J. (2018). Amyloid toxicity in Alzheimer's disease. *Reviews in the Neurosciences*, *29*(6), 613–27. https://doi.org/10.1515/revneuro-2017-0063

Relkin, N., Marmarou, A., Klinge, P., Bergsneider, M., & Black, P. M. (2005). Diagnosing idiopathic normal-pressure hydrocephalus. *Neurosurgery*, *57*(3 Suppl), S4-16; discussion ii-v. https://doi.org/10.1227/01.neu.0000168185.29659.c5

Renner, J. A., Burns, J. M., Hou, C. E., McKeel, D. W., Storandt, M., & Morris, J. C. (2004). Progressive posterior cortical dysfunction: A clinicopathologic series. *Neurology*, *63*(7), 1175–80. https://doi.org/10.1212/01.wnl.0000140290.80962.bf

Revi, M. (2020). Alzheimer's Disease Therapeutic Approaches. *Advances in Experimental Medicine and Biology*, *1195*, 105–16. https://doi.org/10.1007/978- 3-030-32633-3_15

Rissin, D. M., Kan, C. W., Campbell, T. G., Howes, S. C., Fournier, D. R., Song, L., Piech, T., Patel, P. P., Chang, L., Rivnak, A. J., Ferrell, E. P., Randall, J. D., Provuncher, G. K., Walt, D. R., & Duffy, D. C. (2010). Single-molecule enzyme- linked immunosorbent assay detects serum proteins at subfemtomolar concentrations. *Nature Biotechnology*, *28*(6), 595–99. https://doi.org/10.1038/nbt.1641

Robertson, D. S. (2010). The physical chemistry of brain and neural cell membranes: An overview. *Neurochemical Research*, *35*(5), 681–87. https://doi.org/10.1007/s11064-010-0121-7

Roychaudhuri, R., Yang, M., Hoshi, M. M., & Teplow, D. B. (2009). Amyloid beta- protein assembly and Alzheimer disease. *The Journal of Biological Chemistry*, *284*(8), 4749–53. https://doi.org/10.1074/jbc.R800036200

Rudajev, V., & Novotny, J. (2020). The Role of Lipid Environment in Ganglioside GM1- Induced Amyloid β Aggregation. *Membranes*, *10*(9), 226. https://doi.org/10.3390/membranes10090226

Sachdev, P., Kalaria, R., O'Brien, J., Skoog, I., Alladi, S., Black, S. E., Blacker, D., Blazer, D. G., Chen, C., Chui, H., Ganguli, M., Jellinger, K., Jeste, D. V., Pasquier, F., Paulsen, J., Prins, N., Rockwood, K., Roman, G., Scheltens, P., &Internationlal Society for Vascular Behavioral and Cognitive Disorders. (2014). Diagnostic criteria for vascular cognitive disorders: A VASCOG statement. *Alzheimer Disease and Associated Disorders*, *28*(3), 206–18. https://doi.org/10.1097/WAD.0000000000000034

Saido, T., & Leissring, M. A. (2012). Proteolytic degradation of amyloid β-protein. *Cold Spring Harbor Perspectives in Medicine*, *2*(6), a006379. https://doi.org/10.1101/cshperspect.a006379

Saito, R., Kaneko, M., Kitamura, Y., Takata, K., Kawada, K., Okuma, Y., & Nomura, Y. (2014). Effects of oxidative stress on the solubility of HRD1, a ubiquitin ligase implicated in Alzheimer's disease. *PloS One*, *9*(5), e94576. https://doi.org/10.1371/journal.pone.0094576

Saito, R., Kaneko, M., Okuma, Y., & Nomura, Y. (2010). Correlation between decrease in protein levels of ubiquitin ligase HRD1 and amyloid-beta production. *Journal of Pharmacological Sciences*, *113*(3), 285–88. https://doi.org/10.1254/jphs.10118sc

Sajdel-Sulkowska, E. M., & Marotta, C. A. (1984). Alzheimer's disease brain: Alterations in RNA levels and in a ribonuclease-inhibitor complex. *Science (New York, N.Y.)*, *225*(4665), 947–49. https://doi.org/10.1126/science.6206567

Sakono, M., & Zako, T. (2010). Amyloid oligomers: Formation and toxicity of Abeta oligomers. *The FEB Journal, 277*(6), 1348–58. https://doi.org/10.1111/j.1742-4658.2010.07568.x

Samad, N., Ishaq, S., Bano, S., & Manzoor, N. (2017). Calcium Regulation in Alzheimer's Disease: Mechanistic Understanding. *Journal of the College of Physicians and Surgeons--Pakistan: JCPSP*, *27*(9), 566–71.

Santoro, M. M. & Bolen, D. W. Unfolding free energy changes determined by the linear extrapolation method. 1. Unfolding of phenylmethanesulfonyl .alpha.-chymotrypsin using different denaturants. *Biochemistry* **27**, 8063–8068 (1988)

Santos, A. N., Torkler, S., Nowak, D., Schlittig, C., Goerdes, M., Lauber, T., Trischmann, L., Schaupp, M., Penz, M., Tiller, F.-W., & Böhm, G. (2007). Detection of amyloid-beta oligomers in human cerebrospinal fluid by flow cytometry and fluorescence resonance energy transfer. *Journal of Alzheimer's Disease: JAD*, *11*(1), 117–25. https://doi.org/10.3233/jad-2007-11114

Santos, R. X., Correia, S. C., Wang, X., Perry, G., Smith, M. A., Moreira, P. I., & Zhu, X. (2010). A synergistic dysfunction of mitochondrial fission/fusion dynamics and mitophagy in Alzheimer's disease. *Journal of Alzheimer's Disease: JAD*, *20 Suppl 2*(Suppl 2), S401-12. https://doi.org/10.3233/JAD-2010-100666

Savage, M. J., Kalinina, J., Wolfe, A., Tugusheva, K., Korn, R., Cash-Mason, T., Maxwell, J. W., Hatcher, N. G., Haugabook, S. J., Wu, G., Howell, B. J., Renger, J. J., Shughrue, P. J., &McCampbell, A. (2014). A sensitive aβ oligomer assay discriminates Alzheimer's and aged control cerebrospinal fluid. *The Journal of Neuroscience: The Official Journal of the Society for Neuroscience*, *34*(8), 2884-97. https://doi.org/10.1523/JNEUROSCI.1675-13.2014

Scalia, F., Vitale, A. M., Santonocito, R., Conway de Macario, E., Macario, A. J. L., & Cappello, F. (2021). The Neurochaperonopathies: Anomalies of the Chaperone System with Pathogenic Effects in Neurodegenerative and Neuromuscular Disorders. *Applied Sciences, 11*(3), Article 3. https://doi.org/10.3390/app11030898

Schengrund, C.L. (2010). Lipid rafts: Keys to neurodegeneration. *Brain Research Bulletin*, *82*(1–2), 7–17. https://doi.org/10.1016/j.brainresbull.2010.02.013

Scheuner, D., Eckman, C., Jensen, M., Song, X., Citron, M., Suzuki, N., Bird, T. D., Hardy, J., Hutton, M., Kukull, W., Larson, E., Levy-Lahad, E., Viitanen, M., Peskind, E., Poorkaj, P., Schellenberg, G., Tanzi, R., Wasco, W., Lannfelt, L., … Younkin, S. (1996). Secreted amyloid beta-protein similar to that in the senile plaques of Alzheimer's disease is increased in vivo by the presenilin 1 and 2 and APP mutations linked to familial Alzheimer's disease. *Nature Medicine*, *2*(8), 864–70. https://doi.org/10.1038/nm0896-864

Schneider, J. A., Arvanitakis Z., Bang W., Bennett D. A. (2007). Mixed brain pathologies account for most dementia cases in community-dwelling older persons. Neurology. 69:2197–204. doi: 10.1212/01.wnl.0000271090.28148.24.

Schwab, C., Arai, T., Hasegawa, M., Yu, S., & McGeer, P. L. (2008). Colocalization of transactivation-responsive DNA-binding protein 43 and huntingtin in inclusions of Huntington disease. *Journal of Neuropathology and Experimental Neurology*, *67*(12), 1159–65. https://doi.org/10.1097/NEN.0b013e31818e8951

Sciacca, M. F. M., La Rosa, C., & Milardi, D. (2021). Amyloid-Mediated Mechanisms of Membrane Disruption. *Biophysica*, *1*(2), 137-56.

https://doi.org/10.3390/biophysica1020011

Selkoe, D. J. (1999). Translating cell biology into therapeutic advances in Alzheimer's disease. *Nature*, *399*(6738 Suppl), A23-31. https://doi.org/10.1038/399a023

Selkoe, D. J. (2019). Alzheimer disease and aducanumab: Adjusting our approach. *Nature Reviews. Neurology*, *15*(7), 365–66. https://doi.org/10.1038/s41582-019-0205-1

Selles, M. C., Fortuna, J. T. S., Cercato, M. C., Santos, L. E., Domett, L., Bitencourt, A. L. B., Carraro, M. F., Souza, A. S., Janickova, H., Azevedo, C. V., Campos, H. C., de Souza, J. M., Alves-Leon, S., Prado, V. F., Prado, M. A. M., Epstein, A. L., Salvetti, A., Longo, B. M., Arancio, O., … Ferreira, S. T. (2023). AAV- mediated neuronal expression of an scFv antibody selective for Aβ oligomers protects synapses and rescues memory in Alzheimer models. *Molecular Therapy: The Journal of the American Society of Gene Therapy*, *31*(2), 409–19. https://doi.org/10.1016/j.ymthe.2022.11.002

Sengupta, U., Guerrero-Muñoz, M. J., Castillo-Carranza, D. L., Lasagna-Reeves, C. A., Gerson, J. E., Paulucci-Holthauzen, A. A., Krishnamurthy, S., Farhed, M., Jackson, G. R., & Kayed, R. (2015). Pathological interface between oligomeric alpha-synuclein and tau in synucleinopathies. *Biological Psychiatry*, *78*(10), 672– 83. https://doi.org/10.1016/j.biopsych.2014.12.019

Senjem, M. L., Gunter, J. L., Shiung, M. M., Petersen, R. C., & Jack, C. R. (2005). Comparison of different methodological implementations of voxel-based morphometry in neurodegenerative disease. *NeuroImage*, *26*(2), 600–08. https://doi.org/10.1016/j.neuroimage.2005.02.005

Sevigny, J., Chiao, P., Bussière, T., Weinreb, P. H., Williams, L., Maier, M., Dunstan, R., Salloway, S., Chen, T., Ling, Y., O'Gorman, J., Qian, F., Arastu, M., Li, M., Chollate, S., Brennan, M. S., Quintero-Monzon, O., Scannevin, R. H., Arnold, H. M., … Sandrock, A. (2016). The antibody aducanumab reduces Aβ plaques in Alzheimer's disease. *Nature*, *537*(7618), 50–56. https://doi.org/10.1038/nature19323

Sewell, R. D. E. (Ed.). (2007). *Protein Misfolding in Neurodegenerative Diseases: Mechanisms and Therapeutic Strategies*. CRC Press. https://doi.org/10.1201/9781420007145

Shaw, L. M., Vanderstichele, H., Knapik-Czajka, M., Clark, C. M., Aisen, P. S., Petersen, R. C., Blennow, K., Soares, H., Simon, A., Lewczuk, P., Dean, R., Siemers, E., Potter, W., Lee, V. M.-Y., Trojanowski, J. Q., & Alzheimer's Disease Neuroimaging Initiative. (2009). Cerebrospinal fluid biomarker signature in Alzheimer's disease neuroimaging initiative subjects. *Annals of Neurology*, *65*(4), 403–13. https://doi.org/10.1002/ana.21610

Sheu, K. F., Cooper, A. J., Koike, K., Koike, M., Lindsay, J. G., & Blass, J. P. (1994). Abnormality of the alpha-ketoglutarate dehydrogenase complex in fibroblasts from familial Alzheimer's disease. *Annals of Neurology*, *35*(3), 312–18. https://doi.org/10.1002/ana.410350311

Sheu, K. F., Kim, Y. T., Blass, J. P., & Weksler, M. E. (1985). An immunochemical study of the pyruvate dehydrogenase deficit in Alzheimer's disease brain.

Annals of Neurology, *17*(5), 444–49. https://doi.org/10.1002/ana.410170505

Shughrue, P. J., Acton, P. J., Breese, R. S., Zhao, W.-Q., Chen-Dodson, E., Hepler, R. W., Wolfe, A. L., Matthews, M., Heidecker, G. J., Joyce, J. G., Villarreal, S. A., & Kinney, G. G. (2010). Anti-ADDL antibodies differentially block oligomer binding to hippocampal neurons. *Neurobiology of Aging*, *31*(2), 189–202. https://doi.org/10.1016/j.neurobiolaging.2008.04.003

Simrén, J., Elmgren, A., Blennow, K., & Zetterberg, H. (2023). Fluid biomarkers in Alzheimer's disease. *Advances in Clinical Chemistry*, *112*, 249–81. https://doi.org/10.1016/bs.acc.2022.09.006

Sims, J. R., Zimmer, J. A., Evans, C. D., Lu, M., Ardayfio, P., Sparks, J., Wessels, A. M., Shcherbinin, S., Wang, H., Monkul Nery, E. S., Collins, E. C., Solomon, P., Salloway, S., Apostolova, L. G., Hansson, O., Ritchie, C., Brooks, D. A., Mintun, M., Skovronsky, D. M., & TRAILBLAZER-ALZ 2 Investigators. (2023). Donanemab in Early Symptomatic Alzheimer Disease: The TRAILBLAZER- ALZ 2 Randomized Clinical Trial. *JAMA*, *330*(6), 512–27. https://doi.org/10.1001/jama.2023.13239

Sims, R., Hill, M., & Williams, J. (2020). The multiplex model of the genetics of Alzheimer's disease. *Nature Neuroscience*, *23*(3), 311–22. https://doi.org/10.1038/s41593-020-0599-5

Singer, S. J., & Nicolson, G. L. (1972). The fluid mosaic model of the structure of cell membranes. *Science (New York, N.Y.)*, *175*(4023), 720–31. https://doi.org/10.1126/science.175.4023.720

Singh, A., Kukreti, R., Saso, L., & Kukreti, S. (2019). Oxidative Stress: A Key Modulator in Neurodegenerative Diseases. *Molecules (Basel, Switzerland)*, *24*(8), 1583. https://doi.org/10.3390/molecules24081583

Somavarapu, A. K., & Kepp, K. P. (2015). The Dependence of Amyloid-β Dynamics on Protein Force Fields and Water Models. *Chemphyschem: A European Journal of Chemical Physics and Physical Chemistry*, *16*(15), 3278–89. https://doi.org/10.1002/cphc.201500415

Song, S., Kim, S.-Y., Hong, Y.-M., Jo, D.-G., Lee, J.-Y., Shim, S. M., Chung, C.-W., Seo, S. J., Yoo, Y. J., Koh, J.-Y., Lee, M. C., Yates, A. J., Ichijo, H., & Jung, Y.- K. (2003). Essential role of E2-25K/Hip-2 in mediating amyloid-beta neurotoxicity. *Molecular Cell*, *12*(3), 553–63. https://doi.org/10.1016/j.molcel.2003.08.005

Sorbi, S., Bird, E. D., & Blass, J. P. (1983). Decreased pyruvate dehydrogenase complex activity in Huntington and Alzheimer brain. *Annals of Neurology*, *13*(1), 72–78. https://doi.org/10.1002/ana.410130116

Sorbi, S., Nacmias, B., Forleo, P., Latorraca, S., Gobbini, I., Bracco, L., Piacentini, S., & Amaducci, L. (1994). ApoE allele frequencies in Italian sporadic and familial Alzheimer's disease. *NeuroscienceLetters*, *177*(1–2), 100–2. https://doi.org/10.1016/0304-3940(94)90054-x

Sormanni, P., Aprile, F. A., & Vendruscolo, M. (2015). Rational design of antibodies targeting specific epitopes within intrinsically disordered proteins. *Proceedings of the National Academy of Sciences of the United States of America*, *112*(32), 9902–07. https://doi.org/10.1073/pnas.1422401112

Sormanni, P., Aprile, F. A., & Vendruscolo, M. (2018). Third generation antibody discovery methods: In silico rational design. *Chemical Society Reviews*, *47*(24), 9137–57. https://doi.org/10.1039/c8cs00523k

Sperling, R. A., Aisen, P. S., Beckett, L. A., Bennett, D. A., Craft, S., Fagan, A. M., Iwatsubo, T., Jack, C. R., Kaye, J., Montine, T. J., Park, D. C., Reiman, E. M., Rowe, C. C., Siemers, E., Stern, Y., Yaffe, K., Carrillo, M. C., Thies, B., Morrison-Bogorad, M., … Phelps, C. H. (2011). Toward defining the preclinical stages of Alzheimer's disease: Recommendations from the National Institute on Aging-Alzheimer's Association workgroups on diagnostic guidelines for Alzheimer's disease. *Alzheimer's & Dementia: The Journal of the Alzheimer's Association*, *7*(3), 280–92. https://doi.org/10.1016/j.jalz.2011.03.003

Stewart, M. D., Ritterhoff, T., Klevit, R. E., & Brzovic, P. S. (2016). E2 enzymes: More than just middle men. *Cell Research*, *26*(4), 423. https://doi.org/10.1038/cr.2016.35

Strimbu, K., & Tavel, J. A. (2010). What are biomarkers? *Current Opinion in HIV and AIDS*, *5*(6), 463–66. https://doi.org/10.1097/COH.0b013e32833ed177

Sunde, M., & Blake, C. (1997). The structure of amyloid fibrils by electron microscopy and X-ray diffraction. *Advances in Protein Chemistry*, *50*, 123–59. https://doi.org/10.1016/s0065-3233(08)60320-4

Sutphen, C. L., Jasielec, M. S., Shah, A. R., Macy, E. M., Xiong, C., Vlassenko, A. G., Benzinger, T. L. S., Stoops, E. E. J., Vanderstichele, H. M. J., Brix, B., Darby, H. D., Vandijck, M. L. J., Ladenson, J. H., Morris, J. C., Holtzman, D. M., & Fagan, A. M. (2015). Longitudinal Cerebrospinal Fluid Biomarker Changes in Preclinical Alzheimer Disease During Middle Age. *JAMA Neurology*, *72*(9), 1029–42. https://doi.org/10.1001/jamaneurol.2015.1285

Swanson, C. J., Zhang, Y., Dhadda, S., Wang, J., Kaplow, J., Lai, R. Y. K., Lannfelt, L., Bradley, H., Rabe, M., Koyama, A., Reyderman, L., Berry, D. A., Berry, S., Gordon, R., Kramer, L. D., & Cummings, J. L. (2021). A randomized, double- blind, phase 2b proof-of-concept clinical trial in early Alzheimer's disease with lecanemab, an anti-Aβ protofibril antibody. *Alzheimer's Research & Therapy*, *13*(1), 80. https://doi.org/10.1186/s13195-021-00813-8

Swerdlow, R. H. (2018). Mitochondria and Mitochondrial Cascades in Alzheimer's Disease. *Journal of Alzheimer's Disease: JAD*, *62*(3), 1403–16. https://doi.org/10.3233/JAD-170585

Taipale, M., Jarosz, D. F., & Lindquist, S. (2010). HSP90 at the hub of protein homeostasis: Emerging mechanistic insights. *Nature Reviews. Molecular Cell Biology*, *11*(7), 515–28. https://doi.org/10.1038/nrm2918

Tcw, J., & Goate, A. M. (2017). Genetics of β-Amyloid Precursor Protein in Alzheimer's Disease. *Cold Spring Harbor Perspectives in Medicine*, *7*(6), a024539. https://doi.org/10.1101/cshperspect.a024539

Thompson, A. J., Banwell, B. L., Barkhof, F., Carroll, W. M., Coetzee, T., Comi, G., Correale, J., Fazekas, F., Filippi, M., Freedman, M. S., Fujihara, K.,

Galetta, S. L., Hartung, H. P., Kappos, L., Lublin, F. D., Marrie, R. A., Miller, A. E., Miller, D. H., Montalban, X., … Cohen, J. A. (2018). Diagnosis of multiple sclerosis: 2017 revisions of the McDonald criteria. *The Lancet. Neurology*, *17*(2), 162–73. https://doi.org/10.1016/S1474-4422(17)30470-2

Tokunaga, Y., & Takeuchi, K. (2020). Role of NMR in High Ordered Structure Characterization of Monoclonal Antibodies. *International Journal of Molecular Sciences*, *22*(1), 46. https://doi.org/10.3390/ijms22010046

Toledo J. B., Arnold S. E., Raible K., Brettschneider J., Xie S. X., Grossman M., Monsell S. E., Kukull W. A., Trojanowski J. Q. (2013). Contribution of cerebrovascular disease in autopsy confirmed neurodegenerative disease cases in the National Alzheimer's Coordinating Centre. Brain. 136:2697–706. doi: 10.1093/brain/awt188.

Tu, S., Okamoto, S., Lipton, S. A., & Xu, H. (2014). Oligomeric Aβ-induced synaptic dysfunction in Alzheimer's disease. *Molecular Neurodegeneration*, *9*, 48. https://doi.org/10.1186/1750-1326-9-48

Twohig, D., & Nielsen, H. M. (2019). α-synuclein in the pathophysiology of Alzheimer's disease. *Molecular Neurodegeneration*, *14*(1), 23. https://doi.org/10.1186/s13024-019-0320-x

Vadukul, D. M., Papp, M., Thrush, R. J., Wang, J., Jin, Y., Arosio, P., & Aprile, F. A. (2023). α-Synuclein Aggregation Is Triggered by Oligomeric Amyloid-β 42 via Heterogeneous Primary Nucleation. *Journal of the American Chemical Society*, *145*(33), 18276–285. https://doi.org/10.1021/jacs.3c03212

Valdor, R., Mocholi, E., Botbol, Y., Guerrero-Ros, I., Chandra, D., Koga, H., Gravekamp, C., Cuervo, A. M., &Macian, F. (2014). Chaperone-mediated autophagy regulates T cell responses through targeted degradation of negative regulators of T cell activation. *Nature Immunology*, *15*(11), 1046-54. https://doi.org/10.1038/ni.3003

van Dyck, C. H., Swanson, C. J., Aisen, P., Bateman, R. J., Chen, C., Gee, M., Kanekiyo, M., Li, D., Reyderman, L., Cohen, S., Froelich, L., Katayama, S., Sabbagh, M., Vellas, B., Watson, D., Dhadda, S., Irizarry, M., Kramer, L. D., & Iwatsubo, T. (2023). Lecanemab in Early Alzheimer's Disease. *The New England Journal of Medicine*, *388*(1), 9–21. https://doi.org/10.1056/NEJMoa2212948

Veerabhadrappa, B., Delaby, C., Hirtz, C., Vialaret, J., Alcolea, D., Lleó, A., Fortea, J., Santosh, M. S., Choubey, S., & Lehmann, S. (2020). Detection of amyloid beta peptides in body fluids for the diagnosis of alzheimer's disease: Where do we stand? *Critical Reviews in Clinical Laboratory Sciences*, *57*(2), 99–113. https://doi.org/10.1080/10408363.2019.1678011

Vemuri, P., Weigand, S. D., Przybelski, S. A., Knopman, D. S., Smith, G. E., Trojanowski, J. Q., Shaw, L. M., Decarli, C. S., Carmichael, O., Bernstein, M. A., Aisen, P. S., Weiner, M., Petersen, R. C., Jack, C. R., & Alzheimer's Disease Neuroimaging Initiative. (2011). Cognitive reserve and Alzheimer's disease biomarkers are independent determinants of cognition. *Brain: A Journal of Neurology*, *134*(Pt 5), 1479–92. https://doi.org/10.1093/brain/awr049

Vemuri, P., Wiste, H. J., Weigand, S. D., Shaw, L. M., Trojanowski, J. Q., Weiner, M. W., Knopman, D. S., Petersen, R. C., Jack, C. R., & Alzheimer's Disease Neuroimaging Initiative. (2009). MRI and CSF biomarkers in normal, MCI, and AD subjects: Predicting future clinical change. *Neurology*, *73*(4), 294–301. https://doi.org/10.1212/WNL.0b013e3181af79fb

Vermunt, L., Sikkes, S. A. M., van den Hout, A., Handels, R., Bos, I., van der Flier, W. M., Kern, S., Ousset, P.-J., Maruff, P., Skoog, I., Verhey, F. R. J., Freund-Levi, Y., Tsolaki, M., Wallin, Å. K., Olde Rikkert, M., Soininen, H., Spiru, L., Zetterberg, H., Blennow, K., … ICTUS/DSA study groups. (2019). Duration of preclinical, prodromal, and dementia stages of Alzheimer's disease in relation to age, sex, and APOE genotype. *Alzheimer's & Dementia: The Journal of the Alzheimer's Association*, *15*(7), 888–98. https://doi.org/10.1016/j.jalz.2019.04.001

Villemagne, V. L., Burnham, S., Bourgeat, P., Brown, B., Ellis, K. A., Salvado, O., Szoeke, C., Macaulay, S. L., Martins, R., Maruff, P., Ames, D., Rowe, C. C., Masters, C. L., & Australian Imaging Biomarkers and Lifestyle (AIBL) Research Group. (2013). Amyloid β deposition, neurodegeneration, and cognitive decline in sporadic Alzheimer's disease: A prospective cohort study. *The Lancet. Neurology*, *12*(4), 357–67. https://doi.org/10.1016/S1474-4422(13)70044-9

Villemagne, V. L., Pike, K. E., Chételat, G., Ellis, K. A., Mulligan, R. S., Bourgeat, P., Ackermann, U., Jones, G., Szoeke, C., Salvado, O., Martins, R., O'Keefe, G., Mathis, C. A., Klunk, W. E., Ames, D., Masters, C. L., & Rowe, C. C. (2011). Longitudinal assessment of Aβ and cognition in aging and Alzheimer disease. *Annals of Neurology*, *69*(1), 181–92. https://doi.org/10.1002/ana.22248

Vivekanandan, S., Brender, J. R., Lee, S. Y., & Ramamoorthy, A. (2011). A partially folded structure of amyloid-beta(1-40) in an aqueous environment. *Biochemical and Biophysical Research Communications*, *411*(2), 312–16. https://doi.org/10.1016/j.bbrc.2011.06.133

Walsh, D. M., & Selkoe, D. J. (2004). Deciphering the molecular basis of memory failure in Alzheimer's disease. *Neuron*, *44*(1), 181–93. https://doi.org/10.1016/j.neuron.2004.09.010

Walsh, D. M., Klyubin, I., Fadeeva, J. V., Cullen, W. K., Anwyl, R., Wolfe, M. S., Rowan, M. J., & Selkoe, D. J. (2002). Naturally secreted oligomers of amyloid beta protein potently inhibit hippocampal long-term potentiation in vivo. *Nature*, *416*(6880), 535–39. https://doi.org/10.1038/416535a

Walsh, D. M., Tseng, B. P., Rydel, R. E., Podlisny, M. B., & Selkoe, D. J. (2000). The oligomerization of amyloid beta-protein begins intracellularly in cells derived from human brain. *Biochemistry*, *39*(35), 10831–839. https://doi.org/10.1021/bi001048s

Wang, H.-W., Pasternak, J. F., Kuo, H., Ristic, H., Lambert, M. P., Chromy, B., Viola, K. L., Klein, W. L., Stine, W. B., Krafft, G. A., &Trommer, B. L. (2002). Soluble oligomers of beta amyloid (1-42) inhibit long-term potentiation but not long-term depression in rat dentate gyrus. *Brain Research*,

924(2), 133–40. https://doi.org/10.1016/s0006-8993(01)03058-x

Wang, X., Wang, W., Li, L., Perry, G., Lee, H., & Zhu, X. (2014). Oxidative stress and mitochondrial dysfunction in Alzheimer's disease. *Biochimica Et Biophysica Acta*, *1842*(8), 1240–47. https://doi.org/10.1016/j.bbadis.2013.10.015

Wasik, U., Schneider, G., Mietelska-Porowska, A., Mazurkiewicz, M., Fabczak, H., Weis, S., Zabke, C., Harrington, C. R., Filipek, A., & Niewiadomska, G. (2013). Calcyclin binding protein and Siah-1 interacting protein in Alzheimer's disease pathology: Neuronal localization and possible function. *Neurobiology of Aging*, *34*(5), 1380–1388. https://doi.org/10.1016/j.neurobiolaging.2012.11.007

Wasmer, C., Lange, A., Van Melckebeke, H., Siemer, A. B., Riek, R., & Meier, B. H. (2008). Amyloid fibrils of the HET-s(218-289) prion form a beta solenoid with a triangular hydrophobic core. *Science (New York, N.Y.)*, *319*(5869), 1523–26. https://doi.org/10.1126/science.1151839

Weintraub, S., Wicklund, A. H., Salmon, D. P. The neuropsychological profile of Alzheimer disease. Cold Spring HarbPerspect Med. (2012) Apr;2(4):a006171. doi: 10.1101/cshperspect.a006171. PMID: 22474609; PMCID: PMC3312395

Westermark, P. (2005). Aspects on human amyloid forms and their fibril polypeptides. *The FEBS Journal*, *272*(23), 5942–49. https://doi.org/10.1111/j.1742- 4658.2005.05024.x

Westin, K., Buchhave, P., Nielsen, H., Minthon, L., Janciauskiene, S., & Hansson, O. (2012). CCL2 is associated with a faster rate of cognitive decline during early stages of Alzheimer's disease. *PloS One*, *7*(1), e30525. https://doi.org/10.1371/journal.pone.0030525

Whitehouse, P. J., Orgogozo, J. M., Becker, R. E., Gauthier, S., Pontecorvo, M., Erzigkeit, H., Rogers, S., Mohs, R. C., Bodick, N., Bruno, G., & Dal-Bianco, P. (1997). Quality-of-life assessment in dementia drug development. Position paper from the International Working Group on Harmonization of Dementia Drug Guidelines. *Alzheimer Disease and Associated Disorders*, *11 Suppl 3*, 56–60.

Wiatrak, B., Piasny, J., Kuźniarski, A., & Gąsiorowski, K. (2021). Interactions of Amyloid-β with Membrane Proteins. *International Journal of Molecular Sciences*, *22*(11), 6075. https://doi.org/10.3390/ijms22116075

Wiedrick, J. T., Phillips, J. I., Lusardi, T. A., McFarland, T. J., Lind, B., Sandau, U. S., Harrington, C. A., Lapidus, J. A., Galasko, D. R., Quinn, J. F., & Saugstad, J. A. (2019). Validation of MicroRNA Biomarkers for Alzheimer's Disease in Human Cerebrospinal Fluid. *Journal of Alzheimer's Disease: JAD*, *67*(3), 875–91. https://doi.org/10.3233/JAD-180539

Wilkins, H. M., & Swerdlow, R. H. (2017). Amyloid precursor protein processing and bioenergetics. *Brain Research Bulletin*, *133*, 71–79. https://doi.org/10.1016/j.brainresbull.2016.08.009

Winblad, B., Amouyel, P., Andrieu, S., Ballard, C., Brayne, C., Brodaty, H., Cedazo- Minguez, A., Dubois, B., Edvardsson, D., Feldman, H., Fratiglioni, L., Frisoni, G. B., Gauthier, S., Georges, J., Graff, C., Iqbal, K., Jessen, F.,

Johansson, G., Jönsson, L., … Zetterberg, H. (2016). Defeating Alzheimer's disease and other dementias: A priority for European science and society. *The Lancet. Neurology*, *15*(5), 455–532. https://doi.org/10.1016/S1474-4422(16)00062-4

Wojdała, A. L., Bellomo, G., Toja, A., Gaetani, L., Parnetti, L., & Chiasserini, D. (2024). CSF and plasma Aβ42/40 across Alzheimer's disease continuum: Comparison of two ultrasensitive Simoa® assays targeting distinct amyloid regions. *Clinical Chemistry and Laboratory Medicine*, *62*(2), 332–40. https://doi.org/10.1515/cclm-2023-0659

World Health Organization. Geneva, Switzerland: World Health Organization; (2021). Fact sheets of dementia [Internet] [cited 2022 Apr 13].

Yamamoto, N., Fukata, Y., Fukata, M., & Yanagisawa, K. (2007). GM1-ganglioside- induced Abeta assembly on synaptic membranes of cultured neurons. *Biochimica Et Biophysica Acta*, *1768*(5), 1128–37. https://doi.org/10.1016/j.bbamem.2007.01.009

Yamazaki, T., Koo, E. H., & Selkoe, D. J. (1997). Cell surface amyloid beta-protein precursor colocalizes with beta 1 integrins at substrate contact sites in neural cells. *The Journal of Neuroscience: The Official Journal of the Society for Neuroscience*, *17*(3), 1004–10. https://doi.org/10.1523/JNEUROSCI.17-03-01004.1997

Yanagisawa, K. (2007). Role of gangliosides in Alzheimer's disease. *Biochimica Et Biophysica Acta*, *1768*(8), 1943–51. https://doi.org/10.1016/j.bbamem.2007.01.018

Yang, T., O'Malley, T. T., Kanmert, D., Jerecic, J., Zieske, L. R., Zetterberg, H., Hyman, B. T., Walsh, D. M., &Selkoe, D. J. (2015). A highly sensitive novel immunoassay specifically detects low levels of soluble Aβ oligomers in human cerebrospinal fluid. *Alzheimer's Research & Therapy*, *7*(1), 14. https://doi.org/10.1186/s13195- 015-0100-y

Yerbury, J. J., & Wilson, M. R. (2010). Extracellular chaperones modulate the effects of Alzheimer's patient cerebrospinal fluid on Abeta(1-42) toxicity and uptake. *Cell Stress & Chaperones*, *15*(1), 115–21. https://doi.org/10.1007/s12192-009- 0122-0

Yoshihara, T., Takiguchi, S., Kyuno, A., Tanaka, K., Kuba, S., Hashiguchi, S., Ito, Y., Hashimoto, T., Iwatsubo, T., Tsuyama, S., Nakashima, T., & Sugimura, K. (2008). Immunoreactivity of phage library-derived human single-chain antibodies to amyloid beta conformers in vitro. *Journal of Biochemistry*, *143*(4), 475–86. https://doi.org/10.1093/jb/mvm239

Young-Pearse, T. L., Chen, A. C., Chang, R., Marquez, C., & Selkoe, D. J. (2008). Secreted APP regulates the function of full-length APP in neurite outgrowth through interaction with integrin beta1. *Neural Development*, *3*, 15. https://doi.org/10.1186/1749-8104-3-15

Younkin, S. G. (1995). Evidence that A beta 42 is the real culprit in Alzheimer's disease. *Annals of Neurology*, *37*(3), 287–88. https://doi.org/10.1002/ana.410370303

Yu, Y. J., & Watts, R. J. (2013). Developing therapeutic antibodies for neurodegenerative disease. *Neurotherapeutics: The Journal of the American Society for Experimental NeuroTherapeutics*, *10*(3), 459–72. https://doi.org/10.1007/s13311-013-0187-4

Yuan, S., Zhou, G., & Xu, G. (2024). Translation machinery: The basis of translational control. *Journal of Genetics and Genomics = Yi Chuan Xue Bao*, *51*(4), 367–78. https://doi.org/10.1016/j.jgg.2023.07.009

Yusakul, G., Sakamoto, S., Pongkitwitoon, B., Tanaka, H., & Morimoto, S. (2016). Effect of linker length between variable domains of single chain variable fragment antibody against daidzin on its reactivity. *Bioscience, Biotechnology and Biochemistry*, *80*(7), 1306–12. https://doi.org/10.1080/09168451.2016.1156482

Zameer, A., Kasturirangan, S., Emadi, S., Nimmagadda, S. V., & Sierks, M. R. (2008). Anti-oligomeric Abeta single-chain variable domain antibody blocks Abeta- induced toxicity against human neuroblastoma cells. *Journal of MolecularBiology*, *384*(4), 917–28. https://doi.org/10.1016/j.jmb.2008.09.068

Zampagni, M., Cascella, R., Casamenti, F., Grossi, C., Evangelisti, E., Wright, D., Becatti, M., Liguri, G., Mannini, B., Campioni, S., Chiti, F., & Cecchi, C. (2011). A comparison of the biochemical modifications caused by toxic and non-toxic protein oligomers in cells. *Journal of Cellular and Molecular Medicine*, *15*(10), 2106-16. https://doi.org/10.1111/j.1582-4934.2010.01239.x

Zandomeneghi, G., Krebs, M. R. H., McCammon, M. G., & Fändrich, M. (2004). FTIR reveals structural differences between native beta-sheet proteins and amyloid fibrils. *Protein Science: A Publication of the Protein Society*, *13*(12), 3314–21. https://doi.org/10.1110/ps.041024904.

Zetterberg, H., & Bendlin, B. B. (2021). Biomarkers for Alzheimer's disease-preparing for a new era of disease-modifying therapies. *Molecular Psychiatry*, *26*(1), 296–308. https://doi.org/10.1038/s41380-020-0721-9

Zetterberg, H., Alawode, D. O. T., Keshavan, A., O'Connor, A, Weston, P. S. J., Paterson, R. W., Heslegrave, A., Fox, N. C. Fox, Lunn, M. P., Schott, J. M. (2020). *Blood Tests for Alzheimer Disease*. Practical Neurology; Bryn Mawr Communications. Retrieved 8 January 2025, from https://practicalneurology.com/articles/2020-nov-dec/blood-tests-for-alzheimer-disease

Zha, J., Liu, X.-M., Zhu, J., Liu, S.-Y., Lu, S., Xu, P.-X., Yu, X.-L., & Liu, R.-T. (2016). A scFv antibody targeting common oligomeric epitope has potential for treating several amyloidoses. *Scientific Reports*, *6*, 36631. https://doi.org/10.1038/srep36631

Zhao, Y., & Zhao, B. (2013). Oxidative stress and the pathogenesis of Alzheimer's disease. *Oxidative Medicine and Cellular Longevity*, *2013*, 316523. https://doi.org/10.1155/2013/316523

Zheng, F., Pang, Y., Li, L., Pang, Y., Zhang, J., Wang, X., &Raes, G. (2022). Applications of nanobodies in brain diseases. *Frontiers in Immunology*, *13*, 978513. https://doi.org/10.3389/fimmu.2022.978513

Zhu, X., Perry, G., Smith, M. A., & Wang, X. (2013). Abnormal mitochondrial dynamics in the pathogenesis of Alzheimer's disease. *Journal of Alzheimer's Disease: JAD*, *33 Suppl 1*(0 1), S253-62. https://doi.org/10.3233/JAD-2012-129005.

Index of names

FUP Best Practice in Scholarly Publishing (DOI 10.36253/fup_best_practice)

PREMIO TESI DI DOTTORATO CITTÀ DI FIRENZE

TITOLI PUBBLICATI

ANNO 2023-2024

Catani Andrea, *L'indipendenza e l'*accountability *democratica delle banche centrali. Profili comparatistici*
Cinnella Della Porta Silvia, *Traduttori e mercanti. La scoperta inglese del Nuovo Mondo*
Ciravegna Gabriele, *On the Two fold Role of Logic Constraints in Deep Learning*
Colucci Clementina, *Tra ottimizzazione della funzione comando e prospettive di un suo superamento. I nuovi scenari della normatività penale*
Di Gesto Cristian, *Influenze socioculturali, immagine corporea e chirurgia estetica*
Santanni Fabio, *Molecular approaches for quantum technologies. Optimization of electron spin-based quantum bits and quantum logic gates*

ANNO 2025

Arianna Amatruda, *La Dea Diana di Heine. Sopravvivenza e rinascenza del mito nella Parigi del XIX secolo*
Andrea Apollonio, *Politiche della memoria e narrazioni sulla storia nel Parlamento europeo*
Gianluca Damiani, *Looking for a Science of Politics. William H. Riker and the adoption of Game Theory in Political Science*
Sofia Imperatore, *Adaptive spline approximation: data-driven parameterization and CAD model (re-) construction*
Benedetta Masiani, *La città fa scuola, la scuola fa città. Dallo spazio pubblico ai cortili scolastici per una rinnovata permeabilità*
Liliana Napolitano, *A multidisciplinary approach for the early diagnosis of Alzheimer's disease and potential therapeutic applications*

Premio Tesi di Dottorato
Città di Firenze 2025

This thesis presents a multidisciplinary approach to improve Alzheimer's disease (AD) early diagnosis and therapy. The first part, based on the PRAMA cohort, identifies two novel CSF biomarkers using biophysical and cell viability assays to detect proteostasis failure. The second part focuses on the single-domain antibody DesAb-O, demonstrating its ability to selectively detect $A\beta_{42}$ oligomers and neutralize their toxicity in patient-derived CSF. This tool was further engineered into Dimeric-DesAb-O. In the third part, ELISA, ThT, and TEM analyses confirm that dimerization enhances binding avidity, alters fibril morphology, and increases protective efficacy at low concentrations. This study suggests innovative immunodiagnostic and therapeutic strategies for future AD clinical applications.

LILIANA NAPOLITANO is a researcher specializing in Alzheimer's disease and other neurodegenerative disorders. Her work focuses on the $A\beta_{42}$ oligomer proteotoxicity and the engineering and validation of single-domain antibodies as innovative tools for early diagnosis and future therapy.

ISSN 3103-3881 (print)
ISSN 3103-3989 (online)
ISBN 979-12-215-0992-2 (Print)
ISBN 979-12-215-0993-9 (PDF)
ISBN 979-12-215-0994-6 (XML)
DOI 10.36253/979-12-215-0993-9
www.fupress.com